TECHNISCHE UNIVERSITÄT MÜNCHEN
Lehrstuhl für Regelungstechnik

Model-Based Damper Control for Semi-Active Suspension Systems

Enrico Pellegrini

Vollständiger Abdruck der von der Fakultät für Maschinenwesen
der Technischen Universität München zur Erlangung
des akademischen Grades eines

Doktor-Ingenieurs

genehmigten Dissertation.

Vorsitzender:	Univ.-Prof. Dr.-Ing. Georg Wachtmeister
Prüfer der Dissertation:	1. Univ.-Prof. Dr.-Ing. habil. Boris Lohmann
	2. Univ.-Prof. Dr.-Ing. Dr.-Ing. habil. Heinz Ulbrich (i. R.)

Die Dissertation wurde am 27.08.2012 bei der Technischen Universität München eingereicht und durch die Fakultät für Maschinenwesen am 18.12.2012 angenommen.

To my family and Susanne

ABSTRACT

This Thesis presents new approaches for control of semi-active vehicle suspension systems. In particular, towards optimizing the exploiting of the fast dynamic of modern devices, it focuses on three aspects: semi-active device modeling, damper control and optimal control for semi-active suspensions. At first, a new physical model of a semi-active damper is presented, which takes into account the fluid dynamics, the switching elements and the external valves. This model reproduces the real hardware with high precision. Nevertheless, because of its complexity and thus its high demand for computational time, it is not suitable for control in real-time applications. Therefore, a functional damper model, which emulates the main characteristics of the real device, is derived and validated by means of measurements. Next, the obtained model is integrated in a controller structure. Since the state of the art solution utilizes a feedforward approach based on static damper characteristics, the novelty of the presented model-based approach consists of introducing a dynamical feedforward path, which considers the hysteresis effects of the damper. This allows a better force tracking and, hence, a better exploitation of the semi-active hardware. In addition, the dynamical feedforward structure is extended by a force feedback path, which further reduces the control error and allows to increase the semi-active control performance. The low-level actuator control structure, meaning both the newly introduced feedforward and feedback structures, is analyzed by making use of state of the art suspension controllers. The commonly employed suspension controllers do not consider the working range, i.e. the state dependent constraints of the semi-active device in the controller design. Therefore, the third aspect addressed in this Thesis is an optimized high-level suspension controller, which takes the limitation of the controlling hardware into account. Based on the Principle of Optimality, two different suspension controller solutions for the nonlinear quarter-car model are compared in this Thesis. Although the high computational cost does not allow yet to utilize these methods for industrial applications, the importance of these approaches consists in the fact that the desired damper force always lies within the damper working range. Since the force can be continuously generated by the device, the control performance is further increased. The result for both the low-level and the high-level strategies have been experimentally confirmed on a semi-active quarter-car test rig, which has been designed and constructed by utilizing production vehicle components and sensors.

ACKNOWLEDGMENTS

I would like to gratefully and sincerely thank my advisor Prof. Boris Lohmann for his guidance during the time at the Institute of Automatic Control. The freedom in the choice and in the treatment of the research topic as well as his constructive comments, which constituted the basis of this dissertation, and his support in the realization of the quarter-car test rig are very appreciated.

I would also like to thank Prof. Heinz Ulbrich for being the second examiner for this Thesis and Prof. Georg Wachtmeister for chairing the board of examination.

My deepest gratitude goes to Dr. Guido Koch for introducing me to the field of automotive suspension systems as supervisor of my Master Thesis and then involving me in the design and construction of a new mechatronic suspension, whose adjustable damper has been the subject of this Thesis. Moreover, I would like to deeply thank Nils Pletschen, Sebastian Spirk and Dr. Andreas Unger for the excellent teamwork and the fruitful discussions which have been indispensable for successful academic research. Besides the aforementioned colleagues, especially Dr. Michael Buhl, Klaus J. Diepold and Dr. Rudy Eid deserve my gratitude for the long discussions on this work and their precious and constructive comments. I am also grateful to all my colleagues Benjamin Berger, Dr. Sebastian Bürger, Paul De Monte, Oliver Fritsch, Tobias Kloiber, Heiko Panzer, Joachim Pfleghaar, Peter Philipp and Thomas Wolf for their scientific and non-scientific assistance and support, which contributed to the familiar atmosphere at the Institute. I also would like to express my deepest gratitude to Thomas Huber for the realization of the test rig and for bringing me closer to the manufacturing process.

Furthermore, I would like to thank the industrial partner BMW AG, which allowed the Institute to use their mechanical components, damper test rig and data. In particular, the technical and scientific cooperation with Carsten Bischoff, Prof. Marcus Jautze, Dr. Markus Nyenhuis and Dr. Karsten Röski is appreciated.

Moreover, I would like to sincerely thank all my students, in particular Josua Braun, Killian A. Grunauer Brachetti, Christoph Deleye, Ronnie Dessort, Justus Jordan, Martin Mayerhofer, Anh Phan, Michael Rainer and Franciska Völgyi. Their excellent work has significantly contributed to the quality of my research work and its results.

Special thanks go to the ”MPI-Team” for spending their lunch times with me and for investing their money in healthier meals. I take this opportunity to also sincerely thank all friends who supported and motivated me during this venture, even from Italy.

A very special acknowledgment goes to my family, Ermenegildo, Rosamaria, Pietro and Stefano for their care and support throughout all my years of education both in Italy and in Germany. The patience, the understanding and the love of my sunshine Susanne Trainotti gave me the inspiration to face this adventure. Without her support and encouragement this work would not have been possible.

TABLE OF CONTENTS

Page

LIST OF FIGURES

LIST OF TABLES

GLOSSARY

Abbreviation

ACD II	Active Control Damping 2
ADS	Adaptive Damping System
BIBO	Bounded-Input, Bounded-Output (system)
CAD	Computer aided design
CDC	Continuous Damping Control
CES	Continuously controlled Electronic Suspension
ECU	electronic Control Unit
EDC	Electrical Damper Control
EDCC	Electrical Damper Control with Continuously working damping valves
EMPC	Explicit Model predictive control
ER	Electrorheological
FB	Feedback (loop)
FEM	Finite element method
FFW	Feedforward (loop)
GA	Genetic Algorithm
ISO	International Organization for Standardization
LMI	Linear matrix inequality
LPV	Linear parameter-varying
LQR	Linear quadratic regulator
LTI	Linear time-invariant
LVTD	Linear Variable Differential Transformer
MPC	Model predictive control
MR	Magnetorheological
PSD	Power spectral density

SDC	Sensitive Damping Control
SISO	Single input single output (system)

Notation

$G_{a,b}$	Amplitude in the frequency response. Input: b, output: a
$\angle G_{a,b}$	Phase in the frequency response. Input: b, output: a
$\hat{x}(t)$	Estimate of variable x(t)
$\|x\|_{rms}$	Root mean square (rms) value of x(t)
$\|x\|_{std}$	Standard deviation of x(t)
$\|x\|$	Any p-norm of x(t)
x^*	Optimal value of x / reference value for x(t)

Chapter 1

INTRODUCTION

One of the first characteristics which is noted by riding a car, is how the vehicle reacts to external road excitations. Its behavior is mainly influenced by the suspension system, which consists of several components and defines the particular ride feeling. In its conventional configuration a suspension system consists of a chassis, an elastic element (typically a steel or air primary spring), a damping element (typically a hydraulic damper) and of elastomer buffers. Wheels, tires, wishbone structure, steering system and brakes belong to the suspension system as well. The main task of suspension systems is to guarantee ride safety and road holding of a vehicle. In addition to preserving the contact between tire and road, which is essential to ensure good tracking and braking performance, the vibration system also has to provide the best possible ride comfort for car occupants.

While the spring (stiffness c_c), carries all the static loads and delivers a force dependent on the suspension deflection, the damper does not influence the static or quasi-static motion around the equilibrium state but assumes a fundamental role in the dynamic behavior of the suspension. It provides a nonlinear dissipative force and is related to the suspension deflection velocity. These two elements are fundamental for the vibration behavior of the vehicle, while the suspension strut characterizes the kinematic relationships of the components.

As already mentioned, the choice of the spring and the damping setting defines the dynamic behavior of the vehicle. On the one hand the suspension system has to provide a high comfort, which means that soft spring and damping settings are desired for isolating the body mass from the vibration introduced by the road irregularities. On the other hand, the suspension must provide the maximal controllability for the driver to ensure vehicle holding. This task requires a hard damped connection between the vehicle and the road. The suspension strut represents a mechanical low-pass filter, which influences the transmission of forces to the chassis mass and consequently determines the above-mentioned ride feeling.

Hence, considering the ride comfort as main objective, the majority of specialist books define the relevant variable as the body acceleration, whereas if the target is the road-holding the dynamic tire deflection has to be considered. However, as depicted in Figure 1.1, these two aspects are contradictory. The basic design has the task to find the "right" balance between these two demands, according to the industrial politics. It is underlined, that the tradeoff is even more restricted by the limited suspension deflection. By hitting end-stops or by reaching mechanical limits both comfort and ride safety are not guaranteed, [138].

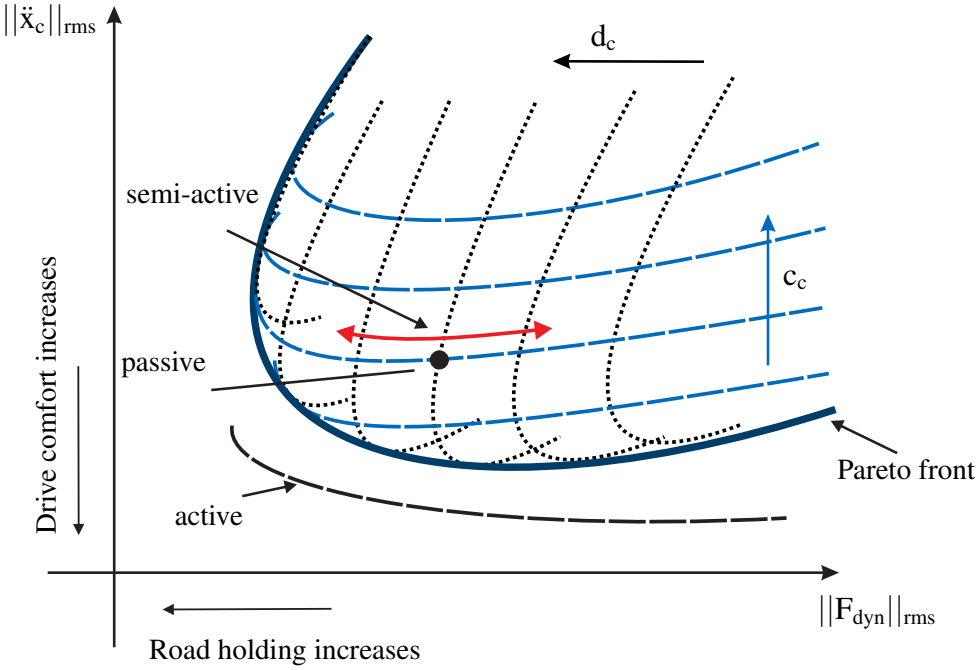

Figure 1.1: Qualitative conflict diagram for suspension systems

One criterion for evaluating the ride comfort is the root mean square (rms)[1] of the vertical acceleration of the passengers' cabin $\|\ddot{x}_c\|_{rms}$, which should be kept as low as possible to isolate the vehicle occupant from the road unevenness. To evaluate the driving safety, the effective value of the dynamic wheel load $\|F_{dyn}\|_{rms}$ is used, which indicates an improved road contact for low values. The latter requirement can also be formulated in terms of bounded rms-value of the dynamical wheel load, [76, 107].

Figure 1.1 illustrates the impact of the variations of the spring constant and damping coeffi-

[1] It represents a statistical measure of the energy of the quantity q: $\|q(t)\|_{rms} = \sqrt{\frac{1}{T}\int_0^T q(t)^2 dt}$.

cient of the two above-mentioned evaluation quantities. The conventional suspension (passive configuration) is determined in the basic design by choosing a combination of the spring-damper characteristic. Once it is designed, it cannot be changed and cannot be adapted to different road profiles. Aiming to mitigate this restriction, mechatronic suspension systems have been developed and from the second half of 1980s introduced into application, [3, 78, 138]. Besides full-active concepts [4, 27, 109], studies on slow-active systems [71, 72, 125, 139, 157] can be found in literature. Mainly because of their high energy consumption, full-active systems have not been further pursued by vehicle manufacture concerns, while slow-active and semi-active configurations can be found in series production. The first ones still allow to introduce energy into the system, however with limited energy requirement, while the second ones are dissipating devices. Due to their minimal energy requirements, they are widespread in the market, [34, 80, 141]. For these devices, the input power is needed only for adjusting the damper's valves, [138].

The passive suspension system configuration is determined by a standard choice of stiffness and damping. Referring to the tradeoff diagram, it is noted that reducing the spring constant mainly leads to an improvement in both objectives, while the damping can be adjusted by a suitable compromise between the two evaluation parameters. In any case, it is clear that comfort and safety are in conflict with one another and they cannot be influenced independently. In addition the mechanical limitation of the suspension deflection restricts the scope, where the stiffness and damping can be varied.

Figure 1.2 underlines the well known suspension tradeoff in case of semi-active suspension system (damping-isolation conflict), in which only the damping constant can be varied, [25, 121]. It depicts the effect of different damping configurations in the frequency response of sprung mass acceleration $G_{\ddot{x}_c,z}$ and of the dynamical wheel load $G_{c_w(x_w-z),z}$, while exciting it with a white noise signal z. Their phase characteristics are also reported ($\angle G_{\ddot{x}_c,z}$ and $\angle G_{c_w(x_w-z),z}$).

While in passive configurations the damping constant does not change, in semi-active controlled suspensions it varies in order to track a desired damper force, calculated by the suspension controller law. Due to the simple controller structure, industrial applications are still mainly based on skyhook laws, [84]. Even if it has been shown, that model-based approaches offer an higher potential to mitigate the tradeoff (see e.g. [57, 63]), there are marginal realizations of such strategies in a vehicle yet. In a very recent work, a study and a design of a linear

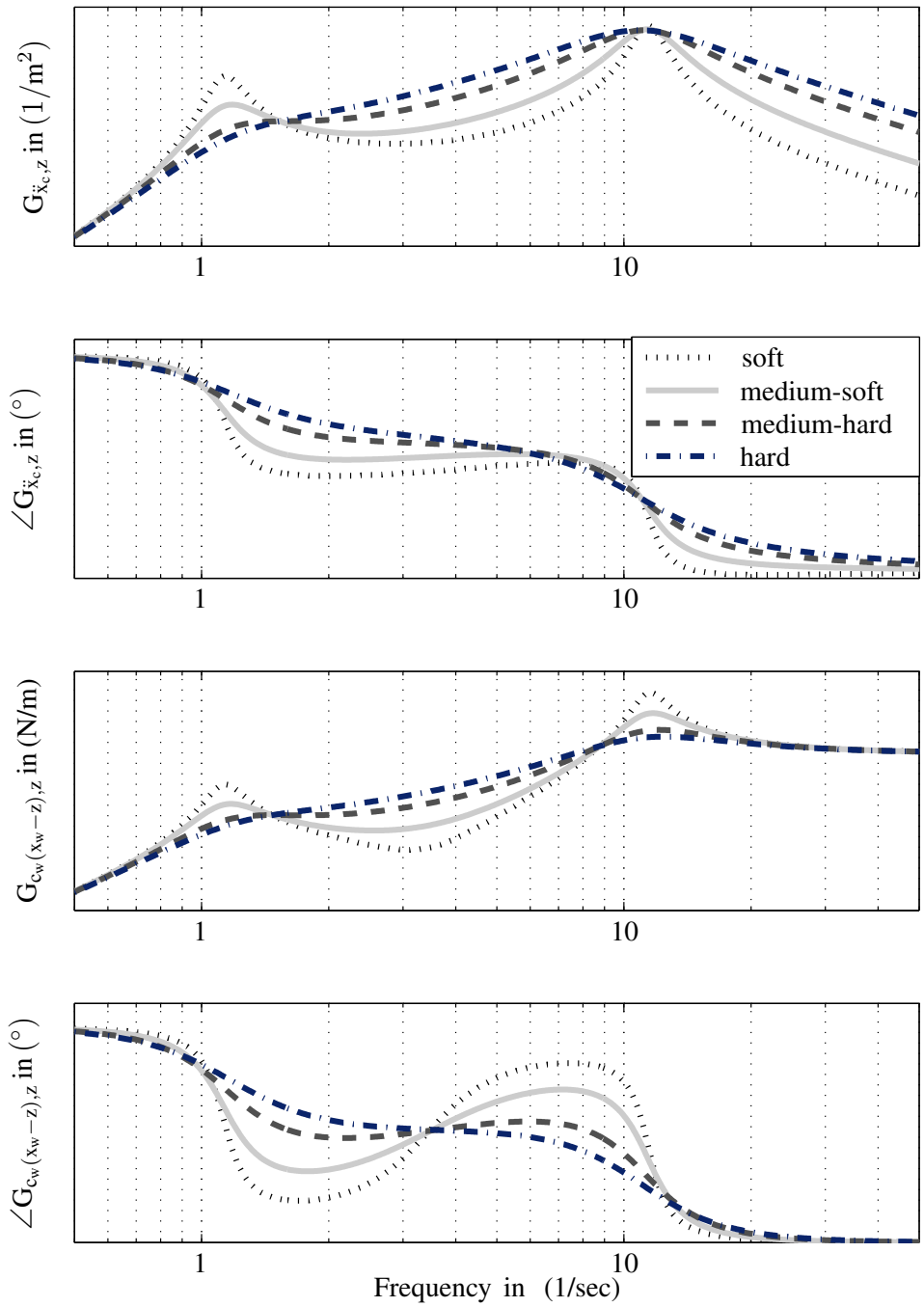

Figure 1.2: Bode diagram: amplitude and phase for different damping configurations

quadratic controller is presented, [161].

This Thesis focuses on semi-active damper modeling and its model-based control considering a realistic framework. The scope is to exploit the full potential of these modern devices by drawing a model-based control strategy which ensures compatibility with series requirements and transparency in the modeling and controller design. The low complexity and the intuitiveness of the proposed approaches are equivalent to the wide established controller structure. Also two suspension controller approaches, based on the principle of optimality, are addressed in this Thesis, which are not yet suitable for industrial application due to the high computational time.

1.1 Aim of the Thesis

Towards maximizing the performance of semi-active vehicle suspension systems, while considering a realistic framework, this Thesis mainly focuses on three aspects: semi-active damper modeling, damper control and modern optimal semi-active suspension control.

In the first part a detailed semi-active damper model is derived, which considers physical aspects of the damping dynamics, including the fluid, geometric characteristics and the valves' dynamics. Due to its complexity, such a model is not suitable for real time application. Therefore a functional modeling is proposed, in order to reproduce the main damper effects, which are not considered by standard models.

In the second part, the control of the semi-active device is addressed. With the aim of maximizing the performance of a semi-active vehicle suspension system while considering different real road profiles, a dynamic force tracking and control strategies are designed. Therefore, the functional dynamic damper model is implemented in a feedforward structure, which is extended by a feedback component. As a result, it is shown that a two degrees of freedom strategy guarantees a better force tracking by considering the nonlinear dynamic damper characteristics and allows to further increase the performance by making use of state of the art suspension controllers.

The commonly used suspension controllers in production vehicles do not take the semi-active device characteristics into account. Moreover, the state-dependent and the energy limitation are not included in the controller design process. Therefore, in the third part of this Thesis

suspension controllers, which take the nonlinear constraints of the controlled hardware into account are studied. The device's control strategy is applied and an additional benefit is obtained due to the suitable choice of the desired force within the real limits.

Many contributions on semi-active suspension control both from research field and automotive industry have been published over the last years. The majority of these works deal with suspension controller laws without considering semi-active devices' characteristics. In contrast, this Thesis considers both aspects of model-based control of the device (low-level controller) and the suspension control (high-level controller) for semi active suspension systems. Therefore, even if the focus lies on the particular type of semi-active device used for measurements, the transparency of the low-level strategy and the feasibility by applying other devices are preserved. In fact, the proposed functional damper model can be easily adapted to different devices using only measurements, which are already made in the automotive industry. Furthermore, the damper control design is firstly developed independently from the adopted suspension control law and the procedures for obtaining the optimal suspension laws (high-level control) are described in general. Moreover, the new control strategies are compared with the passive configuration and to benchmark systems to appreciate the benefits of the proposed solutions.

In order to support the practical aspect of this Thesis, a realistic framework (quarter-vehicle suspension test rig) for the controller design and the performance evaluation has been designed. It is equipped with a sensor architecture similar to the one realized in production vehicles. In addition, measurements of real road profiles are applied as road input signals both for the simulations and for the experiments.

The contributions of the Thesis can be summarized as follows:

- **New physical semi-active damper model for suspension control:** A detailed physical model of a dual tube semi-active hydraulic damper is derived. The passive representation, known form literature, is extended by means of switching elements. Particular attention is given to the external valves, which allow to adjust the damping force, depending on the valves' settings. Both the mechanical and the electrical aspects are analyzed.

- **New functional simplified semi-active damper model suitable for real time applica-**

tion: Based on the main effects reproduced by the precise damper model, a functional hydro-mechanical model is derived. It allows to emulate the nonlinear current depending damper slope and the hysteresis effects. The latter depend on the oil characteristics, the chambers' geometry and the valves' assemblies. Moreover, the functional model reproduces the linear damping by strokes with high velocities. The reduced number of parameters are estimated by means of ISO-standard damper identification procedures, which relate velocities, currents and forces.

- **A new dynamic feedforward control approach for semi-active devices:** To fully take advantage of the potential of modern devices, an open loop solution is presented, which takes the nonlinear dynamic of semi-active devices into account by employing a hysteresis model. The new set of equations reproduces the damper behavior considerably better than static characteristics do. The latter resemble the state of the art for the calculation of the control input of a semi-active damper in order to track reference forces from higher level suspension controllers. The low complexity of the hysteresis model enables its real time capability and thus the applicability of the damper control approach.

- **A new closed loop actuator control strategy - A two degrees of freedom structure:** To overcome significant drawbacks of open loop control strategies, the proposed extended control structure combines a dynamical feedforward approach with a nonlinear feedback component to control the damper valves' currents of a semi-active suspension system. By considering hysteresis effects, the relation between valve current, velocity and force can be represented significantly more accurate when comparing it with conventional approaches. The additional force feedback path is able to enhance force tracking even further. The performance potential of the force tracking controller shows its benefit both in simulation and in real application on a quarter-car test rig, independently from the applied suspension controller laws.

- **Optimal suspension controller for semi-active devices:** To enhance the suspension performance by modern control methods, two optimal control methods for a nonlinear semi-active suspension system subjected to state and input saturation are presented and compared with benchmark control laws. All nonlinearities of the suspension strut are considered in the modeling. The first approach incorporates inequality constraints by

applying the nonlinear programming method, while the second construes the task as an optimal switching problem between predefined nonlinear subsystems. This enables a recursive problem formulation and thus the usage of the Bellman's recurrence equation of optimality. These approaches lead to an optimal state-depending feedforward control and to a switching law, respectively, which are integrated in the feedback loop. The performance benefit of the proposed suspension controllers is confirmed by simulation and experimental application on a quarter-car test rig.

1.2 Structure of the Thesis

A detailed nonlinear model of the suspension system and the kinematic characteristics of the double wishbone are introduced in Chapter 2. Based on the simple quarter-car model (or quarter-vehicle model) of the suspension system, performance criteria for ride comfort and safety as well as the constraint for the suspension deflection are reported. Moreover, an overview on the state of the art regarding semi-active devices and their control techniques are presented.

In oder to exploit the functional principle of the semi-active device, its behavior is analyzed in detail and an accurate physical damper model is derived in Chapter 3. Based on the passive behavior, particular attention is given to the valves' dynamics and the build-up force in the semi-active configuration. Two models for the adjustable valves are derived and compared to real measurements. The complete model allows understanding and analyzing the damper physics, in oder to build a functional model, which is introduced in the next Chapter.

The realization of the functional damper model, suitable for control purposes, is demonstrated in Chapter 4. Based on previous analysis and observations, the phenomena affecting the damping force are singularly analyzed and their impact, considering computational time, model precision and modeling costs is reported. Only the significant effects are held and considered in the further steps. Each physical phenomenon is then emulated by mechanical components, i.e. spring, damper and lag element.

In Chapter 5 the functional damper model is integrated into a dynamical feedforward control structure, which increases the suspension controller performance by additionally considering the dynamic effects of the modern semi-active damper in the controller design. The potential

of the new open loop solution for a semi-active suspension system is analyzed. The structure dynamically adjusts the driving currents, so that the hysteresis and the other nonlinearities are incorporated into the control current signals.

In order to improve the force tracking, the dynamical open loop structure is extended by a feedback component, which takes into account the non-modeled effects, load changes or changing in operational characteristics. The controller structure acts only on minor errors between desired and operating forces, which are not reproduced by the fixed feedforward path. The complete structure is presented and analyzed by means of simulations and measurements in Chapter 6.

The desired force adopted to investigate the new two-degrees-of-freedom structure for semi-active suspension systems in the previous Chapters, is generated by generally valid control laws. That means that they do not consider the passivity constraints, which a semi-active damper is subjected to, thus the desired force could lie outside the velocity-dependent working range of the semi-active device. To this aim, two suspension control strategies, which take into account the nonlinear suspension strut kinematic, suspension nonlinearities and hysteresis effect of the controlling device, are proposed in Chapter 7. Moreover the proposed device control strategies of Chapter 5 and Chapter 6 are applied and the performance of the optimal controllers is further increased.

A summary of the results and an outline of possible future work conclude the Thesis in Chapter 8.

Furthermore, in order to provide a realistic framework for the design and validation of the models and control methods presented in this Thesis, Appendix A describes an experimental setup that has been designed to study the potential of a modern suspension configuration. The Chapter also reports the main nonlinearities of the considered suspension elements.

Chapter 2

SEMI-ACTIVE SUSPENSION SYSTEMS

In this Chapter the framework of this Thesis is introduced. Firstly, in Section 2.1 the semi-active system is sorted between the commonly-used model for analyzing vertical dynamics behavior in vehicle. Hence, in order to present the vehicle model employed in this Thesis, the nonlinear elements, which play a relevant role in the vertical motion, are introduced and the nonlinear model is derived.

Since semi-active suspension struts are already available in production vehicles, Section 2.2 gives a survey on the state of the art of damper hardware. In addition, an overview of already known semi-active suspension control laws is presented in the same Section.

Based on this overview, benchmark controllers, used to evaluate performances in this work, are discussed in Section 2.3. Section 2.4 reports the system requirements and the adopted gains, which quantify the performance of the proposed control laws and of the identification procedures. In order to quantify the identification and controller benefit, some performance indexes are defined in Section 2.5. In Section 2.6, both the damper excitation signal and the test rig road signal are reported. In particular, two type of road excitation signals are introduced, which are utilized both in simulation and on the test rig to excite the system.

2.1 Quarter-car models

The vertical motion of the primarily degree of freedom of a vehicle system can be described by different models. Beside full-car and half-car models, which take more degrees of freedom into account, the simplified and well-known quarter-car model describes the heave movements of only one wheel and a quarter of the chassis mass, [26, 104]. Since it assumes to decouple the four wheels, it can be applied for simulating the one-dimensional vehicle suspension performance in the frequency range of interest, i.e. 0-25Hz, [138]. In fact, it outlines the main

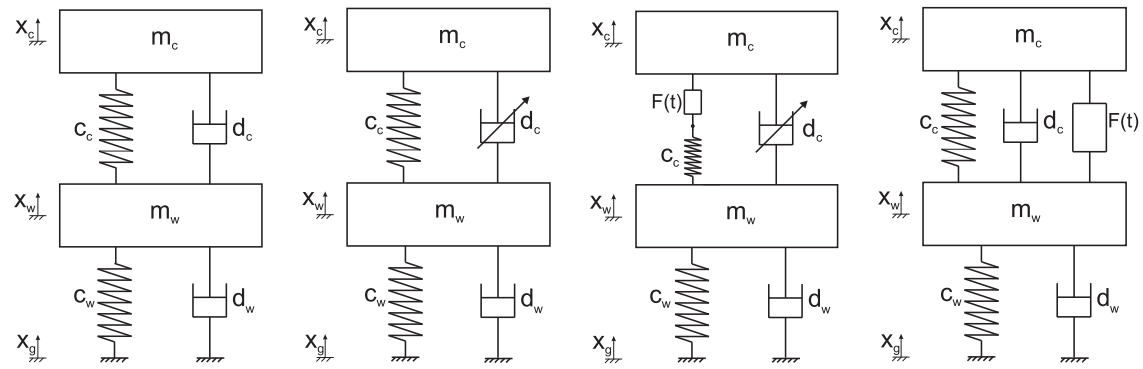

(a) passive (b) semi-active (c) slow-active/hybrid (d) full-active

Figure 2.1: Different quarter-car model configurations

characteristics of the vertical suspension dynamics. Moreover, due to its simplicity, is widely used in automotive engineering for controller design purposes, [76, 104].

A quarter-vehicle model consists of the sprung mass m_c, the unsprung mass m_w and the suspension system, which connects the two masses. While the first one includes a quarter of the total mass of the chassis, considering also passengers and loading, the second one includes the tire, the wheel, the brake and parts of the mass of suspension system. It is noted, that the tire is modeled by a parallel configuration of spring and damper. The suspension system can be categorized, as shown in Figure 2.1, into passive, semi-active, slow- and full-active suspension system according to the external power input and/or the control bandwidth.

Briefly, a passive system is a conventional suspension system, which consists of a non-controlled spring and damper. The semi-active suspension has the same elements but the damper has adjustable damping rate. A slow-active suspension consists of an actuator applying a force F(t) to the system, by working in series to the primary spring, while the damper is a passive device. If the damper is a semi-active one, this configuration is known as hybrid system, [97]. Full-active suspensions consist of passive components which are augmented by actuators (electric or hydraulic) that supply additional force F(t). More information about semi-active suspension systems can be found in Section 2.2.

Since all real suspension struts contain nonlinear elements, the linear quarter-car models drawn in Figure 2.1, have to be extended by these characteristics, in order to reproduce the behavior of the real system with sufficient accuracy.

The main nonlinear components involved in the dynamics are addressed in the following. Based on works describing a similar system [93, 96], the real test rig, including kinematic characteristics and sensors are reported in Appendix A. Through surface irregularities the wheel is excited and the vibrations are transmitted to the chassis mass by the interconnected suspension strut. On the one hand the nonlinear behavior is strongly dependent on the suspension double wishbone strut kinematics. In contrast to the representation in Figure 2.1, the assembly of the suspension unit is inclined. Due to the change of the inclination during suspension deflection $x_{cw} = x_c - x_w$ the transmission factor

$$i_f = \frac{(\dot{x}_c^{FE} - \dot{x}_w^{FE})}{\dot{x}_c - \dot{x}_w} = i_0 - i_x x_{cw} \tag{2.1}$$

varies, [69]. The transmission ratio i_x is assumed to change linearly with the suspension stroke[1], see Appendix A for more details. Accordingly, the following relation for the suspension deflection

$$\begin{aligned} x_{cw}^{FE} &= i_0 x_{cw} - \frac{1}{2} i_x x_{cw}^2 \\ \dot{x}_{cw}^{FE} &= i_f \dot{x}_{cw} \end{aligned} \tag{2.2}$$

can be given, whereas for the force conversion the relation

$$F^{FE} = \frac{F}{i_f} \tag{2.3}$$

holds.

On the other hand, the nonlinearity results from the character of the steel spring and the damper characteristics. Considering the damper adopted in this Thesis (see Figure 2.2), the first one consists of linear primary spring

$$F_{ps}^{FE} = -c_{ps} x_{cw}^{FE}, \tag{2.4}$$

which can be modified applying (2.2) and (2.3) in

$$F_{ps}^{FE} = -c_{ps} x_{cw} i_f^2 = -c_{ps} \left(\frac{i_x^2}{2} x_{cw}^3 - \frac{3}{2} i_x i_0 x_{cw}^2 + i_0^2 x_{cw} \right), \tag{2.5}$$

[1]The superscript FE refers the corresponding variable to the suspension center plane; all variable without it, are referred to the wheel center plane.

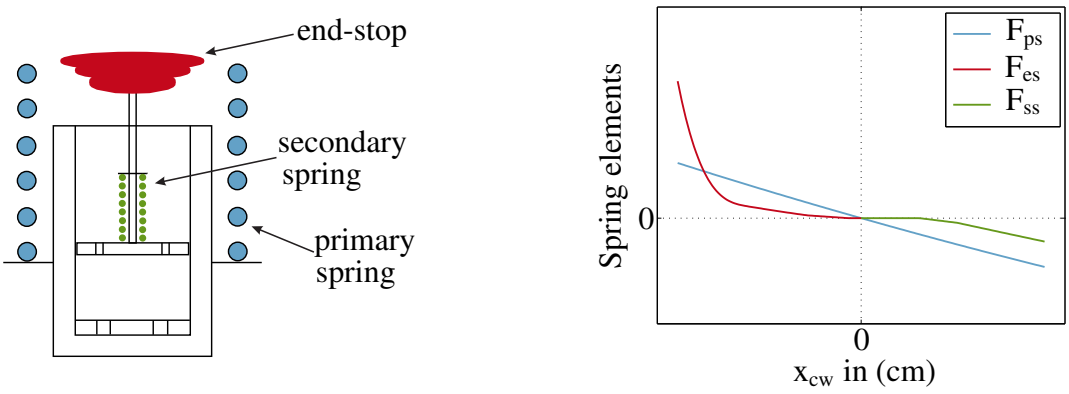

(a) Schematic representation of the spring elements (b) Measured characteristic of the spring elements

Figure 2.2: Spring force of the modeled elements

a piece-wise linear secondary spring and of an elastomer end-stop. It is noted, that the secondary spring, F_{ss}, acts only in rebound direction $(x_{cw} > 0)$ and the end-stop, F_{es}, only in compression direction $(x_{cw} < 0)$. Moreover, the internal spring of the damper exhibits, depending on the absolute value of the upward deflection, two different stiffnesses. In contrast, the end-stop has a linear effect at the beginning of the compression, which then fades to a cubic characteristic. The different force contributions can be clearly distinguished in Figure 2.2(b), in which, mainly in compression, the strong action of the end-stop can be seen.

Considering the spring pre-load and the weight force

$$F_g = \left(\frac{i_f}{i_0} - 1\right) m_c g x_{cw} = -\frac{i_x}{i_0} m_c g x_{cw}, \tag{2.6}$$

where g represents the gravity constant, the total spring force is obtained as sum of primary F_{ps}, secondary F_{ss}, end-stops F_{es} and gravity contributions F_g:

$$F_f = F_{ps} + F_{ss} + F_{es} + F_g. \tag{2.7}$$

The characteristics of the considered semi-active damper can be adjusted between the minimal and the maximal current values $[\mathbf{i}_{min}; \mathbf{i}_{max}]$ both in the compression and in the rebound direction. Usually the damping behavior shows a degressive character and an evident asymmetrical attitude[2], [80].

[2]The compression damping value is 3 to 5 times smaller than the relative rebound value

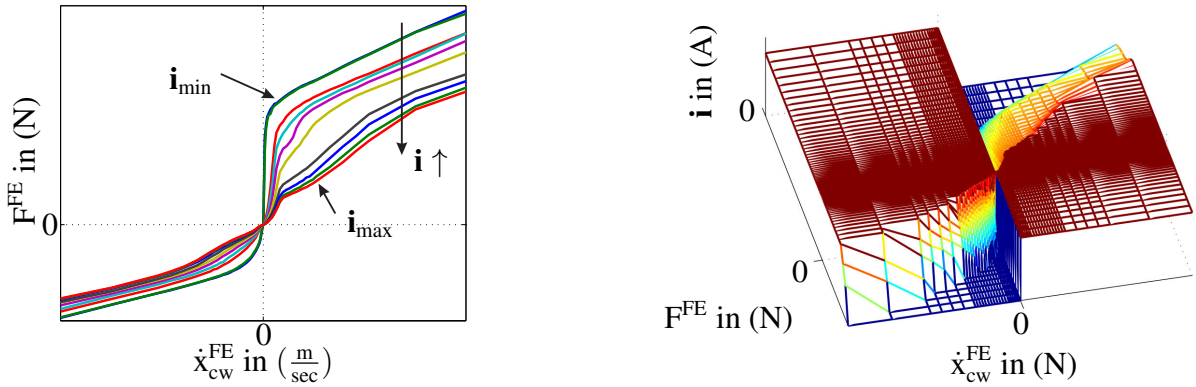

(a) Nonlinear damper characteristics

(b) Inverse damper characteristics field

Figure 2.3: Damper force as function of relative suspension deflection velocity and of applied currents. Image is reproduced with kind permission of BMW AG.

In Chapter 3 and Chapter 4 the damper behavior is extensively discussed. In Figure 2.3(a) the damper's static characteristics are shown, which are obtained by keeping constant current settings and exciting the damper by sine waves with different stroke velocities, according to the procedure described in [128]. During this process the actual suspension deflection velocity $\dot{x}_{cw}^{FE}$ is mapped with the applied current setting to the damper force, whereas the dynamical effects are not considered in this representation. In Figure 2.3(b) the inverse characteristics field are reported.

According to Figure 2.1, it is noted that the viscous-elastic effect of the wheel is modeled by a linear spring c_w and a linear damper element d_w. The increasing of the wheel stiffness due to the vehicle velocity is not included because the rolling motion is neglected by considering only the vertical dynamics.

Considering the described force relations the nonlinear differential equations of the system can be formulated as follows

$$\begin{aligned} m_c\ddot{x}_c &= F_{ps}(x_c - x_w) + F_{ss}(x_c - x_w) + F_{es}(x_c - x_w) + F_g(x_c - x_w) + \\ &\quad + F(\dot{x}_c - \dot{x}_w, \mathbf{i}) + F_{R,cw}(\dot{x}_c - \dot{x}_w) \\ m_w\ddot{x}_w &= -\left[F_{ps}(x_c - x_w) + F_{ss}(x_c - x_w) + F_{es}(x_c - x_w) + F_g(x_c - x_w) + \right. \\ &\quad \left. + F(\dot{x}_c - \dot{x}_w, \mathbf{i}) + F_{R,cw}(\dot{x}_c - \dot{x}_w)\right] - c_w(x_w - x_g) - d_w(\dot{x}_w - \dot{x}_g). \end{aligned} \tag{2.8}$$

Defining

$$\mathbf{x} = \begin{bmatrix} x_1 \\ x_2 \\ x_3 \\ x_4 \end{bmatrix} = \begin{bmatrix} x_c - x_w \\ \dot{x}_c \\ x_w - x_g \\ \dot{x}_w \end{bmatrix} \tag{2.9}$$

as the state-vector and

$$\mathbf{y} = \begin{bmatrix} \ddot{x}_c \\ F_{dyn} \\ x_c - x_w \end{bmatrix} \tag{2.10}$$

as the output vector, where $F_{dyn} = -c_w(x_w - x_g) - d_w(\dot{x}_w - \dot{x}_g)$ denotes the dynamic wheel load. By condensing all nonlinearities in the input signal

$$\tilde{u}\,(\mathbf{x}, \mathbf{i}) = F_{ps}(x_1) + F_{ss}(x_1) + F_{es}(x_1) + F_g(x_1) + F(x_1 - x_2, \mathbf{i}) + F_{R,cw}(x_2 - x_4), \tag{2.11}$$

the system in (2.8) can be reformulated and the input-output linearized system is given by

$$\dot{\mathbf{x}} = \underbrace{\begin{bmatrix} 0 & 1 & 0 & -1 \\ 0 & 0 & 0 & 0 \\ 0 & 0 & 0 & 1 \\ 0 & 0 & -\frac{c_w}{m_w} & -\frac{d_w}{m_w} \end{bmatrix}}_{\mathbf{A}_L} \cdot \mathbf{x} + \underbrace{\begin{bmatrix} 0 \\ \frac{1}{m_c} \\ 0 \\ -\frac{1}{m_w} \end{bmatrix}}_{b_L} \cdot \tilde{u}\,(\mathbf{x}, \mathbf{i}) + \underbrace{\begin{bmatrix} 0 \\ 0 \\ -1 \\ \frac{d_w}{m_w} \end{bmatrix}}_{e_L} \cdot \dot{x}_g \tag{2.12}$$

$$\mathbf{y} = \underbrace{\begin{bmatrix} 0 & 0 & 0 & 0 \\ 0 & 0 & -c_w & -d_w \\ 1 & 0 & 0 & 0 \end{bmatrix}}_{\mathbf{C}_L} \cdot \mathbf{x} + \underbrace{\begin{bmatrix} \frac{1}{m_c} \\ 0 \\ 0 \end{bmatrix}}_{d_L} \cdot \tilde{u}\,(\mathbf{x}, \mathbf{i}) + \underbrace{\begin{bmatrix} 0 \\ d_w \\ 0 \end{bmatrix}}_{f_L} \cdot \dot{x}_g. \tag{2.13}$$

For analysis purposes the nonlinear system is linearized, as shown in the Appendix A.4, by meaning of the Taylor series. According to the analysis in [86], the main characteristics and limitations of the linearized system can still be found in the nonlinear one.

The well-known equations of motion are derived for the passive configuration. The semi-active configuration is obtained by considering a varying damping constant, i.e. $d_c = d_c(t)$.

The equations of motion are

$$\begin{aligned} m_c\ddot{x}_c &= -c_c(x_c - x_w) - d_c(t)(\dot{x}_c - \dot{x}_w) \\ m_w\ddot{x}_w &= c_c(x_c - x_w) + d_c(t)(\dot{x}_c - \dot{x}_w) - c_w(x_w - x_g). \end{aligned} \tag{2.14}$$

These equations can be reformulated for the passive configuration in matrix form as follows

$$\dot{\mathbf{x}} = \mathbf{A}\mathbf{x} + \mathrm{e}v \tag{2.15}$$

$$\mathbf{y} = \mathbf{C}\mathbf{x} + \mathrm{f}v, \tag{2.16}$$

where each element is given as

$$\begin{bmatrix} \dot{x}_1 \\ \dot{x}_2 \\ \dot{x}_3 \\ \dot{x}_4 \end{bmatrix} = \underbrace{\begin{bmatrix} 0 & 1 & 0 & -1 \\ -\frac{c_c}{m_c} & -\frac{d_c}{m_c} & 0 & \frac{d_c}{m_c} \\ 0 & 0 & 0 & 1 \\ \frac{c_c}{m_w} & \frac{d_w}{m_w} & -\frac{c_w}{m_w} & -\frac{d_c+d_w}{m_w} \end{bmatrix}}_{\mathbf{A}} \cdot \begin{bmatrix} x_1 \\ x_2 \\ x_3 \\ x_4 \end{bmatrix} + \underbrace{\begin{bmatrix} 0 \\ 0 \\ -1 \\ \frac{d_w}{m_w} \end{bmatrix}}_{\mathrm{e}} \cdot \underbrace{\dot{x}_g}_{v} \tag{2.17}$$

$$\begin{bmatrix} \ddot{x}_c \\ F_{dyn} \\ x_c - x_w \end{bmatrix} = \underbrace{\begin{bmatrix} -\frac{c_c}{m_c} & -\frac{d_c}{m_c} & 0 & \frac{d_c}{m_c} \\ 0 & 0 & -c_w & -d_w \\ 1 & 0 & 0 & 0 \end{bmatrix}}_{\mathbf{C}} \cdot \begin{bmatrix} x_1 \\ x_2 \\ x_3 \\ x_4 \end{bmatrix} + \underbrace{\begin{bmatrix} 0 \\ d_w \\ 0 \end{bmatrix}}_{\mathrm{f}} \cdot \dot{x}_g. \tag{2.18}$$

2.2 State of the art

In the following a survey on the state of the art of damper hardware and their control laws is given.

2.2.1 Semi-active dampers

During the years, a large number of damper hardwares have been developed and installed on production vehicles. They are based both on mechanical friction and fluid dissipation mechanisms. As already briefly introduced for the modeling (see Section 2.1), automotive

suspension systems can be classified in three major categories on the basis of their hardware: passive, adaptive or semi-active and (slow)-active systems, [69].

A *passive* suspension configuration denotes a purely dissipative system, which absorbs the power of the moving masses. Thereby, since no energy is introduced into the system, the primary spring has its own characteristic and the damper ratio is fixed and cannot be changed at any time. An *adaptive or semi-active* damper system is dissipative as well. Nevertheless the damper characteristic is adjustable; it is controlled by an electronic power unit to absorb the energy of the system according to the control targets, [38]. According to [69] these systems differ due to their switching frequencies: semi-active devices demonstrate a higher switching frequency than adaptive ones. In any case, both configurations limit or delay body movements and variation of wheel load forces. However, a full elimination is not possible. This target is provided by *active* systems. An external power source supplies energy into the system and can, therefore, actively reach predefined control aims.

Passive devices

The passive device represents the oldest damper configuration which is developed to dissipate systems' energy. The earliest devices are based on the principal of abrasion and consisted of springs or parabolic springs, which mechanically convert the motion energy into thermal energy, [34].

Successively, telescopic damper designs were developed as passive systems in form of mono- and twin-tube dampers. These devices operate hydraulically and mechanically. The damping forces of these systems are related to the pressure differences above the internal valves. Mineral oil is usually used as transmitting medium. The interrelationship between pressure difference and damping force can be varied by the use of different valves and their combination, [43].

Due to the fact that the damping factor of telescopic shock absorbers mostly depends on the stroke, various stroke-dependent systems have been developed. This kind of damping is mostly realized by means of control grooves which act as hydraulic bypasses both on the piston rod and along the pressure tube. Generally, the position of the groove influences the damping ratio. Fichtel and Sachs implemented an hardware especially to effect forces in re-

bound direction by adding a notch at the bottom of the piston rod and using a guide washer additionally. A further implementation based on the mentioned principle, where the forces are affected both in traction and in compression directions, was made by Bilstein. Also Boge applied a similar principle by means of two washers with different grooves, however only affecting the traction direction forces. Bores drilled in the inner cylinder can act as an additional bypass, [128].

Referring to bypass grooves formed along the pressure tube, the oil is enabled only to flow trough the groove and not trough the piston valves. This solution reduces the hydraulic resistance of the piston varying the damping factor consequently. The designs mainly vary by means of the position, the length and the number of the grooves. More details can be found in [69].

In other application diverse notches are distributed over the circumference of the damper cylinder in order to improve the damping behavior. Such an example of a twin-tube shock absorber is produced by Fichtel and Sachs. In case of a mono-tube telescopic damper the same implementation of groove has an effect on both directions. A damping concept based on the bypass principal was designed by Subaru for mono-tube shock absorbers, [128]. It consists of a metering rod, which slides within the bored piston rod and allows to increase or reduce the damper force by covering or setting free the oil path.

An amplitude-selective damping system named Sensitive Damping Control (SDC) was developed in 2008 by ZF Sachs. In this design, two separately adjustable piston valves are operating, [49]. An additional valve is introduced in the valve rod assembly. It is mounted leeway to guarantee adjustability and works as an oil reservoir, which controls the volume and the flow speed of the fluid with a shifting piston. The interaction between fluid and mechanic parts allows to distinguish between minor and major suspension deflections and to consequently adjust the damping force characteristic, [131].

Adaptive and semi-active devices

Adaptive and semi-active dampers are designed to work with the same principle of the passive devices. However, they are extended by electrically adjustable valves which allows either to change the damping ratio by varying the internal pressure or to modify the fluid proprieties.

Therefore, the rebound and compression stages can be independently adjusted. Hereby, the switching frequency of an adaptive system is smaller than the switching frequency of a semi-active, [170, 171].

In the last decades both continuously and stepwise solutions are proposed, [70]. While the first allows to interpolate the force in the damper working range, the second one switches between predefined characteristic lines. A solution, which uses a servo motor to realize a stepwise variable damping force has been studied and developed by Delco Products, [70]. The motor is placed within the piston rod and rotates a control element with a defined shape of holes, allowing to change the oil path. The drilled circumference can be differently covered and the damping force is adapted. A similar design with four stages was implemented by Koni for the VW Golf GTI. Due to the invasive construction solution, the mechanical stability of the hardware cannot be guaranteed. In fact, the piston rod's profile is weakened by the hollow volume in which the servo motor is placed. Therefore, the proposal made by Bilstein is to place the motor at the top of the piston rod. For this configuration, eight different damping characteristics are optimized for the Porsche 959. The switch between the generated characteristics takes place manually by the driver, [128]. The solutions reported in this paragraph are classified as adaptive systems, since the switching time lies between $50\,\mathrm{msec}$ and $100\,\mathrm{msec}$, so that no proper influence on the vehicle motion is possible, [33]. However, Fichtel and Sachs succeeded in developing a three-stage device based on the same principle as discussed above, with a switching time of $30\,\mathrm{msec}$, [70].

Besides servo motors, magnetic valves are applied to provide variating damping force as well, [70]. The valve can be placed within the piston or at the main cylinder of the damper. They control the flow path into and out of the tube. The main advantages of utilizing valves compared to the mechanical solution is the less power requirements and the reduced switching time (about $20\,\mathrm{msec}$). In addition, the placement of the valve is widely flexible and no hollow piston rod is needed, so the mechanical stability is not compromised. This kind of technology was developed e.g. by Boge for the BMW M3, where two external valves generate three different damping characteristics [128]. Another electrical adjustable damping implementation made in cooperation with Boge and the VDO Adolf Schilling AG was first introduced in the European market 1987 with the name Electrical Damping Control (EDC). Here the magnetic valve is integrated at the bottom of the piston rod. This concept was first set into the BMW 6 series and was continuously developed further for the 5 and 7 series, [152, 171]. Also

ThyssenKrupp Bilstein developed electronically adjustable damping systems with magnetic valves, such as the Active Control Damping 2 (ACD II), a two stage damping system with an integrated valve or the Adaptive Damping System (ADS), a 4 stage implementation with two external switching valves, [158].

Aiming to increase the potential of semi-active devices, by increasing the range of application, continuously adaptable valves are developed. They work generally according to the same principle discussed before, [70]. The damping force is adjusted via proportional valves which continuously varies a bypass fluid path. In contrast to the previous solution, the generated damper force is not limited to the characteristic lines but includes all forces in the damper working range. Designs of a damper with proportional valves named Continuous Damping Control (CDC) were implemented by ZF Sachs. However, this system presents some disadvantages. In [69] it is reported that its dynamic behavior is strongly influenced by the construction properties of the hardware. In addition, also the kinetic characteristic of the suspension strut (joint, top mount connection, end-stops) have to be taken into consideration. The combination of fluid and suspension strut elasticity can result in delay by the damper response time. Moreover, from practical application, it is noted that the pressure gradient is limited and the maximum should not be exceeded, in order to prevent switching noise.

According to [35], two constructive configurations are established in literature: with integrated or with external valves. For the first one, the adjustable valve replaces the conventional piston valve, while for the external setting the valves act as bypass between chambers [24]. The solution proposed in 2001 for the BMW series 7, the so called Electric Damper Control system with Continuously working damping valves (EDCC) as well as in the case of its forerunner (EDC), is designed with the valve positioned at the end of the piston rod. For such solutions, the electrical feed line is placed within the hollow piston rod. In order to properly control the valves an electronic control unit (ECU) determines the control signal based on acceleration, steer angle, and wheel speed signal values [152, 171]. Generally, mechatronic systems in vehicle application use the information of different sensors mostly from CAN or Flexray, to calculate the control signals of the valve. The driving situation and the vehicle condition are captured and a central control unit optimizes the damping force for each vehicle corner, [83].

TKA-Bilstein developed two semi-active damper models in which either the adjustable valve is placed in the pressure tube (DampTronic I) or mounted outside the device (DampTronic II). The semi-active suspension system with continuously adjustable valves developed by Tenneco

is known as Continuously controlled Electronic Suspension (CES). Each device is individually controlled by the dedicated control unit, which uses the information of the complete vehicle.

As distinguished at the beginning of this Section, devices exist, which adapt the damping force by varying the fluid characteristic. They present an alternative to the hydraulic devices and utilize as operating medium magneto-rheological fluids (MRFs) or electro-viscous fluids (ERFs). The first one is composed of oil and iron particles, which can be activated by exposing them to a magnetic field. In that case the fluid aligns itself along the magnetic flux lines, while if inactivated behaves like ordinary oil. The force varying is obtained by influencing the viscosity of the MR fluid. The principle of magneto-rheological damping can be applied to mono- and to twin-tube telescopic dampers as well, [124]. This technology was used in 2006 in the Audi TT, [69]. ERF dampers operate similar to MRF dampers. The ERF devices are subjected to an externally applied electric field, which controls and regulates the viscosity of the fluid. Typical time constants of ERF are approx. a few milliseconds. The control voltage terminals are usually placed within the pressure tube, [112].

Active devices

In contrast to the systems described in previous Sections, active systems are able to introduce energy into the vibrating systems. The force direction and magnitude, generated between chassis and wheel masses, is independent of the suspension deflection direction as well as on its velocity, [70]. Depending on the acting bandwidth a classification between slow-active and full-active systems is usually made, [170]. While full-active systems work in a very large frequency range, slow-active systems can be applied only in low-frequency range, mainly including the natural frequency of the body. This range is chosen to limit the energy requirements. Generally, high frequency vibrations are damped by passive system components, [56].

A very well-known full-active system was developed by Bose, whereby the conventional spring/damper elements of the suspension are substituted by linear electromagnetic devices, which work both as motor and as generator. Due to a regenerative cycle the suspension system requires only small amount of power, [56, 69].

Mercedes Benz employs a slow-active suspension system called Active Body Control (ABC), which has a control bandwidth of 5Hz, [126]. The hydraulic cylinder is mounted in series

to the primary spring and can actively influence the body natural frequency, by damping the vertical, the roll and pitch motions, [156]. The wheel mass is damped by a passive damper. In [93] a new combination of slow-active and semi-active systems is presented, while in [154] energy analysis has been conducted.

Several theoretical works and patents considering the use of electromechanical actuators instead of conventional dampers were published during the last years. These concepts mostly include linear motors as actuator. However because of disadvantages such as high weight, costs and energy consumption none of them were utilized in series production, [100]. In a recent work an hybrid electromagnetic shock absorber for active suspension system is presented, [47].

More details regarding active and slow-active systems can be found e.g. in [93] and the references therein.

Functionality of semi-active damper devices

Since the core of this Thesis are semi-active suspension systems, more attention is given to these devices. A suspension system has to ensure ride safety, by guaranteeing a constant contact to the ground and to attenuate the vibration transmitted to the vehicle body, in order to ensure the best possible comfort. By adapting the damper's damping ratio, the two main tasks have to be fulfilled.

Safety is mostly associated with the effective value of the wheel load fluctuation with respect to the static wheel load. To increase the handling the dynamical wheel load has to be decreased. In fact, load fluctuations cause lateral and longitudinal forces which influence driving behavior, [126]. The level of comfort which is experienced by the passenger depends on both, the absolute value and the frequency of the vertical body acceleration. Utilizing semi-active dampers, body vibrations should be attenuated as fast as possible, [35].

Aiming to produce high damping force by still keeping a lightweight construction, devices with digressive characteristic curves are preferred, [69]. Therefore, the dampers are designed in order to provide force-velocity characteristics with decreasing slopes for all adjustable valves' settings, both in compression and in rebound stage, [69]. The working range has to be kept as wide as possible, in order to face also critical maneuvers. However, the character-

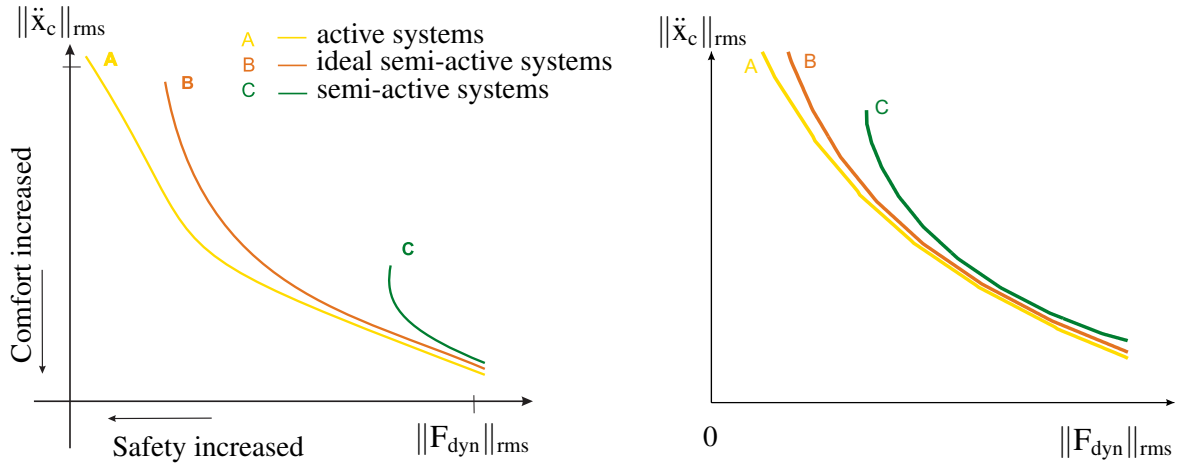

(a) Potential study considering a linear quarter-car model without mechanical limitations

(b) Limit curve obtained in the simulation by considering the nonlinear model and the suspension deflection limitation

Figure 2.4: Limit curves obtained by considering different actuator configurations, [82]

istics of hydraulic damping systems whether passive, adaptive or semi-active are challenging to be determined, due the nonlinear interaction between fluid and valves, [100]. In addition, as reported in [35], the ride can be strongly influenced if the devices are able to provide high damping also in case of slow deflection.

A semi-active system is capable of influencing both the first and the second natural frequency, but the effects of the body and of the wheel motion cannot be completely eliminated, [69]. This task can be reached by (slow-) active systems, which are able to strongly increase the ride performances, [70, 93, 126].

A comparison of the functionality is also apparent from the chart of conflict between comfort and safety (see Figure 2.4). By means of ideal semi-active systems, a semi-active configuration is considered, whereby the semi-active device has the potential to produce the force in complete 1^{st} and 3^{rd} quadrants, without the limitation presented in Figure 2.3(a). It is noted, that dealing with force-velocity limitations leads to a relevant loss of performance compared to the ideal semi-active case. A significant shift of the limit curve in the direction of more comfort and more safety is expected by applying active systems, [70]. In Figure 2.4(b) similar analysis has been conducted by considering the nonlinear quarter-car model and the suspension deflection limitations.

2.2.2 Semi-active control laws

Since this Thesis focuses on controlled semi-active suspension systems, a summary of control concepts found in literature for this kind of configuration is given. An overview can be found in [51, 76, 93, 160, 161].

Because of the intuitive approach and good performance properties of the *skyhook* control law for semi-active control systems, the contributions of Karnopp [84, 85, 87, 88] are widespread. The comfort-oriented control law pursues to reduce the absolute body acceleration, by generating a damper force proportional to the absolute body velocity. Dealing with a semi-active device the passivity condition, meaning that the damper generates forces only in the 1st and 3rd quadrant, and its working range influence the generated force. In particular, only those forces, which are within the adjustment range, can be realized through the semi-active damper. In more recent works, e.g. [80], the idea of Karnopp is extended by a passive contribution proportional to the relative damper velocity, see Section 2.3. Other further developments are analyzed in e.g. [68, 90, 149, 178]. An extension of the original skyhook idea is presented in a work of Hong [73], in which he proposes an adaptive skyhook control. This adaptive law is further described in this Thesis, since it is used as benchmark controller.

Similarly to hardware solutions, where both continuously adjustable and stepwise adjustable dampers have been developed, also in the control theory besides the mentioned continuous control laws, discontinuous variants are proposed (e.g. on-off strategies). Controller performance, in which the force can only vary between the maximal and the minimal characteristic are analyzed in [9, 137, 143]. Some application results can be found in [102, 167]. The idea to reduce accelerations on the passengers' cabin by applying an on-off strategy is also discussed in [135]. Nevertheless, the author based the control concept on acceleration signals instead of velocity ones. This approach is known as *acceleration driven damper* (ADD). The method is further enhanced in [42, 136, 150] to increase its potential.

Equivalently to skyhook, a control law named *ground hook*, which aims to reduce the dynamic wheel load, was presented. It has been studied in two variants: in the one hand, the wheel is connected via a virtual damper to the road [164, 165], in the second hand, the wheel can be damped virtually against an inertial reference system, e.g. [8]. In addition, comfort-oriented and safety-oriented laws are combined and examined in [77, 110, 159, 178].

Optimal control laws with regard to cost functions are also addressed in literature, [76]. In semi-active suspension systems, the linear control theory cannot be directly applied, because of the state-dependent control variable restriction on the input. Butsuen focuses this issue and reformulates the problem in a bilinear form, [29]. Gordon also addresses the question of the optimal semi-active control, by considering a detailed nonlinear structure, [63]. In [11], the nonlinear dynamics of the actuator is considered, while the suspension elements are still assumed to be linear. Also for a novel hardware paring of slow actuator and semi-active damper (hybrid suspension) exists an optimal active component control law, which considers several nonlinearities, [153].

Clipped control approaches do not consider the damper limitation in controller design, so that the law is tuned for an active system, while the generated force can only be applied under the working condition of the damper. In this framework control methods for active system can be utilized. In [29], it is shown, that for a linear semi-active system the obtained optimal control law is the same law, which can be calculated by an LQR, designed for a linear full-active systems.

Aiming to use methods of active systems without neglecting the passivity restriction of the device, a solution is proposed by Johnson, [81]. He suggests to perform controller design for the full-active system in the form of linear matrix inequalities (LMI) and add an additional dissipative constraint to the solution.

In [17] it is analyzed, how the targets in the cost function can be influenced via a linear parameter varying (LPV) approach for an $\mathcal{H}_\infty$-controller. A similar approach is also followed in [59, 134], while an alternative LPV approach for semi-active devices is presented in [123].

Another approach for semi-active suspension control is provided by the *model predictive* control (MPC), [30]. By considering these methods, state and output constraints as well as nonlinearities or variable cost functions can be easily considered. Such investigation was carried out by Giorgetti in [57], where it is shown, that clipped optimal control exactly corresponds to model predictive control with horizon of prediction 1 sampling step. A similar issue is addressed in [162] where it is experimentally shown that clipped LQR achieves the same performance as MPC controller. Since the implementation of model predictive control strategies is difficult especially due to the high computational complexity, [99], Canale suggested in [32] an approach for increasing the computational velocity and guaranteeing the applicability.

Taking the damper dynamics into account by means of predictive methods [46, 58], it reduces the computation time. Further works in the field of semi-active, model predictive control are described e.g. in [31, 114, 138].

In [41, 179] a nonlinear method, sliding mode approach, is applied to semi-active controller purposes. In addition, fuzzy techniques, e.g. [79] or neural networks approaches, e.g. [108, 183] have been already studied for semi-active devices.

An overview of the already mentioned and other methods for controlling semi-active suspensions can be found in [67, 138, 164] and the references therein. In Table 2.1 some control methods applied in production vehicles are reported.

Table 2.1: Overview of the control methods applied in series, [161]

Vehicle	**Literature**	**Control strategy**
Audi A4	[140]	Based on Skyhook
Audi Q3	[5],[61]	Skyhook with extension for wheel vibration
Audi Q5	[141]	Based on Skyhook
BMW 7	[80]	Skyhook with ground damping
BMW X5	[111]	Based on chassis and wheel velocities
Mercedes C	[105]	Skyhook with ground damping
Mercedes E	[55]	Skyhook with ground damping
Opel Astra	[20]	Based on chassis and wheel velocities
Porsche Panamera	[6]	Based on Skyhook
Volvo S60	[5],[115]	Skyhook with extension for wheel vibration
Volvo S80	[5],[115]	Skyhook with extension for wheel vibration
Volvo V70	[5],[115]	Skyhook with extension for wheel vibration
Volvo XC60	[5],[115]	Skyhook with extension for wheel vibration
VW Touareg	[10]	Based on Skyhook

In production vehicles semi-active dampers, independently of the particular control law, are primarily controlled in open loop, generally using static force-velocity relation to determine the damper control inputs $\mathbf{i}$ to track reference forces F^* (control application in Figure 2.5). The obtained currents are applied to the damper characteristics to simulate the velocity-dependent damper force generated by the control inputs.

This model and its control structure ignores the dynamical and hysteresis effects which can influence the behavior of the device. It is underlined that this model does not reproduce the

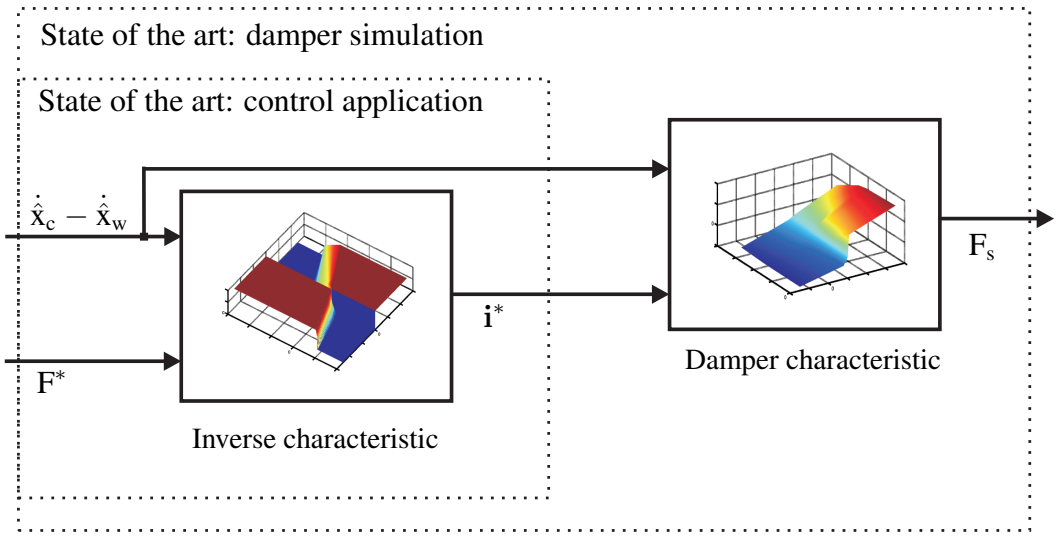

Figure 2.5: Damper model and control structure: state of the art

damper force precisely enough. While for high velocity the real measured force corresponds to the one modeled by the static characteristic lines, in lower velocity range significant discrepancies can be noticed, [117, 119].

The above-mentioned control techniques and feedback laws refer to suspension controllers (high-level controllers). They utilize information (states or outputs) of the complete system to calculate the desired force. However, besides the amount of publications about suspension controllers, there are only few contributions which deal with the force tracking of semi-active devices (low-level controller), e.g. [145, 146]. In fact, most studies on semi-active devices assume that the hardware can track the desired force calculated by the suspension controller perfectly. Due to nonlinearities, time delays, valve dynamics, friction and oil characteristics, this assumption is not accurate. Due to the fact that the only measured signals are the valves' currents, a model- or a signal-based approach are required, in order to obtain the hardware state. An Hardware-in-the-Loop (HiL) approach is presented in [22], while the contribution in [142] presents a force control strategy, which utilizes a hysteresis compensator for MR damper.

2.3 Benchmark systems

To investigate the performance gain of the new strategies presented in Chapter 5, Chapter 6 and Chapter 7, a comparison with well-established control laws is given. The parametrization of the benchmark controllers is adjusted to the considered suspension test rig by means of numerical optimization, [82].

The benchmark systems used in this Thesis are:

- *Passive suspension system*: To evaluate the performance of modern mechatronic systems, a comparison with the passive configuration is a common procedure. Therefore, also in this Thesis, the passive reference, meaning a fixed damping ratio, is considered as a benchmark. In case of the adopted semi-active device, the passive configuration is obtained by holding the valves' currents $\mathbf{i}$ at the 60% of the maximal current value. This configuration represents a comfortable setting for an upper class vehicle, [80, 93].

- *Skyhook control*: Also the skyhook concept is often considered as a benchmark system due to its popularity. According to [22, 93], in this Thesis a skyhook law extended by a passive damping $d_{c,p}$ is applied. The resulting damper force F_{sky} acting on the chassis mass results from

$$u \equiv F_{sky} = -d_{sky}\dot{x}_c - d_{c,p}(\dot{x}_c - \dot{x}_w). \tag{2.19}$$

  Dealing with a semi-active system the force formulated in (2.19) can only be generated by the device if the passivity condition $\dot{x}_c(\dot{x}_c - \dot{x}_w) \geq 0$ is fulfilled and the desired force lies within the damper working range. Otherwise it is clipped by the upper or lower limit.

- *Adaptive control law for a modified skyhook*, formerly presented in [73], is also considered. The adaptation law uses an online Fourier transformation of the road signal estimation $\hat{x}_g$ to determine the characteristic of the road profile at the body and the wheel eigenfrequencies. On the basis of its excitation intensity the road disturbance is classified into various road conditions defined as ISO road classes, see [1]. By applying

$$u \equiv F_{rams} = -\bar{d}_{sky}(\hat{x}_g)\dot{x}_c - \bar{d}_{c,p}(\hat{x}_g)\,(\dot{x}_c - \dot{x}_w)\,, \tag{2.20}$$

the adaptation logic then schedules optimal groundhook-skyhook gains $\bar{d}_{sky}(\hat{x}_g)$ and $\bar{d}_{c,p}(\hat{x}_g)$ depending on the quality of the ground surface. The optimal gains for the different road classes have been optimized based on simulations. In this Thesis the estimation of the road profile is carried out by means of a Kalman filter, [66]. More details about the adaption logic are given in Chapter 6.

- *LQR*: In research applications it is a well-known optimal controller concept, employed for full-active system. In this Thesis it is tuned in oder to realize comfort-oriented or safety-oriented solutions. The optimal force calculated by the law is clipped to the damper working range. Therefore, the semi-active damper can only generate a suboptimal damper force. The closed loop design is tested in the simulation, where constraints on suspension deflection and dynamic wheel load are taken into account. To calculate the optimal solution, the cost function

$$J_{LQR} = \frac{1}{2}\int_0^\infty \left[\mathbf{y}^T(t)\mathbf{Q}_{y,lqr}\mathbf{y}(t) + u(t)^T R_{lqr} u(t)\right] dt \tag{2.21}$$

is minimized, where $\mathbf{y}$ is defined in (2.10), $u \equiv F_{lqr}$ and the quantities $\mathbf{Q}_{y,lqr}$ and R_{lqr} are the weights of the outputs and the input, respectively. The solution of the Riccati equation allows to calculate the state feedback $u \equiv F_{lqr} = -\mathbf{k}^T\mathbf{x}$, where $\mathbf{x}$ is defined in (2.9).

Figure 2.6 qualitatively shows the differences between the desired force and the applied force by the semi-active device. In the depicted case, the desired force is calculated for a full-active system by means of LQR benchmark controller.

For the implementation of the benchmark systems, estimation of the required states are employed, [98]. The state estimation is obtained by using the filter-based approach illustrated in [95]. The damper's relative velocity, needed for the skyhook-based control law is obtained form the chassis and wheel acceleration and the suspension deflection. While the absolute velocity of the body is gained by highpass filtering of the chassis acceleration. Similar procedure has been adopted to obtain the absolute velocity of the wheel mass, which is needed for the optimal state feedback. Furthermore, the tire deflection is obtained from the estimated dynamic wheel load, considering a linear tire stiffness.

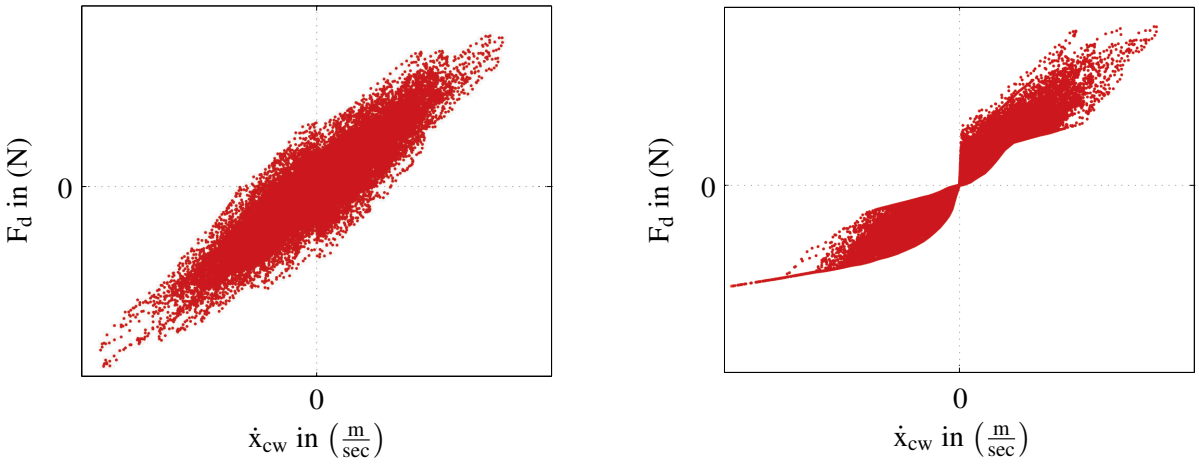

(a) Required force of LQR control law for a full-active linear system

(b) LQR solution clipped to the damper working range

Figure 2.6: Linear quadratic regulator desired force: comparison between required force and applied force, [82]

2.4 System requirements

Aiming to describe the behavior of the quarter-car system excited by the road excitation, the main objectives, meaning the ride comfort and the ride safety, have to be quantified. Since the suspension deflection influences the trade-off it has to be considered as well. In the following the criteria adopted in this Thesis are reported.

A widespread measure reported in literature for ride comfort is the root mean square value of the vertical chassis acceleration $||\ddot{x}_c||_{rms}$. A reduced value indicates an increased ride comfort, meaning that vibration induced by the road irregularities are attenuated. Due to the frequency dependent human sensitivity for vibrations, the frequency range for mechanical excitation between 4 and 8 Hz has to be taken into account for the controller design [2, 107, 168]. Therefore, a shaping filter presented in [2, 168] is adopted. It amplifies this frequency range and, as suggested in [94], for control design purposes can be integrated into the system by modeling it as a fifth-order linear transfer function. Accordingly, also the rms-value of the weighted vertical chassis acceleration $||\ddot{x}_c||_{comf,rms}$ is considered in this Thesis.

Moreover, since the rms-value of the specific variable considers the effect of the vibration over a time period, also the maximum of the absolute value of the chassis acceleration $\max(|\ddot{x}_c|)$

is calculated. It permits to consider the effect of singular event both from the road excitation and/or from the vehicle dynamic (e.g. by hitting the mechanical limitation).

Further evaluation criteria for ride comfort can be found in literature e.g. [107, 161, 177].

Since the main task of a suspension system is to allow the driver to govern the vehicle by steering and braking, it is required that forces can be transmitted between wheel and road at any time. A criterion known from literature to quantify the ride safety is that the dynamic wheel load must not exceed the static wheel load, [107]. To statistically ensure the observance of this condition, the bound

$$\sigma_{F_{dyn}} = ||F_{dyn}||_{std} = \sqrt{\frac{1}{T}\int_0^T F_{dyn}^2(\tau)d\tau} \tag{2.22}$$

over a time period T is adopted. It is assumed that the vertical road displacement is stochastic and that the resulting dynamic wheel load F_{dyn} has a Gaussian probability density, [94]. Assuming a normally distributed zero mean stochastic signal, the 3σ-rule conveys that dynamic wheel load remains within the bounds $\pm F_{stat}$[3] for approx. 99.7% of the considered period of time. Therefore, the bound on the dynamic wheel load in rms-value can be given as $||F_{dyn}||_{rms} \leq \frac{F_{stat}}{3}$, [107, 176]. Particular attention should be given to the negative dynamic wheel load, since this could cause loss of ground contact.

As already mentioned in this Thesis, also the suspension deflection influences the ride characteristic of a vehicle. This variable has to be kept within its limitations in order to avoid unpredictable force transmission to the chassis. Therefore, the suspension deflection $x_c - x_w$ should remain between its lower and upper bounds.

A violation of the limits not only reduces both performance values of comfort and road-holding but could damage the suspension strut components (especially the damper internal valves and end-stops).

Due to the asymmetry of the damper characteristic in compression and rebound direction, the equilibrium point of the suspension is shifted and the suspension deflection exhibits a mean value, which differs from zero.

[3] It represents the static wheel load, $F_{stat} = g(m_c + m_w)$, where g is the gravitational constant

2.5 Optimization, simulation and measurement quality

In Chapter 3 and Chapter 4 parameter estimations are performed, in order to identify the unknown parameters of both damper models. A general cost function, that is minimized during the optimization process, is presented in Section 2.5.1. Moreover to quantify the estimation results, a performance gain is formulated. Similarly, the benefit of the proposed control strategies are compared, based on improvement value defined in Section 2.5.2, while the force tracking index is described in Section 2.5.3.

2.5.1 Performance gain for parameter estimation

Parameters are estimated by minimizing a cost function J that calculates the difference between a measured signal O_{meas} and the signal obtained according to the model O_{mod} in mean square sense

$$J(P) = \sum_{i=1}^{n} (O_{mod}(t, I_{meas}(t_i), P) - O_{meas}(t_i))^2 \tag{2.23}$$

by considering a set of input signal $I_{meas.}$ sampled at time instant t_i and a set of parameters P.

Since most models are nonlinear in the parameters, an iterative optimization is performed, based on genetic algorithm method (GA) in combination with a gradient-based optimization algorithm. The quality of the fits is determined by calculating the cost function:

$$P_{G,e}(\|\cdot\|) = 1 - \frac{\|\cdot\|_{mod,\,rms}}{\|\cdot\|_{meas,\,rms}}. \tag{2.24}$$

2.5.2 Performance gain for simulations and measurements

Besides the described system requirements, the suspension performance relative to benchmark suspension systems is considered to evaluate the suspension controller. Consequently, in order to quantify the respective benefit of the proposed methods, a performance gain

$$P_G(\|\cdot\|) = 1 - \frac{\|\cdot\|_{controlled,\,rms}}{\|\cdot\|_{passive,\,rms}} \tag{2.25}$$

is determined for each considered quantity $\{\cdot\}$ with respect to the passive suspension configuration. Thereby, a reduction of the absolute value of the corresponding quantity and thus a

performance improvement is denoted by a positive value of $P_G(\|\cdot\|)$, [93].

2.5.3 Force tracking index

In order to quantify the force tracking structure, newly proposed in Chapter 5 and Chapter 6 of this Thesis, the index

$$\Gamma = \frac{\|F^* - F_{meas}\|_{rms}}{\|F^*\|_{rms}} = \frac{\|\Delta F_{fb}\|_{rms}}{\|F^*\|_{rms}} \tag{2.26}$$

is introduced. It allows to compare the tracking error between the desired force and the actually generated force of the semi-active damper. Since the applied controllers claim the semi-active device differently, the rms-value of the tracking error is referred to the rms-value of the desired force. A force tracking improvement is denoted by a reduction of the index Γ.

2.6 Design of Experiments

In this Section three excitation signals are described, which are applied in the following Chapters. Section 2.6.1 presents a modified chirp signal, which is employed to identify the parameter of the physical damper model in Chapter 3. In Section 2.6.2 stochastic road profiles, which are utilized in Chapter 4, Chapter 5, Chapter 6 and Chapter 7 are introduced in order to quantify the performance gain of the proposed control strategies. Moreover, a singular disturbance event is reported in Section 2.6.3.

2.6.1 Filtered chirp signal

According to [45, 144], a linear sweep is not ideally feasible for identification of the damper characteristics, because it lacks of sufficient content by low velocities. Therefore, the chirp signal shown in Figure 2.7 is applied, so that the required frequency range is exponentially swept to prevent prolonged excitation at high velocities.

Since the hysteresis effects mainly occur at the beginning of the rebound and compression phases, the measurements are revised, in order to not include hysteresis effects. Samples at the beginning of each stroking phase are eliminated by retaining those, where acceleration and velocity have a different sign, [43].

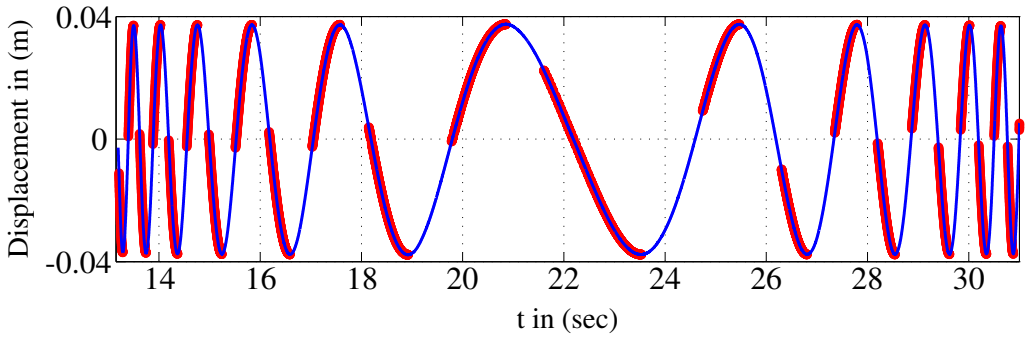

Figure 2.7: Displacement/time plot for chirp signal (blue) and corresponding plot without hysteresis (red), [116]

For the sake of a fast identification, a damper model without oil dynamic effect is considered, therefore an incompressible flow is assumed.

2.6.2 Stochastic road profiles

Generally, public roads induce stochastic vibrations into the vehicle system. The intensity of these vibrations depends on the quality of the road and the ride velocity of the vehicle, [1]. Aiming to maintain a realistic framework, besides the mechanical components of production vehicles, also measurement of real profiles are utilized for simulations and experiments at the designed test rig, see Appendix A.

The two profiles adopted in this Thesis (P1 and P2) are provided by an industrial partner and are recorded on German highways and country roads, see Figure 2.8. The road roughness is analyzed by means of the power spectral density (PSD), reported in the same Figure. The power spectrum referred to the spacial frequency of profile P2 shows, that it contains more energy at the high frequency components than P1.

For the description of road induced vibrations in terms of a disturbance model, different approaches exist in literature, e.g. [76, 107].

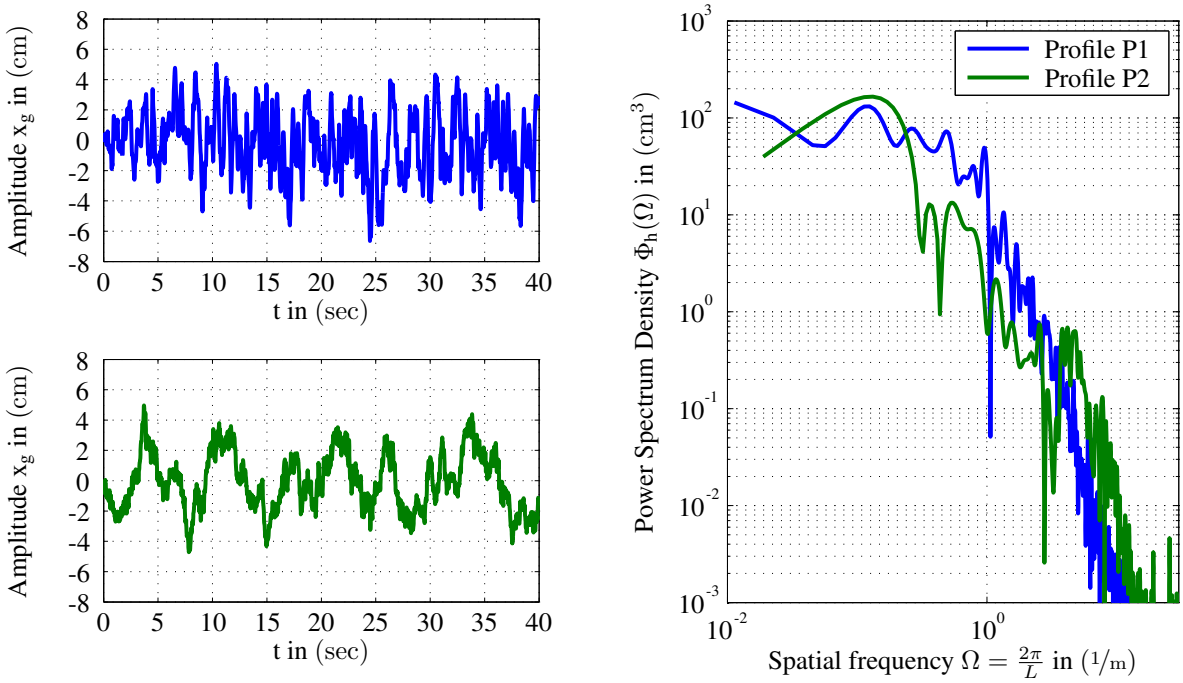

Figure 2.8: Input amplitudes and power spectrum density of the two adopted road profiles – Profile P1 by $50\,\mathrm{km/h}$; Profile P2 by $30\,\mathrm{km/h}$, [122]. Image is reproduced with kind permission of BMW AG.

2.6.3 Singular disturbance event: Bump

In this Thesis also a singular disturbance event is used to test the performance of suspension systems, e.g. in [104, 107]. The model of this kind of input can be given as

$$x_g(t) = \frac{A}{2} \cdot \left[1 - \cos\left(2\pi \frac{v}{L} t\right)\right] \tag{2.27}$$

where $A = 13\,\mathrm{cm}$ is the amplitude, $v = 20\,\mathrm{km/h}$ the velocity and $L = 1.85\,\mathrm{m}$ marks the longitudinal distance. The exciting frequency can be calculated as $\omega = \frac{v}{L}$ and the amplitude is chosen to completely exploit the suspension travel without reaching the mechanical limitation.

Figure 2.9 shows an exemplary parametrization of this model for a singular disturbance event, which is used in Chapter 5.4 to validate the damper control open loop structure and in Chapter 7 to compare the optimal solution to the passive reference.

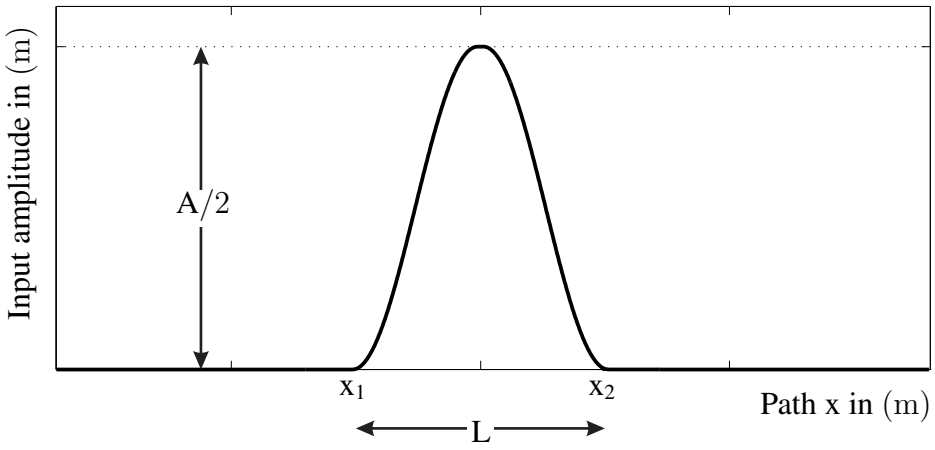

Figure 2.9: Parametric representation of a single obstacle.

2.7 Stability of the controlled suspension system

In the suspension research field, stability analysis of the closed loop is mainly based on Lyapunov theory, which provides conditions for the stability of an equilibrium point, $\mathbf{x}^* = \mathbf{0}$. The stability of the controlled suspension system is studied by means of initial perturbation of the states while neglecting the external excitation, [18, 52]. By dealing with semi-active suspension systems the Lyapunov stability is guaranteed. The energy of the system can be defined as Lyapunov function

$$\mathrm{V}(\mathbf{x},\mathrm{t}) = \frac{1}{2}\left(\mathrm{c_c x_1^2} + \mathrm{m_c x_2^2} + \mathrm{c_w x_3^2} + \mathrm{m_w x_4^2}\right), \tag{2.28}$$

whereby $\mathrm{V}(\mathbf{x},\mathrm{t}) > 0, \forall \mathbf{x} \neq 0$ and $\mathrm{V}(\mathbf{0},\mathrm{t}) = 0$. It is noted, that for the stability analysis the wheel damping can be ignored without loss of generality, since this element dissipates energy. By neglecting the road excitation, the derivative of $\mathrm{V}(\mathbf{x},\mathrm{t})$ is given depending on the damping constant

$$\dot{\mathrm{V}}(\mathbf{x},\mathrm{t}) = -\mathrm{d_c}(\mathrm{t})\left(\mathrm{x_2} - \mathrm{x_4}\right)^2, \tag{2.29}$$

where $\dot{\mathrm{V}}(\mathbf{x},\mathrm{t})$ is negative definite. In the closed loop, the control variable is the damping constant $\mathrm{d_c}(\mathrm{t})$, which can be adjusted between a minimum $\mathrm{d_{c,min}}$ and a maximum value $\mathrm{d_{c,\,max}}$. Dealing with real device, the minimum damping constant is always positive, $\mathrm{d_{c,min}} > 0$. There-

fore, with due regard to the Krasovskii-LaSalle invariance principle, see [89], it can be shown that the semi-active system is asymptotically stable.

However, when operating, vehicles are permanently subjected to road disturbances, which strongly influence ride comfort and ride safety. Since these disturbances introduce energy into the system, they cannot be neglected. Therefore, Lyapunov theory cannot be always applied to the general framework of a suspension system. Theoretical contributions, which guarantee systems' stability under non-vanishing disturbances are discussed in [89, 148].

Under common non-vanishing excitation, such as real measured road profiles, it can be assumed that the amount of power introduced into the system remains bounded, [148]. Since only components of production vehicles have been utilized in this Thesis, which are designed to endure common road excitations unscathed, it can be expected that the suspension system is able to absorb the road excitation. The amount of absorbed power increases by rising of damper relative velocity. Moreover, dealing with semi-active systems, independently of the control law, energy can only be dissipated and a minimal damping force is always guaranteed by the softest characteristic of the device. Hence, it can be stated from the premise that semi-active suspension systems also remain stable under non-vanishing bounded excitations, [148].

Chapter 3

PHYSICAL DAMPER MODELING

Benefits of semi-active systems over passive ones strongly depends on the accuracy of the damper model, [7]. Since the adjustable damper represents the kernel of a semi-active suspension system, a detailed analysis of the characteristic and the dynamics of these devices is needed in order to design a model-based control strategy. Therefore, in this Chapter, a model of a continuously variable semi-active dual-tube damper based on physical insights is presented. In the first Section some basic information about the damper physics and its working principle are given. In addition, the Section briefly presents the physical passive dual-tube damper model, known form the literature, while focusing on the valves and the current device modeling.

In order to obtain a reproduction of a semi-active device, the previous model is extended with two independently adjustable electromagnetic valves, which capture the continuously variable damping effects (Section 3.5). In particular, two models are analyzed: in the first one, a fluid mechanics description of the flow through a restriction, while in the second one a precise hydraulic description of the external valve and its hydraulic model are given. Friction model and temperature effects are also discussed.

The unknown physical model parameters are estimated with a genetic algorithm and a gradient-based optimization method to match measurement data. In Section 3.8, the electrical model of the dampers power unit, which also incorporates an internal current controller, is reported. In the last Section, the simulation results are compared with measurement data.

3.1 Hydraulic dual-tube damper

As mentioned in the previous Chapters, automotive dampers are key elements for suspension systems. They substantially influence the dynamic behavior of vehicles by dissipating energy

introduced by the road disturbances. Due to their complex dynamics, their appropriate modeling (both physical, structural and functional) has been a subject of engineering research, e.g. [67, 138].

The core of a semi-active suspensions struts is the adjustable device. In this Thesis, a continuously variable hardware configuration is utilized, with external adjustable valves. The damping action is obtained by increasing or decreasing the flow resistance through the valve assemblies, while the external valves work as bypass. Depending on geometrical characterizations of the valve, force-velocity characteristics with different forms can be achieved. The benefits of semi-active systems over passive ones are briefly addressed in Section 2.2 and can be also found in [7].

Due to the interaction between mechanical, hydraulical and electrical effects, the modeling of semi-active dampers is challenging. The results of their application for controller design purposes strongly depend on the accuracy and reliability of the modeled behavior. Therefore, the aim of this Chapter is to re-propose the physical model of a passive dual-tube damper already presented in [44] and to extend it by electro-mechanical and fluid-mechanical models, which simulate the external valves that allow to continuously adjust the damping force. The dynamics of the valves and the dynamics of the force generation are especially studied.

While in Figure 3.1(a) the general structure of a dual-tube damper are depicted, in Figure 3.1(b) the hardware, which is a component already applied in production vehicles, is represented. The joint at right side of the picture in Figure 3.1(b), is attached to the suspension strut, while the end of the piston rod is fixed, together with the main spring, to the car body (chassis mass) by means of a top mount element.

As depicted in Figure 3.1(a) the considered continuously variable dual-tube damper consists of an internal, an external cylinder and of three chambers: the rebound chamber, the compression chamber and the reserve chamber. Moreover, it is equipped with two external electromagnetic valves, which connect the reserve chamber to the rebound and the compression chambers respectively, and allow to continuously vary the damper characteristic.

The pressure tube (inner tube) is entirely filled with oil, while the reserve chamber is partially filled with gas, in order to compensate the volumetric changes generated by motion of the piston rod. The internal cylinder, is divided by the piston valve assembly, which is fixed at the lower end of the rod, into the rebound and the compression chambers. The piston

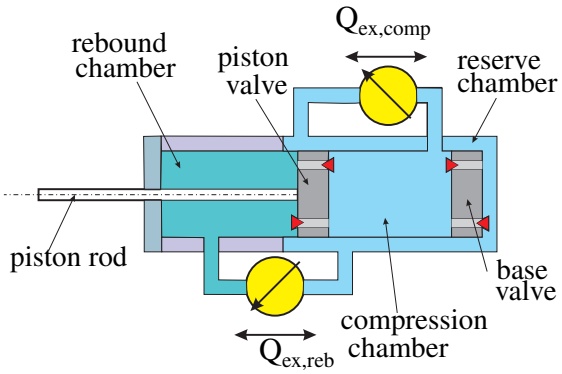

(a) Schematic representation of a dual-tube damper

(b) Semi-active device used on the test rig

Figure 3.1: Semi-active device considered in this work

valve assembly incorporated in the damper piston allows oil to flow between the rebound and compression chamber while the base valve assembly lets the oil flow between the compression and reserve chambers. Both the rebound and the compression chambers are connected to the reserve chamber by the external valves. Rebound and a compression bumpers are utilized to limit the suspension deflection (see Chapter 2.1) both in compression and in rebound direction.

Based on [44] a typical base valve assembly is drawn in Figure 3.2(a) and compared to its schematic architecture view in Figure 3.2(b). A very detailed description of the operation principle of the assembly valve is given in the works of Duym [43, 44, 45] and summarized in the following.

In the upward direction, meaning to the left side in Figure 3.2(a), the pressure behavior is influenced by the intake valve. Once that the pre-load generated by the intake spring is overcome, the intake valve opens offering small resistance to the oil flow, restricting flows in the opposite direction, Figure 3.2(b).

In the opposite direction the oil flows through a disc and orifices. These elements build the blow-off valve. The holes brake the fluid, generating a pressure drop across the valve, due to the viscosity of the fluid. Depending on the stroke's velocity and consequently on the height of the pressure drop above the valve, two operating modes can be described. Firstly, the discs bend and open the flow path until they reach the mechanical limitation (back-up washer). Secondly, once the bending is limited by the maximal angle, the port restriction mainly influences the pressure behavior. According to Duym's works, in this case, the oil

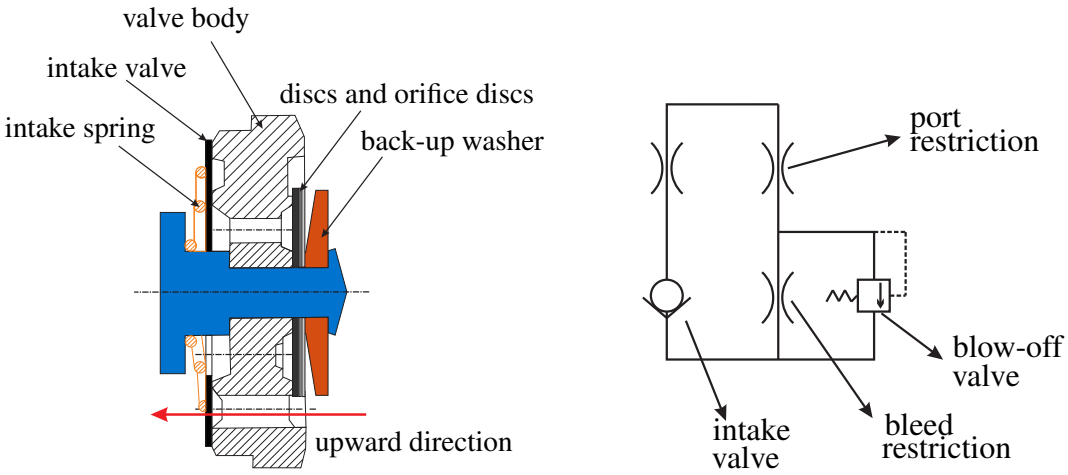

(a) Typical valve assembly (b) Hydraulic schema

Figure 3.2: Valve assembly: Base valve assembly (a) and schema of valving architecture (b), according to [44]

which flows through the holes, the disc and orifice disc, follows the same path as the one flowing through the blow-off valve. Therefore, the common path (port restriction) is kept in series with a parallel combination of the bleed and the blow-off valves, see Figure 3.2(b).

The mechanical construction of the internal valves influences the damping behavior, since the pressure drops mainly determines the force shape. After reaching a certain pressure drop above the bleed valve, which implies a certain damping force behavior (primary damping rate), the blow-off valve opens reducing therefore the damping slope (secondary damping rate). Thereby, it has been shown that the use of blow-off valve improves the vibration and shock isolation performance of the damper. The pressure at which the blow-off valve opens is determined by a pre-load of disc (represented in Figure 3.2(b) by a spring). According to [43], the leaking effects occur gradually before the opening pressure is reached. Thus makes it possible to avoid a sharp blow-off edge at transition between bleed and blow-off resulting in a smoother force transition.

3.2 Physical description

In order to increase the understanding of the physical phenomena, leading the force build-up dynamics depending on valves and geometry characteristic, a model of a passive damper is

summarized, where the damping force is calculated as function of the damper displacement, damper velocity and valve parameters.

3.2.1 Rebound and compression chambers

According to [106] the oil compressibility influences the dynamic effects of the damper. The relative change in volume $\frac{\Delta V}{V_0}$, with respect to the initial volume V_0, the compressibility factor α, and the applied pressure p are considered for physical modeling. They are combined in order to describe the volume equation in the pressure chambers. Moreover, if the flow rate Q between the chambers is considered, the volumetric change in the pressure tube can be expressed by

$$\dot{V} = Q - \frac{V\alpha\dot{p}}{1-\alpha p}. \tag{3.1}$$

Considering geometrical constraints and the linear motion x_{rod} of the damper rod from the static position x_0, the volume of each chamber can be expressed as

$$\text{rebound chamber} \quad V_{reb} = (L_{pt} - x_0 - x_{rod})(A_{pt} - A_{rod}), \tag{3.2}$$

$$\text{compression chamber} \quad V_{com} = (x_0 + x_{rod})A_{pt}, \tag{3.3}$$

where L_{pt} represents the physical length of the pressure tube and A_{pt} and A_{rod} the cross sections of pressure tube and damper rod, respectively. Substituting (3.2) and (3.3) in (3.1) and solving the equations for rebound and compression pressures leads to the relations of the pressure changing for both chambers.

It is noted, that the explicit relations for rebound

$$\dot{p}_{reb} = \frac{\left(\dot{x}_{rod}(A_{pt} - A_{rod}) - Q_{pv}\right)(1 - \alpha p_{reb})}{(L_{pt} - x_0 - x_{rod})(A_{pt} - A_{rod})\alpha}, \tag{3.4}$$

where Q_{pv} represents the oil flow above the piston valve, and for compression chamber

$$\dot{p}_{com} = -\frac{\left(\dot{x}_{rod}A_{pt} - Q_{pv} + Q_{bv}\right)(1 - \alpha p_{com})}{(x_0 + x_{rod})A_{pt}\alpha}, \tag{3.5}$$

where Q_{bv} represents the flow above the base valve, depend on the damper geometry, the applied rod motion and the internal flows. It can be also noticed, that because of the dual-

tube geometry, (3.5) is influenced by the characteristic of the piston valve as well as by the base valve, while (3.4) is only influenced by the piston valve dynamic. A qualitative flow representation is given in Figure 3.3 both for compression and rebound cases.

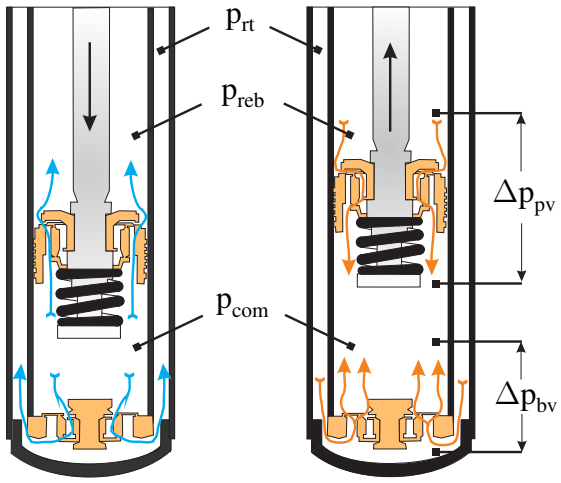

Figure 3.3: Qualitative flow paths in compression (left) and rebound (right) case, according to [130]

The flow rates $Q_{(\cdot)}$ define the main characteristic of the damper behavior and the dynamic damper progression. The flow paths are driven by the nonlinear functions of pressure drops

$$Q_{pv} = f_r\left(\Delta p_{pv}\right) = f_r\left(p_{reb} - p_{com}\right),$$
$$Q_{bv} = f_c\left(\Delta p_{bv}\right) = f_c\left(p_{com} - p_{rt}\right),$$

both over the piston and the base valve, whereas also the gas effective is needed. By knowing the geometry and the pressures in the damper, the damper force can be calculated as

$$F_d = p_{reb}(A_{pt} - A_{rod}) - p_{com}A_{pt} + F_{fr}, \tag{3.6}$$

where F_{fr} represents both the valves and the rod friction (see Section 3.6).

3.2.2 Reserve chamber

The reserve tube contains both oil and a volume of gas $V_{rt,gas}$. The latter is assumed to be compressed and expanded under adiabatic conditions. The gas phase compensates the volumetric changes induced by the rod motion. Considering the equilibrium of the gas volume ($V_{rt,gas,0}$) by the pressure $P_{rt,0}$, the volumetric change in the reserve chamber can be calculated by a polytropic transition. According to [44] an iso-entropic law

$$p_{rt} = p_{rt,0}\left(\frac{V_{rt,gas,0}}{V_{rt,gas}}\right)^{\gamma} = p_{rt,0}\left(\frac{V_{rt,gas,0}}{V_{rt,gas,0} + A_{rod}x}\right)^{\gamma}, \tag{3.7}$$

with γ=1.4 is chosen. Due to the presence of the large gas phase, the effect of oil compressibility in the reserve chamber is negligible and the variation of the pressure is small in comparison with that of the main tube.

In the cut view in Figure 3.3 the pressure drops over the valves and the flow direction are depicted. In this Thesis the internal valves of the damper (piston and base valves) are modeled considering an equal hydraulic model. Therefore, in Section 3.3 general consideration about the flow rates $Q_{(\cdot)}$ are derived. The results can be applied both to the piston and to the base valves.

3.3 State of the art of damper modeling

In this Section the main properties of the valve assembly commonly applied in semi-active damper for vehicle suspension application are summarized. The state of the art description reported in the following is mainly based on the work [45] and it is needed in this Thesis to introduce the working principle of these mechanical components, which are newly integrated in this Thesis, to model external adjustable valves.

Referring to Figure 3.2(b), restriction valves and blow-off valve are depicted. More precisely, in the assembly considered in this Thesis, intake, bleed and the port valves are considered restriction elements. Duym reports in [45] that for turbulent flows the pressure drop Δp over a restriction is a function of the flow Q. Therefore, the three restriction elements mentioned

above can be modeled by the following relations:

$$\text{Leak restriction} \quad \Delta p_{\text{leak}} = K_{\text{leak}} \nu^{1/4} Q_{\text{leak}}^{7/4}, \tag{3.8}$$

$$\text{Port restriction} \quad \Delta p_{\text{port}} = K_{\text{port}} \nu^{1/4} Q_{\text{port}}^{7/4}, \tag{3.9}$$

$$\text{Intake restriction} \quad \Delta p_{\text{intake}} = K_{\text{intake}} \nu^{1/4} Q_{\text{intake}}^{7/4}. \tag{3.10}$$

While the restrictions are characterized by one parameter $K_{(.)}$ and the kinamtic viscosity ν, the blow-off valve is characterized by two independent parameters:

$$K_{\text{spring}} Q_{\text{blow-off}} = (\Delta p_{\text{blow-off}} - \Delta p_0) \sqrt{\Delta p_{\text{blow-off}}}. \tag{3.11}$$

As mentioned in Section 3.1, in the upward direction only the intake valve is considered. While in the downward direction, depending on the pressure drop above the valve, two cases have to be considered: firstly the pressure drop is caused by bleed and port restrictions, secondly the blow-off valve is opened and the bleed restriction is bypassed. In the next Section the flow rate equations leading the three configurations are derived. The total pressure drops over both valve assemblies

$$\Delta p_{\text{pv}} = p_{\text{reb}} - p_{\text{com}} \quad \text{and} \quad \Delta p_{\text{bv}} = p_{\text{com}} - p_{\text{rt}} \tag{3.12}$$

are defined as the difference in pressure of the two chambers that are above and under the assembly. The algebraic sign of the pressure drops define the flow direction, namely upward or downward. In case of the downward direction the absolute value determines, if the blow-off valve is open or closed.

Considering the same model for both internal valves, instead of the definitions in (3.12), a generic total pressure drop Δp_{tot}, is considered and these three different operating states are described.

1. $\Delta p_{\text{tot}} < 0$: intake valve
   Firstly, if pressure drop Δp_{tot} over the considered valve assembly is negative, the oil entirely flows through the intake valve and the total flow rate is obtained by solving

(3.10) for the flow rate and can be calculated as

$$Q_{tot} = -\left(\frac{-\Delta p_{tot}}{K_{intake}\nu^{1/4}}\right)^{4/7} \quad \text{for} \quad \Delta p_{tot} \leq 0. \tag{3.13}$$

2. $\Delta p_{tot} > 0$: blow-off valve closed
   By considering a positive pressure drop, meaning a flow in the opposite direction, the series and parallel combination of valves is used. In parallel configuration, the pressure drops for each valve is equal but the total flow is the sum of the flow through each element while for series combination both flows are equal but the total pressure drop is obtained by summing the individual pressure drops, i.e. $\Delta p_{tot} = \Delta p_{leak} + \Delta p_{port}$. The flow rate consideration in parallel configuration allows to decouple the total port flow into the flows through port valve and blow-off valve (see Figure 3.2(b)).

   In the second case the pressure is smaller than the pre-load and the blow-off valve remains closed, which means that the whole loss is generated by the bleed and port restrictions. In that case, the leak flow equals the total flow and an explicit expression for the total pressure drop as a function of flow can be obtained by solving the equation with respect to the flow rate

$$Q_{tot}|_{closed} = \left(\frac{\Delta p_{tot}}{(K_{intake} + K_{leak})\,\nu^{1/4}}\right)^{4/7}. \tag{3.14}$$

3. $\Delta p_{tot} > 0$: blow-off valve opened
   In the third case, the pre-load of the blow-off valve is overstepped and the bleed restriction is bypassed, which results in the opening of the blow-off valve. Due to the parallel configuration, only the implicit relation between Q_{tot} and Δp_{tot}

$$f(\Delta p_{tot}, Q_{tot}) = \frac{\Delta p_{tot} - K_{port}\nu^{\frac{1}{4}}Q_{tot}^{\frac{7}{4}} - \Delta p_0}{K_{spring}}\sqrt{\Delta p_{tot} - K_{port}\nu^{\frac{1}{4}}Q_{tot}^{\frac{7}{4}}} + \left(\frac{\Delta p_{tot} - K_{port}\nu^{\frac{1}{4}}Q_{tot}^{\frac{7}{4}}}{K_{leak}\nu^{\frac{1}{4}}}\right)^{\frac{4}{7}} \tag{3.15}$$

   can be obtained. Because of its implicit character, (3.15) can be only solved numerically or approximated by Taylor series around the blow-off pressure Δp_0. The inversion takes place by means of Cardano's rule, [44]. Once Δp_{leak} is calculated, Q_{tot} is obtained for

an open blow-off valve

$$Q_{tot}|_{open} = \left(\frac{\Delta p_{tot} - \Delta p_{leak}}{K_{port} \nu^{1/4}} \right)^{4/7} \quad \text{for} \quad p_{tot} > p_{tot,blow\text{-}off}, \tag{3.16}$$

where $p_{tot,blow\text{-}off}$ is the total pressure drop at the blow-off break point.

In order to obtain a continuous transient between the second and the third configurations, the same smoothing function proposed in [43, 44] is adopted in this Thesis. The function is applied for both damping directions and is characterized by the smoothing factors G_{reb} and G_{com}.

The given equations allow to simulate the passive damper behavior. In order to give a general view of the relationship described by the set of equations, Figure 3.4 reports a scheme of a dual tube damper's physics, in case of passive configuration.

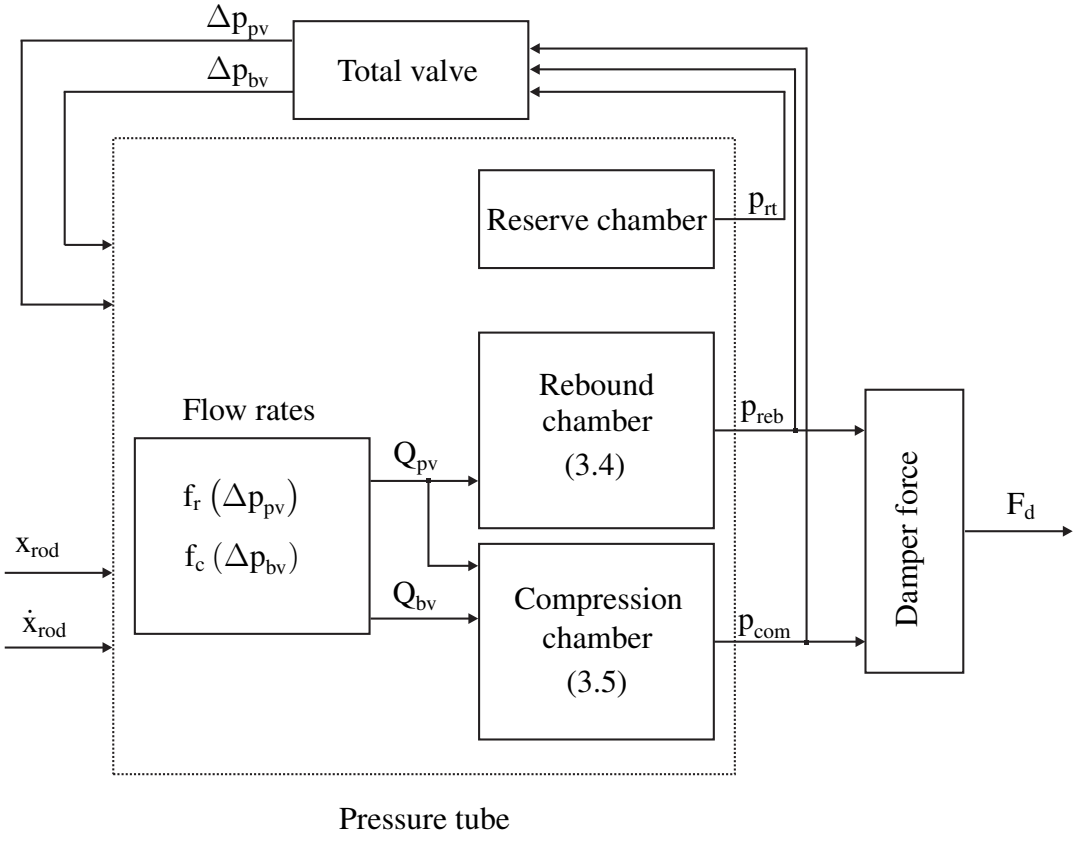

Figure 3.4: Schema of a dual tube damper's physics for the passive configuration

3.4 Influence of the internal valves' parameters

At this point the equations given in the previous Section already describe the complete physical model of a passive damper. However, a better understanding of the valves' parameters influence is necessary in order to identify the unknown parameters.

In the following, the parameters are separately considered for base and piston valve, meaning for compression and rebound motion. All parameters are listed in Table 3.1. It is noted, that only the geometrical ones together with the fluid characteristic are known.

Table 3.1: Paramters for the description of a standard dual-tube damper

Valve parameters		**Fixed parameters**		**Initial values**
Rebound	**Compression**			
$\Delta p_{0,reb}$	$\Delta p_{0,com}$	L_{pt}	x_0	$P_{rt,0}$
$K_{port,reb}$	$K_{port,com}$	A_{pt}	A_{rod}	$V_{rt,gas,0}$
$K_{leak,reb}$	$K_{leak,com}$	ν	α	F_{fr}
$K_{spring,reb}$	$K_{spring,com}$			
$K_{intake,reb}$	$K_{intake,com}$			
G_{reb}	G_{com}			

In Figure 3.5 a typical damper characteristic is shown to illustrate the direct relation and the impact of the parameters on the velocity-force behavior, which in other words is proportional to the relation flow rate-pressure drop on the considered valve.

Even if the relation of valve switching and flow rate is strongly nonlinear, some main effects and trends can be depicted. Because the base and the piston valve are modeled with the same components, the illustration given for the rebound case is transferable to the compression case.

The parameter $\Delta p_{0,reb}$ determines the height of the primary damping rate in the force-velocity diagram. By increasing $\Delta p_{0,reb}$ the corresponding force of the transition from the primary to the secondary damping rate can be increased. Considering the compression plan, $\Delta p_{0,com}$ acts on the negative half.

After the blow-off point, the slope of the characteristic changes and the damper behavior

transits from the primary to the secondary damping rate. The product

$$PSL_{reb} = K_{port,reb} \cdot K_{spring,reb} \cdot K_{leak,reb}$$

represents the damping effect in the low velocity range. While parameters $K_{spring,reb}$ and $K_{leak,reb}$ are only responsible for the slope in the primary damping rate, $K_{port,reb}$ influences also the secondary damping rate. It allows to change the slope from linear to progressive in high frequency range. Moreover, the curvature factor G_{reb} allows a smooth crossing to the high velocity range, see Figure 3.5(b).

The K_{intake} factor describes the shape of the damper at the inversion of motion direction and spreads the hysteresis effect. Both the rebound and the compression factor mutually influence the hysteresis in both directions.

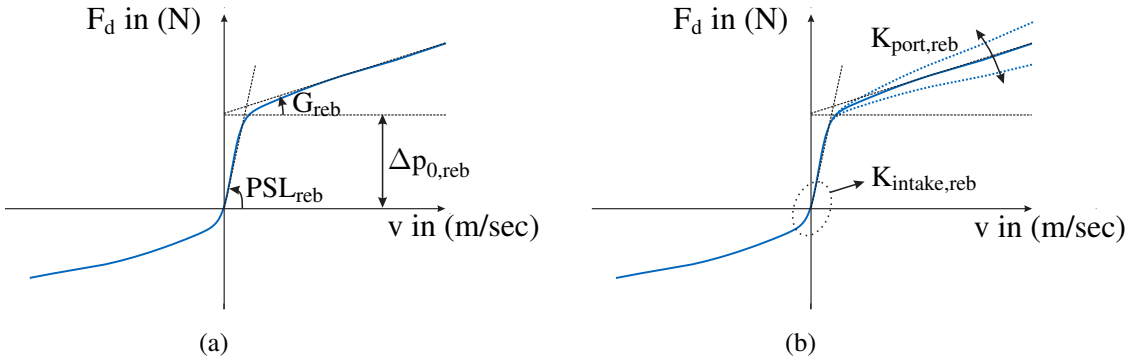

Figure 3.5: Parameter analysis: (a) primary and (b) secondary damping rate

Due to the state-dependent switching behavior of the differential equation describing the damping force, the strong nonlinear relation between valves' parameters, robustness and sensitivity analysis have not been conducted in details. Based on values for the valve parameters given in [43, 44, 45], a range for the unknown values is defined and fitted by numerical optimization algorithms, see Section 2.5.1.

3.5 External valves models

In the following, the passive device is extended by two external valves, which allow to achieve a variable damping effect. The new modeling techniques allow to bypass the internal valves

by rapidly reducing the pressure in the main tube. Two models are derived: the first is based on physical considerations about dynamical effects of oil flowing through a constriction, [116]; the second re-proposes a hydraulic valve model, similar to the one proposed for the internal valves while modifying the pressure differential equations.

3.5.1 Flow dynamics in external valves

The first model for the external valves is based on the knowledge of the fluid dynamics between the chambers of the damper. The principles of conservation of mass, energy and momentum are considered to write the equation of motion of the fluid. In order to calculate the oil flowing through the external valves, once they are activated, firstly the streamline between two sections is considered.

The Bernoulli's principle for a non-viscous fluid is used to calculate the flow rate through the valves by the command voltage signals. According to [174], if a frictionless flow is considered and it is assumed that the density ρ_{oil}, the volume V and the pressure p are uniform over the considered cross section A_i, the integral form of the unsteady frictionless flow along a streamline between section A_1 and A_2

$$\int_1^2 \frac{\partial V}{\partial t} ds + \int_1^2 \frac{\partial p}{\partial \rho} ds + \frac{1}{2}\left(v_2^2 - v_1^2\right) + g\left(h_2 - h_1\right) = 0, \tag{3.17}$$

can be calculated, whereby the term $g\left(h_2 - h_1\right)$ represents the fluid's potential energy and can be omitted in the following considerations. A schematic illustration of the considered situation can be seen in Figure 3.6.

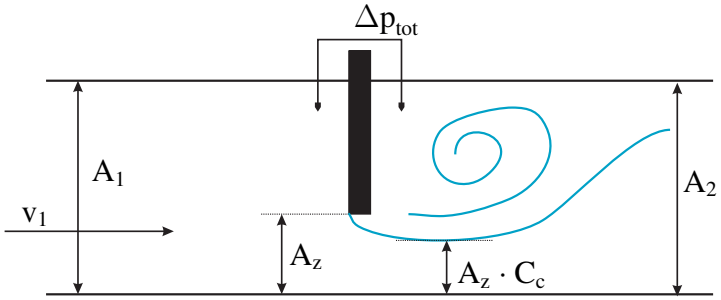

Figure 3.6: External Valve Scheme, [116]

Restricting the consideration only for steady ($\partial V/\partial t = 0$) incompressible flows, meaning that the density is considered constant, the integrals of (3.17) become constant. Furthermore, the pressure drop above the valve ΔH and the losses along the valve tube JL are introduced. Applying these measures, (3.6) can be reformulated and the equation for steady incompressible flow along a streamline

$$p_1 + \frac{1}{2}\rho v_1^2 = p_2 + \frac{1}{2}\rho v_2^2 + \Delta H + JL \tag{3.18}$$

is obtained. In particular, ΔH is the local loss of pressure caused by the valve and the term JL represents the distributed pressure loss along the tube, [65].

According to [50, 69] the minor loss can be modeled as

$$\Delta H = \frac{(V_1 - V_z)^2}{2g} = \frac{V_1^2}{2g}\left(\frac{1}{m \cdot C_c} - 1\right)^2, \tag{3.19}$$

where $m = A_z/A_1$, C_c is the constriction factor due to the valve and the loss effect JL can be modeled depending on the geometry and on the Reynolds number. To simplify the description only the laminar flow configuration is considered. The distributed pressure loss, which is related to the flow velocity in the section previous to the valve, can be obtained from the expression

$$JL = \chi \cdot v_1 = \xi \frac{64}{Re} v_1, \tag{3.20}$$

where ξ represents the geometry of the tube connecting the rebound or compression chamber with the valves.

The coefficient m correlates the discharge flow by opening the valve (A_z) with the cross-section A_1 of the tube connecting the internal to the reserve chambers. It is assumed that A_z changes linearly with the measured current and the value of m is replaced by the ratio of the current i_{eff} to its maximal value i_{max}. This parameter, as well as the original one A_z/A_1, ranges in the interval $[0; 1]$.

Moreover, to take the characteristic of the opening section into account, the pressure drop above the valve is scaled according to [166]. The presented equation allows to calculate the flow velocity across the section. The result is obtained solving a quadratic equation: the positive solution indicates the direction from left to right in Figure 3.6, the negative one the opposite flow. The continuity equation is reformulated and the flow rate through the external

valves is obtained as

$$Q_{ex} = v_{z_{1,2}} A_z = v_{z_{1,2}} \frac{A_z}{A_1} A_1 = v_{z_{1,2}} m A_1. \tag{3.21}$$

For both valves (3.21) can be used. The pressure drop Δp is described in (3.4), (3.5) and (3.7) as the difference between the two chambers that are above and below the electromagnetic valves. The unknown parameters in the flow-rate equations are the section A_1, the geometrical term χ and the constriction factor C_c.

3.5.2 Hydraulic model of external valves

Through the action of the external valve, the flow rate and pressure can be changed and therewith the damper force. To model the flow rate through the external valves, a similar valve architecture to the internal one is used. Based to simulative evidence, the intake path in the external valve is omitted, since it does not significantly improve the model results and it increase the number of unknown parameters.

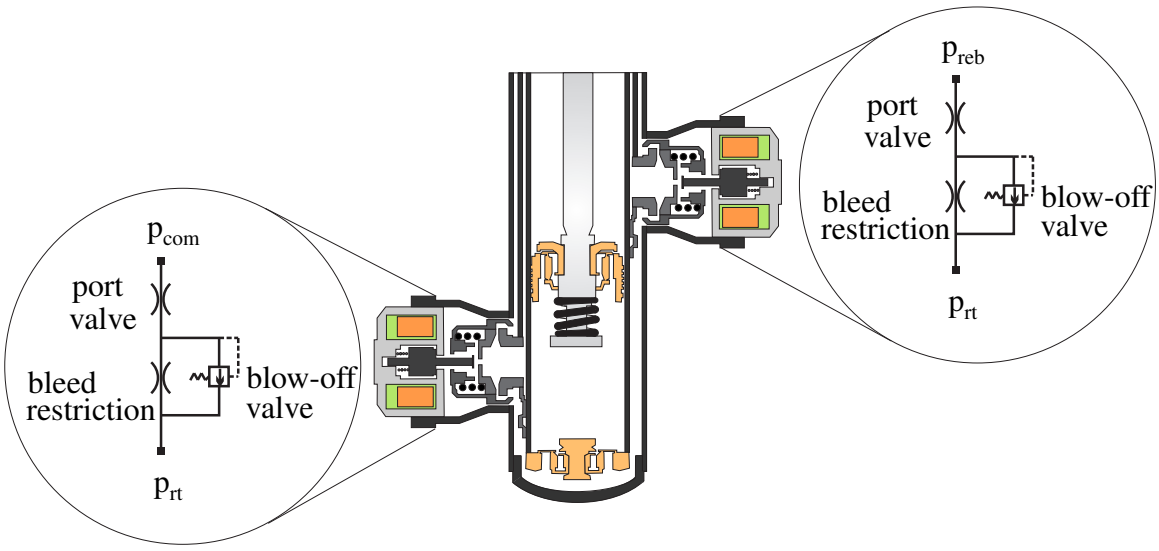

Figure 3.7: Qualitative valve assembly of the external valves, according to [130]

The external valves, qualitatively represented in Figure 3.7, allow the oil to flow from the pressure tube to the reserve chamber directly. By activating them, a sudden pressure drop takes place in the internal pressure tube changing the work states of the internal valves. Therefore,

the main force shape (meaning the passive characteristic curve) experiences significant variation. The external valves characteristics are driven by the pressure drops $\Delta p_{ex,com} = p_{com} - p_{rt}$ and $\Delta p_{ex,reb} = p_{reb} - p_{rt}$ respectively, which determine the external flow rate $Q_{ex,com}$ and $Q_{ex,reb}$ respectively.

Since the essential dynamic is defined by the pressure drops above the valve, the equation structure introduced in Section 3.2.1 is maintained, however equations (3.4) and (3.5) have to be arranged to take the external flow contributions into account. Since the flows have direct influence on the pressure changes, their effects are added to the internal ones in the following analysis and the pressure derivatives

$$\dot{p}_{reb} = \frac{\left(\dot{x}\left(A_{pt} - A_{rod}\right) - Q_{pv} - Q_{ex,reb}\right)\left(1 - \alpha p_{reb}\right)}{\left(L_{pt} - x_0 - x\right)\left(A_{pt} - A_{rod}\right)\alpha}, \tag{3.22}$$

and

$$\dot{p}_{com} = -\frac{\left(\dot{x}A_{pt} - Q_{pv} + Q_{bv} + Q_{ex,com}\right)\left(1 - \alpha p_{com}\right)}{\left(x_0 + x\right)A_{pt}\alpha}, \tag{3.23}$$

are redefined. Furthermore, the damping force can be still considered as in (4.2). Due to the omission of the intake path each valve has now two working configurations: the flow rate has to be calculated for opened or closed blow-off valve, both for rebound and compression direction. The calculation is described in Section 3.3, where the valve parameter are replaced by the ones of the external valves.

Considering the new formulation of the damper, the influence of the applied voltage on the variable components is studied and different analysis of parameter combination are considered, [12]. In Table 3.2, the main results are reported, which are obtained by variations of blow-off, bleed and port valves. It is shown, that by changing the blow-off valve characteristics a parabolic behavior is obtained. By varying the bleed restriction, the point slope remains at the same force level and the relation with the velocity is not parabolic anymore. In case of a port restriction variations, the point slope is changing with the velocity.

According to the measured characteristics reported in Figure 2.3(a), the behavior of adjustable current settings mainly reflects the results obtained by the analysis of port valve variation (third case of Table 3.2). Nevertheless a more detailed observation reveals that for extremal cases, meaning around 0% and 100% of damper current, the measurements resamble the bleed restriction variations too. Therefore, for the optimization a combination of beed restriction and

port valve variation are chosen to reproduce the damping force, when a voltage is applied at the valve.

Table 3.2: Variation of external valve components: 1) blow-off, 2) bleed restriction, 3) port

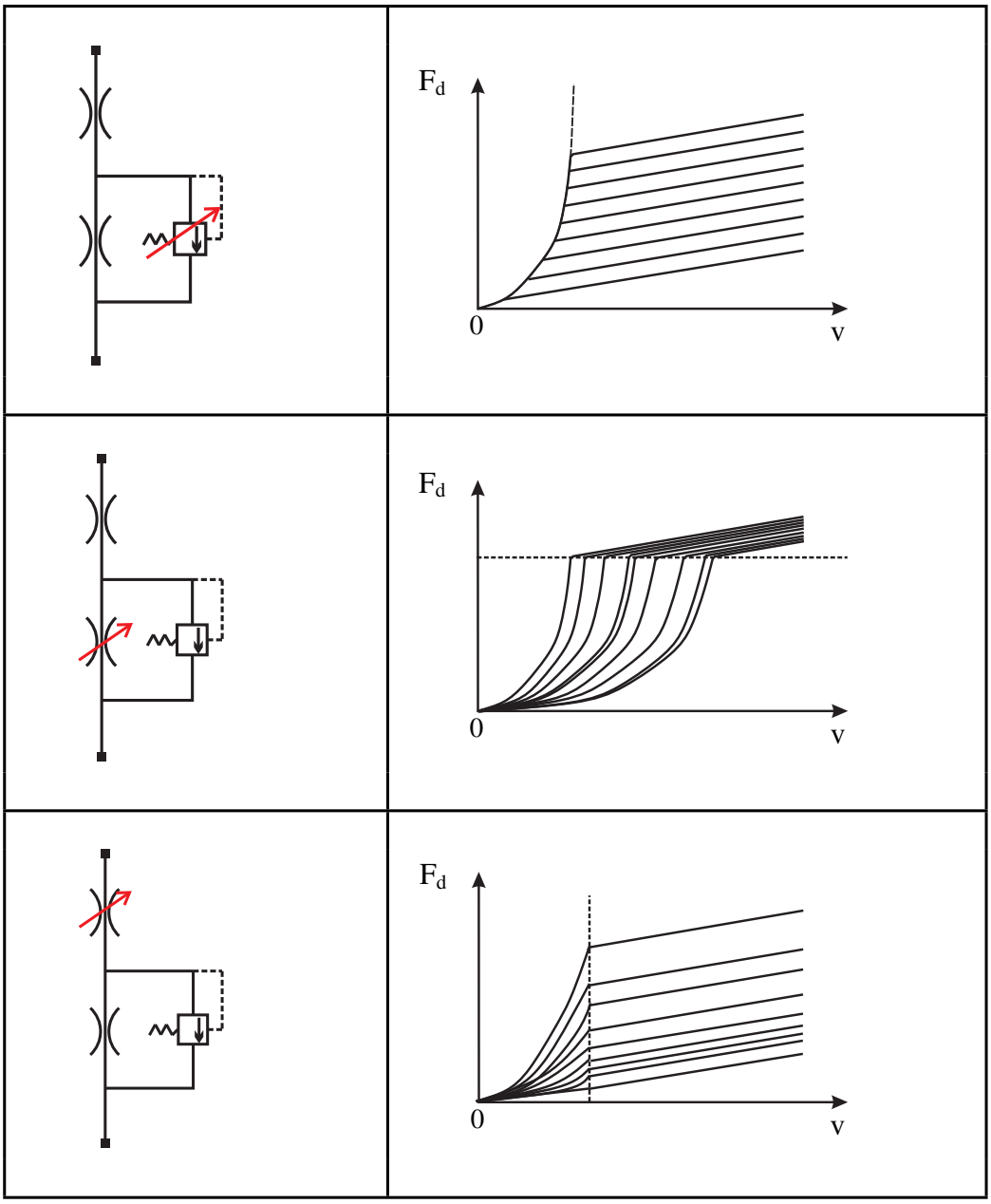

3.6 Friction model

The translational attrition represents contact friction between moving bodies and is adopted in this Thesis to shape the friction effects between piston valve and pressure tube and between piston rod and pressure tube. The friction force F_{fr} is modeled as function of damper rod velocity and is assumed to be the sum of Stribeck, Coulomb and viscous components. For an overview on friction models refer to [15, 16] and the references therein.

3.7 Oil temperature influence

According to [106], the oil temperature has an influence on the damping factor of a shock absorber. In this source a standard shock absorber is considered and the relationships between temperature, viscosity, damping factor as well as damping forces and body acceleration are addressed. In addition, the flow characteristics are studied. The impact of laminar and turbulent flow depends on the Reynold's number which is inversely proportional to the oil viscosity. Therefore, in case of high oil viscosity the laminar flow is dominant, while for higher oil temperatures (the oil viscosity is at a lower level), the turbulent flow is dominant.

A further relevant aspect when considering the influence of the damper oil is the track dependent change of oil viscosity. According to [128] the viscosity increases with increasing track distance and the viscosity of clean oil or used oil strongly influences the damping behavior.

Due to the complexity of including a temperature model and the technical difficulty/impossibility to validate it on the real device, the temperature effects on the damping force are omitted in this Thesis.

3.8 Power electronics

The external valves need a control unit for the current which produces a magnetic field in their coils. They have to be adjusted in order to influence the damper dynamic. This is achieved by varying the input voltage. This direct correlation allows the damping coefficient to be controlled in real-time.

As depicted in Figure 3.8, in the current driver, the control voltages $\mathbf{V} = [v_{reb},\ v_{com}]^T$ are

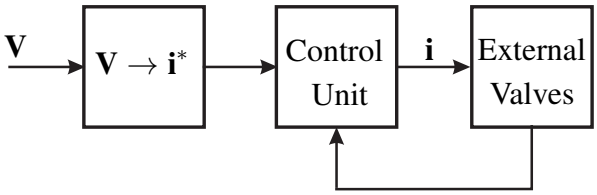

Figure 3.8: Block diagram of the power electronic unit

converted to the corresponding required currents $\mathbf{i} = [\mathrm{i_{reb}},\ \mathrm{i_{com}}]^{\mathrm{T}}$. The power electronic unit controls compares the desired currents to the ones fed back from the internal coil. Detailed information regarding a typical power electronic structure and its components can be found in [36]. The core coil dynamics can be described as a first order lag element by a resistor $\mathbf{R}_{\mathrm{pu}} = [\mathrm{R_{reb}},\ \mathrm{R_{com}}]^{\mathrm{T}}$ and an inductor $\mathbf{L}_{\mathrm{pu}} = [\mathrm{L_{reb}},\ \mathrm{L_{com}}]^{\mathrm{T}}$ connected in series

$$\mathbf{V}(\mathrm{t}) = \mathbf{R}_{\mathrm{pu}}\mathbf{i}(\mathrm{t}) + \mathbf{L}_{\mathrm{pu}}\frac{\mathbf{i}(\mathrm{t})}{\mathrm{dt}}, \tag{3.24}$$

where the voltage $\mathbf{V}(\mathrm{t})$ is assumed to be the input and the current $\mathbf{i}(\mathrm{t})$ the output of the plant. The transfer function of (3.24) is used on the simulation platform on which the proposed controller can be tested. The PI control method based on classical control theory is still widely utilized for the design of the controller (see e.g. [36]).

The PI-controller parameters are known from an industrial partner, while the plant parameters are unknown. For simulation and damper control design purposes, they are obtained from an optimization algorithm comparing simulations and measurement data, [116].

The scheme presented in Figure 3.4 is augmented by the external valve model, by the friction model and by electronic components. The complete representation is reported in Figure 3.9, where the new models of the external valves are emphasized in red.

3.9 Simulation and validation

For simulation purposes the unknown parameters, reported in Table 3.1, are estimated. The resulting model includes geometrical and reserve chamber parameters, parameters for the internal valve assemblies and tunable parameters for the external valves.

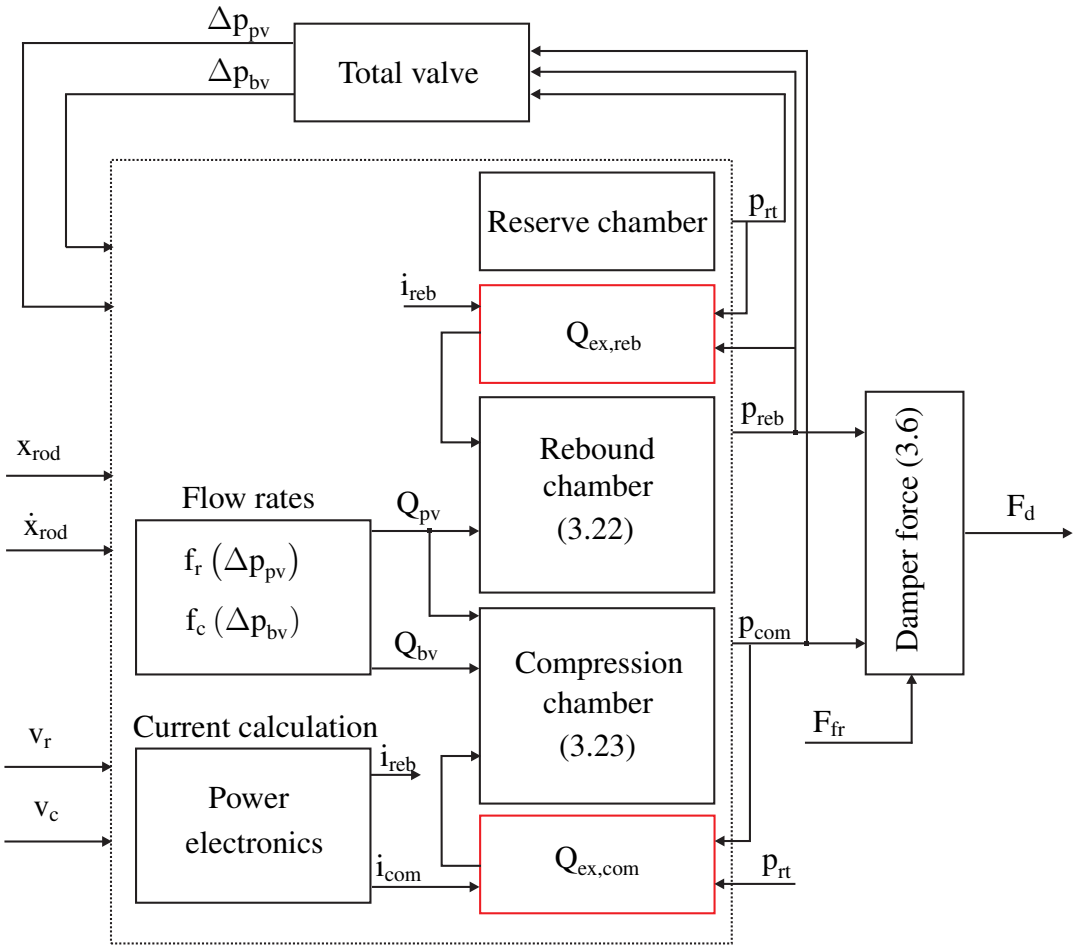

Figure 3.9: Schema of a complete dual tube demi-active damper's physics

While the geometrical parameters can be measured on the real device and therefore do not need to be identified, the reserve chamber ones are obtained by considering a quasi-static excitation signal. Firstly, the passive case is considered and the internal valve assemblies are identified by means of dynamical tests, which excite the damper in the whole frequency range. Since no voltage is applied, it is assumed that the external valves remain closed. The procedure is described in [45].

Secondly, once the internal valve's parameters are optimized, the damper dynamics are studied by applying a voltage on the external valves. Identification results are reported by considering the external valves modeled by the hydraulic representation.

Quasi-static compression test

By means of the quasi-static test, three model parameters are determined: the static gas pressure $p_{rt,0}$, the static gas volume $V_{rt,gas,0}$ in the reserve tube and the friction value F_{fr}. Due to the slow velocity, which characterizes these tests, the latter unknown parameter is considered constant and only the constant friction value $F_{c,fr}$, namely Coulomb friction, is estimated.

The quasi-static motion slowly compresses and then extends the shock absorber at the speed of $2\,{}^{\mathrm{mm}}/_{\mathrm{sec}}$ in order to minimize the damping forces caused by the viscous losses. The damping force is mainly generated by friction and the gas pressure only. Considering the force expression (3.6) and a quasi-static damper state, meaning that only minimal pressure changes around the equilibrium point are notable, it can be assumed that $p_{reb} \approx p_{com}$ during the motion. Without pressure drop above the valve, i.e. no flow rate, the viscous losses are not significantly influencing the measurement. Therefore, (3.6) can be modified as follows

$$F_d = -p_{reb}A_{rod} + F_{fr}, \tag{3.25}$$

while the pressure tube characteristics are neglected. Similar consideration can be done for the pressure behavior between compression and reserve chamber, see Figure 3.2.1, which allows to assume that $p_{com} \approx p_{rt}$. If the three chambers have the same pressure, $p_{reb} \approx p_{com} \approx p_{rt}$, the damper force can be consequently reformulated for the quasi-static case. By considering the pressure relation and applying (3.7) into (3.25), the quasi-static damper force

$$F_{d,qs} = -A_{rod}p_{rt,0}\left(\frac{V_{rt,gas,0}}{V_{rt,gas,0} + A_{rod}x}\right)^{\gamma} + F_{fr} \tag{3.26}$$

is obtained. Using the least squares estimator which minimizes the difference between the measured force and the modeled force in the mean square sense (2.23), the three parameters are identified. The results can be found in [116], where it is shown that a $P_{G,e}(\|F_{d,qs}\|)$ of about 98% is reached.

Dynamic slope identification

The detailed estimation of the internal valve assemblies' parameters is also reported in [116]. During this test the signal in Figure 2.7 excites the test rig (see Appendix A.5). It is noted

that, to identify the internal valve parameters no voltage are applied to the external valves, i.e. the damper is considered as a standard passive dual-tube damper and the viscosity of the oil is considered constant. The hysteresis filter, introduced in Section 2.6.1, is applied to the measurements in order to minimize the effect of the oil characteristic and the oil compressibility is set to zero.

However, even if the static slope is matched sufficiently well, the dynamical hysteresis behavior is not reproduced with enough accuracy. Therefore, the identification procedure proposed in the previous work [116] is refined and the results are proposed in this Thesis. Based on the results obtained by the static slope identification, the fluid characteristics are considered to further improve the estimation performance. Consequently, (2.23) is weighted to better reproduce the build up and the maximal force values.

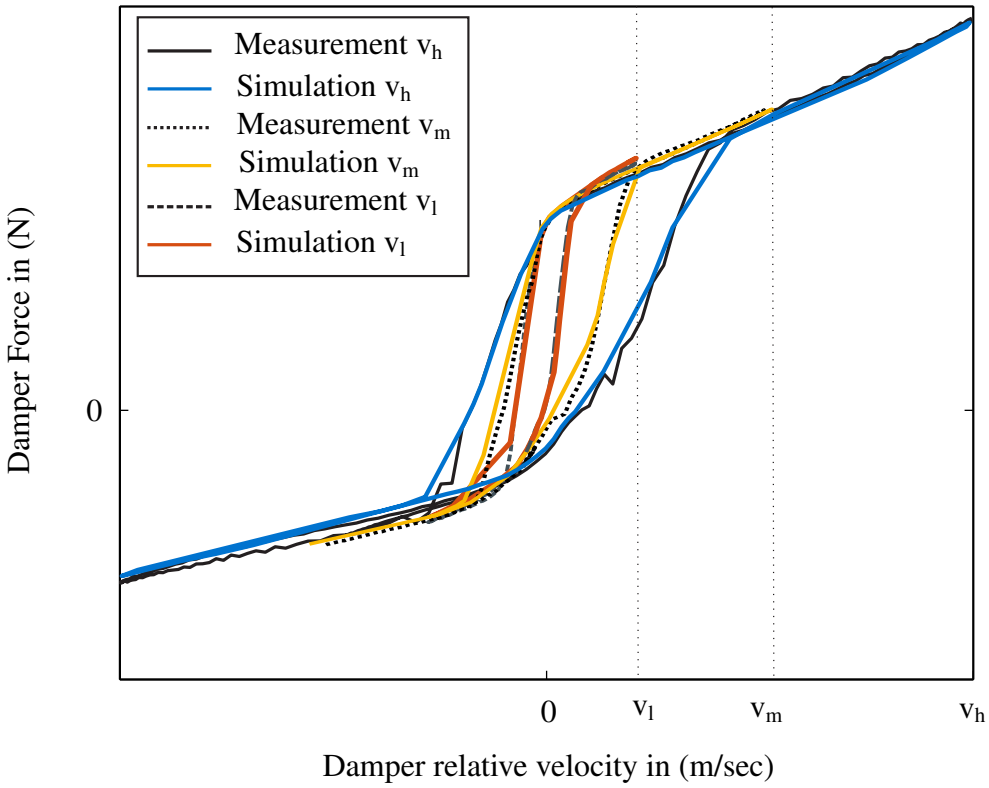

Figure 3.10: Identification result for the dynamic slope of the damper in passive configuration. Image is reproduced with kind permission of BMW AG.

Figure 3.10 illustrates the force-velocity relation for the semi-active damper when the external valve are closed, by exciting the device with low, medium and high symmetrical stroke

velocity, v_l, v_m and v_h respectively. As it can be seen, the model contains enough information, in order to reproduce the main dynamical effects of the damper. Estimation errors can be noticed, mainly in the compression direction, where constant deviations for different stroke velocities are obtained. This is mainly due to the challenging choice of the internal valves' parameters. The chosen rate between leakage and intake parameters of the rebound and compression directions does not allow to reduce this constant error. In any case, the shaping of the real force is outstanding recreated.

The presented detailed model allow to improve the knowledge of the major physical aspects, which influence the damping force. The precise information of time and force constants can be used model based control. Only minor imprecisions, due to the choice of the internal valves' parameters can be noticed mainly in compression direction. By the simulation with medium velocity a smooth force signal is obtained, while in the case of high and low velocities in the compression direction bending points in the force shapes are obtained, see Figure 3.10. The break point is generated by a stepwise change in the valves pressure state. That induces an inauspicious variation of the valves' operating state, the flow rate through the assembly rashly increases and the second damping rate is prematurely achieved.

The main disadvantage of the physical model is the computational time needed to run a simulation. Especially in the identification process, the choice of the parameter set values strongly influences not only the results but also the computation costs. To increase the optimization time, a parameter range is defined. In any case, due to the nonlinear relation of the parameters and the high complexity, a stable numeric solution is not always guaranteed.

External valve dynamic

In Section 3.5 two models are proposed. While the first is described in [116] and therefore is only summarized in this Thesis, the second one is detailed in the following.

Through the description of the flow dynamics in external valves a good prediction of the static and dynamic behavior of the damper are obtained. However, due to the strong model simplification and the assumption of a laminar flow and linear current dependency, a lack of precision in the force shape, in case of high voltages, is noticed, [116]. In this previous work, only the characteristic curves for different currents are simulated, since the model does not

allow to integrate hysteresis effects.

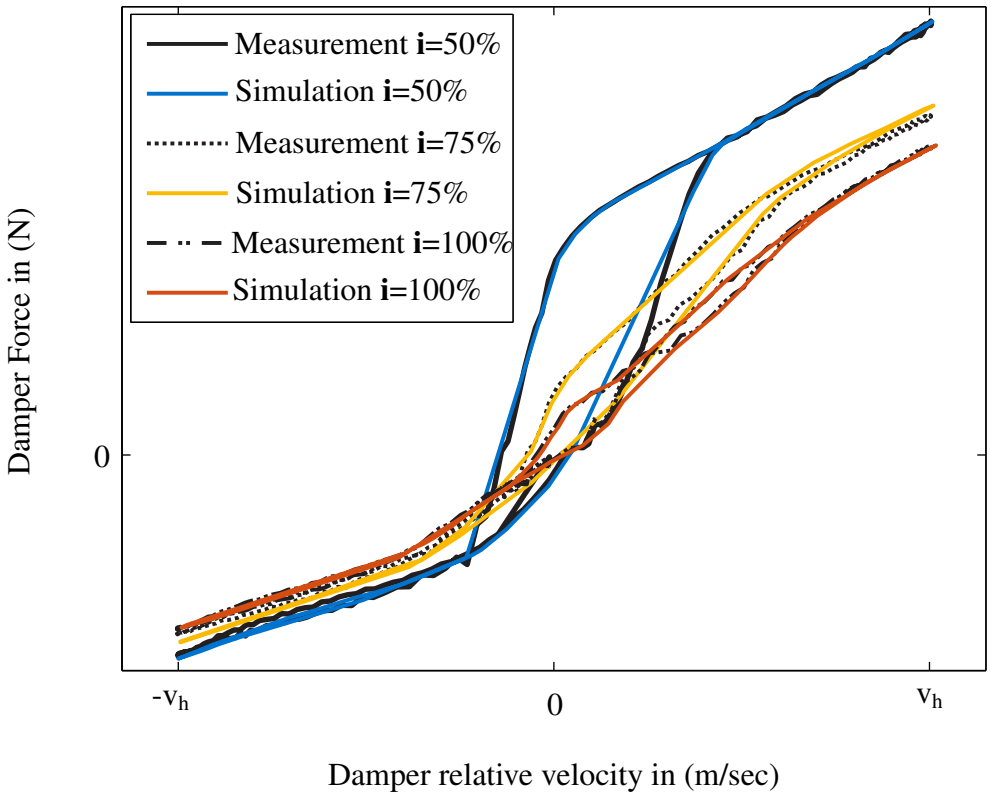

Figure 3.11: Simulation results of the complete physical model of the adjustable damper for high velocity stroke. Image is reproduced with kind permission of BMW AG.

The hydraulic model of the external valves takes this aspects into account. As reported in Section 3.5.2, by applying a voltage the valves open and let oil flow into the reserve chamber. In this process, the pressure of the considered pressure chamber is reduced and consequently the force decreases. Due to the pressure change in the reserve chamber also the pressure drop above the base valve shows traces of dynamics variation, which again influences the flow rate above the piston valve.

Figure 3.11 reports the optimization results for a high velocity stroke (v_h). Three simulations of different current settings are compared with the corresponding measurements. It can be noticed, that the damping effects for high velocity mainly corresponds to the characteristic curves and the are reproduced very well by the physical model. Also the constant error at negative velocities, which was underlined in Figure 3.10 is clearly reduced. However, the

excellent force match is slightly deteriorated the by a lack of precision in the hysteresis effects, when currents are applied. The minor deviation in the hysteresis modeling are increased due to the challenging definition of the relationship between some valves parameters (particularly K_{intake} as described in Section 3.4). The main effects can be noticed considering the **i**=50% simulation and its measurement, mainly in rebound direction around $0\,{}^{\mathrm{m}}/_{\mathrm{sec}}$. Generally, it is noted that the main inaccuracy are at the strokes' beginning. In any case, besides the minor discrepancy between measurement and simulation, an overall very good representation can be achieved for the semi-active dual-tube damper.

3.10 Summary

In this Chapter a precise semi-active damper model, which considers internal and external valves together with fluid dynamic effects is presented. The model of the passive damper is extended with two independently adjustable electromagnetic valves, which capture the continuously variable damping effects. The fluid dynamic effects are derived from the compressibility of the oil, the geometry of the damper and the adiabatic compression of the gas. The electrical model of the damper's power unit also incorporates an internal current controller.

Two basic identification precesses are adopted, to estimate the damper behavior: quasi-static and dynamic tests. The model parameters are classified into three groups: geometrical parameters, valve parameters and quasi-static parameters. The first ones are determined form drawings, while both the quasi-static and the valves ones are estimated by means of identification procedures. The unknown physical model parameters are estimated with a genetic algorithm and a gradient-based optimization method to match measurement data.

Due to the amount of detailed information, the switching differential equations have to be solved using variable step algorithms. Therefore, the presented model is not suitable for model based control in real-time application. Moreover, the identification process is computationally inefficient and it is optimized only for the device used in this Thesis. Hence, there is a need to develop a functional model, which can be easily parametrized and can reproduce the main nonlinear damper effects. This model is presented in the next Chapter.

Chapter 4

FUNCTIONAL DAMPER MODELING

In this Chapter hydro-mechanical and thermodynamical aspects, which are able to modify the damper response, are considered. The aim is to obtain a framework suitable for controller purposes, which allows to exploit the fast dynamic of modern semi-active damper in real time applications. Based on some considerations of Chapter 3, a first model is proposed in Section 4.2, which simplifies the electrical and mechanical damper characteristics with lag elements. Its dynamical frequency response is studied and compared with the state of the art solution. Due to the lack of precision a second model is proposed.

According to examples of physical phenomena already described in literature, a functional damper framework is presented in Section 4.4, which considers the major physical aspects treated in the previous Chapter. The structure of the model is kept suitable for different devices and the number of parameters to be identified is minimized.

Comparing the measurement results to the model output, the simulation performance is considered to introduce or overcome physical effects. Aspects like model costs and complexity, time calculation needed for the determination of parameters and numerical problems in the simulation have been considered and thus only relevant effects are included in the modeling.

The obtained model is extended by the suspension strut components (see Appendix A) and integrated by the top mount element. Simulation and measurement matching results are proposed in Section 4.5.

4.1 Motivation for hysteresis modeling

Hysteresis effects strongly influence the response of a dynamic system, since it represents the characteristic to react in a delay to the applied excitation and in dependence on the previous state. As remarked in Chapter 3, the hysteresis in a damper is usually caused by the high

pressure in the internal tube, which acts on the fluid compressibility and on internal elements (e.g. structural components) that minimally expand and contract during operation. In addition, the hysteresis impact significantly increases with increasing frequency of the damper relative velocity. Therefore, for controller design purposes a model of hysteresis is required, [67]. Several models, like the Chua-Stromsmoe model, the Mayergoyz' monograph, the Preisach and the Bouc-Wen model have been proposed for this purpose: A survey can be found in [133, 169].

Several idealized mechanical model both for ER or MR dampers can be found in the literature. As the considered device is based on hydro-mechanical principles, mainly the latter are considered. A review of models for controllable fluid dampers and phenomenological models based on Bouc-Wen model is reported in [151], while [74] presents a model for a symmetric hydro-mechanical device. However, these models do not reproduce the dynamic behavior of the continuously variable hydraulic damper adopted in this These with sufficient accuracy. The main reasons are the inherent symmetry assumptions of the damper characteristic and consequently the symmetrical hysteresis effect and the presence of magnet field effects. Therefore a new hysteresis model, based on the ones in [74, 151] is presented in this Chapter and compared to the state of the art structure (see Figure 2.5), [117].

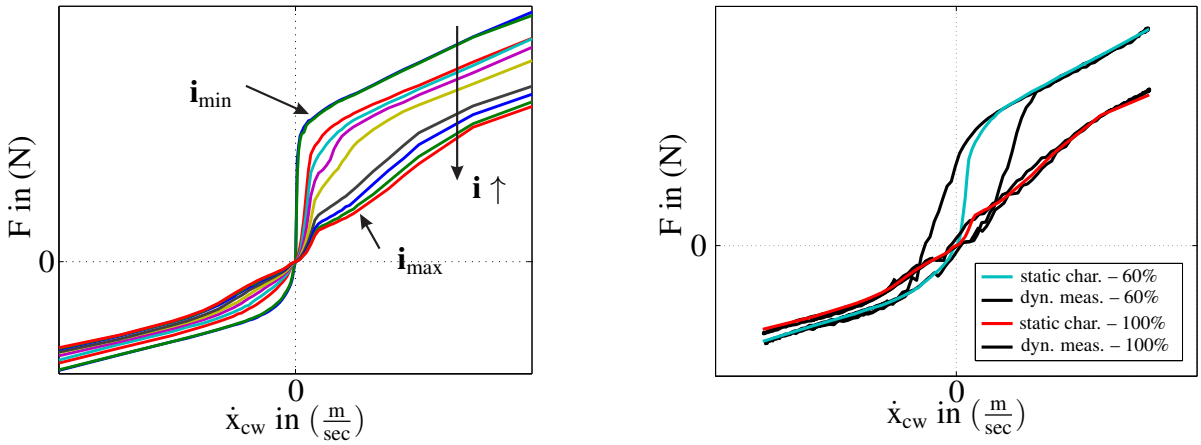

(a) Static characteristics of the continuously variable damper

(b) Static characteristics versus measured damper force

Figure 4.1: Static and dynamic damper behavior at high velocity stroke. Image is reproduced with kind permission of BMW AG.

Figure 4.1 shows the difference between the static damper characteristics and the measured

force produced by the damper. The measurements are taken at the damper test rig, see Appendix A.5, by exciting the device with sine waves, according to [128]. The produced damper force is recorded by a load cell, see Figure A.5. The hysteresis effects are depicted for two different valves' settings, 60% and 100% of the maximal current. As expected an asymmetric current-dependent dynamical effect is noticed: "hard" valves' settings that have a higher damping coefficient lead to more energy dissipation than the "soft" ones. For strokes with higher velocities the static characteristics match the real behavior very well. The area in the centre of a hysteresis loop is the energy dissipated by the damper, which varies depending on the current settings.

In this Chapter, simplified models are proposed, in order to fill the gap between the static characteristics and the real measurable damper force.

4.2 Electrical and mechanical time constants

Although a complex modeling approach based on physical insight for the dynamic behavior of the semi-active dampers has been presented in the previous Chapter, a more transparent, controller design-oriented modeling approach for the semi-active device is intended. By means of the detailed analysis in Chapter 3 the conclusion is that the dynamic behavior of the semi-active damper, in a first approximation, is determined by switching proprerties of the valve and by the fluid characteristics. Since the power electronic unit provides for internal control of the currents, the time constant of the closed loop can be considered an accurate model for electrical terms. Considering that the fluid response depends on the stroke direction and on the valve operating state, including switching direction (from soft to hard or vice versa), the choice of an adequate model is more challenging.

The magnetic valves of the damper are actuated by the valve currents, which are influenced by the inductance of the valve and the properties of the power electronic unit, see Section 3.8. The tracking control of the desired damper current is accomplished by an internal PI-controller of the power electronic unit. As can be seen in the step response of the valve current (Figure 4.2), the resulting current dynamics can be well approximated by a first-order low pass filter with a small time constant of about $1\,\mathrm{msec}$.

Due to the hydraulic properties of the damper and the inertia of the oil, the measured damper

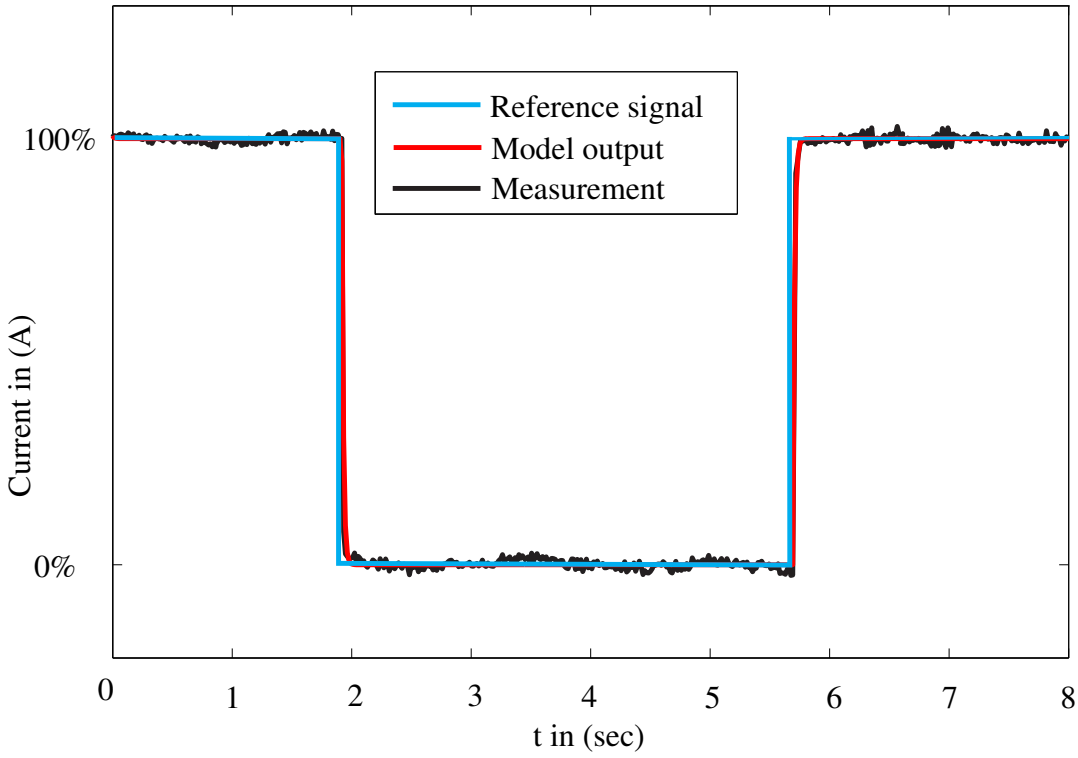

Figure 4.2: Damper current step response (measurement and simulation)

force has a time lag compared to the damper force calculated from the static damper characteristic and the measured relative damper velocity, [116]. Aiming to an approximation of the fluid dynamics, which allows real time applications, although the time constant differs for the distinct operating modes of the damper, a first-order low pass filter is adopted. An average time constant of $10\,\mathrm{msec}$ is considered.

As a result, the damper dynamics are taken into account using the two transfer functions. The mechanical dynamics is described by $G_m(s)$ while the electrical dynamics are characterized by the transfer matrices $\mathbf{G}_{el}(s)$, [93].

By comparison with measurements, the mechanical time constant is chosen such that, the model gives best possible results in the frequency range 4-8 Hz, which is considered an important range for control vehicle control purposes, see Section 2.4.

In Figure 4.4 a frequency analysis of the body acceleration is shown. The frequency response of the sprung mass is compared to the ones modeled by meaning of the nonlinear quarter-car

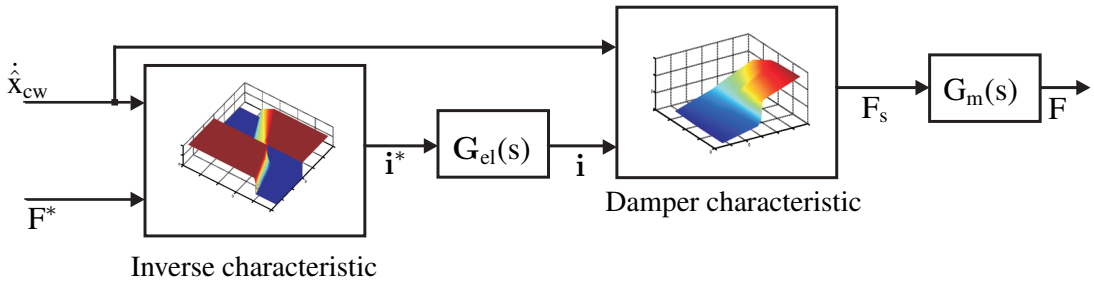

Figure 4.3: Damper model and feedforward control, according to [93, 96, 98]

model (Appendix A), where the damper force is calculated by the static characteristics or by the structure in Figure 4.3, which includes the electrical and simplified mechanical damper dynamics. The results are obtained considering as excitation a chirp-sine wave with maximal frequency of 25 Hz. It is noted, the state of the art solution (SoA) reproduces the amplitude response well but does not match neither the first nor the second natural frequency.

By adding the dynamic components the response at the first natural frequency is amplified and the accuracy is deteriorated, while by the second natural frequency the peak is shifted to the measured one but strongly amplified.

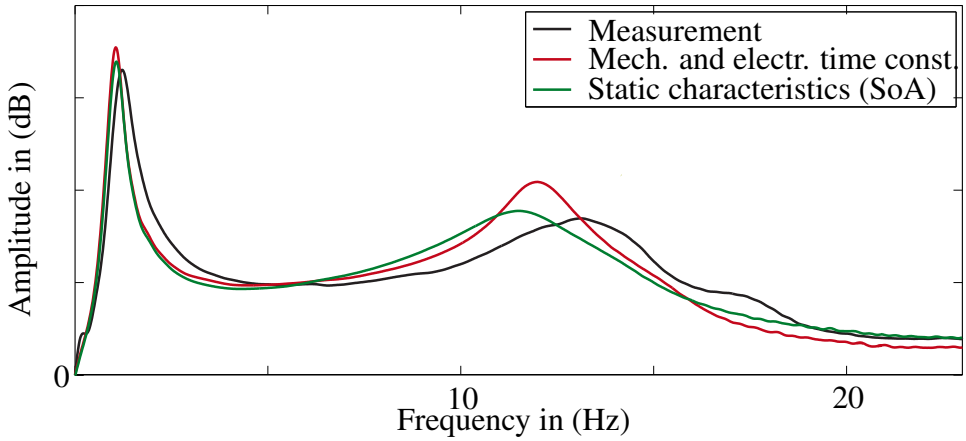

Figure 4.4: Frequency response comparison: $G_{\ddot{x}_c,\dot{x}_g}$

Although the frequency analysis still shows discrepancy between the modeled and the measured response, the electrical and the mechanical dynamics are taken into account for the semi-active damper modeling. The basic structure, presented in state of the art in Section 2.2.2 (Figure 2.5), is kept and extended with the time constants. This model structure (see

Figure 4.3) of the semi-active damper is suitable for controller design and has been already successfully applied, e.g. as presented in [93, 97, 98].

4.3 Description of the main mechanical and physical aspects

In general, dampers are modeled by means of their static characteristics both for application and for controller design purposes, see Figure 2.3(a). However, this framework only roughly reproduces the behavior of a real device and therefore lack of precision is found comparing the simulation with the measurement as shown in Figure 4.4. Even the electrical and mechanical approximation by first order lag elements only slightly improves the performance, more accuracy is required to exploit the hardware device dynamics and successfully apply a model-based control strategy. Based on consideration on fluid and hardware effects, the main physical effects, which occur in the damper tube, are reported and approximated by functional elements, [163].

Firstly, the construction and fluid characteristics of the damper are analyzed. As reported in [44, 101], due to the damper construction material, the damper case is not perfectly rigid. The rigidity of the cylinder walls has the major effect on the oil pressure in the chambers. The fluid itself, which flows through the valves building up pressure in the three chambers, is considered compressible. In addition, the complete behavior of the the damper does not only depend on the fluid characteristics but also on the mechanical switching elements. Moving parts and elasticity of discs in the valves' assembly have influence on the force behavior. Considering the switching time as the interval of time in which 90% of the final force is reached, it has been experimentally investigated, that it varies between $7\,\mathrm{msec}$ and $35\,\mathrm{msec}$ for the considered damper. According to [69], it depends on the absolute damper velocities, on the stroke's direction as well as on the switching direction (from soft to hard or viceversa). This effect relates the strokes velocity, which is generally not the velocity of the oil through the valves' assemblies, to the current applied and the resulting damping force. This phenomenon is strongly nonlinear and very challenging to describe. All these aspects can be reproduced by a spring element with variable stiffness, which emulates the current-depending switching properties, [117]. Moreover, to recreate the effect of inertia of the oil flowing between the chambers, two further elements are introduced: a mass and a lag element. While the first one is constant and represents the fluid and valve assembly characteristics, the second depends on

the oil velocity in the pressure tube and relates the hysteresis effect to the switching behavior.

Moreover, the structure of the internal valves' assemblies, which determine the static characteristics of the damper and consequently the asymmetrical behavior of the damping force (Figure 2.3(a)) have to be included, since they define the slope (first and second damping rates), depending on the damper relative velocity and current.

As reported in Section 3.7, the variation of the viscosity and density of the fluid is omitted and consequently the effect of the hydro-dynamical friction, due to the motion of mechanical components is not included, in order to maintain transparent model structure. Therefore, to guarantee comparable results, it is assumed that the damper is heated up at a constant working temperature before recording measurement data.

Since an elastomer element is attached between the damper and the sprung mass to isolate the body from high frequency vibration induced by the suspension strut, a model of the damper mount has to be included in order to validate the model. Due to the fact that the transmitted force includes not only the contribution of the damper, but also from the spring and the elastomer, the top mount framework is not discussed at this point and it is addressed in Section 4.5.

4.4 Functional semi-active damper modeling

According to Section 4.3 and to the results obtained by considering only time constants in Section 4.2, it is noticed that mainly mechanical effects are given by the hysteresis phenomena, taking place inside the damper. Due to their complexity, hysteresis phenomena have been a subject of intensive mathematical and engineering research, see e.g. [169].

A precise damper model is aspired, in order to fully exploit the potential of these fast modern devices. The impact on control system performance of these phenomena can be significant and in order to better predict the system response, a model-based structure is desired for employing model based control techniques, which incorporate in the controller design hysteresis effects and dynamics of the damper force generation. Since the electrical behavior is well represented by the time constant, the functional model, addressed in the the following, tempts to reproduce the dynamical effects of the device.

The new hysteresis model, based on the ones in [74, 151], reproduces the gas force, the viscous damping without hysteresis for high velocities and the shape of the hysteresis curves depending on the valve settings. The proposed mechanical model of the damper is presented in Figure 4.5, [117].

It allows to reproduce the dynamic part of the gas force (denoted by c_0 associated with the displacement x_{cw}), the damping effects in case of high velocities and the hysteresis damper behavior (c_1,d_1).

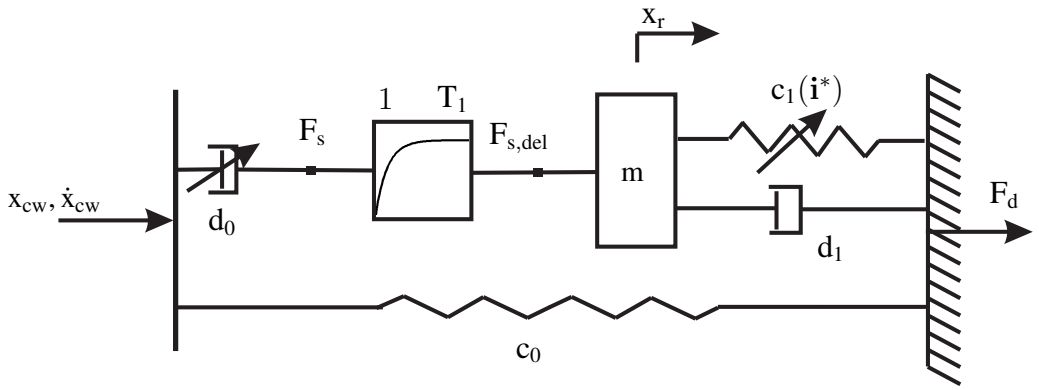

Figure 4.5: Functional hysteresis damper model, [119]

The shape of the damper force is defined by the character of d_0, which is reflected by the static characteristic field. From experimental evidence a first order lag element (time constant T_1) is needed to model the internal force rise time $F_s = f(v, \mathbf{i}^*)$, where $v = \dot{x}_{cw} - \dot{x}_r$ i.e.

$$\dot{F}_{s,del} T_1 + F_{s,del} = F_s, \tag{4.1}$$

where, as shown in Figure 4.5, $F_{0,d}$ represents the internal force after the delay. The hysteresis effects are modeled by the mass-spring-damper system, where the spring characteristic c_1 influences the shape of the curves depending on the current. The dynamic equation for the damping force F_d[1] is obtained as

$$F_d = d_1 \cdot \dot{x}_r + c_1(\mathbf{i}^*) \cdot x_r + c_0 x_{cw}. \tag{4.2}$$

[1] the index d is referred to quantities which include dynamic effects

For the respective model parameters, identification techniques based on genetic algorithms have been performed as to minimize a cost function J (see (2.23) in Section 2.5.1) defined by the mean square error between the measured and the modeled force. It is noted, that the choice of the damper force as referring force for the analysis is the only possible, since the damper force is the only value, beside the valves' currents, which can be measured on the device at the designed test rig. To ensure numerical stability of the model, the mass parameter m is chosen to be $2\,\mathrm{kg}$ and the parameter d_1 is optimized for strokes with high velocity, [117, 119].

The stiffness $c_1(\mathbf{i}^*)$ is analyzed in terms of the cost function J with respect to all current settings. Thereby, the same current is applied for rebound and compression states, respectively. Figure 4.6 shows the optimization results, where J is illustrated as a function of $c_1(\mathbf{i}^*)$.

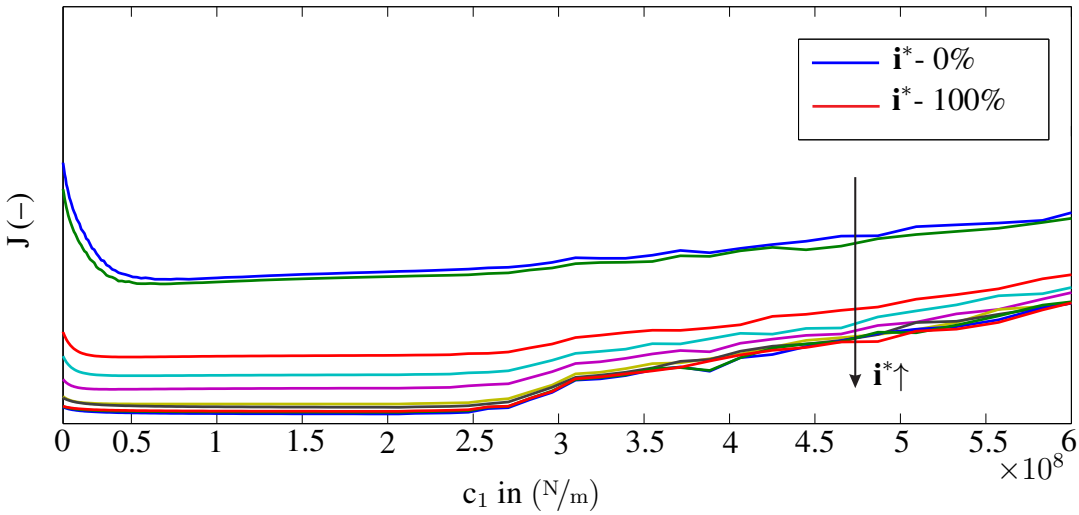

Figure 4.6: Cost function development for different currents at varying damper model stiffness c_1

4.5 Model matching and force rise time

Even if the stiffness tends to increase with the stroke velocity and has a strong dependence on the applied current, the respective cost function J shows only minimal variation, [117]. Therefore, considering that the respective minima in Figure 4.6 are all achieved for similar values of the stiffness, an average value $\bar{c}_1$ is chosen in order improve the real-time application. According to previous analysis in Section 4.2, the electrical dynamics of the damper are

approximated by a first order lag element with a time constant of $1\,\mathrm{msec}$, [119].

In the following, the results obtained by the damper model are compared to the static characteristic ones by taking the measured force signal as reference. The damper is excited by a ramp-input and by a sine wave and the results are reported in Figure 4.7. The variation in time of ramp-input with a current switch from 50% to 100% and the velocity/force devolutions are shown in the upper plots of Figure 4.7. The peak of the force generated from the static damper characteristic is higher compared to the proposed model result and the measurement. The deviation is due to the approximation error introduced by the choice of a constant stiffness and the other model simplifications. Similar conclusions are drawn in [117], where additional analysis on switch behavior from 0% to 100% of current values are reported.

In the previous work [117] the analysis includes a current-depending variable stiffness to model the hysteresis effects. However, due to the cost function behavior (see Figure 4.6), for the following investigations and controller design, the configuration with a average stiffness value is considered, since the the damper force is reproduced.

As underlined in Figure 4.1(b), the hysteresis effects are more evident in case of minimal current, meaning higher damping coefficient. In order to validate the proposed model in such configuration, the hardest settings are chosen and the results of a sine wave excitation are depicted in lower plot of Figure 4.7. It can be noticed, that the measurement shape, due to the mechanical characteristics of the device (primarily the force rise time) is taken into account by the new damper model.

It is possible to conclude, that even if minor prediction errors are still present between the real force and the modeled one, the proposed damper model matches the measurement data better than the static damper model does.

4.6 Top mount strut model and test rig validation

Until the previous Section only the damper device has been considered. Since the model is required to control purposes, its behavior has to be integrated in the complete quarter-car model presented in Appendix A. That means, that the contribution of the suspension strut kinematic, the primary spring force, the end-stop effects, double wishbone friction and connection elements have to be considered. Therefore in this Section the new damper model is extended

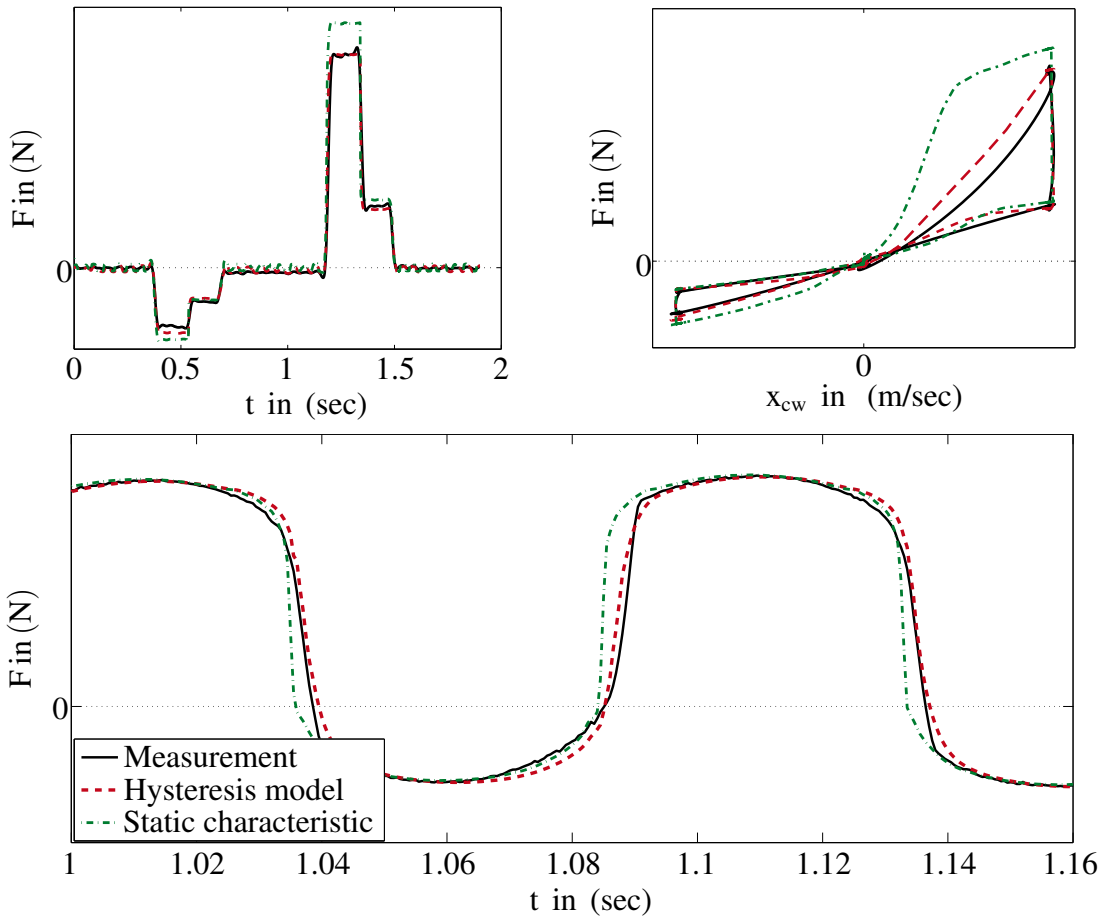

Figure 4.7: Example of ramp-inputs with constant velocity by adjusting external valves and mechanical model response with averaged stiffness by sinus excitation. Image is reproduced with kind permission of BMW AG.

with the top mount model. According to [54] this element can be modeled as a spring-damper device and experimental evidence shows a second order lag element behavior.

Since the load cell is mounted in series to the suspension strut, the measured force consists of the spring force, as well as friction and kinematic contributions of the suspension strut, (see Chapter 2.1 and Appendix A.3). Therefore, test rig nonlinearities are taken into account and their contributions is subtracted from the measured force.

The force transmission between the suspension strut and the chassis mass involves the filtering effect of the strut top mount, i. e. high frequency components of the force signal are absorbed. In Figure 4.8 the effect of this component is depicted in a Bode diagram.

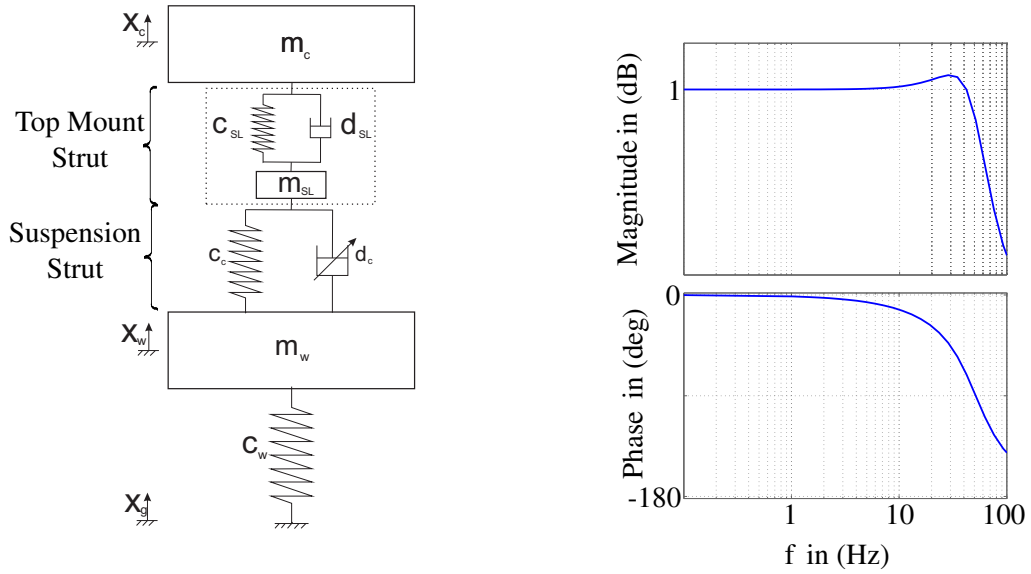

(a) Quarter-car model augmented by top mount, according to [54]

(b) Transfer function of the suspension strut top mount

Figure 4.8: Model and dynamic of top mount strut, [119]

Figure 4.9 shows the quantity calculated from the load cell measurement (black line) in comparison whit both damper models. From the measured signal, recorded by the load cell (see Appendix A.2), the modeled nonlinear effects are subtracted and only the damper force is depicted. Both the quarter-car test rig and the simulation models are excited by a real road profile (P1, see Section 2.6). In order to point out the capability of the new model, two extreme current settings are displayed. The experimental results are reported in terms of the damper force rise.

In the upper plot, the device works on the hardest characteristic, i. e. the damper currents are set and kept to the minimal percent (0%) of the maximal current. It is noted that due to the high damping coefficient, hysteresis effects are significant (see also Figure 4.1(b)). As it can be noticed, the proposed model is able to follow the measurement thoroughly better than the one based on the static characteristics. Not only the maximum force values show enhanced prediction, but also the build-up behavior can be improved. By keeping the current constant, the only difference between the models can be led back to the dynamics. It can be concluded, that the static characteristics have a lack of information in the internal oil dynamics.

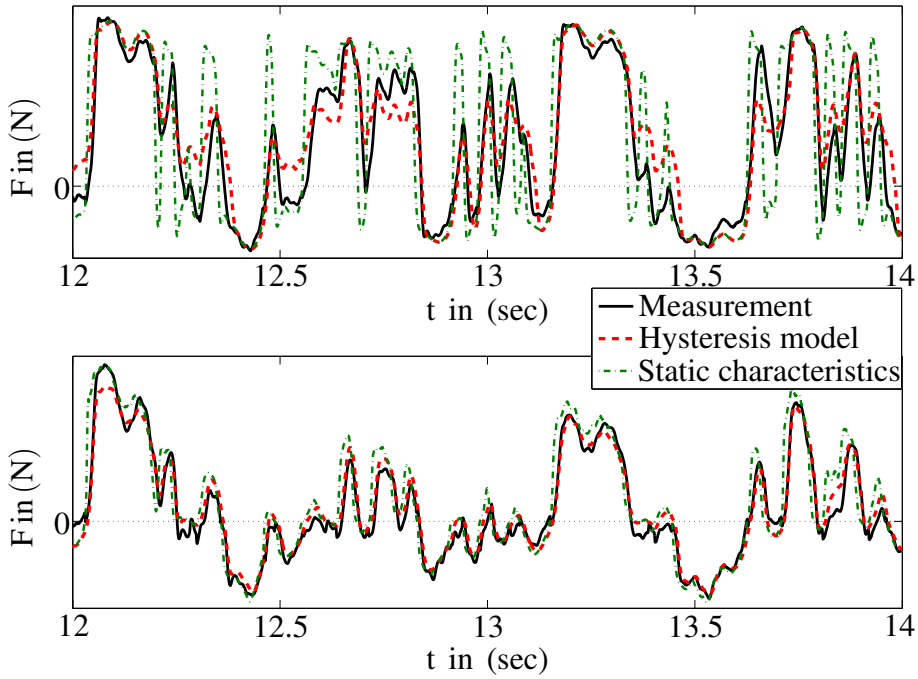

Figure 4.9: Damper force comparison: hard setting ($\mathbf{i} = 0\%$) and soft setting ($\mathbf{i} = 100\%$)

In the lower plot of the same Figure, the device is driven with a valve current of 100%, meaning that both valves are set to the softest characteristic. As already noted in Figure 4.1(b), differences between the static behavior and the hysteresis model are quite limited, due to the minimal damping coefficient. Both models reproduce the measurement to an acceptable extent. Though, particularly the force build-up behavior of the static characteristic model shows a lack of precision, while it is represented sufficiently well by the newly proposed model.

As presented at the beginning of Chapter 4, a frequency analysis of the complete behavior of the suspension system is proposed. The influence of the new damper model is remarked comparing the measurements with the simulated signals of the state of the art (SoA) damper model and the new functional model, proposed in this Thesis, see Figure 4.10.

As it can be clearly seen, for instance considering the sprung mass response (upper plot), the damper model of Section 4.2 shows an excessive increase both by the first and the second natural frequency. Moreover, comparing the response to the measurement, both peaks are shifted to the lower frequency range respectively. A similar behavior is shown by the static characteristic, which does not increase the maximal gain by the natural frequencies as much as

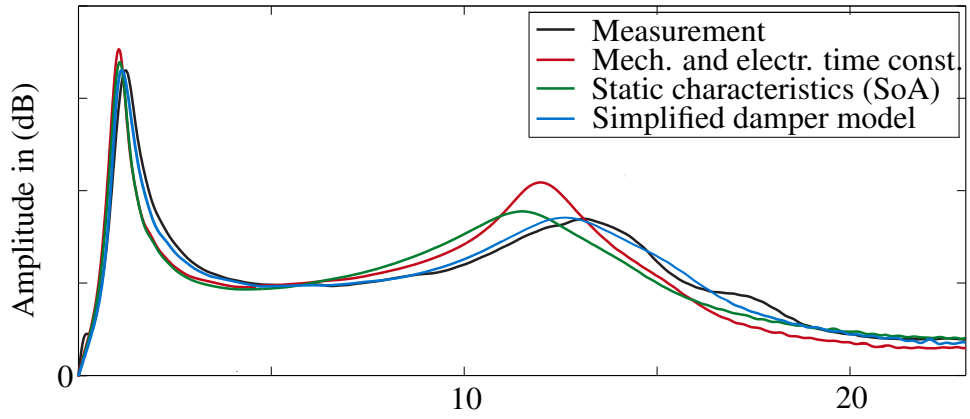

(a) Frequency analysis of the sprung mass acceleration

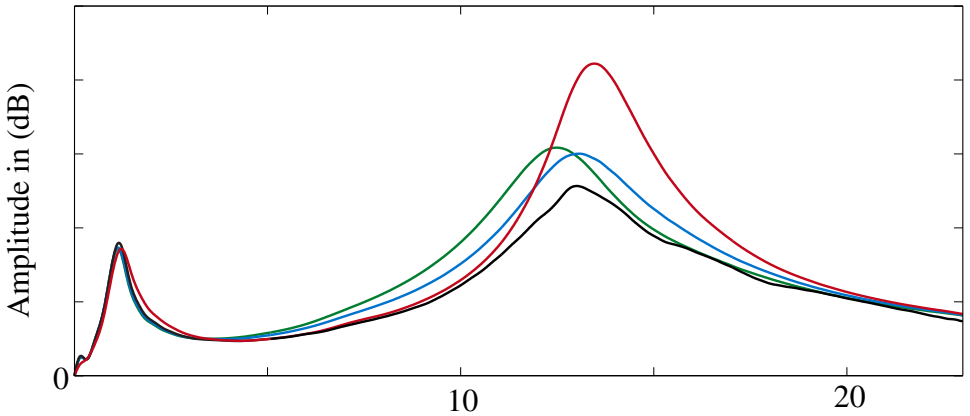

(b) Frequency analysis of the dynamical wheel load

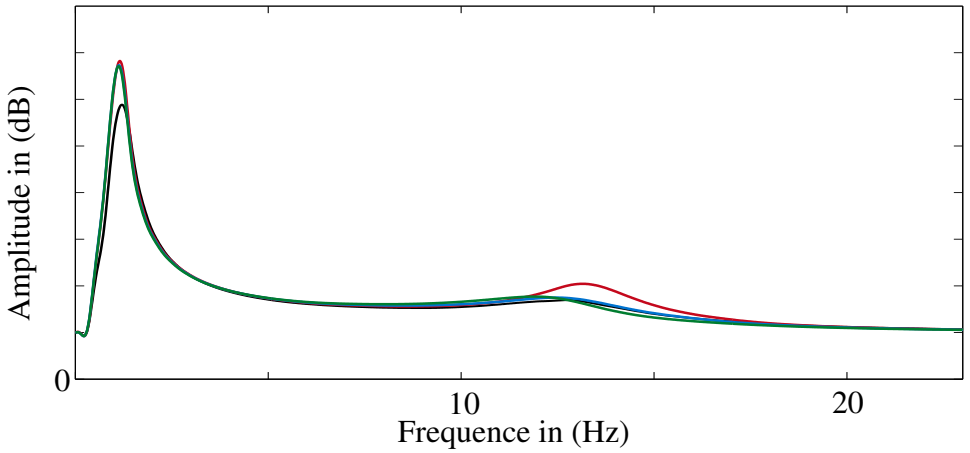

(c) Frequency analysis of the suspension deflection

Figure 4.10: Frequency analysis and comparison of the presented damper models

the model with mechanical and electrical time constant does. Considering the new proposed hysteresis model it can be noticed that, at the sprung mass as well as at the unsprung mass frequency its response follows the measurements well compared to the other models.

Slightly different are the frequency responses given by the dynamical wheel load, see Figure 4.10(b). While the first peak is simulated well by all models, the second eigenfrequency presents a similar situation, as described for Figure 4.10(a). Namely the excessive gain of the model with electrical and mechanical time constant is clearly remarked and the displacement of the static characteristic field is also present. Even if the amplitude is not matched also by the new presented model, however, the shape in the frequency is preserved and the second peaks is simulated with the same frequency of the measured signal.

Marginal differences can be noticed by the third frequency response figure. Analyzing the amplitude in details, it is noted that at the chassis eigenfrequency none of the proposed models match the measurement data. Moreover, the damper model, extended by the electrical and the mechanical constants, presents an elevation at the wheel eigenfrequency.

An interesting discussion can be also drawn considering the frequency range 4-8 Hz, see [2] and the description in Section 2.4. Figure 4.10(a) shows that, even if the time constants are chosen to minimize the gap between measurement and model in this range, a better result can only be obtained by considering the hysteresis effect and including the oil characteristics. The response of simplified damper model and the model with time constants reach comparable results by considering the dynamical wheel load frequency response. In Figure 4.10(b) the minimal gap between the red and the black lines can be noticed. If the third frequency response is considered, due to the minimal differences in this range, none of the models present clear advantages. It can be resumed, that including the dynamic characteristic of the damper by considering the major physical effects studied in Chapter 3 improves the matching between model and measurements. Therefore, in the next Chapters the actuator control structure is designed by considering the new functional damper model.

4.7 Summary

In this Chapter, a novel hysteresis model for a semi-active damper has been presented, which can be used to describe a broad spectrum of dampers. The advantage of the new control-

oriented damper model is that the few unknown parameters can be identified using only measurements, which are already available in the automotive industry in order to obtain the static characteristic of the damper. This support either increases the interest for model-based damper control strategies also in industrial processes, where different devices, for different car classes, can be identified without much effort.

The identification process has been shown for a real damper with strong hysteresis effects and the validation shows, that the model matches the measurement data better than the state of the art solution. Furthermore, a study on the parameter variation has been presented and the influence on the shape of the hysteresis curves has been discussed.

Chapter 5

FEEDFORWARD CONTROL OF A SEMI-ACTIVE DAMPER

In case of suspension systems, the feedforward path represents the direct route within a controller which transforms the controlling signal calculated by the high-level control law (suspension controller) into an electrical signal, used to drive the external valves of the damper. A control system which has only a feedforward path responds to its control signal in a predefined way, without adapting its response to the variable operating conditions. Furthermore, dealing with a semi-active damper, whose characteristics depend on the suspension deflection velocity, a feedback of this variable is needed to obtain the current corresponding to the desired force. The state of the art solution is based on this controller structure. The novelty of the following approach is the introduction of damper dynamic and hysteresis effects to achieve better force tracking and thus a better performance of the suspension system.

This Chapter presents a dynamic feedforward control approach for a continuously variable hydraulic semi-active damper of a vehicle suspension, that makes use of a novel damper model. This model, introduced in Chapter 4, takes into account dynamic effects in the damper force generation by employing a new hysteresis description. The control-oriented model description can be easily adapted to diverse damper types and is suitable for real-time applications. In this Chapter it is underlined that by applying the new model-based structure the relation between valve current, velocity and force can be represented significantly more accurate compared to standard approaches, where static damper characteristics are used.

The pure feedforward controller structure is presented in Section 5.1, while the main characteristics of the two-degrees-of-freedom are depicted in Section 5.2. A detailed analysis of the controller of the feedforward strategy is reported in Section 5.3, where the working principle, the nonlinear gain characteristics as well as the controller parameter are discussed.

The structure is firstly studied in a simulation framework and the performance of the concept is subsequently validated in experiments on a quarter-car test rig by comparing the dynamic

control approach with the state of the art control using a skyhook controller and a linear optimal regulator as suspension controllers in Section 5.4 and Section 5.5. The new dynamic feedforward controller especially improves ride safety by enabling better force tracking in the range of the wheel resonance frequency.

5.1 Dynamic feedforward structure

In theoretical works, many control approaches for semi-active dampers are presented but in most practical applications skyhook and groundhook control laws are used, [3, 24]. At the same time only static force-velocity characteristics are utilized as a damper model by applying the feedforward structure presented in Figure 5.1. Therefore, the static damper behavior reported in Figure 2.5 of Chapter 2, is implemented in the feedforward component (FFW) and the driving current $\mathbf{i}^*$ is generated by the static characteristics to track the desired force F^*.

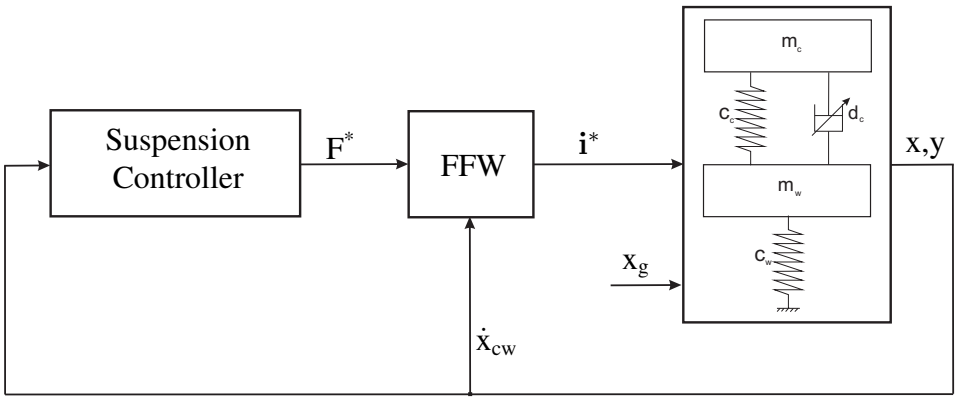

Figure 5.1: Hierarchical quarter-car control structure

Due to the considerations in Chapter 3 and Chapter 4 the enormous potential of modern semi-active dampers remains partly unexploited. Therefore, the aim is to apply the new hysteresis model presented in the previous Chapter, in order to take into account both the dynamic and the static force build-up behavior of the damper and thus improve the tracking of the desired force signal. Hence, the idea is to focus on the adjustable device and to exploit its characteristics in the complete frequency range and independently of the high-level control. The separation between high level control (suspension controller) and low lever controller (device

controller) in this Thesis increases the transparency and feasibility of the proposed control structures which enhance the state of the art solution.

The task of obtaining the dynamic valve currents $\mathbf{i}^* = \mathbf{i}_d$ needed to generate a desired force F^* is performed by means of a dynamic feedforward approach. Therefore, the dynamic model of the continuously adjustable damper is integrated in the feedforward control structure, as depicted in Figure 5.2. A general description of the properties of such a 2-dof control is presented in [14, 53]. Moreover, in [129] this structure is studied for control purposes of linear systems and a new state feedback strategy is discussed, while in a recent contribution a model-based feedforward strategy in frequency domain is discussed, [182].

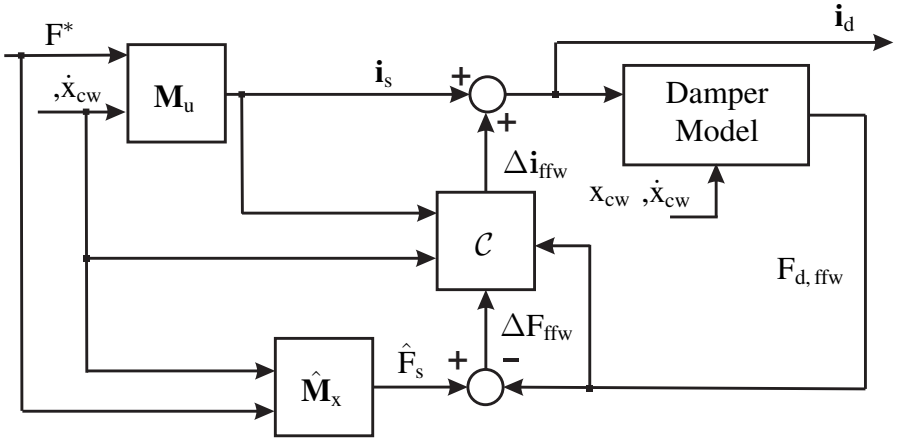

Figure 5.2: Model-based feedforward control structure (FFW), [117]

The static currents $\mathbf{i}_s$ are obtained by inversion of the static damper characteristics $\mathbf{M}_u$ in order to track the desired force F^*, i.e. the well-known state of the art approach is adopted. By means of the damper dynamics effects, i. e. $\hat{\mathbf{M}}_x$, forces are restricted to the working range of the damper including hysteresis effects. The limitations are obtained considering the force shape at the minimum and maximum current settings, respectively, and a high damper stroke velocity. It means, that the desired force is also allowed to be in the 2^{nd} and the 4^{th} quadrants, as the $F_{d,ffw}$ too. In particular the upper and lower bounds, which define the damper working space, are taken from the middle value of the measured hysteresis effect, when the device is excited by a sinusoidal signal, [128].

The limited and the dynamic force, $\hat{\mathrm{F}}_\mathrm{s}$ and $\mathrm{F}_{\mathrm{d,\,ffw}}$, respectively, are compared and a control strategy ($\mathcal{C}$) is applied. Basically, $\mathcal{C}$ compensates for the deviations between static characteristics (static model) and dynamic model. This topology represents a two-degrees-of-freedom (2-dof) structure, which is analyzed in detail in Section 5.2.

In [117] a proportional gain, guided by the sign function of the damper velocity, is proposed. Thereby the gain is experimentally fine tuned, such that a good tracking behavior is achieved, by means of root mean square value, see Section 2.5.1. Thus, a linear relation between force and valve settings is assumed. Since this assumption does not correspond to the reality, there is a need to enhance the control performance. In fact, by considering a linear relation, only the force different is considered, while the damper asymmetry, the stroke-dependent and current-dependent hysteresis are not taken into account. Therefore, a detailed analysis of the nonlinear controller is presented in Section 5.3.

5.2 Preliminaries on two-degrees-of-freedom structure

The degree of freedom of a control system is defined by the number of closed loop transfer functions that can be adjusted separately, e.g. by means of multi-objective optimization. This structure was already stated by Horowitz in 1963, [75]. Although disturbances could act on the plant or influence the measurements, they are not considered in the presented structure and are not further investigated in this Thesis.

To facilitate the analysis, both the plant (Damper Model) and the compensators ($\mathbf{M}_\mathrm{u}$ and $\mathcal{C}$) are considered to be linear elements. Since $\hat{\mathbf{M}}_\mathrm{x}$ only restricts the signal to the damper working range, it can be omitted for the following qualitative analysis. For the linear case, it can be shown, that the steady-state error becomes zero robustly if the plant does not show differentiating behavior and if the requirements on the controller are fulfilled. Indeed, the relations

$$\lim_{\mathrm{s}\to 0} \mathcal{C}(\mathrm{s}) = \infty \qquad \text{and} \tag{5.1}$$

$$\lim_{\mathrm{s}\to 0} \frac{\mathbf{M}_\mathrm{u}(\mathrm{s})}{\mathcal{C}(\mathrm{s})} = 0 \tag{5.2}$$

hold. According to the tutorial paper of Araki, the condition can be satisfy by designing the feedback with an integrative effect, while keeping the feedforward by a proportional ac-

tion, [14].

Since the structure proposed in this Thesis is nonlinear, some considerations about its behavior are discussed in Section 5.3.

5.3 Analysis of the nonlinear controller of the dynamical feedforward structure

The proportional feedforward control approach solution presented in [117] is modified by an integral contribution, in order to reduce the deviation of the feedforward force component $F_{d,\,ffw}$. The integral gain is limited in its working range to prevent wind-up effects, due to the integration effects outside the upper and lower bounds of the damper, [39]. In this case, the force tracking error increases and the algorithm calculates a rising desired damper action, even though the damper cannot be exploited anymore. This precaution slightly increases the tracking performance compared to [117].

As the relation between damper force and valves' currents is nonlinear and due to the asymmetric nature of the damping system, every feedforward force component $F_{d,ffw}$ has to be related to the actual damper relative velocity. In fact, the same feedforward force error ΔF_{ffw} causes different $\Delta \mathbf{i}_{ffw}$ depending on the absolute value and on the sign of $\dot{x}_{cw}$. Therefore, a relation is needed to compensate the nonlinear, asymmetric damper behavior. Hence, the nonlinear gain $\frac{\partial F}{\partial i}\big|_{\dot{x}_{cw}}$, calculated from static characteristics, is introduced, which can be applied to the controller error in order to weight the currents' variation corresponding to the force deviation, see Figure 5.3.

By adopting the nonlinear gain, the force differences between the static characteristics and the hydraulic model are not multiplied by a constant factor anymore. The scaling gain is incorporated into a nonlinear structure relating ΔF_{ffw} to $\Delta \mathbf{i}_{ffw}$, see Figure 5.4. As the mechanical constraint of the damper shall be included in the controller design as well, the controller input ΔF_{ffw}, is also related to the suspension deflection velocity and to the damper force by the signum function of $F_{d,ffw}$. Thus, every ΔF_{ffw} is scaled by a variable positive factor subject to the actual relative damper velocity $\dot{x}_{cw}$ and the already applied current $\mathbf{i}_s$.

Firstly the force error is related to the dynamic model force, by means of its sign, which defines the effect of the hysteresis build in the damper model. The resulting force value is then applied against the nonlinear gain, which scales the force value to the corresponding

current, evaluated by the actual damper relative velocity, $\dot{x}_{cw}$. Hence, the consequent variable current is passed trough the controller $\mathcal{R}_{ffw}$, which generates the variable $\hat{\mathbf{i}}$. The compensator $\mathcal{R}_{ffw}$ is discussed in detail in Section 5.3.2. Before obtaining the output of the structure $\Delta\mathbf{i}_{ffw}$, a weighting function is integrated in the structure shown in Figure 5.4. Thereby a smooth control signal, despite the steep change of the gradient in the transition range between rebound and compression (see Figure 5.3) is generated, which is then added to the static currents i. e. $\mathbf{i}_d = \mathbf{i}_s + \Delta\mathbf{i}_{ffw}$.

By introducing a weighting function in the transition range between rebound and compression a dead zone is defined. It prevents that jerk effects occur in the control variables $\Delta\mathbf{i}_{ffw}$, by allowing only a smooth transient. For this purpose the dead zone is defined as a quadratic function as follows

$$\Delta\mathbf{i}_{ffw}(t) = \begin{cases} \hat{\mathbf{i}}(t), & \text{if } |\dot{x}_{cw}| \geqq \dot{x}_{cw,dead} \\ \left(\frac{|\dot{x}_{cw}|}{\dot{x}_{cw,dead}}\right)^2 \cdot \frac{\partial\hat{\mathbf{i}}(t)}{\partial t}, & \text{if } |\dot{x}_{cw}| < \dot{x}_{cw,dead}. \end{cases} \tag{5.3}$$

Within the dead zone the weighting factor depends on the previous currents value. The choice

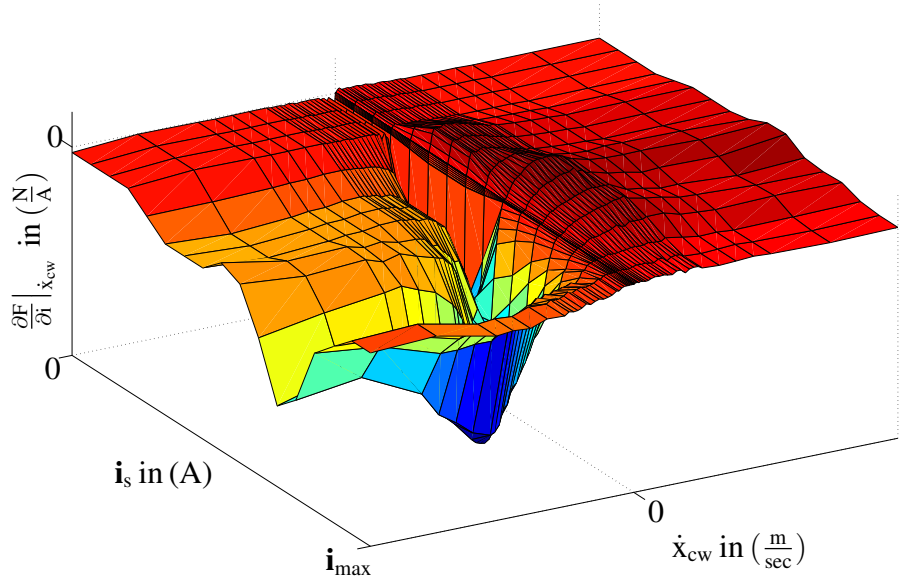

Figure 5.3: Velocity-dependent nonlinear scaling gain

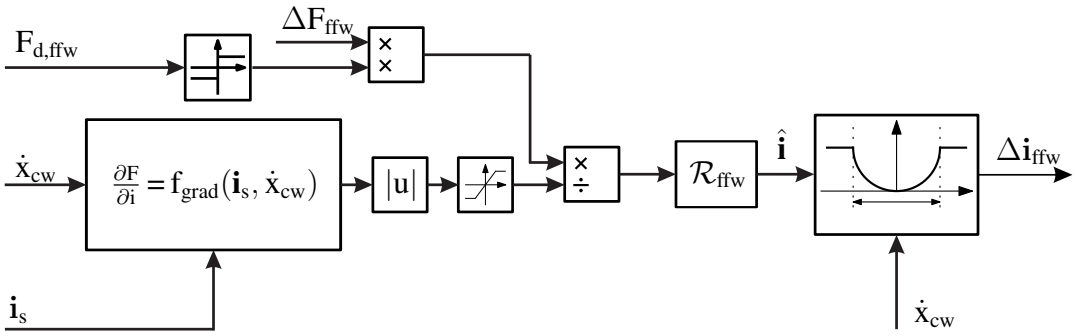

Figure 5.4: Nonlinear gain structure of $\mathcal{C}$

of the width of the weighting function is a trade-off between the intent of smooth signals and the responding performance of the controller. Approaching higher values of $\dot{x}_{cw,dead}$, the benefit of the controller vanishes; as low ones are ineffective regarding current jerks. The latter lead to uncomfortable force transmission to the chassis.

5.3.1 Force-current relation

By applying the controller structure presented in Figure 5.4, the asymmetric behavior of the semi-active device is integrated. Moreover, the difference between the limited and the dynamic force ΔF_{ffw}, meaning the hysteresis contribution in the damper behavior, is referred to the sign of the model force. That is related to the hardware construction, which reaches higher damping by reducing the current in the valves. The fail safe configuration of the device matches with the shortcoming of currents. In this case, the high damping force guarantees contact to the road and therefore safety in the ride maneuvers.

Figure 5.5 presents three exemplary cases, where the actual damper force $F_{d,ffw}$ and the desired damping force F^* do not coincide. The switch current control primarily depends on the absolute value, on the sign of the force deviation ΔF_{ffw} and on the acting damper force $F_{d,ffw}$. It is noted, that the force deviation ΔF_{ffw} is negative for all cases. The arrow indicates the direction in which the force increases by reducing currents. Due to hysteresis effects, the damper can generate force also in second and fourth quadrants for low velocity strokes. Hence, by considering the hysteresis effects, not only the relative damper velocity of the damper influence the choice of the current but also the actual driving force. In fact, the change of the algebraic sign

of the damper velocity in cases 1 and 2 has no effects on the current control strategy; only by change of the sign of $F_{d,ffw}$ changes the sign of Δi_{ffw}.

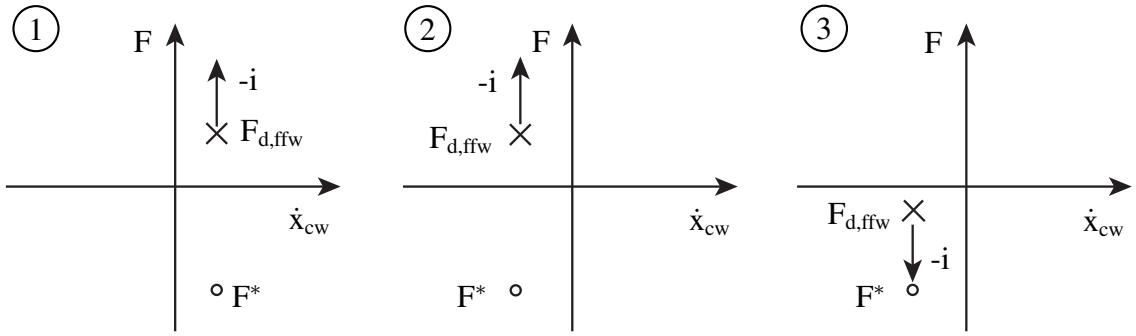

Figure 5.5: Force-current relation

5.3.2 Compensator gain of the feedforward path

In the simulation, various controller structures have been tested with respect to the feedforward compensator $\mathcal{R}_{ffw}$, where the controllers have been tuned in order to minimize the force deviation ΔF_{ffw} in Figure 5.2. In the following the proportional and proportional-integral controllers are considered.

To consider the limitation of the damper force in the controller design phase, dynamical limits are implemented in the PI-compensator. There, it is possible to include the passivity characteristic of the damper and thus limit the integration action, when the device reaches its mechanical and physical limitations. In fact, if the desired force does not lie within the damper working range, the remaining error is not integrated, since the damper is already actuated by the maximal or the minimal current. The saturations are calculated by considering the actual applied currents and the exciting damper velocity.

Some results of simulations and measurements are depicted in Figure 5.6. In the upper plot on the left side the simulation comparison between different $\mathcal{R}_{ffw}$ controllers underlines that the tracking ability of the nonlinear structure are improved by the proportional-integral (PI) controller. The integral component (I) does not increase the force tracking, while the proportional (P) component has a lack of precision in the first damping rate, where the hysteresis effects are dominant, see e.g. Chapter 3.4.

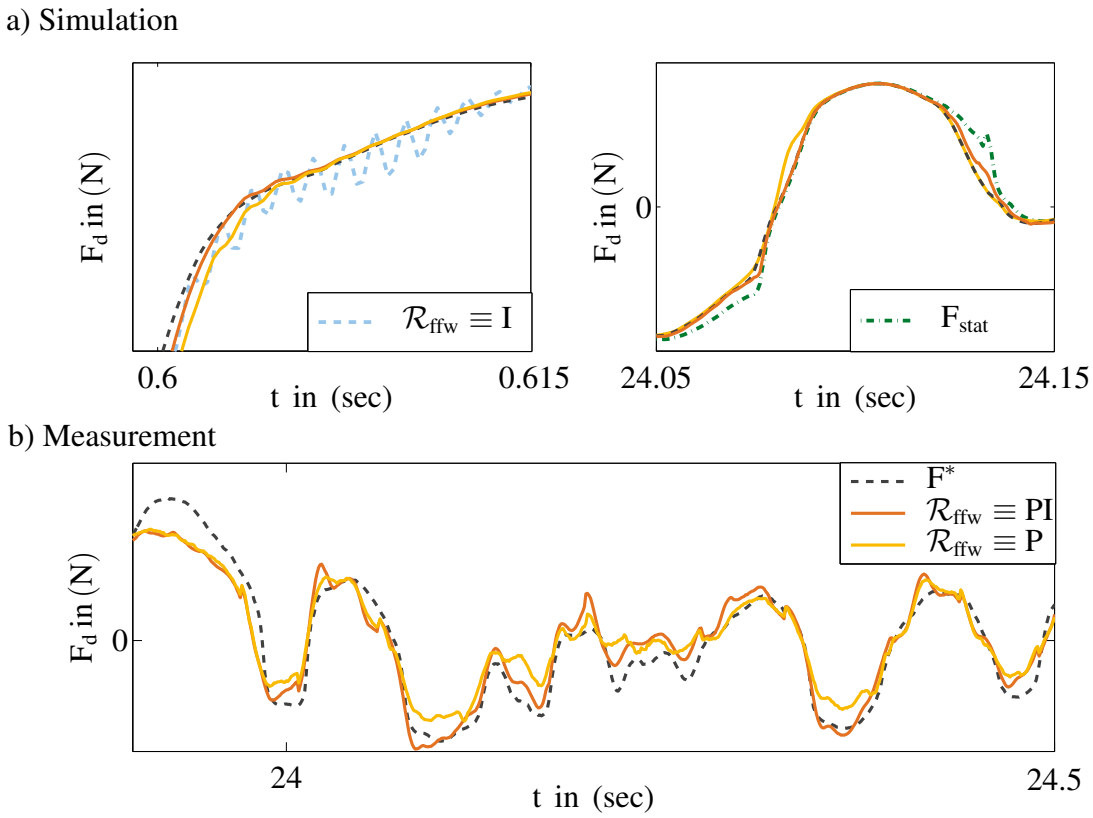

Figure 5.6: a) Simulation and b) measurement comparison of different $\mathcal{R}_{\text{ffw}}$-controllers

In the upper right corner of Figure 5.6 a comparison between the P, PI and static characteristics is reported. Distinct differences can be noticed in this time frame: for high velocity, meaning high force value, the three models respond very well and follow the reference signal properly. At velocities close to the origin, $0\,{}^{\text{m}}/_{\text{sec}}$, the static characteristic provides a wrong value of the force, in same point the signal goes even in the wrong direction. In fact, the static model, does not consider forces in the 2^{nd} or 4^{th} quadrant, therefore the sign of the force is related to the damper velocity (see Figure 4.1) and the control law switches the current to the opposite direction, so that the damping force is increased instead of being reduced. It corresponds to case (2) in Figure 5.5. Minor differences can be noticed in the comparison between P- and PI-controllers.

In the lower plot some measurement results are depicted. The reference force F^* is generated by a safety-oriented linear quadratic regulator, see Section 2.3. This implies a state feedback,

which does not take the damper limitations into account, and thus, the desired force can lie outside the working range of the damper. The desired force generated by the suspension controller, see Figure 5.1, is processed by the feedforward structure or by the static characteristics and clipped within the damper working range. Obviously, the control targets can be achieved if the desired damping force can be completely applied. In the measurements, the best results are achieved by using a proportional-integral element with a time constant of about 5msec. This configuration is applied in the following. The presented structure, has shown a stable behavior both in simulations and in experiments, despite the fact that different controller configurations and different road excitation have been deployed, see Section 2.7.

Since the suspension controllers are not specifically designed for a semi-active device, the desired force cannot always be generated by the damper, both for mechanical limitation and for velocity-dependent behavior of the device. Chapter 7 of this Thesis deals with the issue of generating the optimal force for the semi-active device, by considering the actual damper velocity and the device's limitations.

5.4 Validation of the feedforward control

The dynamic feedforward control structure presented in Figure 5.2 with the nonlinear scaling gain, the current weighting factor and the optimized PI-controller $\mathcal{R}_{\text{ffw}}$ is validated and in this Section a detailed complete analysis of the system response is given. To validate the controller structure on the test rig, the comfort-oriented law, based on the skyhook strategy, is applied. Therefore, the body acceleration is considered and discussed, see Figure 5.7. In addition, the top mount model, presented in Chapter 4.6, is integrated in the controller strategy. Moreover, the test rig is excited by a singular disturbance event (see Section 2.6.3) and the chassis acceleration is measured for the different damper control configurations, which are then compared to each other.

The results for a constant current setting (passive reference), as well as for two variable current settings obtained by the static characteristics (state of the art) and by the dynamical feedforward approach newly proposed here are shown in Figure 5.7. As the description of the force behavior is more accurate, the dynamic structure allows to determine more precise current values, which results in a reduction of the body mass acceleration. Generally, it can be seen that the controlled semi-active damper reduces the acceleration peaks and suppresses the os-

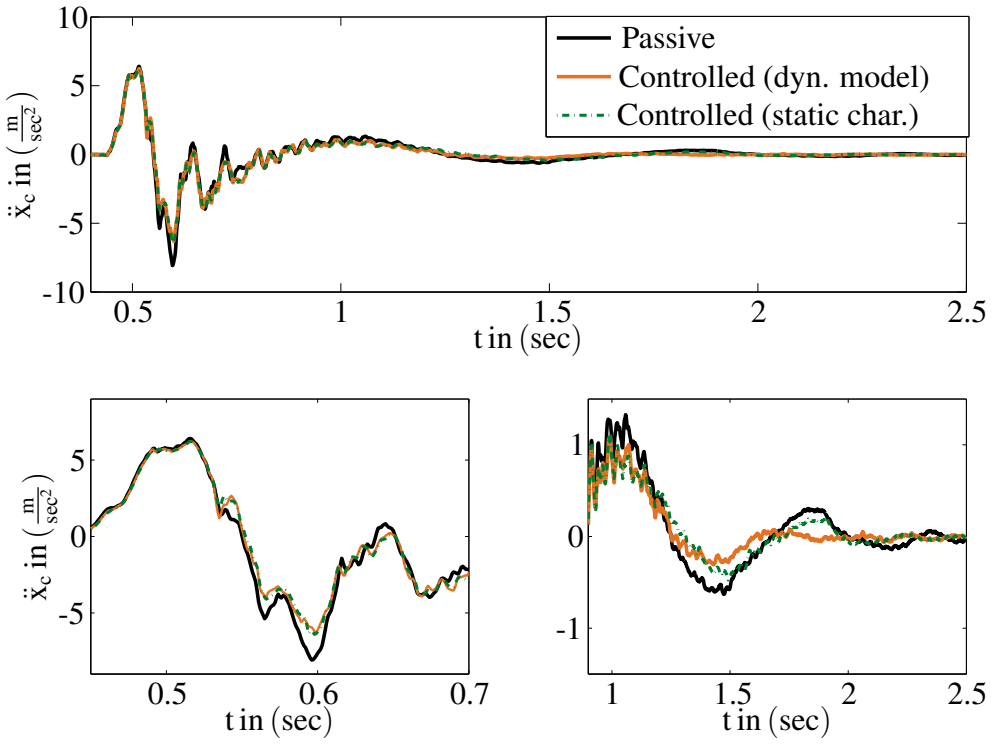

Figure 5.7: Damping action for a 8 cm traffic bump (vehicle speed of $30\,^{\mathrm{km}}/_{\mathrm{h}}$)

cillation wave faster then the passive configuration.

Both semi-active solutions, static and dynamic, almost coincide at the beginning of the event, see Figure 5.7 (bottom left). This is due to the fact that the absolute values of the suspension deflection velocity are large and the differences between the model and the static characteristics are minimal, see Figure 4.1(a).

The advantages of the dynamic feedforward approach can be entirely appreciated by analyzing the damping effect in case of small absolute suspension deflection velocities (around $0\,^{\mathrm{m}}/_{\mathrm{sec}}$), where the hysteresis modeling shows its strength, see Figure 5.7 (bottom right).

5.5 Simulation and measurement results

In this Section representative application results of the presented model-based open loop approach are reported. The performance benefit over the passive configuration is compared with the one of the state of the art solution, which is adopted as strategy in production vehicles. The quarter-car system is exposed to different real road profiles (see Section 2.6.2), in order to excite it in the whole relevant frequency range.

Even when considering $\mathcal{C}$ as a proportional gain, performance benefits can be achieved, [117]. In the previous work a country road (P2 in Section 2.6.2), that contains high frequency components, which make it challenging to provide ride comfort despite the wheel load variations, is considered. Because of the fast valve dynamics of the semi-active device, which allow to influence the behavior of the suspension also in the high frequency range, it is possible to fully utilize its characteristics. The main results are reported in the following by considering a safety-oriented LQR and two skyhook laws. In case of the first control law, the comparison between the state of the art and the new dynamical feedforward structure shows that the proposed model increases the handling index but slightly decreases ride comfort. The minimal and thus most critical value of the dynamical wheel load is reduced considerably. Considering the LQR measurement results, the proposed damper model increases the performance gain over the passive configuration in the dynamical wheel load, while the configuration with the damper static characteristics leads to a negative performance gain both in ride comfort and in ride safety. It can be summarized, that even if the total improvement of the gain indexes do not display significant ameliorations, the benefit of the extension to the state of the art approach can especially be seen at the peak values of the measured signals. This is due to the fact that the damper model takes into account the corresponding hysteresis effects depending on the velocity, [117].

Replacing the proportional gain in $\mathcal{C}$ with the nonlinear control structure, the performance benefit can be increased. A first approach of the comparison between the state of the art solution, meaning the use of the force-velocity characteristics and the feedforward structure based on the hysteresis model proposed in Chapter 4 is presented in the previous work [119]. Both the simulation and the measurement results reported in this contribution underline that the model-based approach achieves better performance as the static characteristics by adjusting the damper control inputs $\mathbf{i}^* = \mathbf{i}_\mathrm{d}$, according to the deviation between the damper model

output and the desired force. Here, the comfort improvement is achieved while maintaining the same value of the dynamical wheel load and making use of the same range of suspension deflection.

The concept is further enhanced by means of optimization and subsequently analyzed for different suspension controllers, [118]. Corresponding results are reported in the following. While in case of FFW_{sc} the damper currents are determined by using the inverted static damper characteristics, FFW_{df} makes use of the hysteresis model and hence a dynamic force is produced in order to track reference forces.

The simulation results are outlined in Table 5.1, where the advantage of the hysteresis model becomes visible. In order to quantify the respective benefit, the performance gain defined in Chapter 2 is calculated for each considered quantity with respect to the passive suspension. Thereby, a reduction of the absolute value of the corresponding quantity and thus a performance improvement is denoted by a positive value of $\text{P}_{\text{G}}(\|\cdot\|)$. Moreover, to evaluate the force tracking for both strategies, the force tracking gain Γ, introduced in Section 2.5.3 is calculated as well. By tracking improvement, the index reduces its value.

Table 5.1: Simulation results for road profile P1 ($50\,\mathrm{km/h}$)

Quantity	Pass.	FFW_{sc}			FFW_{df}		
suspension controller	-	SH	LQR	RAMS	SH	LQR	RAMS
$\|\ddot{\text{x}}_{\text{c}}\|_{\text{rms}}$ in $\frac{\text{m}}{\text{sec}^2}$	1.56	1.38	1.56	1.33	1.34	1.54	1.29
Benefit vs. pass.	-	11.5%	-0.7%	14.5%	13.7%	1.1%	17.1%
$\|\ddot{\text{x}}_{\text{c, comf}}\|_{\text{rms}}$ in $\frac{\text{m}}{\text{sec}^2}$	1.00	0.88	1.21	0.96	0.86	1.20	0.94
Benefit vs. pass.	-	11.7%	-21.0%	3.7%	13.6%	-20.4%	5.6%
$\|\text{F}_{\text{dyn}}\|_{\text{rms}}$ in N	1074	1062	958	969	1056	954	968
Benefit vs. pass.	-	1.1%	10.8%	9.8%	1.7%	11.1%	9.8%
$\min(\text{F}_{\text{dyn}})$ in N	-3140	-3458	-2850	-2715	-3412	-2730	-2639
Benefit vs. pass.	-	-10.1%	9.2%	13.5%	-8.7%	13.1%	15.9%
$\min(\text{x}_{\text{c}}-\text{x}_{\text{w}})$ in cm	-9.4	-7.5	-6.7	-6.5	-7.4	-6.8	-6.4
Benefit vs. pass.	-	19.8%	28.8%	30.2%	21.1%	26.9%	32.1%
Γ in (-)	-	0.26	0.25	0.22	0.23	0.19	0.17

The $\mathcal{R}_{\text{ffw}}$-controller (PI) with optimized parameters has been used with all three different suspension control concepts, described in Section 2.3: a comfort-oriented skyhook law (SH), a

safety-oriented linear quadratic regulator (LQR) and a road-adaptive modified skyhook strategy (RAMS) based on an adaptation logic. For the latter the input road profile has been used in the simulation, while in the experiment the road excitation signal is estimated.

When the skyhook configuration is applied, both damper force controller setups provide a significant reduction of both, the original and the weighted body acceleration quantities in comparison to the passive setting. At the same time also the safety performance with respect to the rms-value is increased. Compared to the state of the art solution, i. e. $\mathrm{FFW_{sc}}$, where the static damper characteristic is used to determine the damper currents, the dynamic approach is able to enhance the ride performance considerably with respect to all criteria.

The application of the proposed model and of the feedforward strategy reduces the tracking error independently of the applied suspension controller. The reducing of the tracking index indicates a better force tracking. This fact implies that the controller goals can be better achieved. In fact, as expected, the LQR strategy clearly improves ride safety while reducing the comfort index, compared to the skyhook controller. The adaptive logic shows a good compromise, strongly increasing the comfort benefit of the measured acceleration over the passive case and at the same time increasing the road holding.

Despite scheduling the gains in order to reach a compromise between ride comfort and ride safety, depending on the roughness of the road profile, the adaptive skyhook-groundhook controller offers good ride comfort by means of the chassis acceleration. For instance, an even better comfort index than in case of the regular skyhook configuration can be obtained. However, due to the choice of high values for the damping parameters in (2.20), insufficient vibration isolation in the comfort range between 4 to 8 Hz results. Thus, considering the weighted acceleration signal the performance profit is drastically reduced.

As can be seen for all of the suspension controllers the dynamic feedforward approach can improve the performance in comparison with the static control by several percentage points.

In order to validate the simulation results and assess the performance under real conditions, experiments have been carried out on the test rig, see Figure A.1. All signals utilized in the control loop are either estimated or measured by sensors usually available in series vehicles, see Section A.2.

The measurement results are summarized in Table 5.2, where the same notation as before is

applied. The suspension controllers show the results that might be expected from the simulations with the regular skyhook (SH) improving ride comfort, LQR enhancing ride safety and the road-adaptive skyhook concept (RAMS) delivering a very good compromise between the two strategies. Similarly to the simulation results, it can be noted, that the force tracking performance is enhanced by introducing the model-based dynamical approach. It allows to better reproduce the device's dynamics and consequently to set more precise currents to reach the controller targets.

Table 5.2: Measurement results for road profile P1 ($50\,\mathrm{km/h}$)

Quantity	Pass.	FFW_{sc}			FFW_{df}		
suspension controller	-	SH	LQR	RAMS	SH	LQR	RAMS
$\|\ddot{x}_c\|_{rms}$ in $\frac{m}{sec^2}$	1.92	1.68	1.82	1.62	1.66	1.83	1.62
Benefit vs. pass.	-	12.9%	5.3%	15.8%	13.5%	4.7%	16.0%
$\|\ddot{x}_{c,\,comf}\|_{rms}$ in $\frac{m}{sec^2}$	1.26	1.07	1.38	1.14	1.07	1.41	1.16
Benefit vs. pass.	-	15.0%	-9.6%	9.4%	15.0%	-11.9%	8.0%
$\|F_{dyn}\|_{rms}$ in N	1275	1290	1106	1157	1283	1105	1149
Benefit vs. pass.	-	-1.1%	13.2%	9.3%	-0.6%	13.3%	9.9%
$\min(F_{dyn})$ in N	-3706	-3795	-3171	-3155	-3737	-3120	-3092
Benefit vs. pass.	-	-2.4%	14.4%	14.9%	-0.8%	15.8%	16.6%
$\min(x_c - x_w)$ in cm	-8.6	-7.7	-7.4	-7.0	-7.7	-7.5	-7.1
Benefit vs. pass.	-	10.4%	13.7%	18.6%	10.2%	12.9%	18.0%
$\Gamma = \|\Delta F_d\|_{rms}/\|F^*\|_{rms}$	-	0.23	0.40	0.33	0.22	0.35	0.31

For profile P2, which contains more high frequency components, the performance can also be increased by the proposed control structure, however, by permitting higher dynamic wheel loads. Due to the increased force tracking behavior, which allows to better apply the desired force and, thus, enhance the realization of the control target, the benefit of the control actions can be increased. The performance gains confirm that the presented approach eases the inherent conflict of suspension systems by offering performance advantages for ride comfort and ride safety simultaneously. The corresponding analysis is addressed in [119].

5.6 Summary

Based on an asymmetric hysteresis model of a hydraulic dual tube semi-active damper that extends the static damper characteristics by the nonlinear dynamic effect of the damper force generation, a new control strategy for the valve currents has been designed. It has been shown that it improves the force tracking of the semi-active damper through a new dynamic feedforward nonlinear control structure. The approach is suitable for real time applications and the experimental results have shown that the proposed model-based feedforward control approach benefits both the ride comfort and the ride safety.

To overcome the modeling uncertainties and measurement inaccuracies a feedback component is introduced in Chapter 6, which completes the actuator control structure proposed in this Thesis and increases the robustness of the presented approach.

Chapter 6

COMBINED FEEDFORWARD AND FEEDBACK CONTROL OF A SEMI-ACTIVE DAMPER

The Chapter presents a two-degrees-of-freedom control structure for semi-active suspension systems. It combines the dynamical feedforward approach presented in Chapter 5 with a nonlinear feedback component to control the damper valves' currents of a semi-active damper.

By extending the damper control loop, the damper action can be adjusted to take into account the quarter-car dynamics. Moreover, unpredictable variations of the damper behavior or changes during its lifetime can be compensated as well. In addition, introducing the feedback further improves force tracking, since information about the force transmitted between wheel and chassis are fed back.

While an additional force feedback path is able to enhance force tracking even further, a measurement signal of the realized damper force is usually not available for control purposes in practice. Hence, a model-based and a signal-based estimation approaches are employed. The impact on ride performance, in the whole frequency spectrum, caused by the reduced tracking error is studied using the same benchmark suspension controllers as in Chapter 5. The reference damper force is thereby determined by either a comfort-oriented (skyhook), a safety-oriented (LQR) or a road adaptive control law (RAMS), see Section 2.3. Similarly to the previous Chapter, the force tracking gain is adopted, in order to evaluate the damper controller behavior. In the ideal case, the desired force is always in the damper working range and can be reached by the device. Otherwise, the force is clipped and the tracking error is minimized in this range.

The performance potential of the force tracking controller as well as of the entire control structure is analyzed in simulations, which are validated on a quarter-car test rig. The effect of improved force tracking on the overall ride performance is comprehensively studied.

6.1 Suspension controllers

Since the adopted high-level controller exploit the semi-active device in different frequency ranges, the characteristic of the adopted controller laws are re-proposed. The suspension controllers are assumed to be one of the following: a skyhook controller, a linear quadratic regulator (LQR) or a road adaptive control law (RAMS), as described in Section 2.3.

In the case of the skyhook law, the reference damping force is given by $F^* \equiv F_{sky}$ in (2.19) depending on the constants d_{sky} and $d_{c,c}$. When applying the LQR the cost functional (2.21) is minimized and the state feedback control law is $F^* \equiv F_{lqr}$ the result of the Riccati equation. Finally, an adaptive control law for a modified skyhook $F^* \equiv F_{rams}$ is employed, see (2.20).

Since the first control law is well-known and widely applied both in research and industrial applications and the linear optimal control is widespread in the research community (see Section 2.3), the road-adaptive modified skyhook presented in [73] is not as common as the others. Therefore in the following, the main characteristics are resumed.

The main disadvantage of this approach is its dependency on the road profile estimation quality. In this Thesis the road characteristic identification takes place by means of an optimized Kalman filter and signal-based approaches, [66]. Applying a Fourier transformation, the main idea is to evaluate the road energy in certain frequency range. For the proposed application, the first f_c and the second f_w natural frequencies of the quarter-car are investigated. The estimated road profile $\hat{x}_g$ is analyzed in its amplitudes and phases over the frequency range is calculated as

$$\bar{X}_g = \sum_{m=0}^{N_s-1} \hat{x}_g(m) \cdot e^{-j(2\pi km/N_s)} = A_{gk} + jB_{gk}, \qquad k = 0, 1, ..., N_s - 1, \tag{6.1}$$

where

$$A_{gk} = \frac{2}{N_s} \sum_{m=0}^{N_s-1} \hat{x}_g(m) \cdot \cos \frac{2\pi km}{N_s}, \qquad k = 1, 2, ..., \frac{N_s}{2} \tag{6.2}$$

$$B_{gk} = \frac{2}{N_s} \sum_{m=0}^{N_s-1} \hat{x}_g(m) \cdot \sin \frac{2\pi km}{N_s}, \qquad k = 0, 1, ..., \frac{N_s}{2} - 1. \tag{6.3}$$

For this application the frequency resolution is chosen to be 1 Hz. Therefore, the approxi-

mations $f_c = 1$ and $f_w = 12$ are considered, [93]. For these two frequencies the amplitudes, meaning the signal energy, are evaluated as follows

$$S(f_c) = \sqrt{A_{g1}^2 + B_{g1}^2} \tag{6.4}$$

$$S(f_w) = \sqrt{A_{g12}^2 + B_{g12}^2}. \tag{6.5}$$

The effective value for both frequencies are weighted and compared with predefined ISO normed road profiles [1], in order to classify the intensity of the surface excitation, [73].

Hong describes the procedure to choose the optimal gains for skyhook $\bar{d}_{sky}$ and passive $\bar{d}_{c,p}$ terms. The range of variation of the gains is chosen in the simulation, by considering the conflict diagram of the semi-active suspension system, [82]. Based on the energy contained in the road excitation, the logic increases comfort as long as the ride safety is guaranteed. Once the dynamic wheel load is high, the passive damping is increased. Depending on the surface class, both gains are scheduled and their effects are combined. When increasing the skyhook gain value the body acceleration is reduced, while by changing the passive damping term the dynamic wheel load is influenced. Results of the choice of the time depending damping coefficients for profile P1 by a velocity of $75\,^{\mathrm{km}}/_{\mathrm{h}}$ are reported in Figure 6.1. The corresponding desired damper force F^* is then obtained according to (2.20).

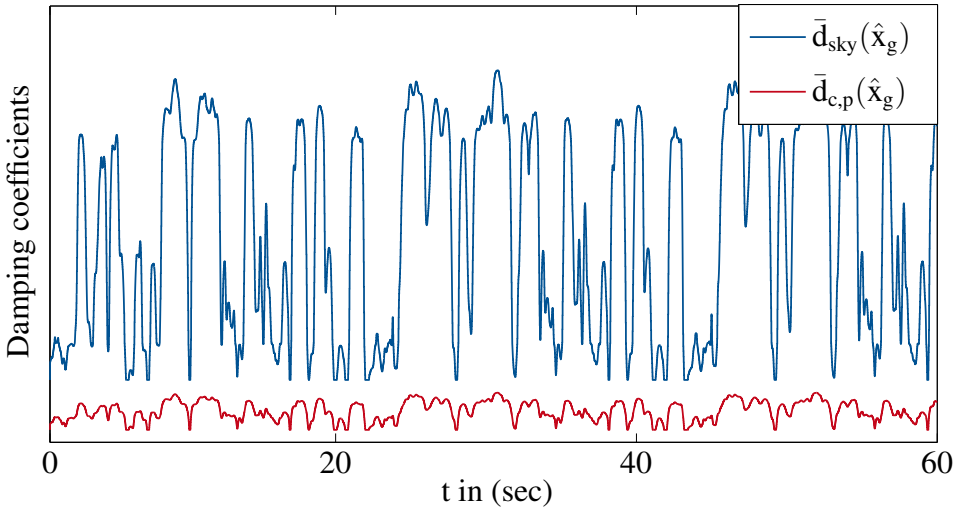

Figure 6.1: Gain scheduling for profile P1

In all three cases, the force F^* can only be realized by the semi-active device, if the condition $\dot{x}_c \dot{x}_{cw} \geq 0$ is fulfilled and F^* lies within the damper characteristic envelope; otherwise the force is clipped by the damper.

6.2 Control approach for mechatronic suspensions

As already mentioned in Chapter 5, when adjustable dampers are employed, the reference forces calculated by a superordinate suspension controller, are mostly tracked by means of static force-velocity characteristics, which allow to determine the damper control inputs, [80]. The nonlinear nature of the semi-active device motivates the use of a more precise model in order to better employ the potential of modern suspensions. The model is adopted to drive a model-based dynamical control approach, which calculates the valve current signals. It allows to better track the desired force and hence to increase the ride performance [117, 119].

Both approaches correspond to an open-loop system with regard to the damper force, since they do not consider the realized damper force acting on the system. That is motivated by the fact, that the only measurable variables are the valve currents. Therefore, in industrial applications, feedforward structures based on the static characteristics are still used. The device complexity (see e.g. Chapter 3) is of course a challenge for the development of effective control strategies. Also in the research field there are only few works dealing with semi-active damper control (e.g. [146, 147]), the most found contributions concentrate on suspension controller strategies.

The basic idea presented in this Chapter is to enhance the quality of the damper force tracking structure by accounting for hysteresis effects and also model inaccuracies in an added closed loop path. With respect to the feedback damper force signal a comparative analysis of a model-based and a new signal-based damper force estimation approach is presented. The hierarchical control approach of the semi-active suspension system, constituted of a feedforward (FFW) and a feedback (FB) component, is represented in Figure 6.2. It is noted, that the status of the switch (S) cannot be changed while operating.

Due to the fact, that the force signal of the realized damper force is usually not available in production vehicles, two approaches are taken here to obviate the missing signal. A damper force estimation either based on the damper model ($\hat{F}_{d,m}$) or based on the damper force cal-

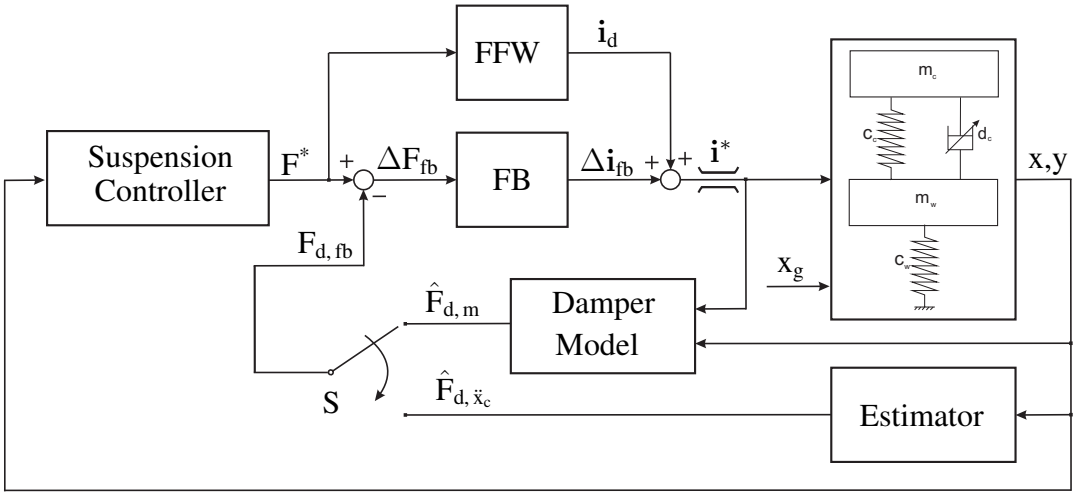

Figure 6.2: Hierarchical quarter-car control structure

culated by an estimator from the measured chassis acceleration ($\hat{F}_{d,\ddot{x}_c}$) is used. The latter case is basically the rearrangement of the chassis equation of motion in (2.14). For analysis purposes, a switch (S) is introduced in the structure. It allows to choose the feedback signal for the damper force control, before starting the application. It is noted, that during operation it does not change its status.

In the following Sections the key elements of the damper control in the feedback loop, shown in Figure 6.2, are discussed in detail, before the results of various suspension controllers are illustrated.

6.2.1 Feedforward component

The approach presented in Chapter 5, which adopted the new damper model introduced in Chapter 4 is extended by a nonlinear feedback compensator. The control structure incorporates dynamical effects of the force rise and increases the force tracking performance. The feedback path, which completes the structure of Figure 6.2, further reduces the tracking errors around the feedforward part, by compensating load changes, temperature influence and model imprecisions. Its action is mainly influenced by the feedback quality: by the model-based feedback, the quality of the damper model is decisive and by the estimator strategy the signal characteristic and the estimation calculation are determinative.

For controller design and simulation purposes, the nonlinear effect of the suspension kinematics, the transmission effect and the top mount effect are included in the feedforward path, see Section 4.6 and Appendix A.

6.2.2 Feedback component

Aiming at a further improved force tracking performance, the damper control algorithm is extended by a force feedback loop. Similarly to the structure proposed for the feedforward path, the feedback compensator has to take into account both the asymmetric nonlinear behavior of the damping force and the hysteresis effects. Therefore, its contribution has to be adapted to the damper working range and to be referred to the actual acting force. Hence, the force-current relation is analyzed as proposed in Section 5.3.1.

The feedback controller structure illustrated in Figure 6.3 is then driven by the force tracking error ΔF_{fb} and also by the signals $\dot{x}_{cw}$, $\mathbf{i}^*$ and $F_{d,\,fb}$, which are omitted in Figure 6.2. In contrast to the approach proposed in [119], where the damper velocity is used to determine the sign of the feedback controller output, here this task is performed by using the estimated damper force $F_{d,\,fb}$. This modification allows the controller to work correctly even if the velocity and the force have different signs due to hysteresis effects of the damper, [127]. However, the controller characteristics are not altered at all when the signs of velocity and force point in the same direction.

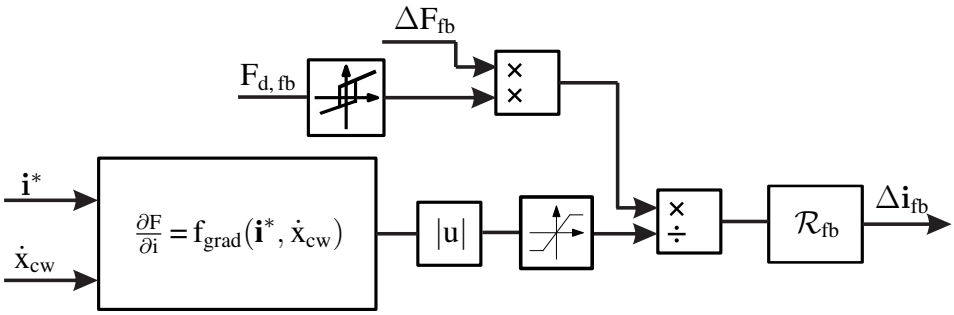

Figure 6.3: Feedback controller structure (FB)

The asymmetrical nature of the considered dual tube damper and thus, the diverging build-

up dynamic in compression and rebound direction is considered in the gradient $\frac{\partial F}{\partial i}\big|_{\dot{x}_{cw}}$, see Figure 5.3. Moreover, the nonlinear gain allows to relate the force difference ΔF_{fb} to the corresponding current variations, taking into account the damper velocity and the already applied currents $\mathbf{i}^*$. Similarly to Chapter 5 in terms of the compensator gain $\mathcal{R}_{fb}$ a proportional, as well as a proportional-integral controller are applied, where both are tuned by means of simulations as to minimize the force tracking error ΔF_{fb}. Similarly to the feedforward path also the feedback path has been tested with different controller settings and different road profiles both in simulations and on the test-rig. No instability issues occurred.

6.2.3 Damper model and estimator

As mentioned before, the feedback signal has to be obtained indirectly, since the approximation of the effective damper force actually realized by the real component is needed for the feedback loop. In the following two feasible methods of damper force feedback $F_{d,\,fb}$ are presented, i. e. a model-based and a signal-based approximation of the actually realized damper force are introduced. In both cases, the feedback signal is compared to the reference damper force F^* requested by the suspension controller, see Figure 6.2.

In case of the model-based approach, the damper force $\hat{F}_{d,\,m}$ is generated by a parallel simulation of the dynamic damper model, driven by the acting relative velocity $\dot{x}_{cw}$ and the currents $\mathbf{i}^*$, see Figure 6.2.

The second method investigated is a signal-based technique, which makes use of the measured body acceleration and of the estimated chassis mass. Solving the chassis equation of motion in (2.14) with respect to $F_d(\mathbf{x}, \mathbf{i}^*)$ and applying the measured and estimated signals, namely the chassis acceleration, the suspension deflection and the mass parameter, an estimation of the acting damper force is given by

$$\hat{F}_{d,\,\ddot{x}_c}(\mathbf{x}, \mathbf{i}^*) = d_c(t)(\dot{x}_c - \dot{x}_w) = -\hat{m}_c\ddot{x}_c - F_c(\mathbf{x}, i_f). \tag{6.6}$$

Therein $\hat{m}_c$ represents an estimation of the chassis mass. Moreover, to increase the precision of (6.6), the spring force contribution $F_c(\mathbf{x}, i_f)$ is obtained by considering the kinematic effects via i_f and the nonlinear spring characteristic as a function of the suspension deflection.

The unknown chassis mass $\hat{m}_c = m_c + \Delta m$ is estimated by using the measurements as well as the spring and damper models, [54]. Since the chassis mass during regular operation is a slowly changing parameter, a lowpass filtered version of the signal $\hat{m}_c$ can be used to estimate it. The structure is presented in Figure 6.4. The contribution of the nonlinear main spring F_c is added to the damper force, calculated by the static characteristic, F_c. The transmitted force is then filtered to obtain the low frequencies' contributions. In contrast, in case of the damper force estimation the high frequency components are considered so as to reproduce the fast damper dynamic. For the estimation of the damper contribution also the damper model has been adopted. However, due to the strong filter effect, only minor differences can be seen in the mass estimation. Therefore, the application takes use of the state of the art damper model.

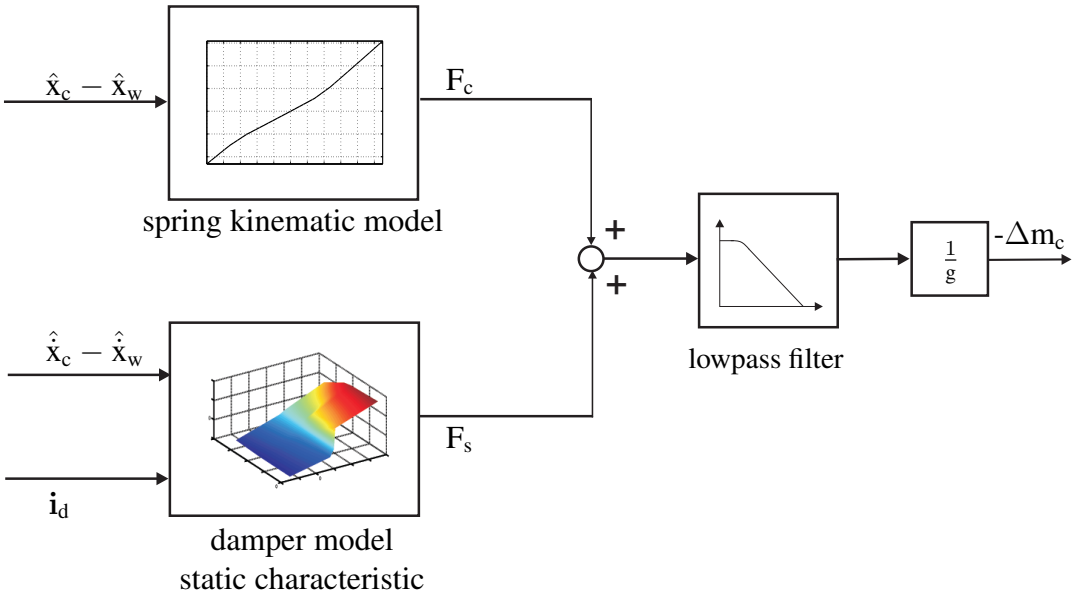

Figure 6.4: Chassis mass tracing estimation structure, [54]

In Figure 6.5, a sequence of the chassis mass estimation is depicted. As it can be seen, the estimated mass attains the real mass value $\hat{m}_c^*$ within about $10\,\mathrm{sec}$. As the additional mass Δm_c causes a permanent suspension deflection, this quantity can be used to find an appropriate initial value. In this case, by starting from the equilibrium point, the effect of the extra mass, meaning the negative suspension deflection, can be seen at $t = 0$.

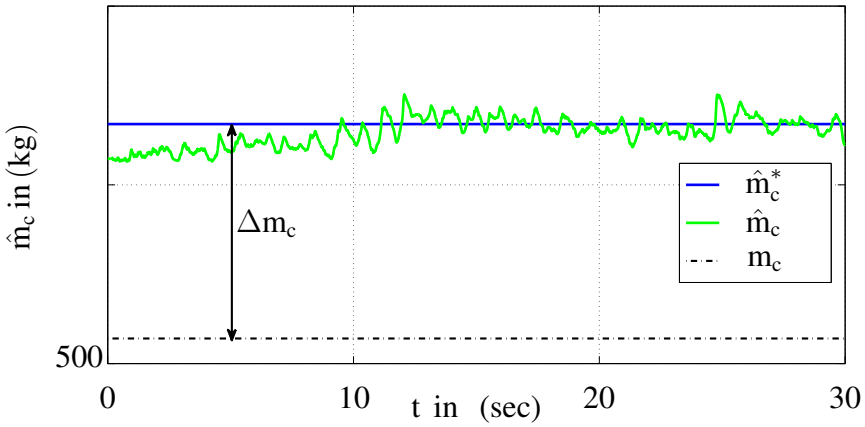

Figure 6.5: Sequence of the chassis mass estimation process ($\Delta m \approx 60\,\mathrm{kg}$)

6.3 Simulation results

In order to tune the various controller parameters as well as to evaluate the performance of the previously described control approaches, the controller structure is analyzed by means of simulation using the nonlinear quarter-car model. Because of the hierarchical layout consisting of a high-level suspension controller and a low-level force tracking controller, the evaluation of the simulation results has also been done separately. In the following, the road excitation signal used for the evaluation is profile P1, while for design purposes of the control parameters, a white noise road input is chosen.

6.3.1 Force tracking controller evaluation

With the aim of increasing the force tracking performance independently of the superordinate suspension controller, the objective is to minimize $\|\Delta F_{fb}\|_{rms}$, which represents the difference between the feedback damper force $F_{d,\,fb}$ and the desired damper force F^*. As the suspension controller goals are related to the desired force F^*, it can be expected that the parameter values that minimize the tracking error, also achieve the best performance for a given suspension control, regardless of whether a comfort-oriented or a safety-oriented concept is applied.

In order to avoid quantifying force tracking deviations caused by the limited valve currents, i. e. where no controller action can enhance the reference tracking, the requested damper force has been clipped to the feasible section of the damper force by calculating the maximum and minimum force values.

In combination with the dynamical structure presented in Chapter 5, two different feedback controller setups are analyzed. More specifically, either a proportional ($FB_{P,m}$) or a proportional integral controller ($FB_{PI,m}$) takes the place of $\mathcal{R}_{fb}$ within the nonlinear gain structure of Figure 6.3. In both cases the feedback force signal $F_{d,fb}$ is obtained by means of the damper model, i. e. $\hat{F}_{d,m}$ is applied (Figure 6.2).

Figure 6.6 depicts a simulation interval, in which the differences in the damper force tracking performance are illustrated. Once again, F^* is the reference force requested by the suspension controller. While $F_{d,ffw}$ represents the force generated by the dynamic feedforward approach only, $\hat{F}_{d,m}$ also incorporates the share of the respective feedback component that is analyzed. As it can be seen from the enlarged section on the upper right of Figure 6.6, the P-controller causes high frequency vibrations at acceleration peaks, which corrupts the force transmitted to the chassis, thereby reducing vibration isolation. In contrast, the PI-controller provides a smoother signal. Even though an increased overshoot behavior is induced, harshness phenomena caused by high frequency signals are reduced and thus ride performance can be improved. In addition, at 46,8 sec the feedforward signal (green line) temporary better approximate the desired force than the feedback solution. However, this jerky force variation deteriorates the chassis signal by increasing the acceleration.

Since the PI-controller is found to be superior to the P-controller, it has also been tested with the signal-based feedback, referred to as $FB_{PI,s}$, meaning that the acting damper force is calculated from (6.6). The simulation results with the optimized compensator parameters, are given in Table 6.1, where not only the feedback but also the feedforward values are given, in order to illustrate the positive effects of the proposed control structure. Moreover, the force tracking index Γ, which reports the quality of the tracking signal, is reported (see Section 2.5.3). It quantifies the tracking error in relation to the desired damper force, calculated by the suspension controller. The quality is increased by increasing the index values. In this case, the clipped force is used as desired force. The tracking parameter value denotes the benefit of the proposed approach.

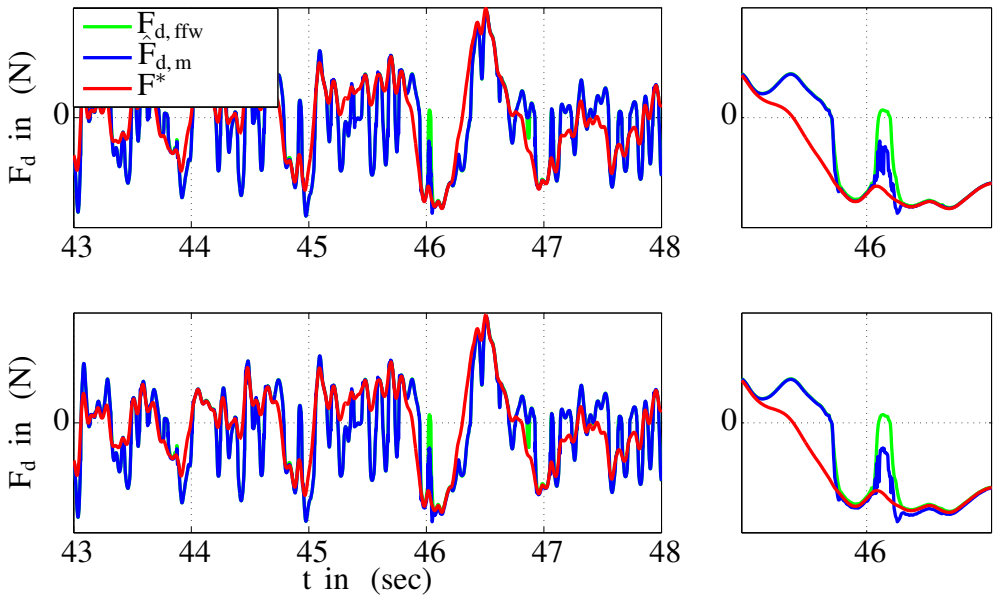

Figure 6.6: Force tracking performance for P- (upper) and PI-controller (lower) using model-based damper force feedback, [118]

Due to the increased force tracking improvement of the control target can be achieved. It can be seen that the data show significant improvements in ride comfort as well as in road-holding, achieved by the dynamic feedforward approach when the feedback component is disabled. Since the skyhook law is applied, both feedback controllers can improve ride comfort even further, however, at the cost of a slight decrease in road-holding.

Table 6.1: Simulation results for the road profile P1

Quantity	Pass.	FFW_{sc}	FFW_{df}	$FB_{PI,m}$	$FB_{PI,s}$
$\|\ddot{x}_c\|_{rms}$ in $\frac{m}{sec^2}$	1.56	1.38	1.34	1.33	1.33
Benefit vs. pass.	-	11.5%	13.7%	14.7%	14.6%
$\|\ddot{x}_{c,comf}\|_{rms}$ in $\frac{m}{sec^2}$	1.00	0.88	0.86	0.85	0.85
Benefit vs. pass.	-	11.7%	13.6%	14.3%	14.3%
$\|F_{dyn}\|_{rms}$ in N	1074	1062	1056	1059	1060
Benefit vs. pass.	-	1.1%	1.7%	1.4%	1.3%
$\Gamma = \|\Delta F_d\|_{rms}/\|F^*\|_{rms}$	-	0.14	0.13	0.12	0.12

6.3.2 Suspension controller evaluation

The strategy proposed in the previous Chapter in Section 5.5 is extended by the feedback solution and the complete damper control approach is applied, by means of the three benchmark suspension controllers. Hence, the PI-controller optimized in the previous Section, has been used with the different suspension control concepts: a comfort-oriented skyhook law (SH), a safety-oriented linear quadratic regulator (LQR) and a road-adaptive modified skyhook strategy (RAMS) based on an adaptation logic. The corresponding results using road profile P1 ($50\,\mathrm{km/h}$) are stated in Table 6.2.

In addition to the benefit achieved by introducing the dynamical feedforward structure (Chapter 5), the application of the feedback components allows a higher ride comfort than the open loop strategy (see Table 6.1). Since the skyhook suspension controller improves the ride comfort, it slightly reduces the ride safety, underlined by the increased $\|\mathrm{F_{dyn}}\|_{\mathrm{rms}}$.

A brief analysis of the suspension controller is summarized in the following. As also expected for the closed loop variation, the LQR strategy clearly improves ride safety while reducing the comfort index, compared to the skyhook controller. The adaptive logic reaches, as expected, a compromise between ride comfort and ride safety. Obviously, the feedback solution enhances the results of the open loop solution even further, no matter which suspension controller is applied.

Since the core of this Chapter is the feedback loop and its effect on the force tracking, the tracking performance gain Γ is reported. The better force tracking reflects the better performance independently of the suspension controller targets. By comparing the result of the tracking parameter to the open loop solutions in Chapter 5 (see Table 5.1), an enhancement of the control performance is achieved, since the knowledge of the applied force can be used and the tracking force performance is increased, since the Γ values are reduced.

In order to validate the simulation results and assess the performance under real test rig conditions, experiments have been carried out. Figure 6.7 shows an exemplary section of a measurement on road profile P1 at a vehicle speed of $50\,\mathrm{km/h}$ using the regular skyhook control law. As before, F^* denotes the reference damper force obtained from the suspension controller, $\mathrm{F_{d,\,meas}}$ represents the actual damper force determined from the load cell measurement described in detail in Appendix A.2 and $\mathrm{F_{d,\,fb}}$ indicates the feedback signal for the controller.

Table 6.2: Simulation results for the road profile P1 ($50\,^{\mathrm{km}}/_{\mathrm{h}}$)

Quantity	Pass.	$FB_{PI,m}$			$FB_{PI,s}$		
suspension controller	-	SH	LQR	RAMS	SH	LQR	RAMS
$\|\ddot{x}_c\|_{rms}$ in $\frac{m}{sec^2}$	1.56	1.33	1.53	1.27	1.33	1.52	1.27
Benefit vs. pass.	-	14.7%	1.8%	18.0%	14.6%	2.0%	18.1%
$\|\ddot{x}_{c,\,comf}\|_{rms}$ in $\frac{m}{sec^2}$	1.00	0.85	1.20	0.93	0.85	1.20	0.93
Benefit vs. pass.	-	14.3%	-20.4%	6.1%	14.3%	-20.3%	6.4%
$\|F_{dyn}\|_{rms}$ in N	1074	1059	954	971	1060	953	971
Benefit vs. pass.	-	1.4%	11.1%	9.6%	1.3%	11.2%	9.5%
$\min(F_{dyn})$ in N	-3140	-3414	-2727	-2640	-3411	-2725	-2647
Benefit vs. pass.	-	-8.7%	13.1%	15.9%	-8.6%	13.2%	15.7%
$\min(x_c - x_w)$ in cm	-9.4	-7.3	-6.9	-6.4	-7.3	-6.9	-6.4
Benefit vs. pass.	-	21.8%	25.8%	32.0%	21.7%	25.9%	31.9%
$\Gamma = \|\Delta F_d\|_{rms}/\|F^*\|_{rms}$	-	0.21	0.15	0.14	0.20	0.15	0.14

In the upper plot the signal-based feedback is illustrated, which employs the measured chassis acceleration to determine the actual damper force by using (6.6). The lower plot depicts the results of the model-based feedback using the output signal of the damper model from the parallel simulation. As it can be seen, the damper model matches the dynamic characteristics of the damper better than the damper force based on the acceleration signal. Due to high frequency vibrations, measurement noise in the signal and inaccuracy in the chassis mass estimation, some errors between the measured and the estimated damper force occur. Since the performance of the two feedback controllers depends highly on the quality of the feedback signal, this imprecision reduces the benefit of the respective feedback controller alternative ($FB_{PI,s}$).

The measurement results are summarized in Table 6.3, where the same notation as before is applied. Similar to the previous Chapter, suspension controllers show the expected results: comparing to the pure feedforward path, the regular skyhook (SH) improves ride comfort, LQR enhances ride safety and the road-adaptive skyhook concept (RAMS) delivers a good compromise. However, due to the noise effect in the signals, the value of Γ shows a decreased force tracking by the configuration $FB_{PI,s}$. The decreased index is reflected in the performance index, which indicates a reduction of ride comfort and ride safety, respectively.

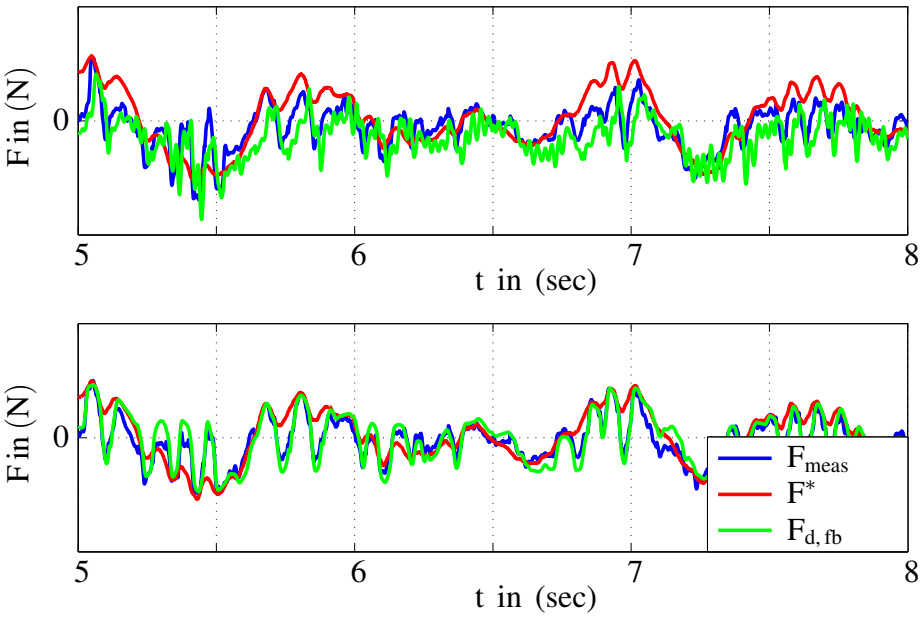

Figure 6.7: Comparison of signal-based (upper) and model-based damper force feedback (lower) at the test rig, [118]

Table 6.3: Measurement results for the road profile P1

Quantity	Pass.	$FB_{PI,m}$			$FB_{PI,s}$		
suspension controller	-	SH	LQR	RAMS	SH	LQR	RAMS
$\|\ddot{x}_c\|_{rms}$ in $\frac{m}{sec^2}$	1.92	1.69	1.80	1.61	1.77	1.83	1.67
Benefit vs. pass.	-	12.3%	6.4%	16.2%	8.2%	4.7%	13.1%
$\|\ddot{x}_{c,\,comf}\|_{rms}$ in $\frac{m}{sec^2}$	1.26	1.06	1.36	1.13	1.08	1.34	1.14
Benefit vs. pass.	-	16.2%	-7.8%	10.2%	13.9%	-6.4%	9.7%
$\|F_{dyn}\|_{rms}$ in N	1275	1319	1101	1163	1337	1160	1207
Benefit vs. pass.	-	-3.5%	13.6%	8.8%	-4.9%	9.0%	5.4%
$\min(F_{dyn})$ in N	-3706	-3949	-3229	-3190	-4022	-3200	-3317
Benefit vs. pass.	-	-6.6%	12.9%	13.9%	-8.5%	13.7%	10.5%
$\min(x_c - x_w)$ in cm	-8.6	-7.9	-7.6	-7.1	-8.2	-7.9	-7.4
Benefit vs. pass.	-	8.1%	12.2%	17.5%	5.1%	8.9%	14.5%
$\Gamma = \|\Delta F_d\|_{rms}/\|F^*\|_{rms}$	-	0.22	0.34	0.30	0.34	0.49	0.41

The consideration of the nonlinear dynamics of the damper as well as the contribution of the feedback component cause a change in the valve switching behavior (see lower plot of Figure 6.8). By using the whole available current range, the switching is more active than in the case based on the static characteristics, see e.g. [93]. In fact, while the feedforward component ensures that the valves' setting are adjusted to track the desired force, the feedback path compensate the error around the feedforward trajectory. Therefore, the dynamic of the damper is exploited by rapidly controlling the semi-active valves.

6.4 Summary

In this Chapter, the enhanced open-loop strategy of Chapter 5 has been extended by a damper force feedback loop. Thus, a two-degrees-of-freedom structure to control the valve currents of a semi-active damper in a vehicle suspension has been realized for the first time.

Similar to the feedforward structure, also the feedback loop has been designed based on a nonlinear damper model, which takes into account the dynamical hysteresis effects of the device. As the effective damper force is needed as a feedback signal, but its measurement is not provided in a realistic sensor configuration, a model-based and a signal-based estimation approach have been analyzed with regard to their respective capabilities.

In order to emphasize the performance potential of the enhanced damper force tracking control, three suspension controllers, each focusing a different performance objective, have been employed. After tuning the controller structure in the simulation, measurements have been conducted at a quarter-car test rig.

Simulation and measurement results have proved that the proposed structure offers additional performance benefit independent of the suspension controller used by providing a more accurate force tracking.

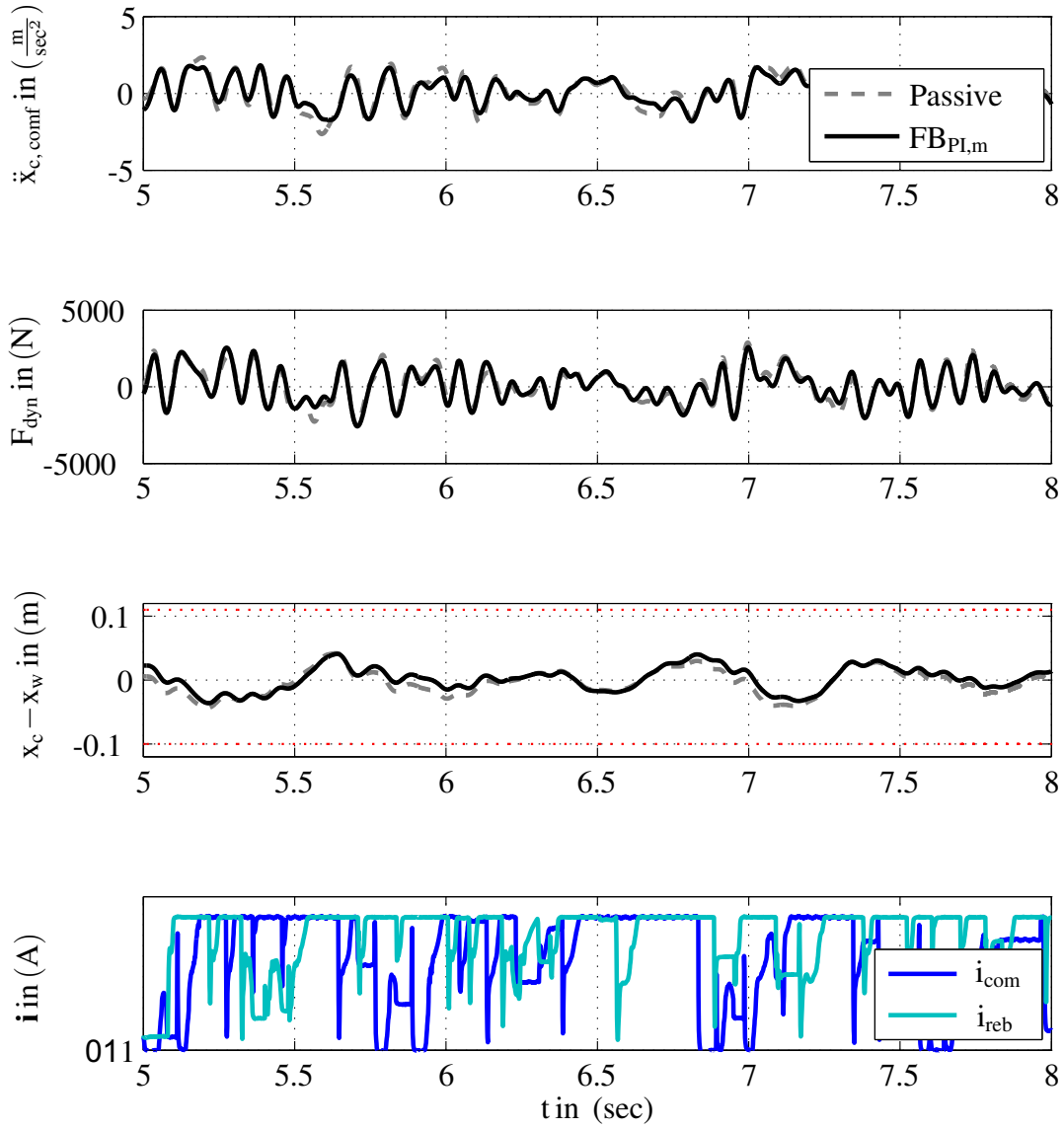

Figure 6.8: Measurement results of $FB_{PI,m}$ versus the passive suspension for profile P1; the red lines indicate the limits for the rms-value of the dynamical wheel load $\left(\|F_{dyn}\|_{rms} \leq \frac{F_{stat}}{3}\right)$ and the suspension deflection limits.

Chapter 7

SUSPENSION CONTROLLER

As already mentioned in this Thesis, the commonly-used suspension controllers, e.g. skyhook and groundhook pointed out in Chapter 2, are not optimized for semi-active dampers, since they generally do not consider the passivity and the state-dependent limitation of these devices in the controller design phase. Therefore, while the previous Chapters have dealt with the low level controller in order to exploit the semi-active device by a given controller law, this Chapter focuses on the high level controller. The desired force is optimized to remain within the damper range and therefore it can always be generated by the device. An overview of the complete control structure is given in Figure 7.1.

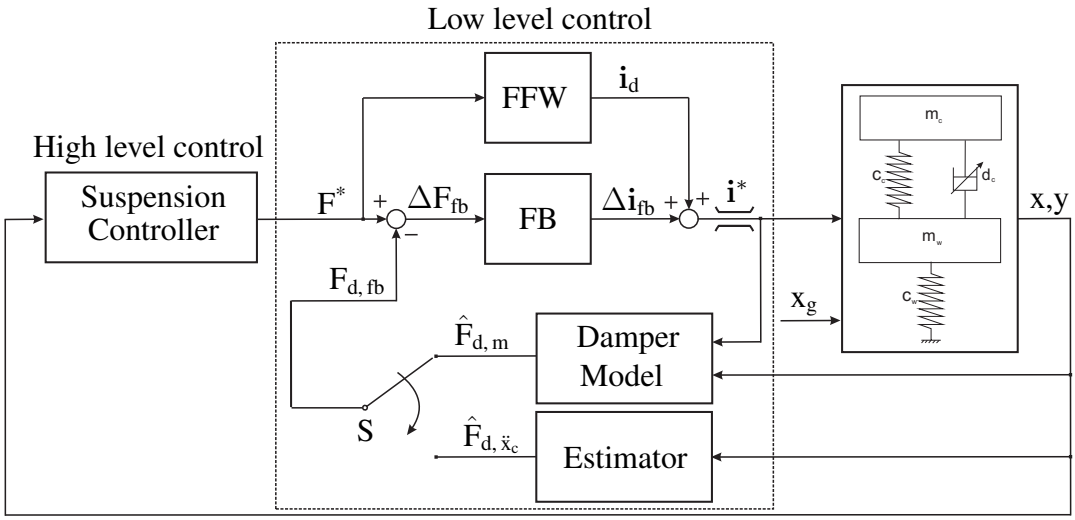

Figure 7.1: Overview of the complete control structure

In this Chapter, two approaches are suggested and compared: an optimal control method and an optimal switching strategy. System nonlinearities and constraints are considered in the general optimization problem in Section 7.1. Section 7.2 deals with suspension strut geometry, spring and damper characteristics, spring deflection limitation and system-specific formula-

tion of the optimization problem.

The first controller is designed based on nonlinear programming (NLP) while the second one (switching strategy) is derived by using the Bellman's recurrence equation of optimality. These two methods are addressed in details in Section 7.3 and Section 7.4 respectively. Section 7.5 shows the feedforward control solutions, obtained off-line for both control strategies. The idea is to integrate them into the control loop, similar to explicit model predictive control (EMPC). The performance of the suggested approaches is confirmed and discussed by simulation as well as by experiments on a quarter-car test rig in Section 7.7. Moreover the comfort filter is added to the controller design in Section 7.8 and its results are reported and compared to the previous ones.

7.1 Preliminaries on optimal control

Mainly two classes of numerical methods are known from the literature to solve optimal control problems: iterative and direct strategies. The first one generates a sequence of improved approximate solutions, considering optimality conditions. In contrast, direct methods attempt to solve the optimization problem by discretizing the state and input space. Aiming to solve the system dynamic with constraint equations, the latter methods are adopted in this Chapter. The nonlinear dynamic system can be represented in the general form

$$\begin{aligned} \dot{\mathbf{x}} &= \mathbf{f}(\mathbf{x},\ \mathbf{v}) \\ \mathbf{y} &= \hat{\mathbf{f}}(\mathbf{x},\ \mathbf{v}), \end{aligned} \tag{7.1}$$

where $\mathbf{x}$ and $\mathbf{v} = [\mathrm{v}_1, \mathrm{v}_2]^{\mathrm{T}}$ represent the state vector and the system inputs, i.e. a control input v_1 and an external excitation v_2, respectively.

General case with fixed final time and no terminal or path constraints

If there are no path constraints on the state or on the control variables and by considering the initial and the final time to be fixed, the general control problem consists in finding the control

vector trajectory $\mathbf{u}^*(\mathrm{t})$ in the time interval $[\mathrm{t}_0, \mathrm{t}_\mathrm{e}]$, such that, the cost function

$$\mathrm{J} = \mathrm{h}\left(\mathbf{x}\left(\mathrm{t}_\mathrm{e}\right), \mathrm{t}_\mathrm{e}\right) + \int_{\mathrm{t}_0}^{\mathrm{t}_\mathrm{e}} \mathrm{g}\left(\mathrm{t}, \mathbf{x}, \mathbf{u}\right)\ \mathrm{dt} \tag{7.2}$$

subject to (7.1) with the initial condition $\mathbf{x}\left(\mathrm{t}_0\right) = \mathbf{x}_0$ is minimized. In (7.2) $\mathbf{x},\ \mathrm{h},\ \mathrm{g},\ \mathbf{f}$, represent the state vector, the terminal cost function, the integral cost function and the vector field, respectively. The described problem is known as Bolza problem. If the integral cost function $\mathrm{g}\left(\mathrm{t}, \mathbf{x}, \mathbf{u}\right) = 0$, then the problem is known as the Mayer problem. Instead, if $\mathrm{h}\left(\mathbf{x}\left(\mathrm{t}_\mathrm{e}\right), \mathrm{t}_\mathrm{e}\right) = 0$, it is known as the Lagrange problem. Applying the calculus of variation it can be shown that the optimal trajectory has to satisfy the well known Euler-Lagrange differential equation and the transversality condition

$$\begin{aligned} \frac{\partial \mathrm{g}}{\partial \mathbf{x}} - \frac{\mathrm{d}}{\mathrm{dt}}\frac{\partial \mathrm{g}}{\partial \dot{\mathbf{x}}} &= 0 \qquad \text{Euler-Lagrange-diff. equation} \\ \left.\frac{\partial \mathrm{h}}{\partial \mathbf{x}}\right|_{\mathrm{t}_\mathrm{e}} + \left.\frac{\partial \mathrm{g}}{\partial \dot{\mathbf{x}}}\right|_{\mathrm{t}_\mathrm{e}} &= 0 \qquad \text{Transversality condition} \end{aligned} \tag{7.3}$$

The calculus of the variations can be extended to consider the dynamic of the system. By the use of time-varying Lagrange multiplier vector $\boldsymbol{\psi}(t)$, the constraint is incorporated to the cost function and the problem can be analytically solved. Without changing the definition of the cost function, its structure is manipulated with the system dynamics by adding the term $\mathbf{f}\left(\mathbf{x}, \mathbf{u}, t\right) - \dot{\mathbf{x}} = \mathbf{0}$ and multiplying it by the Lagrange multiplier so that the following expression is obtained:

$$\mathrm{J} = \mathrm{h}\left(\mathbf{x}\left(\mathrm{t}_\mathrm{e}\right), \mathrm{t}_\mathrm{e}\right) + \int_{\mathrm{t}_0}^{\mathrm{t}_\mathrm{e}} \underbrace{\left[\mathrm{g}\left(\mathbf{x}, \mathbf{u}, \mathrm{t}\right) + \boldsymbol{\psi}^{\mathrm{T}}(\mathrm{t})\mathbf{f}\left(\mathbf{x}, \mathbf{u}, \mathrm{t}\right) - \boldsymbol{\psi}^{\mathrm{T}}(\mathrm{t})\dot{\mathbf{x}}\right]}_{\bar{g}}\ \mathrm{dt}. \tag{7.4}$$

The definition of the Hamilton function as

$$\mathrm{H}\left(\mathbf{x}, \boldsymbol{\psi}, \mathbf{u}, \mathrm{t}\right) = \mathrm{g}\left(\mathbf{x}, \mathbf{u}, \mathrm{t}\right) + \boldsymbol{\psi}^{\mathrm{T}}\mathbf{f}\left(\mathbf{x}, \mathbf{u}, \mathrm{t}\right) \tag{7.5}$$

simplifies the following consideration. The problem consists to find the trajectories of $\mathbf{x}^*(\mathrm{t})$, $\boldsymbol{\psi}^*(\mathrm{t})$, $\mathbf{u}^*(\mathrm{t})$, which minimize the cost function (7.4), which already includes the constraints.

Defining the vector $\bar{\mathbf{x}}(t) = \left[\mathbf{x}(\mathrm{t}), \quad \boldsymbol{\psi}(\mathrm{t}), \quad \mathbf{u}(\mathrm{t})\right]^{\mathrm{T}}$ the following problem

$$\mathrm{J} = \mathrm{h}\left(\bar{\mathbf{x}}\left(\mathrm{t_e}\right), \mathrm{t_e}\right) + \int_{\mathrm{t_0}}^{\mathrm{t_e}} \mathrm{g}\left(\bar{\mathbf{x}}, \dot{\bar{\mathbf{x}}}, \mathrm{t}\right)\ \mathrm{dt} \tag{7.6}$$

has to be solved. It can be figured out by applying (7.3) which leads to

$$\dot{\mathbf{x}} = \frac{\partial \mathrm{H}}{\partial \boldsymbol{\psi}} = \mathbf{f}\left(\mathbf{x}, \mathbf{u}, \mathrm{t}\right) \qquad \text{State equation} \tag{7.7}$$

$$\dot{\boldsymbol{\psi}} = -\frac{\partial \mathrm{H}}{\partial \mathbf{x}} = -\frac{\partial \mathrm{J}}{\partial \mathbf{x}} + \left(\frac{\partial \mathbf{f}}{\partial \mathbf{x}}\right)^{\mathrm{T}} \boldsymbol{\psi} \qquad \text{co-state equation} \tag{7.8}$$

$$\mathbf{0} = \frac{\partial \mathrm{H}}{\partial \mathbf{u}} \qquad \text{stationarity condition} \tag{7.9}$$

$$\boldsymbol{\psi}\left(\mathrm{t_e}\right) = \left.\frac{\partial \mathrm{h}}{\partial \mathbf{x}}\right|_{\mathrm{t_e}} \qquad \text{free terminal point} \tag{7.10}$$

Equations (7.7),(7.8),(7.9) and (7.10) are the first-order conditions for the minimum of (7.4). Depending on the terminal constraints some additional equations can be formulated

$$\text{fixed final state:} \quad \mathbf{x}\left(\mathrm{t_e}\right) = \mathbf{x_e} \tag{7.11}$$

$$\text{free terminal time:} \quad \mathrm{H}\left(\mathbf{x}\left(\mathrm{t_e}\right), \boldsymbol{\psi}\left(\mathrm{t_e}\right), \mathbf{u}\left(\mathrm{t_e}\right), \mathrm{t_e}\right) + \frac{\partial \mathrm{h}\left(\mathbf{x}\left(\mathrm{t_e}\right), \mathrm{t_e}\right)}{\partial \mathrm{t_e}} = 0. \tag{7.12}$$

The general formulation can be extended by state and input constraints. Considering the first ones, the calculus of variation, which considered the system dynamics, can be extended with a general inequality boundary

$$\mathbf{c}(\mathbf{x}, \mathrm{t}) \geq \mathbf{0}, \tag{7.13}$$

in order to describe the state constraint conditions, [91, 132]. Thereby the only requirement is that the constraint **c** holds continuous first and second partial derivatives with respect to **x**. The approach transforms all inequalities into one equality equation and adjusts the cost function and the Hamiltonian in order to take all conditions into account.

An alternative method is presented in [28, 113]. It consists in calculating separately the solution for the restricted and the non-restricted case and to combine them by means of slip functions. Furthermore, in [64] a method to transform the state constraints into a non-restricted

problem by meaning of polynomial saturation functions is presented where a new coordinate system is needed.

Since realistic problems mostly have actuators subjected to physical limitations, the optimal control problem has to be adapted to deal with inequality constraints associated with the input variables, so that the input variable $\mathbf{u}$ is restricted to be within an admissible compact region Ω, such that $\mathbf{u}(\mathrm{t}) \in \Omega$, see e.g. [180]. For the considered system the stationary condition (7.9) has to be replaced by the formulation of the Pontryagin's minimum principle

$$\mathrm{H}\left(\mathbf{x}, \boldsymbol{\psi}, \mathbf{u}, \mathrm{t}\right) \stackrel{!}{=} \min_{\mathbf{u}}. \tag{7.14}$$

The introduction of general state-dependent input boundaries $\mathbf{c}\left(\mathbf{x}, \mathbf{u}, \mathrm{t}\right) \geq 0$ implies to adopt a new state $\dot{\mathbf{z}}^2 = \mathbf{c}\left(\mathbf{x}, \mathbf{u}, \mathrm{t}\right),\ \mathbf{z}(0) = \mathbf{0}$, which is included into the optimization problem. The new integrand becomes

$$\bar{\mathrm{g}}\left(\bar{\mathbf{x}}, \dot{\bar{\mathbf{x}}}, \mathrm{t}\right) = \mathrm{H} - \boldsymbol{\psi}^{\mathrm{T}}\dot{\mathbf{x}} - \boldsymbol{\gamma}^{\mathrm{T}}\left(\dot{\mathbf{z}}^2 - \mathbf{c}\right), \tag{7.15}$$

where $\boldsymbol{\gamma}$ is the Lagrange multiplier. After modulating the co-state equation and the stationarity condition

$$\dot{\boldsymbol{\psi}} = \frac{\partial \mathrm{H}}{\partial \mathbf{x}} + \left(\frac{\partial \mathrm{c}}{\partial \mathbf{x}}\right)^{\mathrm{T}}\boldsymbol{\gamma}, \qquad \frac{\partial \mathrm{H}}{\partial \mathbf{u}} - \left(\frac{\partial \mathrm{c}}{\partial \mathbf{u}}\right)^{\mathrm{T}}\boldsymbol{\gamma} = \mathbf{0} \tag{7.16}$$

the problem can be solved.

Different approaches for solving such optimization problems exist. For instance, equality constraints can be considered by use of the Lagrange function while inequality constraints can be taken into account by nonlinear programming (NLP), which is used in Section 7.3.

If the cost function can be subdivided into a series of subproblems, dynamic programming can be applied to ease the optimization process based on the optimality principle of Bellman, [91]. This approach will be applied in Section 7.4 in order to derive an optimal switching sequence.

Linear quadratic regulator

The optimal solution by considering linear dynamic equations and a quadratic cost function

$$\mathbf{J} = \frac{1}{2}\mathbf{x}\left(\mathrm{t_e}\right)^{\mathrm{T}}\mathbf{S}\mathbf{x}\left(\mathrm{t_e}\right) + \frac{1}{2}\int_{\mathrm{t_0}}^{\mathrm{t_e}} \mathbf{x}\left(\mathrm{t}\right)^{\mathrm{T}}\mathbf{Q}\mathbf{x}\left(\mathrm{t}\right) + \mathbf{u}\left(\mathrm{t}\right)^{\mathrm{T}}\mathbf{R}\mathbf{u}\left(\mathrm{t}\right)\ \mathrm{dt} \tag{7.17}$$

can be considered a special case of the optimal control problem, presented in the previous Section. The feedback law, in this case, is known as linear quadratic regulator (LQR) (see e.g. Section 2.3) and is analyzed in Section 7.7 for different $\mathrm{t_e}$ conditions.

7.2 Optimal control problems for semi-active suspension system

As already mentioned in this Thesis, mainly skyhook and optimal control laws are designed for active suspension controller, whereby a linear suspension dynamics is assumed, e.g. in [94, 175]. In fact, dealing with semi-active devices, these optimal control laws have to be clipped to the corresponding damper working range in order to be applied, [163]. Even if it has been shown in previous works, that optimal semi-active and clipped active controllers are equivalent concerning the linear suspension strut case, e.g. [29], nonlinearities in the suspension strut geometry and state as well as input limitations can significantly influence the system dynamics. Therefore, in different contributions the nonlinear dynamics both of the actuator and of the suspension strut have been considered, [11, 181]. In a recent work a modified optimal control concept is applied to a nonlinear active suspension system [92], while for a novel hardware paring (hybrid suspension) an optimal active component control considering several nonlinearities exists, [153]. Moreover, for active and slow-active systems an optimal solution is calculated and proposed in [48, 155].

However, the inclusion of system nonlinearities in the semi-active suspension controller design has not gained such an attraction yet. In [63], a comparison between optimal control laws, taking symmetric nonlinear damper characteristics into account is presented. Also optimal solution based on switching systems are proposed in the literature. In fact, such optimal switching problems offer an alternative to conventional optimal control problems, [19, 59, 60, 62, 173]. They consider the system nonlinearities as several linear models and transform the optimization set into a discrete (finite) formulation. In [37], an optimal switching problem is

formulated for linear hybrid automaton and applied to a semi-active quarter-car system. In this Chapter, the studies presented for an active systems in [48, 155] are reformulated and the nonlinear boundaries of a semi-active suspension system are introduced, [40].

Considering the nonlinear quarter-car model derived in Section 2.1, which represents the basis for the following optimal control problem, in this Section the analytic problem formulation referred to the semi-active system is presented, [40].

As the rms-values of the vertical dynamic targets, meaning chassis acceleration and dynamical wheel load, play an important role in the evaluation of the ride performance, a quadratic cost function $g(\mathbf{y}) = \frac{1}{2}\mathbf{y}^{T}\mathbf{Q}_{y}\mathbf{y}$ is adopted, whereby the weight matrix is defined as $\mathbf{Q}_{y} = \mathrm{diag}(q_{\ddot{z}_c}, q_{F_{dyn}}, q_{x_1})$. As reported in Chapter 1, also the maximal values of the ride signals are relevant for the performance. Therefore, also weighting factors for the maximal values of the chassis acceleration and of the dynamic wheel load are introduced. This allows to reduce the peaks of these variables.

Aiming to influence the suspension deflection limitation, the goal can be achieved by weighting the term in $\mathbf{Q}_{y}$, such that its quadratic behavior can be influenced. By suitable choice of q_{x_1} an overstep of the mechanical limitation can be prevented. However, increasing the weighting entries of the matrix in order to preserve the violation of limits in critical ride situation, could lead to small suspension deflection values even in non-critical deflections. That is correlated with an increase of damping (hart damper setting) which comes to a reduction of the ride comfort, due to the rise of the acceleration. According to the controller target in Section 2.4, only the adherence of the maximal suspension deflection value has to be guaranteed. In contrast to the weighted terms, the suspension deflection can be exactly represented by an inequality side equation $x_1 \geq x_{1,min}$, whereas $x_{1,min} < 0$ represents the maximal deflection value. In fact, the observance of the suspension deflection is ensured without influencing the other target variables in the cost function.

The semi-active suspension represents a stable system, which always dissipates energy. That means, that the states asymptotically converge to the equilibrium point $\mathbf{x} = \mathbf{0}$. As a consequence the final time t_e and the final state $\mathbf{x}(t_e)$ can be chosen to be fixed or free. Basically there are no requirements for the end time.

In the optimization problem also the damper force characteristics have to be taken into account. It is noted, that considering the nonlinear quarter-car model (2.12) and (2.13), the

damper currents $\mathbf{i}$ are the input of the system. Analogous to suspension deflection an upper and a lower limitation $\mathbf{i}_{\text{min}} \leq \mathbf{i} \leq \mathbf{i}_{\text{max}}$ can be defined. However, if instead of the limitations on the current, the ones on the damper force are considered, nonlinear limits can be derived.

In order to take the hysteresis effects into account, it can be claimed that the damper force exclusively remains within the colored solid lines, as reported in Figure 7.2(a). By choosing a wider damper working range, also forces in the second and fourth quadrant are allowed. Thereby, the hysteresis effect is emulated and by neglecting the discontinuity in $0\,{}^{\text{m}}/_{\text{sec}}$ the numeric is simplified.

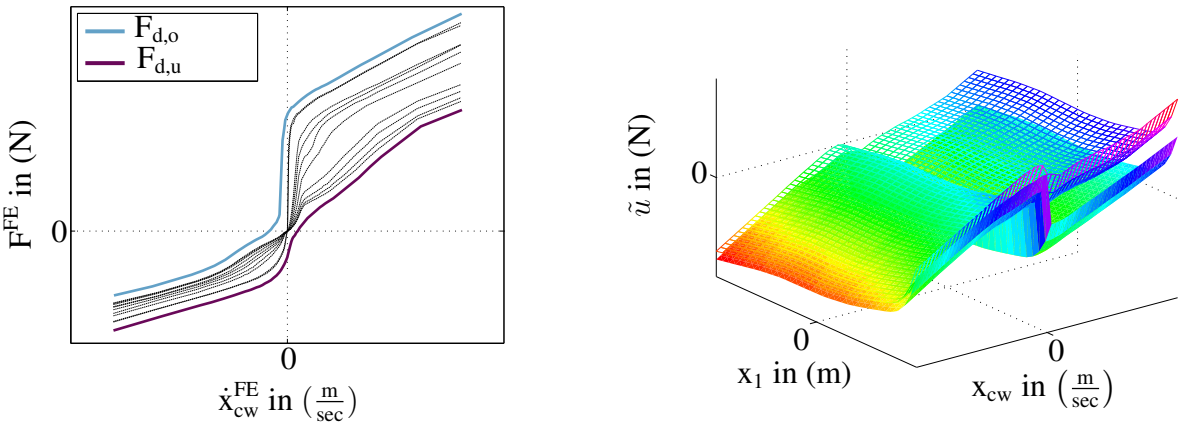

(a) Upper and lower limitations of the damper force

(b) Limitation of the cumulative force between chassis and wheel

Figure 7.2: State-dependent input limitation. Image is reproduced with kind permission of BMW AG.

By applying the dynamical factor in (2.1) the limit equation can be written as

$$\mathrm{F}_{\mathrm{o,u}}(\mathbf{x}) = -\mathrm{F}^{\mathrm{FE}}_{\mathrm{u,o/\,VDA}}\left(\left(\mathrm{x}_2 - \mathrm{x}_4\right)\mathrm{i}_{\mathrm{f}}(\mathrm{x}_1)\right)\mathrm{i}_{\mathrm{f}}(\mathrm{x}_1). \tag{7.18}$$

If the input-state linearized system, defined in (2.12) and (2.13) is considered, a nonlinear state-dependent limit equation of the input can be formulated as

$$\tilde{u}(\mathbf{x}) = \mathrm{F}_{\mathrm{ps}}(\mathrm{x}_1) + \mathrm{F}_{\mathrm{ss}}(\mathrm{x}_1) + \mathrm{F}_{\mathrm{es}}(\mathrm{x}_1) + \mathrm{F}_{\mathrm{g}}(\mathrm{x}_1) + \mathrm{F}_{\mathrm{o,u}}(\mathrm{x}_2 - \mathrm{x}_4) - \mathrm{F}_{\mathrm{d,lin}}(\mathrm{x}_2 - \mathrm{x}_4) - \mathrm{F}_{\mathrm{f,lin}}(\mathrm{x}_1). \tag{7.19}$$

In this set of equations all nonlinearities have been placed in the input and the resulting func-

tion is illustrated in Figure 7.2(b). Therefore, the optimal control problem deals with a linear system dynamic and a nonlinear state-dependent input function. This problem's formulation is in contrast to the one which considers the current as linear input, while the system dynamic remains nonlinear, see Section 7.4.

Summarizing the observations presented in this Section the following optimization problem is derived. Its solution represents the optimal feedforward solution, which will be used as base of the feedback strategy presented in Section 7.6:

$$\begin{aligned}
\text{Cost function:} \quad & \mathrm{J} = \frac{1}{2}\mathbf{x}^{\mathrm{T}}\left(\mathrm{t_e}\right)\mathbf{S}\mathbf{x}\left(\mathrm{t_e}\right) + \frac{1}{2}\int_{\mathrm{t_0}}^{\mathrm{t_e}} \mathbf{y}^{\mathrm{T}}\mathbf{Q}_{\mathrm{y}}\mathbf{y}\ \mathrm{dt} + \mathrm{c}\ \max\left|\ddot{\mathrm{z}}_{\mathrm{c}}\right| + \mathrm{b}\ \max\left|\mathrm{F_{dyn}}\right|, \\
& \min_{\mathbf{u}(\mathrm{t})\in[0,\mathrm{t_e}]} \mathrm{J} \\
\text{Side condition:} \quad & \dot{\mathbf{x}} = \mathbf{A}\mathbf{x} + \mathbf{b}\mathrm{u} \\
\text{Inequality constraint:} \quad & -\mathrm{x}_1 + \mathrm{x}_{1,\min} \leq 0 \\
& \mathrm{u_u}(\mathbf{x}) \leq \mathrm{u} \leq \mathrm{u_o}(\mathbf{x}) \\
\text{Initial condition:} \quad & \mathbf{x}\left(\mathrm{t}_0\right) = \mathbf{x}_0 \text{ arbitrary but fixed, } \mathrm{t}_0 = 0 \\
\text{Final condition:} \quad & \mathbf{x}\left(\mathrm{t_e}\right) \text{ fixed or free, } \mathrm{t_e} \text{ fixed or free.}
\end{aligned} \tag{7.20}$$

Boundary of the analytical solvability of the problem

The solution of the optimal problem for a linear full-active (or slow-active) suspension system, without input or state boundaries, can be solved by applying the Hamilton equations, derived in Section 7.1, [48, 155]. According to [172], input limitation described by upper and lower bounds can be solved deploying the MATLAB©-function *bvp4c*. The addition of state and state-dependent input limitations, as presented in Section 7.1, enhances the complexity of statement of the problem, which has to be solved. Hence, the unsteadiness in the input signals, which influences the system dynamics, increases and does not allow an analytic solution of the optimization problem (7.20). However, there are numerous numerical procedures, which can be implemented to solve the optimal feedforward problem, [21, 23, 91]. In Section 7.3 the one utilized to solve the optimal control problem in this Thesis is explicitly reported.

7.3 Nonlinear programming

Because of the system nonlinearities, the optimization problem has to consider side conditions. Allowing inequality constraints, the approach for nonlinear programming generalizes the method of Lagrange multipliers, which considers only equality constraints, [23, 91]. Applying an input-state linearization the quarter-car model can be reformulated as

$$\begin{aligned} \dot{\mathbf{x}} &= \mathbf{A}_{\mathrm{L}}\mathbf{x} + \mathbf{b}_{\mathrm{L}}\mathrm{u} + \mathbf{e}\dot{\mathrm{x}}_{\mathrm{g}} \\ \mathbf{y} &= \mathbf{C}_{\mathrm{L}}\mathbf{x} + \mathbf{d}_{\mathrm{L}}\mathrm{u} + \mathbf{f}\dot{\mathrm{x}}_{\mathrm{g}}, \end{aligned} \tag{7.21}$$

where the matrices are defined in (2.12) and (2.13). The dynamic matrix $\mathbf{A}_{\mathrm{L}}$ includes only linear spring and linear damping coefficients, while all nonlinear effects are merged in the input signal

$$\mathrm{u} = -\mathrm{F}_{\mathrm{ps}} - \mathrm{F}_{\mathrm{ss}} - \mathrm{F}_{\mathrm{es}} - \mathrm{F}_{\mathrm{d}} - \mathrm{F}_{\mathrm{g}} - \mathrm{F}_{\mathrm{R,cw}} + \mathrm{F}_{\mathrm{d,lin}} + \mathrm{F}_{\mathrm{f,lin}}. \tag{7.22}$$

Towards to obtain the optimal solution by considering the state behavior in open loop configuration, only initial perturbation of the states are considered. Therefore, for the following analysis the contribution of the road excitation x_{g} is omitted.

7.3.1 System dynamics and cost function

In order to use computational solvers with a fixed step size Δt, which allows an analytical derivation of the Lagrange function, the dynamical optimization problem is converted into a static one by discretizing the system dynamics. Note, a small step size leads to a higher accuracy of the integration but at the same time the number of optimization parameters can significantly rise, increasing the computation time. In this Chapter, the Runge-Kutta approach of 4^{th}-order with $\Delta\mathrm{t} = 8\mathrm{ms}$ is applied whereby the discrete system formulation

$$\begin{aligned} \mathbf{x}[\mathrm{k+1}] &= \mathbf{A}_{\mathrm{d}}\mathbf{x}[\mathrm{k}] + \mathbf{b}_{\mathrm{d,1}}\mathrm{u}[\mathrm{k}] + \mathbf{b}_{\mathrm{d,2}}\mathrm{u}[\mathrm{k+1}], \\ \mathbf{y}[\mathrm{k}] &= \mathbf{C}_{\mathrm{d}}\mathbf{x}[\mathrm{k}] + \mathbf{d}_{\mathrm{d}}\mathrm{u}[\mathrm{k}], \end{aligned} \tag{7.23}$$

is obtained. The corresponding matrix and vectors are given by

$$\begin{aligned} \mathbf{A}_\mathrm{d} &= \sum_{\mathrm{i}=0}^{4} \frac{\Delta \mathrm{t}^\mathrm{i}}{\mathrm{i}!} \cdot \mathbf{A}^\mathrm{i}, \qquad \mathbf{b}_{\mathrm{d},2} = \left(\frac{\Delta \mathrm{t}}{2}\mathbf{I} + \frac{\Delta \mathrm{t}^2}{6}\mathbf{A} + \frac{\Delta \mathrm{t}^3}{24}\mathbf{A}^2 \right) \cdot \mathbf{b} \\ \mathbf{b}_{\mathrm{d},1} &= \left(\frac{\Delta \mathrm{t}}{2}\mathbf{I} + \frac{\Delta \mathrm{t}^2}{3}\mathbf{A} + \frac{\Delta \mathrm{t}^3}{8}\mathbf{A}^2 + \frac{\Delta \mathrm{t}^4}{24}\mathbf{A}^3 \right) \cdot \mathbf{b}. \end{aligned} \tag{7.24}$$

Note that the matrix $\mathbf{C}_\mathrm{d}$ and the vector $\mathbf{d}_\mathrm{d}$ remain identical to the continuous ones in (7.21), since the output equations represent a linear combination of the calculated states, $\mathbf{x}[\mathrm{k}]$. Because of the recursive system formulation (7.23), it can be compactly written depending only on the initial state vector and the applied control sequence

$$\hat{\mathbf{x}} = \Theta \cdot \hat{\mathbf{u}} + \Xi \cdot \mathbf{x}_0 \tag{7.25}$$

with $\hat{\mathbf{x}} = [\mathrm{x}[0] \ \cdots \ \mathrm{x}[\mathrm{N}]]^\mathrm{T}$, $\hat{\mathbf{u}} = [\mathrm{u}[0] \ \cdots \ \mathrm{u}[\mathrm{N}]]^\mathrm{T}$ and $\hat{\mathbf{y}} = [\mathrm{y}[0] \ \cdots \ \mathrm{y}[\mathrm{N}]]^\mathrm{T}$. The number of iterations is given by $\mathrm{N} \in \mathbb{N}$. The matrices in (7.25) are defined as

$$\begin{aligned} \underbrace{\begin{bmatrix} \mathbf{x}[0] \\ \mathbf{x}[1] \\ \mathbf{x}[2] \\ \vdots \\ \mathbf{x}[\mathrm{N}] \end{bmatrix}}_{\hat{\mathbf{x}}} &= \underbrace{\begin{bmatrix} \mathbf{0} & \mathbf{0} & \mathbf{0} & \cdots & \mathbf{0} \\ \mathbf{b}_{\mathrm{d},1} & \mathbf{b}_{\mathrm{d},2} & \mathbf{0} & \cdots & \mathbf{0} \\ \mathbf{A}_\mathrm{d}\mathbf{b}_{\mathrm{d},1} & \mathbf{A}_\mathrm{d}\mathbf{b}_{\mathrm{d},2} + \mathbf{b}_{\mathrm{d},1} & \mathbf{b}_{\mathrm{d},2} & \cdots & \mathbf{0} \\ \vdots & \vdots & \vdots & \ddots & \vdots \\ \mathbf{A}_\mathrm{d}^{\mathrm{N}-1}\mathbf{b}_{\mathrm{d},1} & \mathbf{A}_\mathrm{d}^{\mathrm{N}-1}\mathbf{b}_{\mathrm{d},2} + \mathbf{A}_\mathrm{d}^{\mathrm{N}-2}\mathbf{b}_{\mathrm{d},1} & \mathbf{A}_\mathrm{d}^{\mathrm{N}-2}\mathbf{b}_{\mathrm{d},2} + \mathbf{A}_\mathrm{d}^{\mathrm{N}-3}\mathbf{b}_{\mathrm{d},1} & \cdots & \mathbf{b}_{\mathrm{d},2} \end{bmatrix}}_{\Theta} \underbrace{\begin{bmatrix} u[0] \\ u[1] \\ u[2] \\ \vdots \\ u[\mathrm{N}] \end{bmatrix}}_{\hat{\mathbf{u}}} \\ &+ \underbrace{\begin{bmatrix} \mathbf{I} & \mathbf{A}_\mathrm{d} & \mathbf{A}_\mathrm{d}^2 & \cdots & \mathbf{A}_\mathrm{d}^\mathrm{N} \end{bmatrix}^\mathrm{T}}_{\Xi} \cdot \mathbf{x}[0] \end{aligned} \tag{7.26}$$

and

$$\underbrace{\begin{bmatrix} \mathbf{y}[0] \\ \vdots \\ \mathbf{y}[\mathrm{N}] \end{bmatrix}}_{\hat{\mathbf{y}}} = \underbrace{\begin{bmatrix} \mathbf{C}_\mathrm{d} & \cdots & \mathbf{0} \\ \vdots & \ddots & \vdots \\ \mathbf{0} & \cdots & \mathbf{C}_\mathrm{d} \end{bmatrix}}_{\Psi} \cdot \hat{\mathbf{x}} + \underbrace{\begin{bmatrix} \mathbf{d}_\mathrm{d} & \cdots & \mathbf{0} \\ \vdots & \ddots & \vdots \\ \mathbf{0} & \cdots & \mathbf{d}_\mathrm{d} \end{bmatrix}}_{\Omega} \cdot \hat{\mathbf{u}}. \tag{7.27}$$

The output relation can be further rewritten as follows

$$\hat{\mathbf{y}} = \underbrace{(\Psi\Theta + \Omega)}_{\mathbf{G}} \cdot \hat{\mathbf{u}} + \underbrace{\Psi\Xi}_{\mathbf{N}} \cdot \mathbf{x}_0. \tag{7.28}$$

The considered cost function (see (7.20))

$$\mathrm{J} = \underbrace{\frac{1}{2}\mathbf{x}^{\mathrm{T}}\left(\mathrm{t_e}\right)\mathbf{S}\mathbf{x}\left(\mathrm{t_e}\right) + \frac{1}{2}\int_0^{\mathrm{t_e}} \mathbf{y}^{\mathrm{T}}\mathbf{Q}_y\mathbf{y}\,\mathrm{dt}}_{\mathrm{J_{quad}}} + \underbrace{\mathrm{c_{max}} \cdot \max\left|\ddot{\mathrm{z}}_{\mathrm{c}}\right| + \mathrm{b_{max}} \cdot \max\left|\mathrm{F_{dyn}}\right|}_{\mathrm{J_{max}}}. \tag{7.29}$$

consists of a quadratic term $\mathrm{J_{quad}}$ and a term $\mathrm{J_{max}}$, which explicitly considers the maximal values of the two ride objective variables (see Section 2.4). $\mathbf{S}$, $\mathbf{Q}_{\mathrm{y}}$, $\mathrm{c_{max}}$ and $\mathrm{b_{max}}$ represent the weighing matrices and coefficients, respectively.

7.3.2 Analytic determination of the Lagrange function

In order to solve the optimization problem according to (7.20) with the cost function (7.29), the interior-point-algorithm is adopted, which allows to solve nonlinear problems with linear and nonlinear inequality constraints, [23]. The required gradients and the Hessian of the obtained Lagrange function $\mathcal{L}\left(\mathbf{x}, \boldsymbol{\lambda}, \boldsymbol{\nu}\right)$

$$\mathcal{L}\left(\mathbf{x}, \boldsymbol{\lambda}, \boldsymbol{\nu}\right) = \mathrm{f}(\mathbf{x}) + \boldsymbol{\lambda}^T\mathbf{c}_{\mathrm{eq}} + \boldsymbol{\nu}^T\mathbf{c} \tag{7.30}$$

can be derived analytically as

$$\nabla_{\hat{\mathbf{u}}}\mathcal{L}\left(\mathbf{x}, \boldsymbol{\lambda}, \boldsymbol{\nu}\right) = \nabla_{\hat{\mathbf{u}}}\mathrm{f}\left(\mathbf{x}\right) + \sum_{\mathrm{i}} \lambda_{\mathrm{i}}\nabla_{\hat{\mathbf{u}}}\mathrm{c}_{\mathrm{eq,i}}\left(\mathbf{x}\right) + \sum_{\mathrm{j}} \nu_{\mathrm{j}}\nabla_{\hat{\mathbf{u}}}\mathrm{c}_{\mathrm{j}}\left(\mathbf{x}\right), \tag{7.31}$$

and

$$\nabla^2_{\hat{\mathbf{u}}\hat{\mathbf{u}}}\mathcal{L}\left(\mathbf{x}, \boldsymbol{\lambda}, \boldsymbol{\nu}\right) = \nabla^2_{\hat{\mathbf{u}}\hat{\mathbf{u}}}\mathrm{f}\left(\mathbf{x}\right) + \sum_{\mathrm{i}} \lambda_{\mathrm{i}}\nabla^2_{\hat{\mathbf{u}}\hat{\mathbf{u}}}\mathrm{c}_{\mathrm{eq,i}}\left(\mathbf{x}\right) + \sum_{\mathrm{j}} \nu_{\mathrm{j}}\nabla^2_{\hat{\mathbf{u}}\hat{\mathbf{u}}}\mathrm{c}_{\mathrm{j}}\left(\mathbf{x}\right), \tag{7.32}$$

where the equality term $\mathbf{c}_{\mathrm{eq}}$ can be written as

$$\mathbf{c}_{\mathrm{eq}} = \begin{bmatrix}\mathbf{A}_{\mathrm{d}}^{\mathrm{N\text{-}1}}\mathbf{b}_{\mathrm{d},1} & \cdots & \mathbf{b}_{\mathrm{d},2}\end{bmatrix} \cdot \hat{\mathbf{u}} \quad + \mathbf{A}_{\mathrm{d}}^{\mathrm{N}}\mathbf{x}_0, \tag{7.33}$$

if the end point is considered to be fixed. The first derivative $\nabla \mathbf{c}_{\text{eq}} = \frac{\partial \mathbf{c}_{\text{eq}}}{\partial \hat{\mathbf{u}}}$ is constant. The second derivative of the constraint does not influence the Hessian-matrix because of the linear characteristic of this constraint, i.e. $\nabla^2 \mathbf{c}_{\text{eq}} = \mathbf{0}$. In order to take the constructive limitation of the suspension deflection into account, the inequality constraint $\mathbf{c}_1$ can be formulated to maintain the suspension deflection under the minimal value $|\mathrm{x}_{1,\min}|$ in every time step. This condition is given by $\nabla \mathbf{c}_1 = \frac{\partial \mathbf{c}_1}{\partial \hat{\mathbf{u}}}$. Since this constraint is linear the second derivate is equal to zero and does not influence the Hessian, analogous to the previous case.

Because of the state-dependent characteristics of the damper force, a working range limited by an upper ($\mathrm{F_o}$) and a lower bound ($\mathrm{F_u}$) needs to be defined. The damper force must lie within this range in every time step. The associated constraint inequalities are expressed as

$$\mathbf{c_2} = \hat{\mathbf{u}} - \hat{\mathbf{F}}_{\text{ps}} - \hat{\mathbf{F}}_{\text{ss}} - \hat{\mathbf{F}}_{\text{es}} - \hat{\mathbf{F}}_{\text{g}} - \hat{\mathbf{F}}_{\text{R,cw}} + \hat{\mathbf{F}}_{\text{d,lin}} + \hat{\mathbf{F}}_{\text{c,lin}} - \hat{\mathbf{F}}_{\text{o}} \leq \mathbf{0} \tag{7.34}$$

$$\mathbf{c_3} = -\left(\hat{\mathbf{u}} - \hat{\mathbf{F}}_{\text{ps}} - \hat{\mathbf{F}}_{\text{ss}} - \hat{\mathbf{F}}_{\text{es}} - \hat{\mathbf{F}}_{\text{g}} - \hat{\mathbf{F}}_{\text{R,cw}} + \hat{\mathbf{F}}_{\text{d,lin}} + \hat{\mathbf{F}}_{\text{c,lin}}\right) + \hat{\mathbf{F}}_{\text{u}} \leq \mathbf{0}, \tag{7.35}$$

To supply the algorithm with the corresponding first and the second derivative, each term of (7.34) is calculated analytically.

7.3.3 Choice of the initial control sequence

In order to decrease the required computational time, the linearized system (7.21) is considered to calculate the starting control sequence $\hat{\mathbf{u}}_\mathbf{0}$. For the initial choice of the input, inequality constraints are not considered, $\mathbf{x}(\mathrm{t_e}) = \mathbf{x}_\mathrm{e} = \mathbf{0}$ and $\mathrm{t_e}$ can be considered fixed or free. The cost function[1] is considered with respect to the output variables

$$\begin{aligned} \mathrm{J} &= \frac{1}{2}\mathbf{x}^{\mathrm{T}}(\mathrm{t_e})\mathbf{S}\mathbf{x}(\mathrm{t_e}) + \frac{1}{2}\int_{\mathrm{t_0}=0}^{\mathrm{t_e}} \mathbf{y}^{\mathrm{T}}\mathbf{Q}_{\mathrm{y}}\mathbf{y}\ \mathrm{dt} \\ &= \underbrace{\frac{1}{2}\mathbf{x}^{\mathrm{T}}(\mathrm{t_e})\mathbf{S}\mathbf{x}(\mathrm{t_e})}_{\mathrm{h}(\mathbf{x}(\mathrm{t_e}),\mathrm{t_e})} + \frac{1}{2}\int_{0}^{\mathrm{t_e}} \mathbf{x}^{\mathrm{T}}\underbrace{\mathbf{C}^{\mathrm{T}}\mathbf{Q}_{\mathrm{y}}\mathbf{C}}_{\mathbf{Q}}\mathbf{x} + \underbrace{\mathbf{d}^{\mathrm{T}}\mathbf{Q}_{\mathrm{y}}\mathbf{d}}_{\mathrm{R}}\mathrm{u}^2 + 2\mathrm{u}\underbrace{\mathbf{d}^{\mathrm{T}}\mathbf{Q}_{\mathrm{y}}\mathbf{C}}_{\mathbf{s}^{\mathrm{T}}}\mathbf{x}\ \mathrm{dt}. \end{aligned} \tag{7.36}$$

[1] if $\mathrm{t_e}$ is fixed, then $\mathbf{S} = \mathbf{0}$

The Hamiltonian takes the following form

$$\mathbf{H} = \frac{1}{2}\left(\mathbf{x}^{\mathrm{T}}\mathbf{Q}\mathbf{x} + \mathrm{R}\mathrm{u}^2 + 2\mathrm{u}\mathbf{s}^{\mathrm{T}}\mathbf{x}\right) + \boldsymbol{\psi}^{\mathrm{T}}\left(\mathbf{A}\mathbf{x} + \mathbf{b}\mathrm{u}\right), \tag{7.37}$$

while the Lagrange function has the following form

$$\mathcal{L}\left(\hat{\mathbf{u}}, \boldsymbol{\lambda}\right) = \frac{1}{2}\hat{\mathbf{u}}^{\mathrm{T}}\mathbf{H}\hat{\mathbf{u}} + \mathbf{g}^{\mathrm{T}}\hat{\mathbf{u}} + \mathrm{c} + \boldsymbol{\lambda}^{\mathrm{T}} \cdot \left[\mathbf{T}_{\mathrm{N}} \cdot \left(\Theta\hat{\mathbf{u}} + \Xi\mathbf{x}_0\right)\right]. \tag{7.38}$$

The latter is derived with respect to the control sequence and the Lagrange multiplier $\boldsymbol{\lambda}$ the derivatives are

$$\nabla_{\hat{\mathbf{u}}}\mathcal{L} = \mathbf{H}\hat{\mathbf{u}} + \mathbf{g} + \left(\mathbf{T}_{\mathrm{N}}\Theta\right)^{\mathrm{T}}\boldsymbol{\lambda}, \quad \nabla_{\boldsymbol{\lambda}}\mathcal{L} = \mathbf{T}_{\mathrm{N}}\left(\Theta\hat{\mathbf{u}} + \Xi\mathbf{x}_0\right). \tag{7.39}$$

That leads to the following linear system

$$\begin{bmatrix} \hat{\mathbf{u}} \\ \boldsymbol{\lambda} \end{bmatrix} = \begin{bmatrix} \mathbf{H} & \left(\mathbf{T}_{\mathrm{N}}\Theta\right)^{T} \\ \mathbf{T}_{\mathrm{N}}\Theta & \mathbf{0} \end{bmatrix}^{-1} \cdot \begin{bmatrix} -\mathbf{g} \\ -\mathbf{T}_{\mathrm{N}}\Xi\mathbf{x}_0 \end{bmatrix} \tag{7.40}$$

whose solution is adopted as initial sequence.

7.4 Optimal switching system

Switched linear systems are a practical relevance subclass of hybrid dynamical systems, [103]. They consist of a finite amount $\mathrm{i} \in \{1, 2, \ldots, \mathrm{s}\}$, $\mathrm{s} \in \mathbb{N}$ of continuous dynamical LTI-subsystems. The actual active subsystem changes at a specific switching time τ which can be extrinsically (time-depending switching) or intrinsically (state-depending) given. Applying this notation, the nonlinear semi-active suspension defined in (7.21) becomes a state-depending switched system

$$\dot{\mathbf{x}} = \mathbf{f}\left(\mathbf{x}, \mathrm{u}_{\mathrm{I}(\tau)}\right). \tag{7.41}$$

The different dynamics are characterized by discrete damper currents

$$\mathrm{I} \in \{\mathrm{I}_1, \ldots, \mathrm{I}_{\mathrm{s}}\}, \quad \mathrm{I}_{\mathrm{min}} \leq \mathrm{I}_1 < \ldots < \mathrm{I}_{\mathrm{s}} \leq \mathrm{I}_{\mathrm{max}}, \tag{7.42}$$

within the possible range $[\mathrm{I}_{\mathrm{min}}, \mathrm{I}_{\mathrm{max}}]$. Note that, the parameter I does not represent the real current **i** applied to the damper. Thereby, the damping force F changes according to Figure 2.3(a).

Based on that, the input signals $\mathbf{u}$ in (7.22) switch accordingly.

In order to decide which dynamics should be activated, an optimal feedforward control law for an initialization $\mathbf{x}_0$ is achieved by solving the optimization problem

$$\min_{\mathcal{I},\mathcal{T}} \left[\int_0^\infty \mathbf{x}^{\mathrm{T}} \mathbf{Q}_{\mathrm{i(t)}} \mathbf{x} \, \mathrm{dt} + \sum_{\mathrm{k=1}}^{\mathrm{N}} \mathrm{h_k}\left(\tau_{\mathrm{k}}\right) \right], \quad \text{s.t.} \begin{cases} \dot{\mathbf{x}} = \mathbf{A}_{\mathrm{i(t)}} \mathbf{x}; \quad \mathbf{x}(0) = \mathbf{x}_0 \\ \mathrm{i(t)} = \mathrm{i_k} \text{ for } \tau_{\mathrm{k}} \leq \mathrm{t} < \tau_{\mathrm{k+1}} \\ \mathrm{i_{k+1}} \succ \mathrm{i_k} \\ \tau_0 = 0, \ \tau_{\mathrm{N+1}} = \infty \\ \tau_{\mathrm{k+1}} \geq \tau_{\mathrm{k}} + \delta_{\mathrm{min}} \\ \mathbf{x}\left(\tau_{\hat{k}}^{+}\right) = \mathbf{M}_{\mathrm{i}_{\hat{k}-1},\mathrm{i}_{\hat{k}}} \mathbf{x}\left(\tau_{\hat{k}}^{-}\right) \\ \mathrm{h}_{\hat{k}}\left(\tau_{\hat{k}}\right) = \mathrm{H}_{\mathrm{i}_{\hat{k}-1},\mathrm{i}_{\hat{k}}} \text{ if } \tau_{\hat{k}} < \infty \\ \mathrm{h}_{\hat{k}}\left(\tau_{\hat{k}}\right) = 0 \text{ if } \tau_{\hat{k}} = \infty. \end{cases} \tag{7.43}$$

The corresponding optimization variables are the sequence of active dynamics by a sequence of damper currents $\mathcal{I} = \{\mathrm{I}(\tau_0), \ldots, \mathrm{I}(\tau_{\mathrm{N}})\}$ and the moments of switching between them $\mathcal{T} = \{\tau_1, \ldots, \tau_{\mathrm{N}}\}$. The value $\mathrm{N} \in \mathbb{N}$ expresses the amount of allowed overall switches. Each dynamics $\mathbf{A}_{\mathrm{i(t)}}$ is characterized by a stable behavior, which means $\Re\left(|\mu\mathbf{I} - \mathbf{A}_{\mathrm{i_k}}|\right) < 0 \ \forall \ \mathrm{i_k}$.

In contrast to the NLP approach, physical switching restrictions of the damper are considered in two ways, analogous to the linear case shown in [58]: First, by a time constant δ_{min}, which represents the minimal dwell time of remaining in an activated dynamics and thus between two sequenced switching moments τ^- and τ^+. Second, $\mathrm{I}_{\tau^+} \succ \mathrm{I}_{\tau^-}$, meaning that switching is only allowed to the nearest dynamics

$$\mathrm{I}_{\tau^+} \in \begin{cases} \{\mathrm{I}_{\tau^-}, \mathrm{I}_{\tau^-} + 1\}, & \text{if } \mathrm{I}_{\tau^-} = 1 \\ \{\mathrm{I}_{\tau^-} - 1, \mathrm{I}_{\tau^-}, \mathrm{I}_{\tau^-} + 1\}, & \text{if } \mathrm{I}_{\tau^-} = \{2, \ldots, \mathrm{s} - 1\} \\ \{\mathrm{I}_{\tau^-} - 1, \mathrm{I}_{\tau^-}\}, & \text{if } \mathrm{I}_{\tau^-} = \mathrm{s}. \end{cases} \tag{7.44}$$

The quadratic cost function in (7.43) can be interpreted as a sum of costs $\mathrm{J}_{\mathrm{I}(\tau_{\mathrm{k}})}^{(\rho_{\mathrm{k}})}$ arising by the

active dynamics $\mathrm{I}(\tau_\mathrm{k})$ within the interval $\rho_\mathrm{k} = [\tau_\mathrm{k}, \tau_{\mathrm{k+1}}]$, $\mathrm{k} \in \mathbb{N}_0$ between switching, meaning

$$\mathrm{J}_{\mathrm{I}(\tau_\mathrm{k}),\mathrm{N}-l} = \sum_{\mathrm{k}=0}^{\mathrm{N}-l} \underbrace{\int_{\tau_\mathrm{k}}^{\tau_{\mathrm{k+1}}} \mathbf{y}^\mathrm{T} \mathbf{Q}_{\mathrm{I}(\tau_\mathrm{k})} \mathbf{y} \, \mathrm{dt}}_{\mathrm{J}_{y,\mathrm{I}(\tau_\mathrm{k})}^{(\rho_\mathrm{k})}} . \tag{7.45}$$

A qualitative illustration is given in Figure 7.3, in which the switch sequence and the respective costs are drawn. Accordingly, $\mathrm{J}_{\mathrm{I}(\tau_\mathrm{k}),\mathrm{N}-l}$ expresses the actual costs by $l \leq \mathrm{N}$, $l \in \mathbb{N}$, remaining switches and a currently active dynamic $\mathrm{I}(\tau_\mathrm{k})$.

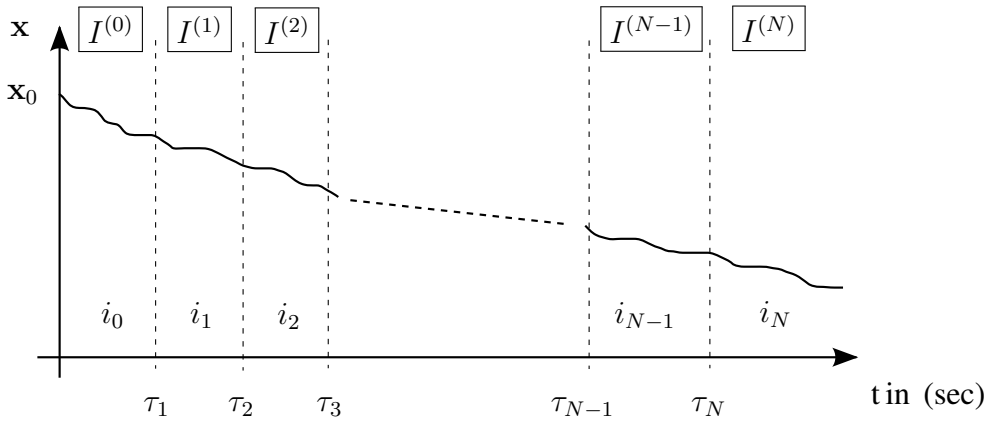

Figure 7.3: Qualitative illustration of the switch sequence and its costs

The resulting problem can be numerically efficiently handled by the well-known principle of dynamic programming [91]. Thus, according to the optimality principle of Bellman [13], the overall strategy can be only optimal, if and only if each partial sequence of (7.45) is optimal. The corresponding formulation of the Bellman's recurrence equation is

$$\mathrm{J}^*_{\mathrm{I}(\tau_\mathrm{k}),\mathrm{N}-l} = \min_{\mathrm{I},\, \rho_k} \left\{ \mathrm{J}^{(\rho_\mathrm{k})}_{\mathrm{I}(\tau_\mathrm{k})} \right\} + \mathrm{J}^*_{\mathrm{I}(\tau_{\mathrm{k+1}}),\mathrm{N}-l-1}, \tag{7.46}$$

The upper index $*$ denotes the optimal solution of the corresponding time intervals.

Compared to the linear suspension system case [58], the whole state space of interest has to be discretized into grid points $\bar{\mathbf{x}} \in \bar{\mathbb{X}} \subset \mathbb{R}^\mathrm{n}$. Figure 7.4 shows an equidistant grid for $\mathbb{R}^2$ exemplarily. Such a grid is considered for $\mathbb{R}^\mathrm{n}$ at every switching moment τ_k. A simultaneous

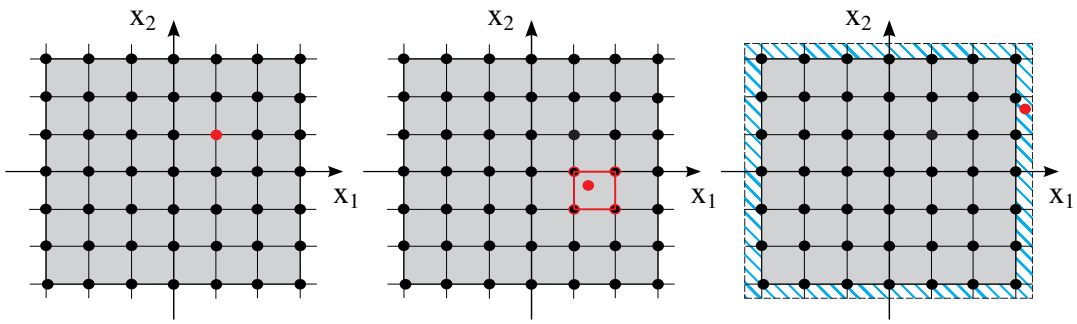

(a) Grid $\bar{\mathbf{x}}(\tau_k)$ (b) Grid $\bar{\mathbf{x}}(\tau_{k+1})$ (c) Grids for $\Phi_{i(\tau_N)}$

Figure 7.4: State space discretization

inclusion of space restrictions, like spring deflection limits, is achieved by bounding the state range of discretization

$$x_i^{(min)} \leq x_i \leq x_i^{(max)}, \quad i \in [1;n]. \tag{7.47}$$

Trajectories $\Phi_{I(\tau_k)}$ between $\mathbf{x}(\tau_k) = \bar{\mathbf{x}}(\tau_k)$ and $\mathbf{x}(\tau_{k+1})$ will not end at a discretization point $\mathbf{x}(\tau_{k+1})$, as illustrated for the marked grid point in Figure 7.4(a) and Figure 7.4(b), respectively. Therefore, the corresponding recursive cost function value according to (7.46) will be obtained by interpolating the values of the surrounding mesh points $\mathbf{x}(\tau_{k+1})$, [37].

The question arises how trajectories $\Phi_{I(\tau_k)}$ which do not remain within $\bar{\mathbb{X}}$ should be treated. The part of the cost function (7.45) considering the final interval ρ_N, is subdivided into

$$J_{I(\tau_N)}^{(\rho_N)} = \begin{cases} \int_0^\infty \mathbf{y}^T \mathbf{Q}_{y,I(\tau_k)} \mathbf{y} \, dt, & \text{if (7.47) holds true,} \\ \infty, & \text{else.} \end{cases} \tag{7.48}$$

This means, if $\Phi_{I(\tau_N)}$ get out of $\bar{\mathbb{X}}$ (see Figure 7.4) then its cost function is set to ∞ and thus, $\Phi_{I(\tau_N)}$ becomes unfeasible for the optimization. For all other intervals ρ_k, $k < N$, such a penalization is not required. The maximum allowed time interval $\rho_k = [\tau_k, \tau_{k+1}]$ for staying within a dynamic $I(\tau_k)$ can be directly restricted by

$$\tau_{k+1} = \begin{cases} \infty & \text{if } \mathbf{x}(t) \in \bar{\mathbb{X}}, \\ \{\min(t^-) > \tau_k | \mathbf{x}(t^+) \notin \bar{\mathbb{X}}\} & \text{else} \end{cases} \tag{7.49}$$

for the optimization. In other words, the switching moment τ_{k+1} is at the time t^- right before the trajectory leaves $\bar{\mathbb{X}}$ at time t^+. Based on (7.45) and (7.46), respectively, the optimal overall cost $J^*_{I(\tau_k),N}$ can be recursively calculated for each grid point $\bar{\mathbf{x}}(\tau_k) \in \bar{\mathbb{X}}$ beginning with the final interval. Is the dynamic system at the switching time of τ_k in state $\mathbf{x}(\tau_k)$, the optimization problem is to minimize the residual cost function $J_{i_k,N-k}$, at which the (k+1)-th interval, the dynamics of $i_k = \{1, \cdot, s\}$ is active and still (N-k) switching are going to be executed. The optimal rest function $J^*_{i_k,N-k}(\mathbf{x}(\tau_k))$ is defined as the smallest possible value of the quality measure $J_{i_k,N-k}$. On the basis of the principle of optimality, the optimal residual cost function $J^*_{i_k,N-k}(\mathbf{x}(\tau_k))$, due to its additive property, can be split into (k+1)-th intervals and into optimal residual costs $J^*_{i_{k+1},N-k-1}(\mathbf{x}(\tau_{k+1}))$. The overall strategy can only be optimal if the same is true for the rest strategy.

On the switch time τ_k at each discrete time point many information are taken into account, see Figure 7.5.

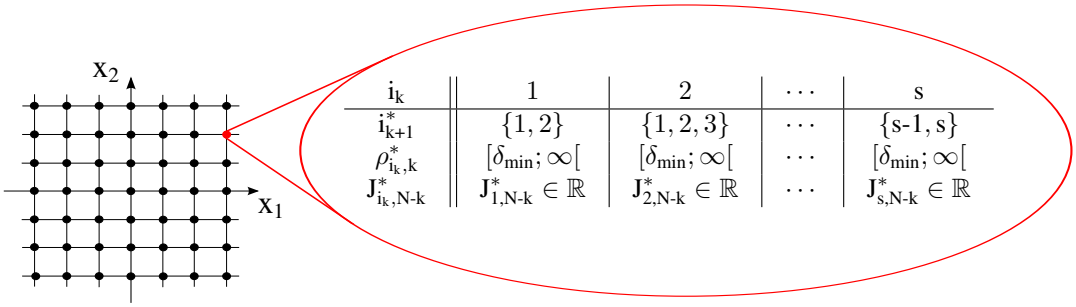

Figure 7.5: Information saved at each time instant τ_k for the discrete state

The final obtained optimization problem can be solved by any appropriate numerical method. For instance, applying the Runge-Kutta method for discretization and the trapezoidal numerical integration method for approximating the integral cost function, analoguous to Section 7.3. The finally obtained optimization results are a sequence of optimal dynamics $\mathcal{I}^* = \{I^*(\tau_0), \ldots, I^*(\tau_N)\}$ and corresponding switching moments $\mathcal{T}^* = \{\tau_1^*, \ldots, \tau_N^*\}$ for each $\bar{\mathbf{x}}(\tau_0)$.

The presented strategy is adopted both for the linear and the nonlinear model. Considering the linear case, the system is allowed to switch only to the nearest dynamic, i.e. to the nearest higher or lower damping coefficient. Moreover a direct change of the dynamic is avoided by the time delay δ_{min}. Thus, the actuator dynamic (e.g. electrical or mechanical time constant)

can be included into the optimization problem. Due to the solution of the problem by means of the minimization of (7.46), discretization of the states and simplification of the algorithm, the integration of the state limitation becomes inapplicable, [40, 58].

For the nonlinear model the optimization problem remains equal to the linear case but in (7.43) the dynamic matrix, the cost function and the calculation of the solution cannot be obtained analytically. Moreover, due to the nonlinear damper characteristics, the $s \in \mathcal{S}$ possible dynamics cannot be related to the damping coefficient anymore. In the nonlinear case, they are associated to the damper currents $\mathbf{i}$, i.e. to the nonlinear characteristics. Due to the nonlinear characteristics the problem is extended by the introduction of state constraints. A new weighting function is applied, which allows to assign a value to the state leaving the grid. For the last interval the modified cost function can be written as

$$J^{*}_{i_N,0} = \begin{cases} \int_0^{\infty} \mathbf{x}^{T}\mathbf{Q}_{i_N}\mathbf{x}\ dt, & \text{for } x_i^{(min)} \leq x_i(t) \leq x_i^{(max)}, \quad i \in [1;n] \wedge t \in [0;\infty[\\ \infty, & \text{else.} \end{cases} \tag{7.50}$$

The length of the remaining intervals $\rho_{i_k,k}$ is defined by the instant of time, in which the state trajectory with dynamics i_k leaves the grid, i.e.

$$\rho_{i_k,k} = \left\{ t \in [\tau_k;\tau_{k+1}[\mid \mathbf{x}(t) \in \mathbb{X} \right\}. \tag{7.51}$$

Most of the states $\mathbf{x}(\tau_{k+1})$ do not hold an exact value of the cost function, therefore it has to be determined by interpolation. In Figure 7.6 this case is underlined. As contrast of the linear case, it can happen, that the interpolation takes place between finite and an infinite values $J_{i_k,N\text{-}k} = \infty$. In this case also the point between the grid obtains an infinite value.

Alternative, at each grid point with finite cost values, a neighborhood ξ can be defined, in which J assumes a finite values. Thus, within the framework of the possible characteristics, the procedure always try not to leave the state space minimizing, at the same time, the cost function.

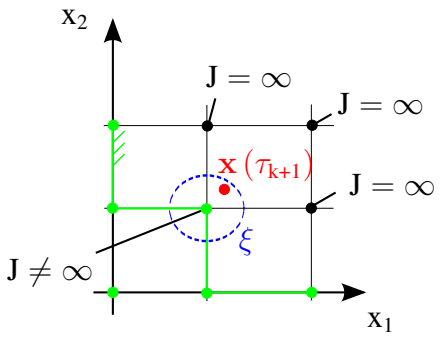

Figure 7.6: Interpolation problem at the switching time τ_{k+1}

7.5 Parameter analysis of the optimal control solutions

In this Section the single optimal control solutions, which are depending on the initial values of the state, are analyzed. Moreover, the influence of the design parameter presented in the previous Sections is pointed out. Due to the similar results, a detailed analysis is explicitly presented only for the nonlinear programming solutions.

Generally, the optimal solutions and the resulting closed loop control strategy depend on the choice of the cost function and on the boundary conditions. As result, four different parameters, which influence the ride comfort and ride safety, can be analyzed:

1. free or fixed terminal time t_e,

2. free or fixed terminal path $\mathbf{x}(t_e)$,

3. suspension deflection weight in the cost function ($q_{x_1} \neq 0$) or as inequality constraint ($q_{x_1} = 0$),

4. choice of the weighting factors (q_{x_1}, $q_{\ddot{z}_c}$, $q_{F_{dyn}}$, b_{max}, c_{max}) or their relation to each other and to the quadratic nonlinear or mixed cost function.

In order to compare the optimal single control solutions, two start state vectors have been chosen, which differently exploit the semi-active device. By the first configuration $\mathbf{x}_0^{(1)}$, the

passive configuration of the quarter-car model, is strongly excited and the damper at the beginning is already in the saturation. Instead, by the second state $\mathbf{x}_0^{(2)}$, the damper force can be in saturation or within the working range of the damper, depending on the choice of the weighting factors.

7.5.1 Influence of the terminal time and the terminal state

One way to influence the solution of the problem is in the choice of the final time $\mathrm{t_e}$ and the final state $\mathbf{x}(\mathrm{t_e})$. In this analysis, the end time in the interval $[0, \infty[$ can be fixed or free, and the final states are selected as fixed or free.

For the choice of a possible combination to determine a terminal condition, the definiteness of the integrand $\mathrm{g}(\mathbf{x}, \mathrm{u}, \mathrm{t})$ in the quality measure (7.20) is crucial. If the integrand is positive semi-definite, i.e. it is assumed that it can be zero also outside of the equilibrium point, then for an end time $\mathrm{t_e} = \infty$ and a free final state, it cannot be ensured that all states have been transferred within a finite time interval to the equilibrium. It occurs only by an appropriate choice of the cost function, i.e. by consideration of the body acceleration in the square measure of quality, however it is only guaranteed when the arbitrary control variables $\mathbf{u}$ act on the system. Since the semi-active suspension can work with its state-dependent variable attenuation exclusively dissipative, and thus energy is always deprived from the system, the integrand of (7.20) is always positive definite, i.e. $\mathbf{y}^T\mathbf{Q}\mathbf{y} > \mathbf{0}$ for any weighting matrices, $\mathbf{Q}_y$. For this reason, any combination of the possible end states and end times for the formation of a terminal condition is acceptable.

In general, no request is made on the time interval, in which the quarter vehicle should reach the end position. However, it influences the computation time in which the solution has to be reached. This should satisfy both the requirements of the system dynamics as well as the optimization method. In terms of the numerical integration method, with which the system dynamics is discretized and solved, the step size should be chosen as small as possible, in order to dissipate the motion of the quarter-car. However, this should be chosen as small as necessary due to the increasing computational effort with decreasing step size. An estimate of the maximum step size (or minimum sampling frequency of a signal) can be carried out using Shannon's sampling theorem,

$$\frac{1}{\Delta \mathrm{t_{max}}} = \mathrm{f_s} > 2 \cdot \mathrm{f_{max}}, \tag{7.52}$$

wherein, in the case of the quarter-vehicle, the maximum occurring oscillation frequency caused by the wheel movement is considered. By the choice of such sampling, the original signal can be approximated with arbitrary precision, with almost no information loss. According to (7.52), from the natural frequency of the wheel results a maximum increment of $\Delta t_{max} = 0.042$ sec.

A detailed analysis is reported in [40] and is briefly summarized in the following. It can be underlined, that both the optimal damper force F^* and the optimal cost function J^* exhibit a small variation with respect to t_e. The rms-values of chassis acceleration and dynamical wheel load increase with respect to the final time, but their relative changes remain fairly constant compared to the passive case. In this context it should be mentioned that the damper force for the initial state $\mathbf{x}_0^{(1)}$ is always at the upper limit, whereas for $\mathbf{x}_0^{(2)}$ the possibility of variation exists, which is evident by the minimal variation in the optimum damping forces.

Comparing the rms-values of body acceleration and dynamic wheel load with those of the passive quarter-car to the corresponding time points, then the relative change in behavior for both initial states is nearly constant and independent of the choice of the final condition (performance increase of about 27% by $\mathbf{x}_0^{(1)}$ and 23% by $\mathbf{x}_0^{(2)}$). In addition it is noted, that if the suspension deflection is taken into account as inequality constraint, the relative change of the rms-value of the suspension deflection shows high fluctuations.

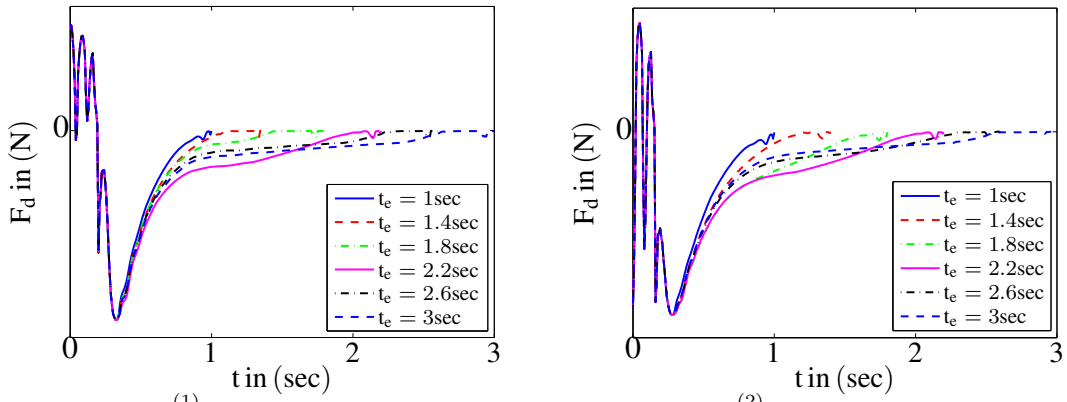

(a) Initial state $\mathbf{x}_0^{(1)}$ (b) Initial state $\mathbf{x}_0^{(2)}$

Figure 7.7: Damper force comparison for different end time in case of $\mathbf{x}(t_e) = \mathbf{0}$

Figure 7.7 presents the optimal solutions, in case of $\mathbf{x}(t_e) = \mathbf{0}$ for the first and the second

initial state. In view of the applied feedback strategy (see Section 7.7), it is noted that different solutions present almost identical course in the first part of the plot.

Moreover, in Figure 7.8 the number of iterations needed to calculate the optimal solution and the related computational time are depicted[2]. They are presented with respect to the final time. Noticeable is here, that only a minor fluctuation in the number of iterations is observed and the required computational time rises almost exponentially by increasing t_e. To guarantee low computation time and a maximum integration step size given by the system dynamic, t_e was set to 1sec and a free final state was chosen.

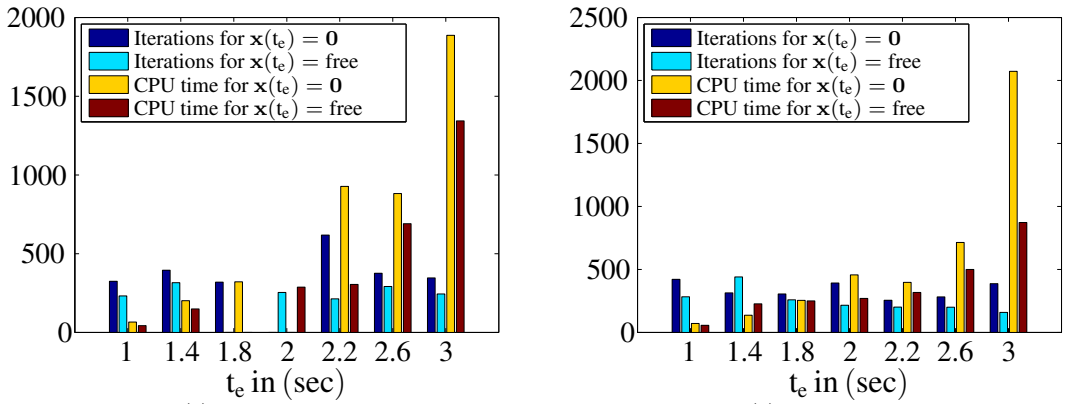

(a) Initial state $\mathbf{x}_0^{(1)}$: Iterations and computational time comparison for different t_e

(b) Initial state $\mathbf{x}_0^{(2)}$: Iterations and computational time comparison for different t_e

Figure 7.8: Time and state influence in the optimal solution

7.5.2 Weighting factors and suspension deflection limitation

The main impact on the solution is given by the weight factors of the cost function matrix. By directly changing the entries of the matrix $\mathbf{Q}_y$, the two ride objectives or a trade-off solution can be reached, see Figure 7.9(b). In order to consider the constructive suspension deflection limitation, the state x_1 can be either weighted in the cost function (7.29) or considered as inequality constraint. In Figure 7.9(a) the result concerning the influence of a weight in the cost function is compared to the state constraint. It becomes clear that increasing the weight of

[2]determined on an AMD Phenom II X4 955 3.2 GHz and 8 GB of RAM

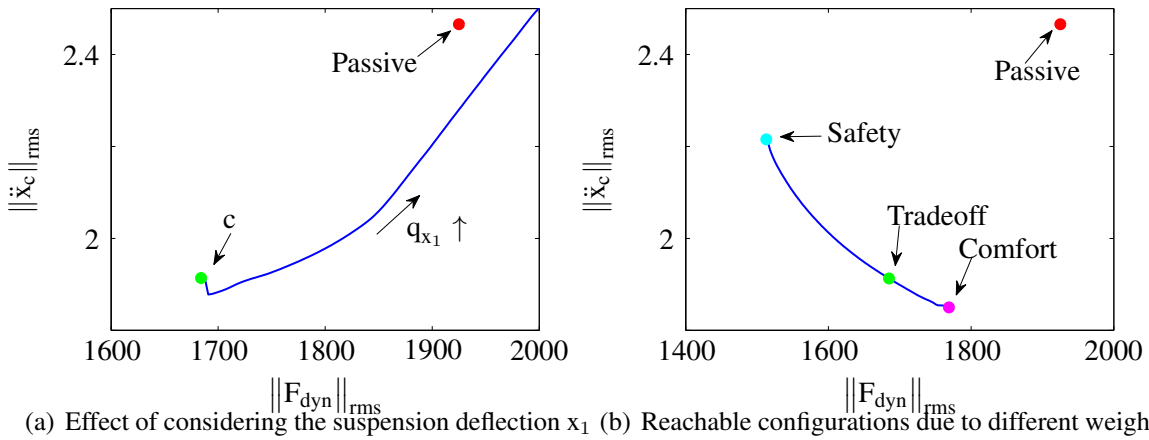

(a) Effect of considering the suspension deflection x_1 as weight in (7.29)

(b) Reachable configurations due to different weighting factors in (7.29)

Figure 7.9: Conflict diagrams for different weighting settings

the suspension deflection, which tends to reduce its rms-value, yields to a significant rise of both performance indices. Moreover, taking the state limitation as inequality constraint into account is more useful for control purposes. Otherwise, the weighting factor of $\mathbf{Q}_y$ should be adapted in every single solution to ensure, that the limitation is not violated, [94].

Similar analyses have been conducted for the switched strategy where also in this case a free final state by final time $t_e = \infty$ is chosen. In addition the same weighting entries in the matrix $\mathbf{Q}_{y,\mathrm{I}(\tau_k)}$ are selected. Therefore the comfort, safety or tradeoff settings of both strategies can be compared.

7.6 Control structure

For controller design purposes and to reduce the calculation time, the tire is modeled as a linear spring and damper. Moreover, a model is included, to detect if the wheel lifts up.

The ideal case consists in analytical solution of an optimal control problem as function of an arbitrary initial condition $u^*(t, \mathbf{x}_o)$, which can be transformed - together with the optimal state trajectory $\mathbf{x}^*(t, x_o)$ - into a time variant optimal control law $u^*(t, \mathbf{x})$, [23, 91]. An analytic solution is not possible for the complex problems, therefore the control strategy is based on

a n-dimensional numerical solution for the feedforward approach. In Figure 7.10 the control concept is depicted, whereby both control appraoches are reported. It is noted, that they are considered separately and it is not switched between the lookup tables while operating. The nonlinear quarter-car test rig is excited to oscillation by the road profile with the excitation vertical speed $\dot{x}_g$.

To determine the optimal damper force, the measured and the estimated actual state $\hat{\mathbf{x}}$ is fed back into the n-dimensional lookup-table, which contains the optimal feedforward solutions. More precisely, the state space is discretized consistently in the respective state directions and the starting value $u^*(0)$ of the optimal control solution u^* is associated to the respective grid point, according to the control law $F = f(\mathbf{x})$. Between the discrete points a linear interpolation takes place.

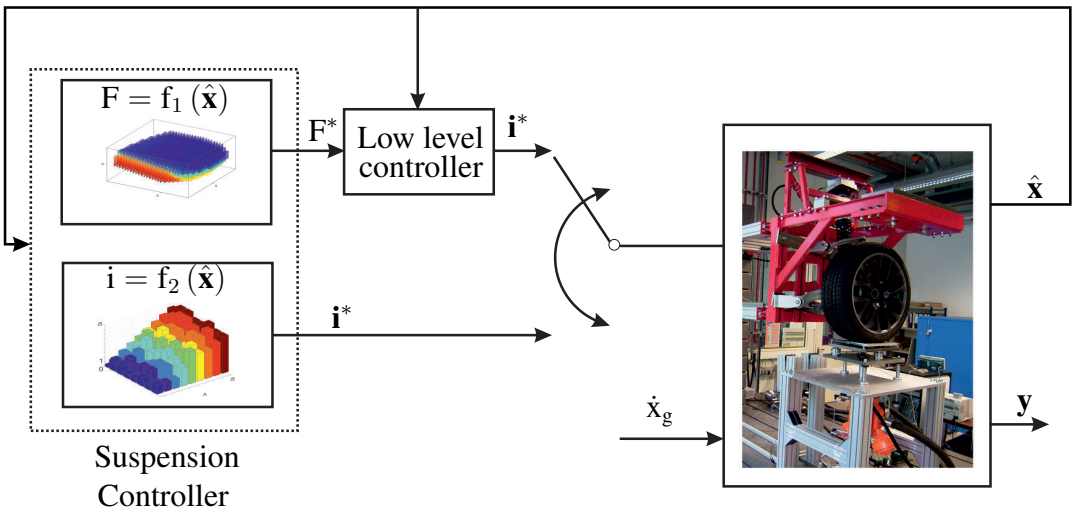

Figure 7.10: Control structure

It is noted, that the nonlinear programming leads to a nominal damper force which can be converted by an inverse semi-active damping characteristic to a target current needs. In contrast, the switch control logic, based on the optimal dynamics, produces directly the desired target current.

7.7 Simulation and measurement results

In real application on the test rig, the tire deflection $x_3 = x_w - x_g$ is not measurable and it has to be estimated. However, since the quality of the estimation is not sufficient, this signal is not fed back.

Therefore, when determining the optimal control solutions by means of nonlinear programming, besides the fully discretized state space also an alternative is considered, which starts always from an initial state of the tire deflection $x_{30} = 0$. The variation in the state x_3 still follows the dynamics of this system and have to reach at the end time t_e the equilibrium point. This has two effects on the computational complexity and the quality of the numerical control law. First, there is a marked reduction in the number of grid points, for which an optimal control solution has to be determined, which implies a reduction in computing time, required for generating the lookup table. Second, for the same number of grid points, a finer discretization of the remaining states can occur, which reduces the interpolation error in the feedback loop, [40, 155].

According to the principle of dynamic programming, which by determining the optimal control solution is based on switching systems, the possibility of a constant tire deflection is not given. The state x_3 is required for each switching time, in order to correctly calculate the cost function and has to be discretized with the remaining states.

7.7.1 Simulation by a single obstacle

In this Section the possible control options are examined in terms of a critical excitation signal in the form of a high single obstacle. It is a time-delayed positive wave of the forcing function, (see Chapter 2.6.3). The road surface is chosen so that the suspension travel limits still comply in case of the passive configuration. The simulation results for the NLP optimal strategy are reported in Figure 7.11.

The chosen input leads after the bump at the time of about 0.6 sec to a wheel lift off ($F_{dyn} < -(m_c + m_w)\, g$), by complete rebound extension of the passive suspension. Within this time interval, no longitudinal and lateral forces are transferable, which is an undesirable in terms of driving safety and generally avoidable condition. Since a controlled suspension is consid-

ered, the results show that this safety-critical state is avoided by all variants, by significantly reducing the absolute minimum dynamic wheel load (in the range of 10.2% to 28.4%).

Simultaneously, a small reduction of the absolute maximum deflection is compared to the passive configuration (in the range of 0.8% to 4.4%). This is also reflected in the pronounced reduction of the rms-value of the dynamic wheel load. The clipped solution (of the compromise solution) offers the largest improvement of about 31.0%, without consideration of the condition x_3 as well as the weighting factors. Similar considerations can be done for the rms-value of body acceleration, in which this variant achieves a reduction of 31.8%. In general, all schemes show a strong improvement, whereby the semi-active safety-oriented variant achieved (without tire deflection feedback) the minimal improvement of 26%. In addition, the rms-value of frequency weighted body acceleration also results in a significant reduction from 21.1% to 28.5%.

The optimal control by means of switching systems shows a less pronounced improvement of about 16.5% to 23.1%. Here it is noticeable that the clip variation reaches, in nearly all rms-values, a better performace then the semi-active configuration.

Finally, it can be seen that the passive suspension until the time of about 0.4 s has a nearly identical behavior as the controlled one and thus shows a similar initial reaction to the bump. The significant difference, in terms of all characteristic values of body acceleration and dynamic wheel load and travel through the decay process, becomes evident after the bump. Here, the controlled vehicle is much faster in reducing oscillation amplitude of body acceleration and dynamic wheel load (for example, at time of about 0.9 s).

7.7.2 Measurement of the road profile

Considering, firstly the NLP case, the control structure presented in Figure 7.10 is adopted, where the upper path is activated and the optimal force is related to the corresponding currents by means of the static characteristics. Each optimization results in a sequence of optimal control moves, but only the first move is saved in the lookup table and applied to the process; its input is the quarter-car state. The absolute values and the benefit are summarized in Table 7.1. A direct comparison between the two optimal solutions, designed for a full-active system and then clipped to the damper working range, shows that the $t_e \rightarrow \infty$ integration time

Table 7.1: Measurement results of NLP strategies (Profile P1 at $50\,\mathrm{km/h}$)

Quantity	Pass.	$\mathrm{Sky_{kf}}$	$\mathrm{LQR_{kf}}$	$\mathrm{CLIP_{kf}}$	$\mathrm{SA_{kf}}$	$\mathrm{SA_{so}}$
$\|\ddot{x}_c\|_{rms}$ in $\frac{m}{sec^2}$	1.92	1.68	1.61	1.68	1.57	1.68
Benefit vs. pass.	-	12.7%	15.8%	12.8%	18.2%	12.2%
$\max(\|\ddot{x}_c\|)$ in $\frac{m}{sec^2}$	6.07	5.04	4.64	5.07	4.97	4.76
Benefit vs. pass.	-	17.0%	23.5%	16.0%	29.6%	17.2%
$\|F_{dyn}\|_{rms}$ in N	1246	1264	1139	1179	1191	1144
Benefit vs. pass.	-	-1.5%	11%	7.9%	6.9%	10.6%
$\min(F_{dyn})$ in N	-3643	-3782	-3296	-3253	-3300	-3098
Benefit vs. pass.	-	-3.8%	10.5%	11.7%	10.4%	15.9%
$\min(x_c - x_w)$ in cm	-7.8	-6.9	-7.2	-7.7	-7.7	-7.3
Benefit vs. pass.	-	11.5%	7.6%	9.0%	6.4%	7.7%

($\mathrm{LQR_{kf}}$) reaches better results both in the ride comfort and in the ride safety. In fact, it obtains a performance gain of about 3% for the acceleration as well as for the dynamical wheel load comparing to $\mathrm{CLIP_{kf}}$. Taking in the controller design the nonlinearities of the system and the state dependent damper force into account, it shows its strengh in the results of the configuration $\mathrm{SA_{kf}}$. The rms-value of the body acceleration can be even more reduced by decreasing the dynamical wheel load of about 7% with respect to the passive configuration.

The same benefit in comfort obtained by $\mathrm{CLIP_{kf}}$ is also obtained with the well-known skyhook law and the proposed $\mathrm{SA_{so}}$, nevertheless only $\mathrm{Sky_{kf}}$ does not ensure ride safety. The dynamical wheel load rms-value of the proposed safety-oriented solution is comparable to the LQR-feedback. In all controller design configuration the suspension deflection limitation is kept.

By applying the switching optimal solution, the lower path in Figure 7.10 is activated. Since the results of this logic are the valves' currents, the damper is directly driven. Simulation as well as measurement results are summarized in Table 7.2. As remarked in Section 7.5.1 the design parameters allow to influence the system similarly to NLP. Hence, a comfort-oriented solution for linear $\mathrm{SW_{l,kf}}$, [58], the nonlinear $\mathrm{SW_{nl,kf}}$ switched dynamics of this Thesis and a tradeoff solution $\mathrm{SW_{nl,to}}$ are compared in the simulation. The performance values are referred to the passive simulation reported in Table 7.2. It can be noted, that due to the consideration of the nonlinearities the performance gain increases of about 6.4% and at the same time the nonlinear system improves safety of about 5.4% comparing to the passiv reference, meaning a relativ gain of about 8.3%. Also the maximum value of the chassis accelaration gets some

benefit from the feedback action.

Table 7.2: Simulation and measurement results of switching strategy (Profile P1 at $50\,\mathrm{km/h}$)

	Simulation				Measurement	
Quantity	Pass.	$SW_{l,kf}$.	$SW_{nl,kf}$	$SW_{nl,to}$	$SW_{nl,kf}$	$SW_{nl,to}$
$\|\ddot{x}_c\|_{rms}$ in $\frac{m}{sec^2}$	1.84	1.66	1.55	1.75	1.79	2.09
Benefit vs. pass.	-	9.2%	15.6%	4.8%	6.6%	-9.3%
max $(\|\ddot{x}_c\|)$ in $\frac{m}{sec^2}$	7.50	7.25	6.52	5.7	5.5	5.8
Benefit vs. pass.	-	3.5%	13.0%	24.0%	7.7%	2.7%
$\|F_{dyn}\|_{rms}$ in N	1201	1238	1136	1159	1232	1253
Benefit vs. pass.	-	-3.1%	5.4%	3.5%	3.7%	2%
$\min(F_{dyn})$ in N	-3448	-3804	-2915	-2835	-3330	-3279
Benefit vs. pass.	-	-10.3%	15.5%	17.8%	9.5%	11.0%
$\min(x_c - x_w)$ in cm	-7.7	-7.3	-7.2	-6.6	-7.3	-7.8
Benefit vs. pass.	-	4.8%	6.3%	13.2%	15.5%	9.69%

Changing the weighting factors in the cost function (7.43) to $SW_{nl,to}$ yield a higher rms-values of the chassis acceleration, while its maximum value is reduced. The minimum value of the dynamical wheel load is increased about 17.8%. However, the rms-value of the dynamical wheel is lightly decreased in comparison to $SW_{nl,kf}$.

The last two columns of Table 7.2 show measurement results obtained at the test rig. The performance gain is referred to the passive measurement given in Table 7.1. It becomes clear, that the comfort solution $SW_{nl,kf}$ improves the ride comfort and the ride safety of about 6.6% and 3.7% , respectively. Identical to the simulation, $SW_{nl,to}$ reduces only the minimum value of the dynamical wheel load, while the rms-value does not gain performance compared to $SW_{nl,kf}$.

Both, in simulation and in measurements, all controller design configurations keep the suspension deflection within the limitations.

Comparing the two proposed control strategies it becomes clear that the NLP-based control solutions provide better results, even if the feedforward results of both strategies are comparable.

While the NLP provides the desired damper force in the whole damper working range (see Figure 7.2(a)), the switching strategy does not. This is because it is designed based on dis-

crete system dynamics (damper currents and thus damper forces) and the switching restriction (7.44). However, the required time for solving the optimization problem of the latter method is very low compared to the NLP case (roughly 15% of the NLP computational speed). A case specific adjustment of the considered amout of discrete dynamics and the minimal dwell time $\delta_{\min}$ can improve the results towards the NLP variation, but the computational time for solving the optimization problem will increase simultaneously. Especially an optimal $\delta_{\min}$ can impove the results significantly.

This means that the latter method is based on the knowledge of the damper characteristics and has no permission to interpolate between them, (see Figure 2.3(a)). Due to the control logic, the jump between currents is not a smooth signal, which on the test rig produces impacts on the chassis and therewith a reduction of the ride comfort. By including more damper characteristics, i.e. discrete dynamics, the currents reference signals become smoother. At the same time it increases the computational time.

7.8 Extension of the proposed optimal control strategy

In the following, two extensions of the proposed optimal strategies are briefely reported. Firstly, the comfort filter is integrated in the calculation of the optimal solution, in order to take into account the frequency range in which the human body is mostly sensible. Secondly, the force tracking is increased by applying the structure proposed in Chapter 5 and Chapter 6.

7.8.1 Integration of the comfort filter in the optimal structure

The shaping filter introduced in Section 2.4 is integrated in the optimal problem, which has to be solved either with the nonlinear programming or with the Bellman's principle. The optimal solution is consequently obtained considering the frequency response of the complete system. Indeed, not only the damper force is chosen in the working range of the damper, but also the frequencies contained in the acceleration signal are weighted and the range 4-8 Hz is preserved from excitations.

7.8.2 Extension by the damper control strategy

As reported in this Chapter, the optimization of the damper force is conducted without considering the damper dynamics, in order to not increase the model complexity and therewith the computational time. Therefore, the semi-active device control proposed in Chapter 5.4 and Chapter 6 is applied and the result are reported in Table 7.3. They are compared to the passive configuration, the skyhook law Sky_{kf} and the the optimal solution calculated by the LQR configuration, designed to increase the ride comfort LQR_{kf}.

The NLP_{kf} configuration represents the solution of the optimization problem, by considering the state of the art structure to calculate the corresponding currents. The results reported in the measurement NLP_{ffw} are obtained by considering the dynamical feedforward approach, which takes into account the damper characteristics (Chapter 5.4). The complete force tracking is reported in NLP_{fb}, where the feedback force is obtained by the model-based variant, see Chapter 6.

It is noted, the the results of the NLP strategies reach better performance in term of body acceleration compared with the skyhook solution. The LQR configuration ensures similar results to the ones obtained with the solution of the nonlinear programming both in the rms-values of $\ddot{x}_c$ and of $\ddot{x}_{c,comf}$.

Table 7.3: Measurement results of NLP strategy with integration of the comfort filter and augmented by the damper control approach

Quantity	Pass.	Sky_{kf}	LQR_{kf}	NLP_{kf}	NLP_{ffw}	NLP_{fb}
$\|\ddot{x}_c\|_{rms}$ in $\frac{m}{sec^2}$	1.92	1.68	1.61	1.60	1.60	1.59
Benefit vs. pass.	-	12.7%	15.8%	16.0%	15.9%	16.6%
$\|\ddot{x}_{c,\,comf}\|_{rms}$ in $\frac{m}{sec^2}$	1.28	1.09	1.08	1.08	1.07	1.06
Benefit vs. pass.	-	14.8%	15.3%	15.2%	16.0%	16.8%
$\max(\|\ddot{x}_c\|)$ in $\frac{m}{sec^2}$	6.07	5.04	4.64	4.97	4.91	4.94
Benefit vs. pass.	-	17.0%	23.5%	18.1%	19.1%	18.6%
$\|F_{dyn}\|_{rms}$ in N	1246	1264	1139	1193	1196	1203
Benefit vs. pass.	-	-1.5%	11%	4.3%	4.2%	3.4%
$\min(F_{dyn})$ in N	-3643	-3782	-3296	-3358	-3445	-3464
Benefit vs. pass.	-	-3.8%	10.5%	7.9%	5.5%	5.0%
$\min(x_c - x_w)$ in cm	-7.8	-6.9	-7.2	-7.1	-7.3	-7.2
Benefit vs. pass.	-	12.1%	17.1%	8.9%	8.0%	8.4%

By considering the damper dynamic the proposed feedforward control approach reduces the rms-value of the acceleration both in the acceleration and in the filtered signal, by keeping the dynamical wheel load at the same value of the NLP_{kf}.

The feedback component further improves the ride comfort by reducing the acceleration and guaranteeing a maximum of 16.6% comfort gain comparing to the passiv configuration. Also in the filtered signal the best performance of 16.8% are reached by the feedback configuration. By aiming to a reduction of the body acceleration, the dynamical wheel load is increased. Only the skyhook contoller does not ensure ride safety, by allowing higher rms-values in the dynamical wheel load signal. While the results of the optimization problem slightely improve the vehicle holding, a very good result is obtained by the LQR solution.

The suspension deflection are within the limits for all considered controller configurations.

7.9 Summary

Nonlinear programming and a Bellman-based switching method, which both take state and input saturations into account are presented and applied for optimal control of a nonlinear semi-active suspension system. The proposed approaches are validated in simulation and experiments and compared with LQR and skyhook controllers. It has been shown that the proposed control structures offers additional performance, as system nonlinearities and limitations are incorporated in their design.

Moreover, the acceleration weight is included in the optimization design by integrating an ISO shape filter, which offers a frequency range weighting due to the human bodys vertical vibration sensitivity. Furthermore, the analysis is completed by extending the optimal solution by the damper force tracking strategy proposed in this Thesis. It has been shown, that the ride comfort can be further increased, by ensuring road holding without breaking the suspension deflection limitations.

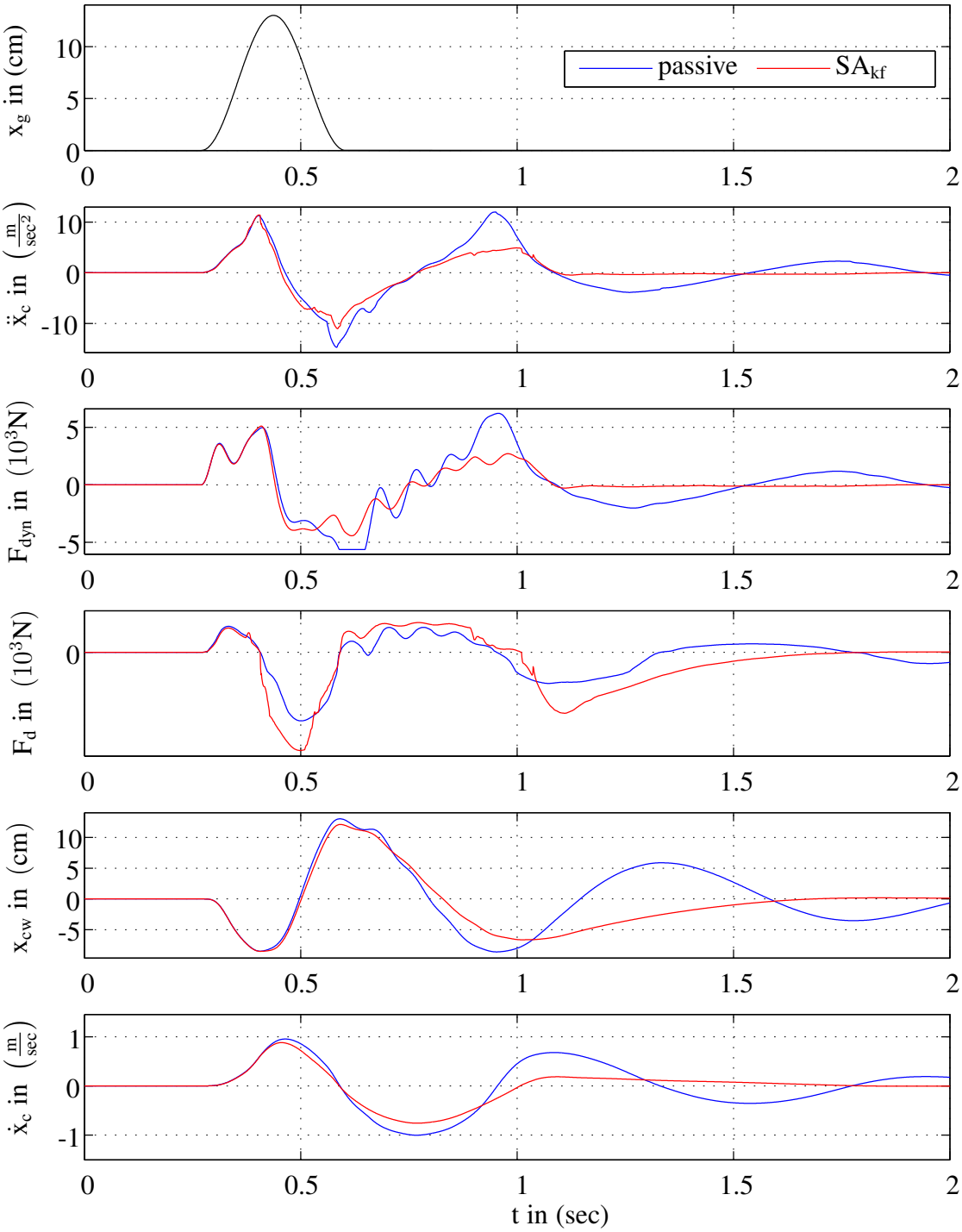

Figure 7.11: Bump simulation: comparison between passive and controlled configuration (SA_{kf}, without x_3)

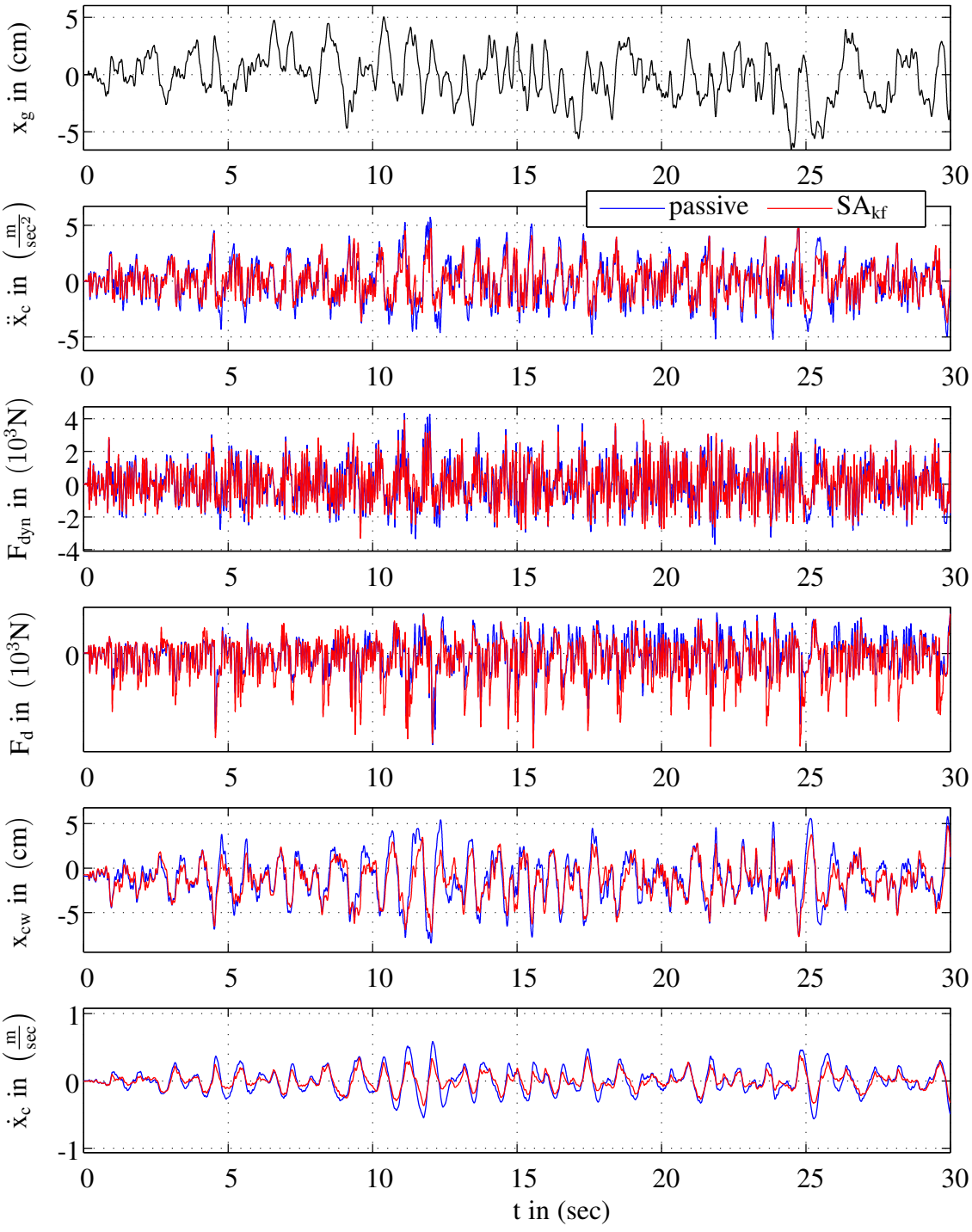

Figure 7.12: Measurement results for the passive and the controlled configurations (semi-active, without x_3, comfort-oriented) by excitation with a real road profile

Chapter 8

CONCLUSION AND FUTURE WORK

Due to their minimal energy demand and their performance potential, semi-active suspension systems are mainly integrated in production vehicles. Mainly skyhook control approaches based on static damper characteristics are used in industrial applications due to their simple parameterability and integrability in global chassis control laws. Moreover, since these devices are strongly nonlinear and work under passivity constraints, meaning that no energy can be introduced into the system, primarily signal based approaches are utilized in industrial applications.

Towards improvements of the state of the art control strategy, this Thesis presents a model-based control concept that enables to exploit the dynamics of these modern mechatronic devices. Towards increasing comfort and road handlig characteristics of the modern production vehicles, in this work semi-active damper modeling, actuator model-based strategies and suspension controllers are discussed. It spreads from the new detailed physical model over a therefrom derived functional semi-active damper model suitable for control purposes to a new dynamical feedforward approach completed by a feedback component. Moreover, to the aim of a suspension controller which includes the state-dependent input limitation of the controlling element, two new suspension controllers, based on the principle of optimality, are derived and compared with the state of the art solutions.

While the physical model allows to enhance understanding of the behavior of a semi-active dual tube hydraulic damper, the simplified semi-active model is requested for control purposes. The first one treats the hydro-dynamical, electrical and valve switching dynamics in detail. Based on this knowledge, two simplified damper representation are proposed. The first one condenses the electrical and the mechanical characteristics into two time constants. However, this representation has a lack of precision, therefore a functional model is derived. The latter allows to reproduce the main semi-active damper effects including force shaping, damping by high stroke velocities, gas force and variable hysteresis behavior. Its few unknown

parameters can be identified by minimal effort, considering the only measurements which are already done in the production vehicle industry to obtain the static damper characteristics.

The equations of the latter model are integrated into a feedforward control strategy, which take into account the hysteresis effect of the controlling device. While the state of the art solution is based on static characteristics, the proposed structure takes advantage of the precise modeling. Furthermore, the feedforward path is extended by a feedback component, which acts on minor force deviations, improving the force tracking. The dynamic behavior of the real damper is matched with enough accuracy and its response is adopted to the control objectives. This approach is studied and analyzed both in open and in closed loop, by meaning of different designed suspension controllers.

Moreover, two strategies based on the principle of optimality are proposed, which take into account the hardware limitations. Thereby, significant performance enhancements in terms of ride comfort and ride safety are achieved without violating the suspension deflection limitation. The solution of the optimal problem is extended by the device control strategy, which further increases the performance gain.

All concepts have been analyzed and experimentally validated on a realistic framework, which includes a double wishbone structure kinematic, suspension strut nonlinearities, road profiles as well as sensors configuration from production vehicle.

Aiming to a transparent concept, the functional model and the control structures are separately designed. Both the feedforward and the feedback paths have been applied, discussed and tested separately and independently of the suspension controller objectives. In addition, to complete the feedback component a new damper force estimation is proposed and compared to a measured signal. Each strategy is compared with the passive and the state of the art configurations. Variations of the suspension controller laws do not affect the low-level controller, meaning the tracking force task. It has been shown that the performance of semi-active suspension systems can be improved by applying model-based approach to control the damper currents and that the proposed hierarchical controller structure is a realizable configuration which is well suited to be implemented in global chassis control architectures.

The following areas of research are proposed to enhance the strategies proposed in this Thesis and further exploit the dynamics of the semi-active device:

1. *Full-car vehicle dynamics:* Since the control concepts have been presented for a quarter-vehicle framework, the structure can be extended for a full-car model. Including the additional effects of the full vehicle and extending the damper control concept to the four wheels, the structure remains transparent and does not further increase the complexity of the system. While the tracking force can be easily extended, the optimal suspension controller has to be integrated according to the global chassis strategy.

2. *Use of preview information:* The controller performance can be increased by taking advantage of the signal measured by the front wheels and making it available for controlling purposes of the rear wheels. To exploit the potential of the preview information, the road profile has to be reliably estimated or detected by additional sensors.

3. *Frequency-selective damping:* The application of semi-active dampers is increasing, since they achieve great comfort performance while maintaining road holding by keeping the energy requirement limited. In addition, these devices operate without additional sensors besides the ones already used for global chassis strategies. In any case, the state of the art controllers partially underachieve the hardware potential. Their fast dynamics allows to differently influence the chassis motion within the frequency range of the excitation. By applying frequency selective damping, high damping forces can be transmitted around the first natural frequency, whereas at the second natural frequency the damping forces can be reduced. While at the chassis natural frequency the motion are damped, at the second one wheel motion are allowed and the force transmission is reduced.

4. *Energy efficient integration:* It has been shown that the combination of semi-active devices with active actuators in suspension systems offers significant advantage in terms of power demand over the full-active suspension systems, [97, 98]. An interesting but open question regarding the optimal energy allocation between the two actuators remains, [154]. Aiming to reduce the energy requirement, the proposed damper control strategy can be utilized to exploit its dynamical characteristics, utilizing the slow-active actuator only if the semi-active device has reached its limits.

5. *On-line optimal solution for suspension controller:* Explicit model predictive control techniques (EMPC) can be further analyzed in order to solve the mathematical optimization problem in each step and calculate the control action. Model simplifications have to be considered and modern computation tools have to be applied in order to guarantee the solution of the problem within the sampling time.

BIBLIOGRAPHY

[1] *ISO 8608: Mechanical vibration - Road surface profiles - Reporting of measured data*, 1995.

[2] *ISO 2631 -1 :Mechanical vibration and shock Evaluation of human exposure to whole-body vibration*, 1997.

[3] Weiterentwicklung von Fahrwerksystemen. *Automobiltechnische Zeitschrift (ATZ)*, 6(114), June 2012.

[4] Bose Suspension System. http://www.bose.de/DE/de/index.jsp, Status: 02/2011.

[5] Tenneco Integrated Kinetic H2 CES System. http://www.tenneco.com/, Status: 02/2011.

[6] Der neue Panamera S Hybrid. www.porsche.com, Status: 11/2010.

[7] M. Ahmadian. On the Isolation Properties of Semiactive Dampers. *Joural of Vibration and Control*, 5:217–232, 1999.

[8] M. Ahmadian and E. Blanchard. Non-dimensionalised closed-form parametric analysis of semi-active vehicle suspensions using a quarter-car model. *Vehicle System Dynamics*, 49(1-2):219–235, 2011.

[9] M. Ahmadian, X. Song, and S. C. Southward. No-jerk skyhook control methods for semiactive suspensions. *Journal of Vibration and Acoustics*, 126(4):580–584, 2004.

[10] S. Albrecht. Der VW Touareg. *Automobiltechnische Zeitschrift*, ATZ extra:36–39, 2010.

[11] A. Alleyne and J. K. Hedrick. Nonlinear control of a quarter car active suspension. *Proceedings American Control Conference*, pages 21–25, 1992.

[12] T. Althoff. Feder-Dämpfer-Systeme: Grundfunktionen. Spezialfall Gasfederdämpfer. Auslegung und Regelung. Umsetzung. FTM: Ausgewählte Kapitel der Fahrzeugentwicklung aus der Sicht der Industrie (BMW Group), 2010.

[13] E. Angel and R. Bellman. *Dynamic programming and partial differential equations*, volume 88. Academic Press, New York, 1972.

[14] M. Araki and H. Taguchi. Tutorial Paper: Two-Degree-of-Freedom PID Controllers. *International Journal of Control, Automation and Systems*, 1(4):401–411, December 2003.

[15] B. Armstrong and C.C. de Wit. *Friction Modeling and Compensation*. The Control Handbook, 1995.

[16] B. Armstrong-Hélouvry, P. Dupont, and De Wit C.C. A survey of models, analysis tools and compensation methods for the control of machines with friction. *Automatica*, 30(7):1083–1138, 1994.

[17] S. Aubouet, L. Dugard, O. Sename, C. Poussot-Vassal, and B. Talon. Semi-active H_∞ / LPV control for an industrial hydraulic damper. In *Proc. of the European Control Conference, 2009*, pages 3628–3633, 2009.

[18] A. Bacciotti and L. Rosier. *Liapunov Functions and Stability in Control Theory*. Springer, 2005.

[19] M. Balandat, W. Zhang, and A. Abate. On the infinite horizon constrained switched LQR problem. In *Proc. IEEE Conference on Decision and Control*, pages 2131 –2136, december 2010.

[20] W. Balandat and T. Kutsche. Systemintegration der CDC-Dämpfung beim neuen Opel Astra. *Automobiltechnische Zeitschrift*, 4:24–28, 2004.

[21] D. P. Bertsekas. *Dynamic Programming and Optimal Control*. Athena Scientific, 2007.

[22] FH. Besinger. Force control of a semi-active damper. *Vehicle System Dynamics*, 24(9):695–723, 1995.

[23] J. T. Betts. *Practical methods for optimal control using nonlinear programming*. Advances in Design and Control. Society for Industrial and Applied Mathematics (SIAM), Philadelphia, PA, 2001.

[24] BMW. *Der neue BMW 7er - Entwicklung und Technik*. ATZ/MTZ- Typenbuch. Vieweg+Teubner Verlag, April 2009.

[25] C. Bohn, H.-J. Karkosch, and F. Svaricek. Zustandsbeobachter für periodische Signale: Anwendungen zur aktiven Kompensation von motorerregten Karosserieschwingungen. *Automatisierungstechnik*, 53:525–536, November 2005.

[26] H.-H. Braess and U. Seiffert. *Handbuch Kraftfahrzeugtechnik*. Vieweg Verlag, Wiesbaden, 2003.

[27] S. N. Brown. *Active vehicle suspension system*. Patent, EP 1 440 826 B1, 11 2010.

[28] A. E. Bryson and Y.-C. Ho. *Applied Optimal Control: Optimization, Estimation and Control*. Hemisphere Publishing, 1975.

[29] T. Butsuen. *The design of semi-active suspensions for automotive vehicles*. PhD thesis, Massachusettes Institute of Technology, 1989.

[30] E. F. Camacho and C. Bordons. *Model Predictive Control*. Springer-Verlag London, 2005.

[31] M. Canale, M. Milanese, Z. Ahmad, and E. Matta. An improved semiactive suspension control strategy using predictive techniques. In *Proc. of the International Conference on Information and Communication Technologies: From Theory to Applications*, pages 53–54, April 2004.

[32] M. Canale, M. Milanese, and C. Novara. Semi-active suspension control using "fast" model-predictive techniques. *IEEE Transactions on Control Systems Technology*, 14(6):1034–1046, 2006.

[33] P. Causemann. *Kraftfahrzeugstoßdämpfer*, volume 185. Bibliothek der Technik, 1999.

[34] P. Causemann. Moderne Schwingungsdämpfung. *Automobiltechnische Zeitschrift*, 11:1072–1079, 2003.

[35] P. Causemann and T. Kutschem. CDC (Continuous Damping Control) Ausführungen mit integriertem oder extern ausgeführten Proportional - Dämpfer - Ventile - Eine Bewertung zweier unterschiedlicher Konzepte. In *Reifen - Fahrwerk - Fahrbahn (VDI Berichte)*, pages 135–153. VDI-Gesellschaft Fahrzeug- und Verkehrstechnik, VDI-Verlag, 1997.

[36] B. Cho, D. Lee, D. Lee, and K. Boo. Design of a current driver controller for MR CDC dampers. In *Control, Automation and Systems, 2007. ICCAS '07. International Conference on*, pages 283 –286, October 2007.

[37] D. Corona, A. Giua, and C. Seatzu. Optimal control of hybrid automata: design of a semiactive suspension. *Control Engineering Practice*, 12(10):1305–1318, 2004. Analysis and Design of Hybrid Systems.

[38] D.A. Crolla. *Automotive Engineering: Powertrain, Chassis System and Vehicle Body*. Elsevier, 2009.

[39] C. Deleye. Hysterese Modellierung und Regelung eines semi-aktiven Dämpfers. Project Thesis at the Institute of Automatic Control (Technische Universität München), 2011, Supervisor: E. Pellegrini.

[40] R. Dessort. Nichtlineare Programmierung und Bellman-basierte Schaltstrategie zur optimalen Steuerung und Regelung eines semi-aktiven Fahrwerks. Master's Thesis at the Institute of Automatic Control (Technische Universität München), 2012, Supervisor: E. Pellegrini.

[41] R. K. Dixit and G. D. Buckner. Sliding mode observation and control for semiactive vehicle suspensions. *Vehicle System Dynamics*, 43(No. 2):83 – 105, February 2005.

[42] A. L. Do, O. Sename, L. Dugard, and B. Soualmi. Multi-objective optimization by genetic algorithms in H_∞ / LPV control of semi-active suspension. *Proc. of the 18th IFAC World Congress 2011*, 1:7162–7167, 2011.

[43] S. Duym. Simulation tools, modelling and identification for an automotive shock absorber in the context of vehicle dynamics. *Vehicle System Dynamics*, 33:261–285, April 2000.

[44] S. Duym and K. Reybrouck. Physical characterization of nonlinear shock absorber dynamics. *European Journal of Mechanical and Environmental Engineering*, 43(4):181–188, 1998.

[45] S. Duym, R. Stiens, and K. Reybrouck. Evaluation of Shock Absorber Models. *Vehicle System Dynamics*, 2(2):109– 127, February 1997.

[46] M. Ebau, A. Giua, C. Seatzu, and G. Usai. Semiactive suspension design taking into account the actuator delay. In *Proc. of the 40th IEEE Conference on Decision and Control*, pages 93–98, 2001.

[47] B. Ebrahimi, H. Bolandhemmat, M. B. Khamesee, and F. Golnaraghi. A hybrid electromagnetic shock absorber for active vehicle suspension systems. *Vehicle System Dynamics*, 49(1-2):311–332, 2011.

[48] M. Eichstetter. Regelung eines aktiven Fahrwerks mit Methoden der optimalen Steuerung. Project Thesis at the Institute of Automatic Control (Technische Universität München), 2011.

[49] M. Eickoff, G. Fenn, and S. Heyn. Sensitive Damping Control - More ride comfort without loss of safety. World Automotive Congress (FISITA), September 2008.

[50] D. Findeisen. *Ölhydraulik: Handbuch für die hydrostatische Leistungsübertragung in der Fluidtechnik*. Springer-Verlag Berlin Heidelberg, 5^{th} edition, 2006.

[51] D. Fischer and R. Isermann. Mechatronic semi-active and active vehicle suspensions. *Control Engineering Practice*, 1:1353–1367, 2004.

[52] O. Föllinger. *Nichtlineare Regelungen 2. Anwendung der Zustandsebene; Ljapunow-Theorie; Popow- und Kreiskriterium*. Methoden der Regelungstechnik. Oldenbourg, 1989.

[53] G. F. Franklin, J. D. Powel, and A. Emami-Naeini. *Feedback Control of Dynamic Systems*. Pearson Prentice Hall, 6th edition, 2010.

[54] M. Fröhlich. *Ein robuster Zustandsbeobachter für ein semiaktives Fahrwerksregelsystem*. PhD thesis, Technische Universität München, 2008.

[55] C. Früh, J. Hermann, M. Tietke, M. Niestegge, F. Scheyhing, A. Neteler, and G. Steller. Die neue E-Klasse von Mercedes Benz: Komfort bei erlebbarer Dynamik und Agilität. *Automobiltechnische Zeitschrift*, ATZ extra:128–143, 2009.

[56] F. Frühauf. Aktive Fahrzeugfederung. In M. Mettner, editor, *Elektronik im Kraftfahrzeugwesen - Steuerungs-, Regelungs- und Kommunikationssysteme*, volume 437, pages 304–315. Kontakt & Studium - expert Verlag, 4 edition, 2002.

[57] N. Giorgetti, A. Bemporad, H. E. Tseng, and D. Hrovat. Hybrid Model Predictive Control Application Towards Optimal Semi-Active Suspension. In *Proc. IEEE International Symposium on Industrial Electronics ISIE 2005*, pages 391–398, June 2005.

[58] A. Giua, M. Melas, C. Seatzu, and G. Usai. Design of a predictive semiactive suspension system. *Vehicle System Dynamics*, 41(4):277–300, April 2004.

[59] A. Giua, C. Seatzu, and G. Usai. Semiactice Suspension Design with an Optimal Gain Switching Target. *Vehicle System Dynamics*, 31(4):213 – 232, 2011.

[60] A. Giua, C. Seatzu, and C. Van Der Mee. Optimal control of autonomous linear systems switched with a pre-assigned finite sequence. In *Proc. of IEEE International Symposium on Intelligent Control (ISIC '01)*, pages 144 –149, 2001.

[61] H. Glaser, T. Rossie, R. Nieboer, J. Rüger, S. Revelant, A. Hopf, R. Wagner, and H.-G. Spengel. Der neue Audi Q3: Fahrwerk. *Automobiltechnische Zeitschrift*, ATZ extra:32–39, 2011.

[62] H. Gonzalez, R. Vasudevan, M. Kamgarpour, S.S. Sastry, R. Bajcsy, and C. Tomlin. A numerical method for the optimal control of switched systems. In *Proc. IEEE Conf. on Decision and Control*, pages 7519 –7526, December 2010.

[63] T. J. Gordon and M. C. Best. Dynamic optimizationof nonlinear semi-active suspension controllers. *Proceedings International Conference on Control*, 1:332–337, 1994.

[64] K. Graichen, N. Petit, and A. Kugi. Transformation of optimal control problems with a state constraint avoiding interior boundary conditions. In *Proc. of the 47th IEEE Conference on Decision and Control*, pages 913 –920, December 2008.

[65] I. Granet. *Fluid Mechanics for Engineering Technology*. Queensborough Community College, 1989.

[66] K. A. Grunauer Brachetti. Design and Implementation of State and Mass Estimators for Semi-Active Suspension System. Project Thesis, 2011, Supervisor: E. Pellegrini.

[67] E. Guglielmino, T. Sireteanu, C. W. Stammers, G. Ghita, and M. Giuclea. *Semi-active Suspension Control*. Springer-Verlag London Limited, 2008.

[68] S. Guo, B. Xu, H. Xing, and C. Pan. Skyhook isolation with magnetorheological damper. In *Proc. Sixth World Congress on Intelligent Control and Automation WCICA*, pages 7860–7863, 2006.

[69] B. Heißing and M. Ersoy. *Chassis Handbook: Fundamentals, Driving Dynamics, Components, Mechatronics, Perspectives*. Vieweg+Teubner Verlag, 2010.

[70] G. Heyer. Trends in Stoßdämpferentwicklung. In O. Krettek, editor, *Federungs- und Dämpfungssysteme*, pages 233–260. Fortschritte der Fahrzeugtechnik - Vieweg, 1992.

[71] C. Hilgers, J. Brandes, H. Ilias, H. Oldenettel, A. Stiller, and C. Treder. Aktives Luftfederfahrwerk für eine größere Bandbreite zwischen Komfort- und Dynamik-Abstimmung. *Automobiltechnische Zeitschrift*, 9:600–609, 2009.

[72] J. Hohenstein, A. Schulz, and D. Gaisbacher. Das elektropneumatische Vorderachslift-system des Porsche 997 GT3. *Automobiltechnische Zeitschrift*, 09:622–626, 2010.

[73] K.-S. Hong, H.-C. Sohn, and J. K. Hedrick. Modified skyhook control of semi-active suspensions: A new model, gain scheduling, and hardware-in-the-loop tuning. *Journal of Dynamic Systems, Measurement and Control*, 124:158–167, 2002.

[74] S.R. Hong, S.B. Choi, Y.T. Choi, and N.M. Wereley. A hydro-mechanical model for the hysteretic damping force prediction of ER damper: experimental verification. *Journal of Sound and Vibration*, 285:1180–1188, 2005.

[75] I.M. Horowitz. *Synthesis of Feedback Systems*. Academic Press, 1963.

[76] D. Hrovat. Survey of advanced suspension developments and related optimal control applications. *Automatica*, 33:1781–1817, 1997.

[77] K. Hudha, H. Jamaluddin, P. M. Samin, and R. A. Rahman. Effects of control techniques and damper constraint on the performance of a semi-active magnethorheological damper. *International Journal of Vehicle Autonomous Systems*, 3:230–251, 2005.

[78] R. Isermann. *Fahrdynamik-Regelung*. Vieweg Verlag, 2006.

[79] A. F. Jahromi and A. Zabihollah. Linear quadratic regulator and fuzzy controller application in full-car model of suspension system with magnetorheological shock absorber. In *Proc. of IEEE/ASME International Conference on Mechatronics and Embedded Systems and Applications (MESA)*, pages 522 –528, July 2010.

[80] M. Jautze, A. Bogner, J. Eggendinger, G. Rekewitz, and A. Stumm. Der neue BMW 7er: Das Verstelldämpfersystem Dynamische Dämpfer Control. *Automobiltechnische Zeitschrift*, ATZ extra:100 – 103, 2008.

[81] E. A. Johnson and B. Erkus. Investigation of dissipativity for control of smart dampers via LMI synthesis. In *Proc. of American Control Conference*, pages 3084–3089, June 2005.

[82] J. Jordan. Implementierung und Vergleich moderner Regelungskonzepte für semiaktive Fahrwerke. Project Thesis at the Institute of Automatic Control (Technische Universität München), 2011, Supervisor: E. Pellegrini.

[83] T. Jungbluth. Federungs- und Dämpfungsinnovationen von ThyssenKrupp Bilstein. *Fachpresse-Mitteilung IAA PKW*, 2005.

[84] D. Karnopp. Active damping in road vehicle suspension systems. *Vehicle System Dynamics*, 12:291–316, 1983.

[85] D. Karnopp. Active suspensions based on fast load levelers. *Vehicle System Dynamics*, 16(5-6):355–380, 1987.

[86] D. Karnopp. How significant are transfer function relations and invariant points for a quarter car suspension model? *Vehicle System Dynamics*, 47:457–464, 2009.

[87] D. Karnopp, M. J. Crosby, and R. A. Harwood. Vibration control using semi-active force generators. *ASME Journal of Engineering for Industry*, 96:619–626, May 1974.

[88] D. Karnopp and G. Heess. Electronically controllable vehicle suspensions. *Vehicle System Dynamics*, 20:207–217, May 1991.

[89] H. K. Khalil. *Nonlinear Systems*. Prentice Hall, 3 edition, 2001.

[90] R.-K. Kim and K.-S. Hong. Skyhook control using a full-vehicle model and four relative displacement sensors. In *Proc. International Conference on Control, Automation and Systems ICCAS '07*, pages 268–272, October 2007.

[91] D. Kirk. *Optimal Control Theory - An Introduction*. Dover Publications, 1998.

[92] T. Kloiber, G. Koch, and B. Lohmann. Modified optimal control of a nonlinear active suspension system. In *Proc. IEEE Conf. on Decision and Control*, pages 5572 –5577, December 2010.

[93] G. Koch. *Adaptive Control of Mechatronic Vehicle Suspension Systems*. PhD thesis, Technische Universität München, 2011.

[94] G. Koch, K. J. Diepold, and B. Lohmann. Multi-objective road adaptive control of an active suspension system. In H. Ulbrich and L. Ginzinger, editors, *Motion and Vibration Control*, pages 189–200. Springer, 2009.

[95] G. Koch, T. Kloiber, and B. Lohmann. Nonlinear and filter based estimation for vehicle suspension control. In *Proc of the 49th IEEE Conference on Decision and Control*, pages 5592 –5597, 2010.

[96] G. Koch, E. Pellegrini, S. Spirk, N. Pletschen, and B. Lohmann. Actuator control for a hybrid suspension system. Technical Report TRAC-6, Number 2, Institute of Automatic Control at Techinische Universität München, 2011.

[97] G. Koch, S. Spirk, and B Lohmann. Reference model based adaptive control of a hybrid suspension system. *Proc. of the IFAC Advances in Automotive Control*, 2010.

[98] G. Koch, S. Spirk, E. Pellegrini, N. Pletschen, and B. Lohmann. Experimental validation of a new adaptive control approach for a hybrid suspension system. In *American Control Conference*, pages 4580 –4585, July 2011.

[99] J.J. Kok, J.G.A.M. van Heck, R.G.M. Huisman, J.H.E.A. Muijderman, and F.E. Veldpaus. Active and semi-active control of suspension systems for commercial vehicles based on preview. In *Proceedings of the American Control Conference 1997*, pages 2992 –2996, June 1997.

[100] C. Kraft. *Gezielte Variation und Analyse des Fahrverhaltens von Kraftfahrzeugen mittels elektrischer Linearaktuatoren im Fahrwerksbereich*. Band 5 von Karlsruher Schriftenreihe Fahrzeugsystemtechnik, KIT Scientific Publishing, 2010.

[101] H. H. Lang and L. Segel. The mechanics of automotive hydraulic dampers at high stroking frequencies. In *7th IAVSD Symp Dynamics of Vehicles on Roads and Tracks*, 1981.

[102] C. Lauwerys, J. Swevers, and P. Sas. Model free control design approach for a semi-active suspension of a passenger car. In *Proc. of the American Control Conference, 2005*, pages 2206–2211, 2005.

[103] D. Liberzon. *Switching in Systems and Control*. Birkhäuser, 2003.

[104] W. Matschinsky. *Road Vehicle Suspensions*. John Wiley & Sons, 1998.

[105] R. Michalski, M. Tietke, G. Krger, F. Scheyhing, G. Steller, and R. Klingel. Die neue C-Klasse von Mercedes Benz: Fahrwerk - Neudefinition der Synthese von Komfort und Agilität. *Automobiltechnische Zeitschrift*, ATZ extra:82–101, 2007.

[106] M. Mitschke and K.-O. Riesenberg. Stoßdämpfererwärmung und Dämpferwirkung. *Automobiltechnische Zeitschrift (ATZ)*, 74:133, 1972.

[107] M. Mitschke and H. Wallentowitz. *Dynamik der Kraftfahrzeuge*. Springer Verlag Berlin, 4. edition, 2004.

[108] A. Moran, T. Hasegawa, and M. Nagai. Continuously controlled semi-active suspension using neural networks. *Society of Automotive Engineers of Japan (JSAE Review)*, 16:217–223, 1995.

[109] M. Münster, U. Mair, H.-J. Gilsdorf, A. Thom, C. Müller, M. Hippe, and J. Hoffmann. Electromechanical Active Body Control. *ATZ autotechnology*, 3:24–29, 2009.

[110] C. S. Namuduri, M. A. Golden, and J. Praeckel. Concurrent research an development of a magnetic ride control system. In *Proc. of the 29th Annual Conference of the IEEE Industrial Electronics Society, 2003*, pages 2853–2858, 2003.

[111] M. Nyenhuis and M. Fröhlich. Das Verstelldämpfersystem des BMW X5: Entwicklung des Sensor- und Beobachterkonzepts. *Automobiltechnische Zeitschrift*, 3:248–255, 2007.

[112] E.C. Obinabo and O. Ighodalo. The utilisation of an electric field sensitive effect for vibration control of viscous isolation system. *Research Journal of Applied Sciences, Engineering and Technology*, 3:153–158, 2011.

[113] M. Papageorgiou. *Optimierung - Statische, dynamische, stochastische Verfahren für die Anwendung*. Oldenbourg, 1991.

[114] T. Paschedag, A. Giua, and C. Seatzu. Constrained optimal control: an application to semiactive suspension systems. In *14th Mediterranean Conference on Control and Automation, 2006*, pages 1 –8, June 2006.

[115] M. Pazikas. Tenneco automotive press release 14.09.2005.

[116] E. Pellegrini, G. Koch, and B. Lohmann. Physical modeling of a nonlinear semi-active vehicle damper. In *Proc. of Advances in Automotive Control*, 2010.

[117] E. Pellegrini, G. Koch, and B. Lohmann. A dynamic feedforward control approach for a semi-active damper based on a new hysteresis model. In *Proc. of the 18th IFAC World Congress*, pages 6248–6253, 2011.

[118] E. Pellegrini, N. Pletschen, S. Spirk, M. Rainer, and B. Lohmann. Application of a model-based two-dof control structure for enhanced force tracking in a semi-active vehicle suspension. *In Proc. of the IEEE Multi-conference on System and Control*, 2012.

[119] E. Pellegrini, S. Spirk, N. Pletschen, and B. Lohmann. Experimental validation of a new model-based control strategy for a semi-active suspension system. In *American Control Conference*, pages 515–520, 2012.

[120] A. Phan. FEM Modellierung eines CATIA-Viertelfahrzeugprfstandsmodells. Project Thesis at the Institute of Automatic Control (Technische Universität München), 2010 Supervisor: E. Pellegrini.

[121] A. G. Piersol, C. M. Harris, and T. Paez. *Harris shock and vibration handbook*. 2009.

[122] N. Pletschen. Implementierung eines adaptiven Regelungskonzepts auf einem Viertelfahrzeugprüfstand für ein hybrides Fahrwerk. Project Thesis at the Institute of Automatic Control (Technische Universität München), 2011.

[123] C. Poussot-Vassal, O. Sename, L. Dugard, P. Gáspár, Z. Szabó, and J. Bokor. A new semi-active suspesion control strategy through LPV technique. *Control Engineering Practice*, 16:1519–1534, 2008.

[124] J. C. Poynor. Innovative designs for magneto-rheological dampers. Master's thesis, Faculty of Virginia Polytechnic Institute and State University, 2001.

[125] M. Puff, P. Pelz, and M. Mess. Beeinflussung der Fahrdynamik durch geregelte Luftdämpfer. *Automobiltechnische Zeitschrift ATZ*, 04:286–291, 2010.

[126] M. Pyper, W. Schiffer, and W. Schneider. *ABC - Active Body Control, Von der Blattfederung zum aktiven System für mehr Fahrsicherheit und Fahrkomfort*. Verlag Moderne Industrie, 2003.

[127] M. Rainer. Modellbasierte Zwei-Freiheitsgrade-Regelung zur Verbesserung des Kraftfolgeverhaltens eines semi-aktiven Dämpfers. Project Thesis at the Institute of Automatic Control (Technische Universität München), 2012 Supervisor: E. Pellegrini.

[128] J. Reimpell and H. Stoll. *Fahrwerktechnik: Stoß- und Schwingungsdämpfer*. Vogel Verlag Würzburg, 2 edition, 1989.

[129] G. Roppenecker. Zustandsregelung linearer Systeme - Eine Neubetrachtung. state feedback control of linear systems - a renewed approach. *AT - Automatisierungstechnik*, 57:491–498, 2009.

[130] ZF Sachs. *Technisches Training - Fahrzeugteile im Pkw Fahrwerk - Aufbau, Funktion und mögliche Schäden*. Sachs ZF.

[131] ZF Sachs. No compromises with chassis technology by ZF. Press Information (IAA), September 2009.

[132] A. P. Sage and C. C. White. *Optimum Systems Control*. Prentice Hall, 1977.

[133] P.M. Sain, M.K. Sain, and B.F. Spencer. Models for hysteresis and application to structural control. In *Proc. of the American Control Conference*, pages 16–20, 1997.

[134] D. Sammier, O. Sename, and L. Dugard. Skyhook and H_∞ control of semi-active suspensions: some practical aspects. *Vehicle System Dynamics*, 4:279–308, 2003.

[135] S. M. Savaresi, E. Silani, and S. Bittanti. Acceleration-driven-damper (ADD): An optimal control algorithm for comfort-oriented semiactive suspensions. *Journal of Dynamic Systems, Measurement, and Control*, 127(2):218–229, 2005.

[136] S. M. Savaresi and C. Spelta. Mixed sky-hook and ADD: Approaching the filtering limits of a semi-active suspension. *Journal of Dynamic Systems, Measurement, and Control*, 129(4):382–392, 2007.

[137] S. M. Savaresi and C. Spelta. A single-sensor control strategy for semi-active suspensions. In *Proc. of IEEE Transactions on Control Systems Technology*, pages 143–152, 2009.

[138] S.M. Savaresi, C. Poussot-Vassal, C. Spelta, O. Sename, and L. Dugard. *Semi-Active Suspension Control Design for Vehicles*. Elsevier Ltd., 2010.

[139] A. Schindler. *Neue Konzeption und erstmalige Realisierung eines aktiven Fahrwerks mit Preview-Strategie*. Dissertation, Karlsruher Institut für Technologie, 2009.

[140] A. Schöpfel, H. Stingl, R. Schwarz, W. Dick, and A. Biesalski. Der neue Audi A4: Audi Drive Select. *Automobiltechnische Zeitschrift*, ATZ extra:124–138, 2007.

[141] R. Schwarz, A. Biesalski, A. Schöpfel, and H. Stingl. Der neue Audi Q5: Audi Drive Select. *Automobiltechnische Zeitschrift*, ATZ extra:60–64, 2008.

[142] M.-S. Seong, K.-G. Sung, and S.-B. Choi. Damping force control of mr damper for passenger vehicle considering hysteretic compensator. *Advanced Materials Research*, 47-50:145–148, 2008.

[143] A. Shamsi and N. Choupani. Continuous and discontinuous shock absorber control through skyhook strategy in semi-active suspension system (4DOF model). *International Journal of Aerospace and Mechanical Engineering*, 2:254–258, 2008.

[144] A. Simms and D. Crolla. The influence of damper properties on vehicle dynamic behaviour. In *Proc. of SAE Word Congress Steering and Suspension Technology Symposium*, 2002.

[145] N. Sims and R. Stanway. Semi-active vehicle suspension using smart fluid dampers: a modelling and control study. *Int. Journal of Vehicle Design*, 33:76–102, 2003.

[146] N. Sims, R. Stanway, D. Peel, W. Bullough, and R. Johnson. Controllable viscous damping: an experimental study of an electrorheological long-stroke damper under proportional feedback control. *Smart Mater. Struct.*, 8:601–615, 1999.

[147] N.D. Sims, D.J. Peel, R. Stanway, R. Johnson, and W.A. Bullough. The electrorheological long-stroke damper: a new modelling technique with experimental validation. *Journal of Sound and Vibration*, 229(2):207–227, 2000.

[148] J.J.E. Slotine and W. Li. *Applied nonlinear control*. Prentice Hall, 1991.

[149] H.-C Sohn, K.-S Hong, and J. K. Hedrick. Semi-active control of the Macpherson suspension system: hardware-in-the-loop simulations. In *Proc. IEEE International Conference on Control Applications*, pages 982–987, 2000.

[150] C. Spelta, M. Cutini, S. A. Bertinotti, S. M. Savaresi, F. Previdi, C. Bisaglia, and P. Bolzern. A new concept of semi-active suspension with controllable damper and spring. In *Proceedings of the European Control Conference*, pages 4410–4415, 2009.

[151] B. F. Spencer, S. J. Dyke, M. K. Sain, and J. D. Carlson. Phenomenological model of a magnetorheological damper. *Journal of Engineering Mechanics, ASCE*, 123:230–238, 1997.

[152] M. Spielmann. Elektronische Dämpfkraftregelung EDCC. In *Elektronik im Kraftfahrzeugwesen - Steuerungs-, Regelungs- und Kommunikationssysteme*, pages 8–14. Kontakt & Studium - expert Verlag, 2002.

[153] S. Spirk, G. Koch, and B. Lohmann. Improving suspension control by an optimal control component and disturbance compensation. In *Proc. of the 18th IFAC World Congress*, pages 6272–6278, aug. 2011.

[154] S. Spirk, G. Koch, E. Pellegrini, and B. Lohmann. Dynamik- und energieoptimale Stellgrößenaufteilung für die Regelung eines hybriden Fahrwerks. In W. Schfer A. Trchtler J. Gausemeier, F. Rammig, editor, *Intelligente Technische Systeme - Entwurf mechatronischer Systeme*, number 294, pages 107–119. Heinz Nixdorf Institut Verlagsschriftenreihe, 2011.

[155] S. Spirk and B. Lohmann. Controlling an active suspension using methods of optimal control. *Accepted and to be presented at the Conference on Decision and Control*, 2012.

[156] R. Streiter. *Entwicklung und Realisierung eines analytischen Regelkonzeptes für eine aktive Federung*. PhD thesis, Technische Universität Berlin, 1996.

[157] R. Streiter. ABC Pre-Scan im F700. *Automobiltechnische Zeitschrift*, 05:388–397, 2008.

[158] TyssenKrupp Bilstein Suspension. Damper adjustment, 12, 2011.

[159] E. Teramura, S. Haseda, Y. Shimoyama, T. Abe, and K. Matsuoka. Semi-active damping control system with smart actuator. *Society of Automotive Engineers of Japan (JSAE Review)*, 18:323–329, 1997.

[160] M. Tomizuka and J. Hedrick. Advanced control methods for automotive applications. *Vehicle System Dynamics*, 24:449–468, 1995.

[161] A. Unger. *Serientaugliche quadratisch optimale Regelung für semiaktive Pkw-Fahrwerke*. PhD thesis, Technische Universität München, 2012.

[162] A. Unger, G. Koch, and B. Lohmann. Benchmark of semi-active suspension controllers in real-time application. *AUTOREG 2011, VDI-Berichte*, 2135:333–344, 2011.

[163] A. Unger, E. Pellegrini, K.-U. Henning, and B. Lohmann. A model for dynamic feedforward control of a semi-active damper. In *Proc. of the 5th International Conference on Integrated Modelling and Analysis in Applied Control and Automation (IMAACA 2011)*, 2011.

[164] M. Valasek and W. Kortm. Semi-active suspension systems II. *Vehicle System Dynamics*, 44:479–488, 2000.

[165] M. Valek, M. Novak, Z. Łika, and O. Vaculin. Extended ground-hook - new concept of semi-active control of trucks suspension. *Vehicle Systems Dynamics*, 27:289–303, 1997.

[166] VDI. *VDI- Wärmeatlas*, 7th edition, 1994.

[167] P. J.Th. Venhovens. *Optimal Control of Vehicle Suspensions*. PhD thesis, Delft University of Technology, 1993.

[168] Verein deutscher Ingenieure (VDI). *VDI Richtlinie 2057 - Einwirkungen mechanischer Schwingungen auf den Menschen*, 2002.

[169] A. Visintin. *Differential Models of Hysteresis*. Springer- Verlag Berlin Heidelberg, 1994.

[170] H. Wallentowitz. *Aktive Fahrwerkstechnik*. Vieweg, 1991.

[171] H. Wallentowitz and T. Schrüllkamp. Elektronik im Kraftfahrzeugwesen - Steuerungs-, Regelungs- und Kommunikationssysteme. In *Geregelte Fahrwerke*. Kontakt & Studium - expert Verlag, 2002.

[172] X. Wang. Solving optimal control problems with Matlab - Indirect Methods. *NCSU, ISE department*, 2009.

[173] Y. Wardi, P. Twu, and M. Egerstedt. On-line optimal timing control of switched systems. In *Proc. IEEE Conf. on Decision and Control*, pages 2137 –2142, dec. 2010.

[174] F.M White. *Fluid Mechanics*. McGraw-Hill Book Company, 1986.

[175] D. A. Wilson, R. S. Sharp, and S. A. Hassan. The application of linear optimal control theory to the design of active automotive suspensions. *Vehicle System Dynamics*, 15(2):105–118, 1986.

[176] P.H. Wirsching, T.L. Paez, and K. Ortiz. *Random Vibrations - Theory and Practice*. John Wiley & Sons, Inc., New York, 1995.

[177] J.Y. Wong. *Theory of ground vehicles*. John Wiley & Sons, Inc., New York, 2008.

[178] K. Yi and B. S. Song. A new adaptive sky-hook control of vehicle semi-active suspensions. In *Proc. of the Institution of Mechanical Engineers, Part D: Journal of Automobile Engineering*, pages 293–303, 1999.

[179] M Yokoyama, J.K. Hedrick, and S. Toyoma. A model following sliding mode controller for semi-active suspension systems with mr dampers. *Proc of the American Control Conference*, 4:2652–2657, 2001.

[180] K. Yoshida, Y. Nishimura, and Y. Yonezawa. Variable gain feedback for linear sampled-data systems with bounded control. *Control Theory and Advanced Technology*, 2(2):313 – 323, 1986.

[181] T. Yoshimura, A. Kume, M. Kurimoto, and J. Hino. Construction of an active suspension system of a quarter car model using the concept of sliding mode control. *Journal of Sound and Vibration*, 239(2):187 – 199, 2001.

[182] M. Zeitz. Vorsteuerungs-Entwurf im Frequenzbereich: Offline oder Online - Feedforward Control Design in Frequency Domain: Offline or Online. *AT - Automatisierungstechnik*, 60:375–383, July 2012.

[183] A. Zikrija, C. Senad, and K. Samim. Reducing vibration of the seat with semi-active damper using the artificial neural networks. In *Proceedings of International Joint Conference on Neural Networks*, 2007.

Appendix A

QUARTER-CAR AND DAMPER TEST RIGS

In oder to identify the suspension elements and their kinematics and to validate controller strategies, a quarter-car test rig for the semi-active suspension is constructed, which is based on a double wishbone suspension adopted in a modern upper class vehicle, [24, 96]. The configuration adopted by the design reflects the original design of the automotive industry. Since the applied components are used in upper class vehicles (limousine), the choice of the primary spring and of the passive damping offers a comfort-oriented ride. The corresponding test rig configuration and suspension model was already presented in [93] and is re-proposed in Section A.3 with particular attention to the nonlinearities, which strongly influence the dynamic behavior of the vehicle.

A.1 Automotive quarter-car test rig

The quarter-car test rig reported in Figure A.1 is designed using hardware components and common settings of an upper class vehicle. The design at the department of Automatic Control of the Technische Universität München was supported by technical draws and components' data made available by the industrial partner. Dealing with a limousine vehicle the nominal values of the sprung mass $m_c \approx 500$kg and the unsprung mass $m_w \approx 70$kg are chosen. It results in a static wheel load of $F_{stat} \approx 5640$N. As already mentioned, the suspension kinematic is governed by a wishbone structure and the suspension is equipped with a hydraulic semi-active suspension system with two independently adjustable external valves.

It is noted that the suspension strut depicted in Figure A.1(b) is extended by an hydraulic component (slow-active actuator), which allows to introduce forces by working in series to the primary spring, see e.g. [93, 97, 98]. In this Thesis, this component is not described, by assuming its inoperative state in the semi-active configuration. The actuator is kept in the rest position and it does not influence the primary spring position. The description of the

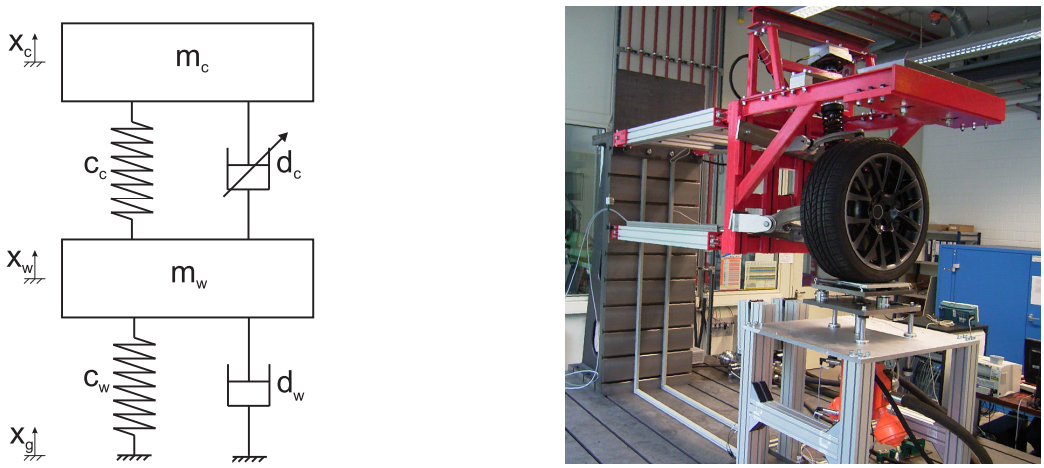

Figure A.1: Quarter-car model (left) und realization (right) of the semi-active suspension test rig.

new extended suspension strut and actuator control strategies are addressed in [93, 96]. The kinematic relationships of the original series suspension configuration including the deflection depending transmission factor (see [104]) are preserved.

A hydraulic actuator (see Figure A.2) is used to vertically excite the tire and thus to simulate the road excitation x_g. Since its bandwidth is above the frequencies of a common road profile, it is suitable for the considered applications. The cylinder's rod position is controlled by a 4-port/3-way-servovalve and the nominal maximum displacement amplitude $\max(x_g)$ of the rod is ± 10 cm. The input signal u_h is control by a subordinate actuator structure for position tracking. Conditioned by mechanical arrangements, apt to protect the internal end-stop of the piston rod, the travel length of the piston rod is mechanically limited to ± 9 cm. During the experiments, the hydraulic system is actuated by a supply pressure p_v of 240 bar and a tank pressure p_t of 1 bar. More information about cylinder modeling and signal tracking controller can be found in [96].

Only the vertical motion of the test rig is allowed. A parallel kinematics guide system is designed to not influence the vertical kinematics of the suspension car by considering the road excitations limited by the nominal value of the the hydraulic cylinder rod. The parallel kinematic consists of aluminum profiles, which guarantee mechanical stability by minimal weight.

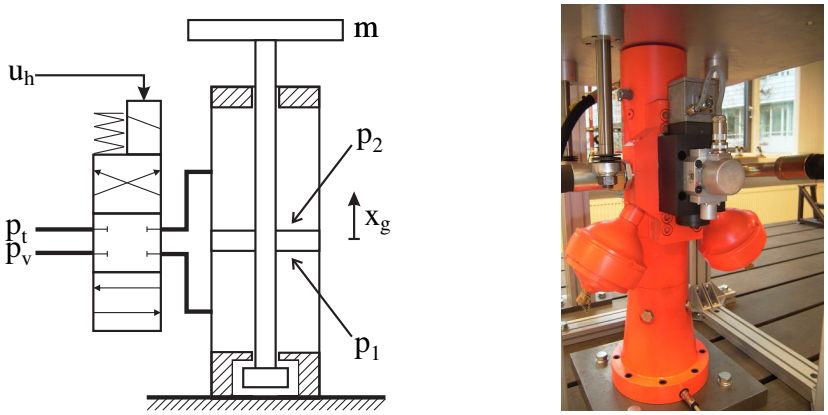

Figure A.2: Hydraulic system: Scheme (le.) and cylinder (ri.), [96]

In the earlier design phases, besides the construction elements (performed with *Dassault Systemes - CATIA V5*) also frequency response of the complete structure (performed with *Ansys*) are considered. In fact, the minimization of the structural vibration of the test rig within the frequency range, in which the suspension control takes place is required. Particularly the suspension unit and the newly designed quarter-car chassis are studied, see Figure A.3.

Therefore, finite element methods (FEM) and a modal analysis of the construction have been completed and the design of the structure has been optimized accordingly, [120]. Figure A.3(b) shows the simulation result of the first eigenmode at approx. 40 Hz, which is above the frequency range of interest for suspension control purposes. Moreover, the details of the the spring-damper unit are illustrated in Figure A.3(a).

A.2 Sensor configuration

The sensor configuration adopted for performing the controller strategies, is similar to the one adopted in production vehicle. Besides the capacitive accelerometers with measurement range of $\pm$10g and $\pm$50g for chassis and wheel respectively, the original encoder from the production vehicle is adopted to measure the suspension deflection. For controller purposes also the damper valves' currents $\mathbf{i}(t)=[i_{com}(t)i_{reb}(t)]^T$ are measured by the power electronic unit.

For validating purposes both the wheel load and the strut force transmitted by the suspension unit are recorded. While the first $F_w(t) = F_{dyn}(t) + F_{stat}$ is received by three cell loads and

then summed by means of an electronic component, the second is recorded by means of a force transducer (measurement range $\pm$ 25 kN), which measures both static and dynamic forces. This sensor is suitable for measuring tensile and compressive forces. The load cell is integrated in the measurement chain by a 600 Hz measuring amplifier. Since the suspension strut consists of spring and damper, both contributes are contained in the measured signal.

The rod position of the hydraulic actuator, $x_g(t)$, is measured by an LVDT-position transducer integrated in the hydraulic cylinder itself.

To run the application the platform *dSpace DS1103 PPC Controller Board* and the software *dSpace Control Desk* are utilized, which are integrated in a *Intel Core2* personal computer. The system operates with a sampling frequency of f_s = 1kHz.

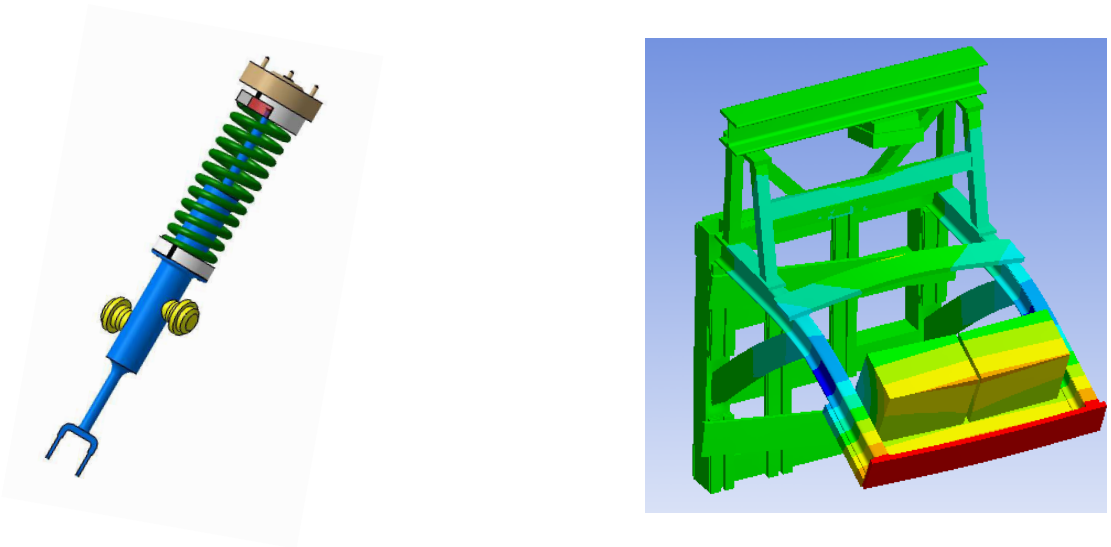

(a) Design of Spring-Damper unit

(b) Structure frequency response: Eigenmode at the first eingenfrequency of 39.95 Hz

Figure A.3: CAD-Design of the semi-active suspension strut and FEM analysis of the vibration modes of the quarter-car test rig

A.3 Suspension kinematics

While the operational behavior of the damper is the kernel of this Thesis and is addressed in Chapter 3 and 4, the characteristics of the suspension spring are described in Section 2.1. Moreover, its characteristic curve and the tire characteristics are already published in a previous works [93, 96] and they do not occur in this Thesis. Some relevant details of suspension kinematics are condensed in the following.

The inclined assembly and the geometry of the double wishbone suspension define the kinematics of the suspension. Due to suspension compression or rebound motion, the suspension strut changes the inclination, thus the kinematic transmission factor i_f can be calculated, according to [104], as follows

$$i_f(t) = i_0 - \underbrace{\frac{\Delta i}{\Delta x_{cw}}}_{i_x}(x_c(t) - x_w(t)), \tag{A.1}$$

where i_0 is a constant transmission factor and the term i_x describes the linear change depending on the suspension deflection of the kinematic transmission factor. The kinematic transmission factor transform the forces and kinematic relations acting in the direction of the suspension strut central line to the coordinates of the quarter-car model, [107].

A.4 Linearization

In this Section the linearization of the nonlinear spring elements, which are applied to build the spring force in (2.8), is performed. The procedure is based on the Taylor series expansion.

It can be noted, that the linear behavior is limited to a small range around $0\,\mathrm{m}$. Due to the linear model assumption of the tire, only the force action between sprung and unsprung mass has to be linearized. The cumulative force F_f is given by the sum of the primary spring, the secondary spring and the pre-load, due to the chassis mass weight. Due to the shape of of the secondary spring characteristic, at the equilibrium point x_1 its effect is omitted. Thus a

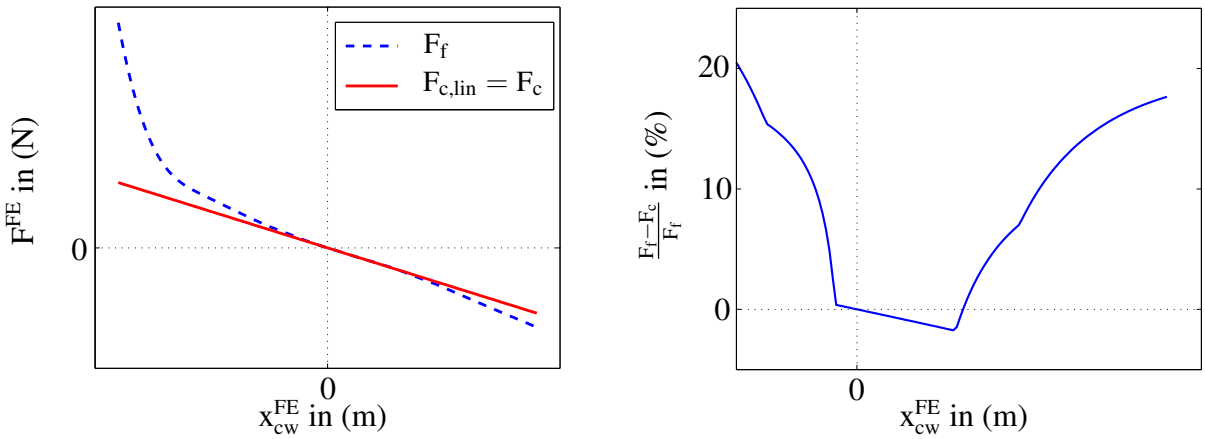

(a) Nonlinear and linear spring forces (b) Relative error

Figure A.4: Comparison between the forces of the nonlinear and linear models

linearized spring stiffness

$$c_c = \left.\frac{dF_f}{dx_1}\right|_{x_1} = -\left(c_{ps} \cdot i_0^2 + \frac{i_x}{i_0} m_c g\right) \tag{A.2}$$

can be calculated. Figure A.4(a) shows a comparison between the linearized and the effectively acting spring force, whereby in Figure A.4(b) the effect of the secondary spring is pointed out by depicting the relative error.

The different damper characteristics both in rebound and in compression are linearized by $\pm 0.4\,{}^{m}/_{s}$ and subsequently the mean value of each current setting is considered as linear damping coefficient d_c. By allowing a freely acting force between sprung and unsprung mass, the state space form in (2.17) and (2.18) has to be modified. The quarter-car equations for the active configuration can be found e.g. in [93].

A.5 Damper Test Rig

The damper test rig structure is shown in Figure A.5. The semi-active device is excited axially by the hydraulic cylinder. The rod position is measured and the rode velocity is derived after filtering. The shock absorber is fixed to load cells so that the internal force can be measured directly. The same real-time system described in A.2 is used to control the test rig.

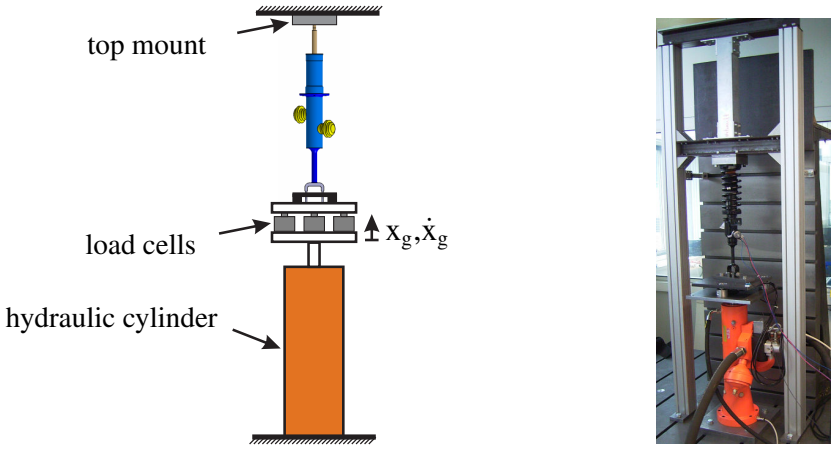

Figure A.5: Damper test rig: (a) Design schema and (b) realization

Both the static and the dynamic damper characteristics are obtained at the presented test rig. Moreover, this setup has been utilized to validate the proposed electrical and the mechanical models of the semi-active damper.